Master's thesis

NTNU
Norwegian University of Science and Technology
Faculty of Engineering
Department of Geoscience and Petroleum

Gaute Magnushommen

Distribution of Th and U in the Fe-dolomite carbonatite from the Fen REE deposit

Master's thesis in Geology
Supervisor: Kurt Aasly
Co-supervisor: Stefanie Lode
June 2022

NTNU
Norwegian University of
Science and Technology

Gaute Magnushommen

Distribution of Th and U in the Fe-dolomite carbonatite from the Fen REE deposit

Master's thesis in Geology
Supervisor: Kurt Aasly
Co-supervisor: Stefanie Lode
June 2022

Norwegian University of Science and Technology
Faculty of Engineering
Department of Geoscience and Petroleum

NTNU
Norwegian University of
Science and Technology

Abstract

A detailed characterisation of thorium and uranium is presented based on 12 specimens taken from material from the Fen carbonatite complex in Ulefoss, Telemark, Norway. The specimens were sorted based on radioactivity into three categories and studied. It was concluded that thorium is found mainly as thorite, and there are some instances of low thorium concentrations along Rare Earth Element (REE) mineral grain boundaries. Most thorite grains are smaller than 50 µm and no larger than 200 µm except a very small fraction of outliers that are no larger than 400 µm. Thorite has a wide range of associations with a consistent high relation to calcite, quartz, and ankerite. There was significantly less uranium in the specimens, and it occurs in uraninite and coffinite. Most of the uraninite and coffinite grains were below 25 µm and no larger than 100 µm. The uraninite and coffinite grains are strongly associated with pyrite and calcite and somewhat with ankerite. Both thorium and uranium only show a possible weak correlation towards the REEs at lower thorium, uranium and REE concentrations. As the element concentrations increase, the correlation lowers, indicating little to no correlation at higher concentrations.

The Light Rare Earth Elements (LREEs) are found in varying concentrations throughout each specimen. Lanthanum, cerium, and neodymium are found mainly in the following minerals: parisite, bastnäsite, monazite and synchysite. While praseodymium and samarium are both found mainly in carbonates, quartz and samarium is also found in apatite. These minerals correlate to previous studies in the area.

A range of methods was used and proved useful for characterising the radioactive minerals: radioactive reading on specimen surfaces gave a general idea of thorium content, and optical microscopy was viable when the radioactive grains were on the larger end. X-ray fluorescence (XRF) proved useful to quantify each element, inductively coupled plasma mass spectrometry (ICP-MS) also worked, and it also quantified more REEs than XRF. Micro-computed tomography (µCT) might prove a useful tool to view textural information in 3D, assuming the resolution matches the general grain size of the radioactive minerals in the analysed specimen. SEM-based automated mineralogy (AM) was the main method used and was critical to quantify grain size, element distribution, and associations. The method works well when the step-size closely matches grain size, therefore some knowledge of the specimen is required for the best result.

Sammendrag

En detaljert karakterisering av thorium og uran er presentert basert på 12 prøver tatt fra materiale fra Fensfeltet i Ulefoss, Telemark, Norge. Prøvene ble sortert i tre kategorier og studert, basert på radioaktivitet. Det ble konkludert med at thorium hovedsakelig finnes som thoritt, og det er i noen tilfeller, lave thorium konsentrasjoner langs sjeldne jordarts (REE) mineralkorngrenser. De fleste thoritt kornene er mindre enn 50 µm og ikke større en 200 µm, unntatt en veldig liten fraksjon med avvik som når opptil 400 µm. Thoritt har et bredt spekter med assosiasjoner, men en konsistent høy relasjon til kalsitt, kvarts og ankeritt. Det var betydelig mindre uran i alle prøvene, og det forekom som uranitt og coffinitt. Majoriteten av uranitt og coffinitt kornene var under 25 µm og ikke større enn 100 µm. uranitt og coffinitt kornene er sterkt assosiert med svovelkis, kalsitt og i svakere grad ankeritt. Både thorium og uran viser kun en mulig svak korrelasjon til REE-ene ved lavere thorium, uran og REE konsentrasjoner. Når element konsentrasjonene stiger så synker korrelasjonen. Dette indikerer at det ikke er lite til ingen korrelasjon på høyere konsentrasjoner

De lette sjeldne jordartene (LREE) finnes i varierende konsentrasjoner i hver prøve. Lantan, cerium og neodym finnes hovedsakelig i følgende mineraler: parisitt, bastnäsitt, monazitt og synchysite. Mens praseodym og samarium hovedsakelig finnes i kalsitt karbonater, kvarts og apatitt for samarium. Disse mineralene korrelerer med tidligere studier fra området.

En rekke metoder ble brukt og viste seg nyttige for å karakterisere de radioaktive mineralene: radioaktiv avlesning på prøveoverflater ga en generell idé om thoriuminnhold, og optisk mikroskopi var brukbart når de radioaktive kornene var av større kornstørrelser. Røntgenfluorescens (XRF) viste seg nyttig for å kvantifisere hvert element, induktivt koblet plasma masse spektrometri (ICP-MS) fungerte også, og det kvantifiserte også flere REE enn XRF. Mikrocomputertomografi (µCT) kan vise seg å være et nyttig verktøy for å se teksturinformasjon i 3D, forutsatt at oppløsningen samsvarer med den generelle kornstørrelsen til de radioaktive mineralene i den analyserte prøven. SEM-basert automatisk mineralogi (AM) var hoved metoden som ble brukt og var kritisk for å kvantifisere kornstørrelse, elementfordeling og assosiasjoner. Metoden fungerer bra når trinnstørrelsen stemmer godt overens med kornstørrelsen, derfor kreves det litt kunnskap om prøven for best resultat.

Preface

This master thesis marks the end of my MSc Studies and hopefully the start of a new chapter.

I would like to thank everyone who have helped during this work period. First of all I would like to thank my advisors Kurt Aasly who I've had weekly meetings throughout the year that has helped keep me on track and Stefani Lode who has been fantastically helpful with her previous experience on the Fen material and SEM knowledge. I would like to thank Camilo Mena Silva, Torill Sørløkk, Laurentius Tijhuis for the help during the sorting and chemical lab work. Haili Long-Sanouiller and Jostein Røstad for help creating the µCT model. I would like to thank REN for providing the material used for this thesis.

I would like to thank Marte Helene Homleid for bearing with me during these last stressful months. I would like to thank my friends that have helped with encouragement and editing during these last few months and the group of online individuals that have kept me sane when not working on this thesis, you know who you are.

And lastly, I would like to thank my cat at home who has surely forgotten all about me during the final stages of this thesis.

Gaute Magnushommen

Trondheim, 30th of June 2022

Contents

Figures

Tables

Abbreviations & Dictionary

Abbreviations	*Meaning*
REE	Rare earth element
LREE	Light rare earth element
HREE	Heavy rare earth element
TREE	Total rare earth element
FDC	Fe-dolomite carbonatite
XRD	X-ray diffraction
XRF	X-ray fluorescence
LOI	Loss on ignition
ICP-MS	Inductively coupled plasma mass spectrometry
μCT	Micro-computed tomography
SEM	Scanning electron microscope
AM	Automated mineralogy
BSE	Back-scatter electrons
BPS	Bright phase search
OV	Overview
Sc	Scandium
Y	Yttrium
La	Lanthanum
Ce	Cerium
Pr	Praseodymium
Nd	Neodymium
Pm	Promethium
Sm	Samarium

Dictionary

Norwegian	*English*
Rødberg	Redrock
Kjerne	Drill-core
Gamle gruva	Old mine

1 Introduction

1.1 Goals and motivations

The aim of this thesis is to answer the following questions: where are the radioactive elements thorium, uranium located? Is there a connection between the minerals containing rare earth elements (REE), thorium and uranium? What analytical methods are effective to classify thorium and uranium? What minerals does the light rare earth elements (LRRE) make up?

To answer the research questions, material from Tuftestolen mine in the Fen area, Ulefoss, Norway, was sorted and 12 specimens were selected based on the sorting results. The specimens were prepared for thin-sections, and parts of each specimen were crushed for other analytical methods. A drill core was created from one specimen for use in Micro-computed tomography (μCT).

The focus of the thesis will be on the methods, characterisation of thorium and uranium with a secondary focus on the REEs. The formation of the minerals that these elements make up, and when they were made will not be a focus in this thesis.

The Fen carbonatite complex is thought to be a considerable potential source of REEs in Europe, but thorium and to lesser degrees uranium have been found associated with the same minerals as the REEs in the area (Dahlgren, 2012). This means that any extraction of the REEs will have to account for and extract thorium and uranium at the same time. A proper characterisation of these elements is necessary because of their radioactive nature. Improper handling of these elements could cause considerable environmental damage (Reisman et al., 2013), including but not limited to birth defects and lung burden (Chen et al., 2005). There is also possible markets for thorium within medical ((Duchemin et al., 2015) and energy sectors in the future.

The main reason for extracting the REEs is because they are crucial components in various electronics, electric cars, and more (Dushyantha et al., 2020). The need for these elements is expected to rise as the world moves to reduce emissions and decarbonisation of energy production (Guyonnet et al., 2015). Currently, the EU has classified REEs as critical raw material, meaning it is crucial to Europe's economy. Today REEs are supplied almost

exclusively by China. This, combined with rising global political tension, means that REEs are currently a significant supply risk for Europe (Gauß et al., 2021).

Because of the complex nature of the deposits where the REEs typically forms, a full characterisation of their mineralogy and geology needs to be done to be able to create a tailor made beneficiation process that fits each deposit (Jordens et al., 2013).

1.2 Fen Carbonatite Complex

The Fen area is assumed to be an old feed tube to a volcano that lay over the area that dates back 580 million years. The bulk of the area is east of Ulefoss in Telemark County, Norway (Figure 1-1). The magmas that made up the feed tube are of an uncommon carbonatite variety that over a multitude of magmatic pulses have created a complex set of intersecting magmatic breccia (Dahlgren, 2012). These pulses have been generalized down to five main events that are somewhat interconnected (Coint & Dahlgren, 2019; Dahlgren, 2019) and make up the bulk origin of what is found in the area today. An interpretation of the area (Figure 1-2) has previously been made based on exposed rocks.

Figure 1-1 Shows the location of the Fen complex right east of Ulefoss

1.3 Geological background

The Fen area was firstly theorised to be magmatic in origin back in 1921 (Brøgger, 1921) and is the origin behind the terms “fenite” and “fenitization”. These terms are used to describe this type of metasomatized alkaline rocks and their creation. The Fe-dolomite carbonatite (FDC) is the main group of interest and the host rock to the specimens used in this study. The FDC (Figure 1-2) seem to concentrate in the middle of the Fen complex.

The creation of the Fen complex stems from five major geological events (Dahlgren, 2019) that were not totally separated, especially the later ones. Firstly, alkaline silicate rocks were emplaced in the area, then came several dike intrusions of various carbonates. The FDC came next and around the same time there were intrusions of damtjernite (an ultra-mafic intrusion). Finally Hydrothermal alteration and hematitization.

The enrichment of REEs in the FDC is believed to be a result of this hydrothermal activity (Dietzel et al., 2019). There was likely three main late/ post stage hydrothermal alteration

events in the area. Firstly, a fluid with a high sulphide content led to widespread pyrite formation in the whole fen complex. The next two hydrothermal fluids likely happened around or at the same time. Of the two there was a REE-rich fluid that redistributed Aluminium and iron that lead to the creation of multiple REE-F-carbonates. The second fluid is thought to be quartz-rich and oxidized that then produced the distinct Redrock ("Rødberg") phase by in-situ oxidation and mixing with the REE-rich fluid.

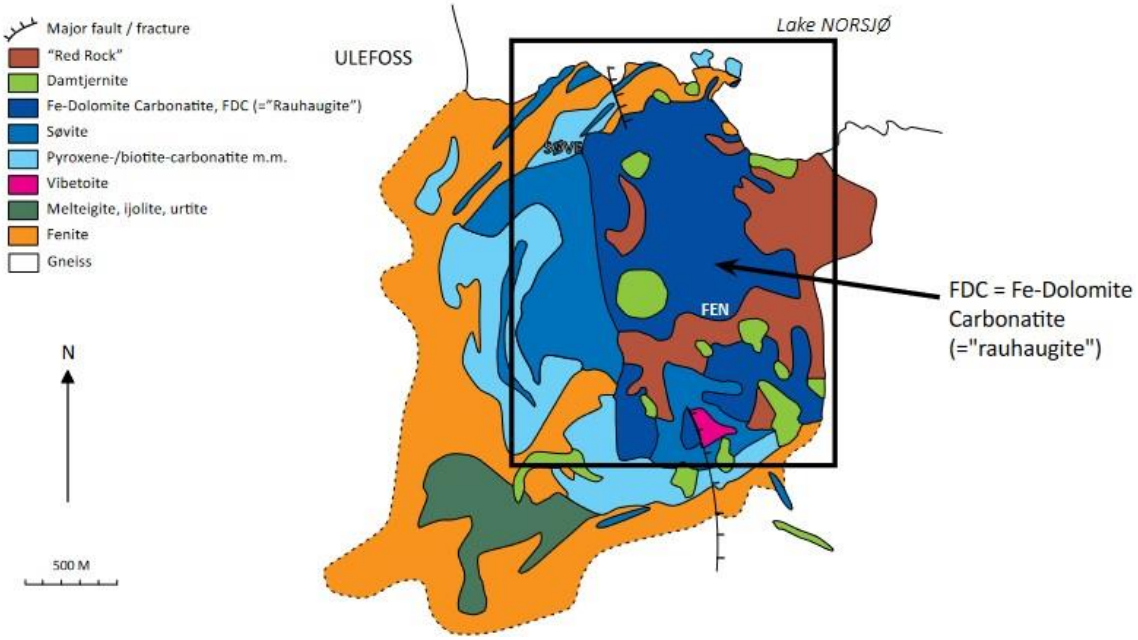

Figure 1-2 Map showing a interpreted area of the Fen complex based upon exposed rocks in the area (Dahlgren, 2016)

The FDC group has had many names since it's discovery, first it was called rauhaugite (Brøgger, 1921), afterwards it was split into two distinct rauhaugite types depending on the iron content (Sæther, 1957). They were named "type 1" and "type 2" rauhaugite, "type 1" was low in iron content and is considered part of the first dikes introduce into the Fen complex, while "type 2" had a higher iron content and came presumedly after "type 1". Both are rather distinct rock types but were never properly defined at the time and this is the reason for their many names. Rauhaugite "type 2" is the more interesting of the two as it has been shown to contain enriched concentrations of rare earth elements (REE) and some considerable concentrations of thorium and uranium. This increased interest has prompted multiple renaming conventions to try to better represent the rock group. In the mid 80's it got the name ferrocarbonatite (Andersen, 1986), which was later deemed unreliable and it was classified as ankerite carbonatite (Dahlgren, 2016). After more groundwork it was determined

that there was little actual ankerite in the rock group and rather increased levels of iron rich dolomite. Therefore it is called Fe-dolomite carbonatite (Coint & Dahlgren, 2019) or FDC today to better represent the rock group.

1.4 Relevant elements

Thorium is no. 90 in the periodic table and together with uranium is placed in the actinide group. It was first found in Norway by an amateur geologist in 1828, he then sent the sample to a Swedish chemist that in 1829 named it thorium (Alstad & Bjørnstad, 2020). Thorium was only discovered to be radioactive in 1889 in Paris and Erlangen independently of each other. It averages around 9.7 ppm in the continental crust. It has been severely neglected as a potential energy source for nuclear reactors because it cannot be used to make nuclear weapons. Thorium can today be a source of multiple medical isotopes.

Uranium is no. 92 in the periodic table and naturally consists of three different isotopes, ^{238}U being the most common, ^{235}U and ^{234}U (Kofstad et al., 2019) appearing in significantly smaller quantities. It was first discovered and named in 1789 and first isolated in 1841. It was discovered to be radioactive in 1896. The continental crust contains on average 2.7 ppm uranium. It has higher notoriety than thorium because of its uses in energy, weapons production, and the waste material it leaves behind.

The group commonly described as rare earth elements (REE) consists of the 15 lanthanides from the periodic table and is subdivided into two somewhat arbitrary groups known as light rare earth elements (LREE) and heavy rare earth elements (HREE). The distinction of which elements are LREE and HREE varies between works and sometimes include a third mid-REE category. In this work LREEs are the lanthanides up to samarium as used in previous works covering the same area (Dahlgren, 2019) and are shown in Figure 1-3. The name rare earth elements can be considered a misnomer, as the name implies that they are rare in the crust, which is untrue. The REEs are commonly found in the earth's crust but there are few deposits around the world where they can be economically extracted. They are often found in carbonatites or alkaline igneous rocks and today there are estimated over 850 deposits around the world (Wall, 2021). Today the main source of REEs comes from China with Australia and USA producing only small amounts. As of now the Fen complex is one of four identified

potential deposits in Norway and is estimated to be a significant source of REEs within Europe.

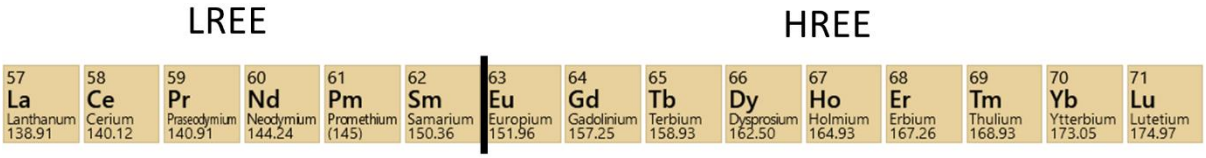

Figure 1-3 Shows the Rare earth elements with the distinction of Light and Heavy REEs (Modified from Dayah, 1997)

The elements Yttrium (Y) and Scandium (Sc) are in many cases included in the REE classification because of their similar chemical characteristics, but this work will refrain from including them. This is because Sc have little relevance to the Fen complex and Y is only included as an add-on is most other literature. Promethium (Pm) is rarely included in the wide variety of chemical tests because it naturally forms no stable isotopes (Chakhmouradian & Wall, 2012). In nature it only occurs in traceable amounts from natural fission, making it a poor element to extract from the crust.

Previous work in the Fen complex have identified four main REE bearing minerals (Table 1-1). REE in the formulas is replaced with the most common REE for each mineral. Three of these minerals are fluorocarbonatites (bastnäsite, parisite, synchysite), the fourth mineral is a phosphate (monazite). The table shows that these minerals are associated with LREE enrichment (Coint & Dahlgren, 2019).

Table 1-1 Shows the REE bearing minerals found in previous studies on the Fen complex (Coint & Dahlgren, 2019), second column shows the most common REEs in each mineral.

Mineral	*Composition*	*Most common REE*
Bastnäsite	(REE)CO3F	La, Ce, Nd
Parisite	$Ca(REE)_2(CO_3)_3F_2$	La, Ce, Nd
Synchysite	$Ca(REE)(CO_3)_2F$	Ce
Monazite	$(REE)PO_4$	La, Ce, Nd

1.1. Bayan obo

Baya obo is a carbonatite deposit in northern China and is currently the world's biggest supplier in RREs. The REEs are hosted mainly in dolomitic marble of fine and coarse grain varieties (K. Yang et al., 2019). The main REE bearing minerals in the deposit is monazite and bastnäsite.

1.5 Background on Equipment

Over the course of the last year several common instruments have been used. These include but are not limited to Optical microscopy, x-ray fluorescence (XRF), X-ray diffraction (XRD), Inductively coupled plasma mass spectrometry (ICP-MS), SEM- (Scanning electron microscopy-) based automated mineralogy (AM) and micro-computed tomography (µCT).

X-ray diffraction (XRD) is a method used to find the crystal structure of a measured object. It uses the principle of each element having differing diffractions. An x-ray gets sent out and hits a desired object. The ray's diffraction is then measured on a receiver plate (JoVE Science Education Database, 2022). A waveform is made based on where on the plate the ray hits, the strength of the ray and the ray angle. This waveform is then compared to known minerals to give an estimate on what the object contains (JoVE Science Education Database, 2022).

X-ray fluorescence (XRF) work by using secondary x-rays, these are produced by ionising the subject with an x-ray (Wirth & Barth, 2020). If this induced energy is high enough it can loosen an electron from the inner ring of the differing atoms that make up the subject. This makes the atom unstable and an electron from the outer ring wants to move inwards to a more stable position, this releases photons that have a characteristic energy/ wavelength for each atom. This can then be used to classify each atom in the subject (Wirth & Barth, 2020).

Inductively coupled plasma mass spectrometry (ICP-MS) works by ionizing in most cases a liquid sample, it does this using an electronic induction to create a plasma (the inductively coupled plasma) that has temperatures around 6000-8000 °C (Wibetoe, 2019). First the sample liquid is pumped into the machine and an argon gas is added in the nebulizer, the sample comes out of the nebulizer as an aerosol because of the injected gas. The areosol then moves into the plasma torch and is ionized (Thomas, 2008). These ions then get converted into an electrical signal that is picked up by the machine. It then presents the data as counts per second, this means that the machine must be calibrated with samples that have known quantity for each element that is to be tested. Using standard solutions allows for the creation of a graph that is used to represent how many counts respond to ppm in the tested sample.

Scanning electron microscope (SEM) works on the same principle as an optical microscope except that the light source is replaced with a focused electron beam produced from a tungsten cathode (Reimer, 1998). The chamber is then placed in a vacuum to remove atoms that could potentially diffract the electron beam. This allows for a much higher resolution (down to 1-2 µm). To focus the emitted beam a set of electron magnets that can be adjusted

are used (Swapp, 2017). The main instrument used is backscatter electrons (BSE), it works on a ricochet principle where the trajectory of the electron changes as it hits an atom, but constant speed is upheld. The chance that the beam will be redirected by an atom is proportional with the atoms size, therefore will the heavier atoms appear brighter than the lighter atoms (Goodge, 2016). The energy of the electron beam determines how many counts each scanned point gets, therefore would a stronger electron beam produce more accurate results, except in certain cases. One such case is when atoms with similar wavelengths can be classified as each other because of a peak overlap (Liao, 2007). To increase accuracy and to be able to separate the peaks better a lower beam energy can be used. An example of this peak overlap is between thorium (Lα 2.996) and silver (Lα 2.983). Generally, a SEM will be equipped with multiple different sensors to cover a wide range of situations. These are usually secondary electron (SE), Cathodoluminescence (CL), Micro diffraction (EBSD) and characteristic x-rays (exiting electrons) detectors.

SEM based automated mineralogy (AM) is essentially a software that can be used together with a SEM to take multiple inputs and use them to categorise a section of a specimen (Schulz et al., 2020). It categorises these sections based on classifications specified by the operator. One such software is Zeiss mineralogic that characterises specimens based on chemical composition to produce a map of a specified area. The map is pixel based where one pixel is a set size, smaller pixels give better overall resolution but uses exponentially more time to map the same area. It creates the pixels in a similar way to point counting, which is an optical microscopy method to determine mineral proportions in an area.

Micro-computed tomography (μCT) is a technique that uses an x-ray to project a slice of a specimen onto a detector that records it as a 2D cross section, the projection will be dependent on differing element compositions and densities (Mees et al., 2003). Resolution is highly dependent on specimen size. The resulting image can show the differing densities or compositions in the analysed specimen if there is sufficient difference between the materials being analysed. The cross sections are then combined into a 3D model to represent the whole scanned specimen. This represents a non-destructive way to view valuable specimens without risk of damaging them. This technique within geoscience is mostly used in studying fluid flow and rock porosity (Ketcham & Carlson, 2001).

RadEye B20 is an instrument that measures α, β, γ and x-ray radiation, and uses a compact Geiger-Muller tube (otherwise known as a pancake tube) to detect low to medium radiation

(Geiger & Müller, 1928). The Geiger-Muller tube works by detecting ionising radiation that strikes within the tube. The tube itself is filled with a low-pressure inert gas, when ionising radiation enters the tube it creates ion pairs. The now positively charged ions move towards the negatively charged outer wall and the free electrons from the ion pair moves towards a positively charged inner rod. This reaction then produces a charge that is detectable as a count in the circuit (Radiation Dosimetry, 2019). This instrument is rated for 17-1300 keV of gamma dose measurements (if a proper shield is used for the higher doses (Thermoscientific, 2017)).

2 Materials and methods

2.1 Materials

2.1.1 Origin

The material used in this study comes from the old “Tuftestolen” mine in Ulefoss Telemark. It is from two mineralized zones located at 504-505 m W and 510-512 m E (Figure 2-1), measured from a mark created during the mine’s operation at the entrance of the mine.

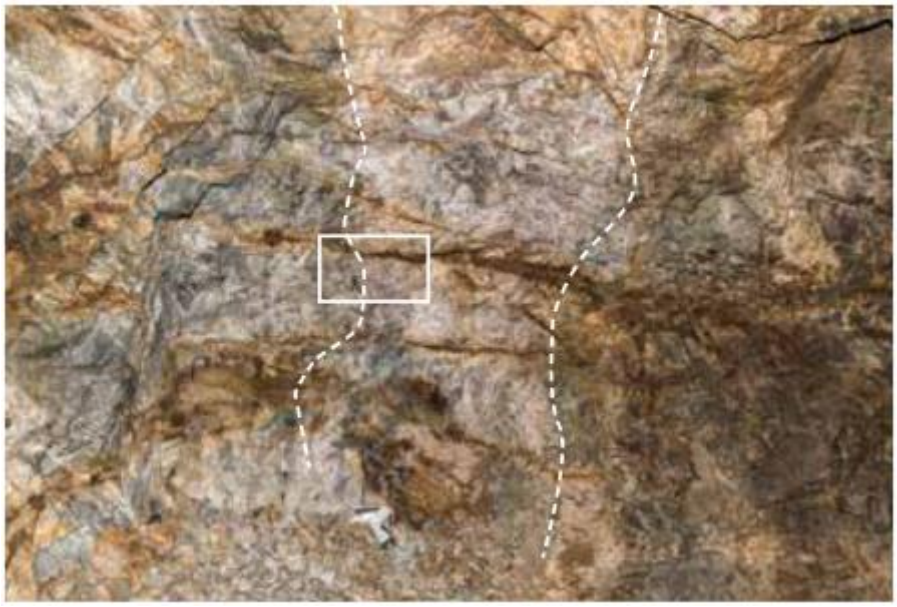

Figure 2-1 Shows the 510-512 m E REE mineralized zone in between the dashed lines, Handheld XRF for scale. (Dahlgren, 2019)

The material was blown out and collected by Sven Dahlgren before it was transported to NTNU. The criteria for sampling were based on visual observation and only the apparent REE mineralized samples were collected. In total there were about 300 kg material in varying sizes. The material was stored in several unsorted plastic boxes, dirt covered most of the material to varying degrees. The sorting started after some material had already been procured and used in a lab scale flotation experiment and was not included in the sorting.

2.1.2 Sorting

Before sorting the material, it was cleaned by running a hose in the specimen box and letting the water and sediments drain out. The specimens were then sorted twice, firstly based on radioactive measurements and second on visual characteristics. Measuring the apparent radioactive dosage for the first sorting was done with a Rad-eye B20. The measurement was taken by applying the scanner as close as possible to a roughly flat area on the specimen, taking care to make sure that no part of the specimen touched the inside of the detector. The

instrument was held in a stable position against the specimen until an apparent stable reading was reached, the time to reach a stable reading varied between each specimen. The material was placed in three categories based on measured radioactivity, first under 0.3 μSv/h, next between 0.3-0.67 μSv/h and last over 0.67 μSv/h. These classifications represent a low, medium, and high amount of radiation relative to the test material. The categories were created based on one category being the background radiation, the highest category was anything over the value the measuring instrument reacted to. The specimens were then sorted into the appropriate container with the highest group being placed in a steel barrel as a safety precaution. After every specimen had been sorted, four representatives were taken out of each category for further testing.

For the second sorting every specimen was sorted again, this time based on colour and texture with categories being made as they appeared during sorting. The category list is shown in Table 2-1

Table 2-1 Shows the final categories from the sorting of the hand specimens based on texture

Nr.	*Description*
1	Mainly white matrix (+ yellow-ish weathering) with some small red REE mineralisation
2	White matrix with larger amounts of visible pyrite grains
3	White matrix with light red small to medium REE mineralisation clasts
4	White matrix with dark red medium REE mineralisation clasts
5	White matrix with dark grey to black mineralisation in cracks
6	White matrix with high amounts of small red REE mineralisation grains

2.1.3 Specimen overview

A table was created to keep track of the various tests that were performed on the specimens, the table was amended every time a new test was done on differing specimens. The finished table is shown in Table 2-2

*Table 2-2 Shows the dictionary for what the 12 differing specimens were used for and for convenience it has been filled with the results obtained in the Results chapter. Green represents that the method was used for that specimen, red indicates that the specimen was not used for that method, yellow are non-applicable for the drill cores. Crossed out test indicates technical problems. *Both elements were scanned.*

Nr.	Specimen	Thin-section	XRD	XRF	ICP-MS	SEM	CL	Drill core	Detail
1	FenREE_GGH_2810_<0,3_1					Batch 2			
2	FenREE_GGH_2810_<0,3_2					Batch 2			
3	FenREE_GGH_2810_<0,3_3					Batch 2			
4	FenREE_GGH_2810_<0,3_4					Batch 2			~~U~~
5	FenREE_GGH_2810_0,3-0,67_1					Batch 2			~~Th~~
6	FenREE_GGH_2810_0,3-0,67_2					Batch 1			
7	FenREE_GGH_2810_0,3-0,67_3					Batch 1			
8	FenREE_GGH_2810_0,3-0,67_4					Batch 1			
9	FenREE_GGH_2810_>0,67_1					Batch 1			U
10	FenREE_GGH_2810_>0,67_2					Batch 1			*Th/U
11	FenREE_GGH_2810_>0,67_3					Batch 1			Th
12	FenREE_GGH_2810_>0,67_4					Batch 1			
12a		Kjerne_V				Batch 2			~~Th~~
12b		Kjerne_H				Batch 2			

= Method used = Method not used = N/a for drill cores

The specimens were named based on the following criteria. First “FenREE” denoting general area and identifier for the specimen, next is GGH was “gamle gruva” + hand specimen, it denotes Tuftestolen and the general size of the specimen. 2810 was the date the specimens were chosen and finally the last part denotes what category (first) and internal classification (second) for each specimen (Table 2-3). The table also includes other aliases used when referring to specific specimens. The retroactively filled specimen overview (Table 2-2) has also been made into a flowchart (Figure 2-2) showing every method used with what specimens.

Table 2-3 Shows an overview of different aliases used to denote the different specimens. FenREE is where the specimen came from, GGH is “gamle gruva” also known as Tuftestollen and hand specimen. 2810 refers to day and month of sorting. Lastly the first number references category and second number within that category.

Full name	*Alias 1*	*Alias 2*
FenREE_GGH_2810_<0,3_1	<0,3_1	3_1
FenREE_GGH_2810_<0,3_2	<0,3_2	3_2
FenREE_GGH_2810_<0,3_3	<0,3_3	3_3
FenREE_GGH_2810_<0,3_4	<0,3_4	3_4
FenREE_GGH_2810_0,3-0,67_1	0,3-0,67_1	3-6_1
FenREE_GGH_2810_0,3-0,67_2	0,3-0,67_2	3-6_2
FenREE_GGH_2810_0,3-0,67_3	0,3-0,67_3	3-6_3
FenREE_GGH_2810_0,3-0,67_4	0,3-0,67_4	3-6_4
FenREE_GGH_2810_>0,67_1	>0,67_1	6_1
FenREE_GGH_2810_>0,67_2	>0,67_2	6_2
FenREE_GGH_2810_>0,67_3	>0,67_3	6_3
FenREE_GGH_2810_>0,67_4	>0,67_4	6_4

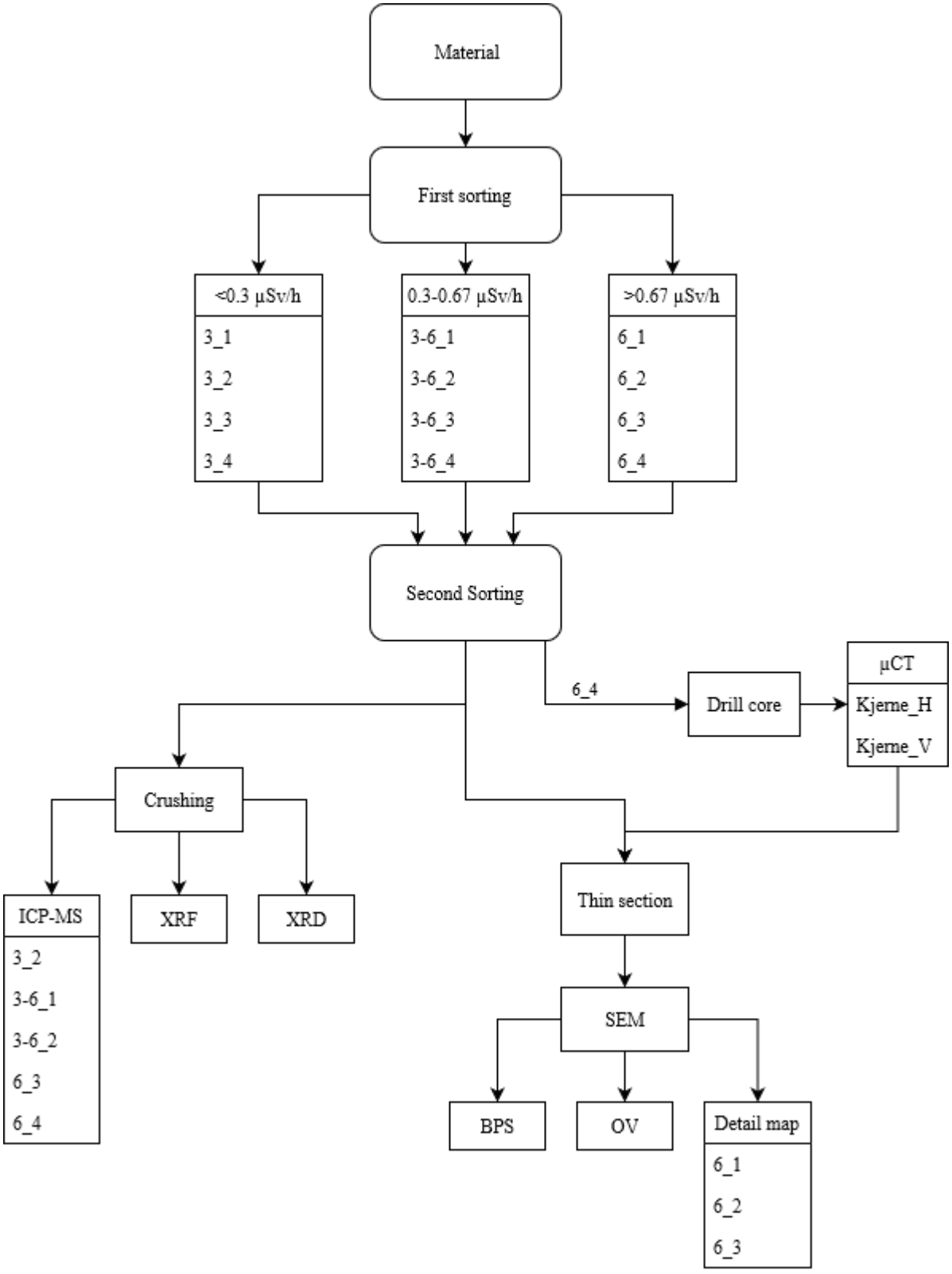

Figure 2-2 Flowchart showing a representation of every test performed and what specimens were used. Every specimen was tested in each method unless specified otherwise. The first sorting was based on radioactivity and the second was colour and texture.

2.2 Methods

Firstly, a range of laboratory methods were applied with the aim of identifying thorium and uranium within the 12 specimens. Secondary was to determine the methods effectiveness at identifying these elements. The third lesser objective was the identification of what minerals the LREE made up. Not every method was used on every specimen as seen in Table 2-2.

2.2.1 XRD & XRF

First approximately 30-40 g for each specimen was weighted and placed in a manually operated "fly press rock crusher" until it attained a size of around 0.5 cm. The crushed material was then placed in the chamber of a Retsch RS 200 disk mill until it produced an even material with grain sizes under 40 µm. The crushed material was then stored in a marked paper specimen bag for later use.

The material used in XRD needs to be around 10 µm and have a uniformly rounded grain shape, this was achieved with a McCRONE micronizing-mill. Approximately 1-2 g material was placed in a container with jade grinding media together with alcohol as a wetting agent and put in the mill. The resulting material was then removed from the container using more alcohol. The material was dried overnight in a Memmert drying oven until the specimens were entirely dry. The material was then collected and placed in a plastic disk and given a flat and even surface before it was placed in the D8 Advanced XRD for analysis.

When preparing materials for XRF two methods were used, one for main elements and one for trace elements. "Loss on ignition (LOI)" was also calculated together with the main element analysis. This was done by measuring a platinum crucible and measuring out 2.4 g material into that crucible. The crucible was then heated at 1000°C for 1 hour in a muffle furnace, immediately after the crucible cooled down it was weighted and LOI was calculated based on the weight difference. The material was then crushed by hand in a pestle back into a powder. Afterwards 0.5 g material was weighed into a platinum crucible together with 5.0 g Litiumtetraborat/Litiummetaborat (66/34). 120 µl Litiumiodid was added to the specimen before it was placed into a Claisse Teox Advanced oven for approximately 25 minutes. The melted specimen was then poured into a mould that made a glass pill that was analysed in the Panalytical Zetium XRF. The trace elements were analysed by taking 9.6 g material together with 2.4 g licowax C micro-powder into a small container. A small plastic marble was placed into the container and then placed into a Fine Vortex FINEPCR for Two minutes. The plastic marble was then removed, and the material was placed in a Horzog pill-press that compressed

the specimen under 200 kbar pressure. The resulting pill was placed into the Panalytical Zetium XRF container without touching the scanning surface.

1.1.1. Optical microscopy

Optical microscopy is used to get the general picture of the thin-sections, using a "Nikon eclipse ci pol" microscope together with the magnifications 5 x, 20 x, 50 x. To capture specific areas of interest in the thin-sections at the best resolution a "Nikon eclipse e600" together with the Spot 5.3 capture program was used. A magnification range of 5 x, 10 x, 20 x, 50 x was available to capture the features of the specimen. To get a complete image of the whole thin-section a Olympus BX51 microscope was used together with a 5x magnification and the Stream motion software. Using the whole thin-section image some assumptions can be made, these will then lay the foundations for further work in the SEM.

2.2.2 ICP-MS

For each specimen 1.00 g of the same material as used in XRD/XRF was measured and added together with 1.35 g borate and 100 µl Litiumiodid into a crucible. A separate control with no specimen material was also created. Then approximately 80 ml of 10 % hydrochloric acid was prepared in an open container with a magnetic stir bar. The crucibles and the open containers were placed in a Claisse Teox Advanced oven where the crucibles were heated and poured into the stirring containers. The material is stirred until it was completely dissolved and allowed to cool. Afterwards it was measured and diluted to 100 ml. The solution was shaken, and 0.1 ml of the solution was diluted with 9.9 ml 1 % hydrochloric acid. The now strongly diluted solution was then analysed in a Perkin Elemr Elan DRC II. First the machine was calibrated to the series of elements that would be searched for by using a set of standard solutions. The calibrated graph from these standard solutions gave measurement of each analysed element. Two rounds were necessary each repeating the calibration step with differing standard solutions, one for REE and thorium and a second one for uranium

2.2.3 µCT

A large specimen rock was chosen to have a drill core with 28 mm diameter taken out from it. The core was extracted with a fixed boring rig. The core was then analysed with a Nikon XT H 225 Xray Computed Tomography CT using a helical continuous scan type, with 180 kV and a current of 78 µA. This gave a resolution down to about 9 µm. The 3D core was then studied to correlate indicator minerals and areas that could be used to correlate the model to the physical core. The densities of the minerals found in the area (Table 2-4) were used to

adjust the model to find two suitable slices to turn into thin sections. The core was then cut as accurately as possible with the tools available, using a fixed diamond blade circular saw. For every cut approximately 0.5 mm was removed by the saw. First a lengthwise cut was made and then the small side was used for a thin-section. The remaining half was then cut perpendicularly to the long side to create the second thin-section.

Results from the SEM were the basis for an element map made from the µCT data. This was done by cross-referencing the AM image to isolate different minerals based on their densities (Table 2-4) to create an approximation of where Thorium, uranium and REE minerals were.

Table 2-4 Shows calculated densities (Barthelmy, 1997) for reported minerals from the Fen complex. The REE minerals have differing densities depending on what REE is included.

Mineral	*Density*	*Mineral*	*Density*
Calcite	2,71	Parisite	4,34 – 4,49
Dolomite	2,82	Bastnäsite	4,72 – 5,07
Ankerite	3,15	Synchisite	3,54 – 4,21
Quartz	2,65	Monazite	5,04 – 5,34
Pyrrhotite	3,95	Thorite	6,75
Pyrite	5,01	Uraninite	10,97
Barite	4,48	Coffinite	5,44

2.2.4 SEM-base automated mineralogy (AM)

The SEM used for this study was a Zeiss Sigma 300 VP, equipped with a Sigman 500 chamber together with Bruker quantax xflash 6 EDS detector (60 mm^2 x 2). The main Tools utilised are backscatter electrons (BSE) in conjunction with automated mineralogy (AM) The first step is to calibrate the SEM to get the highest possible resolution and then using the previous observations in optical microscope as a general guide to find thorium and uranium minerals. To work with the collected data the program mineralogic with software version 1.6 SP3 was used and later upgraded to 1.8. “The mining plugin” was the basis for the classification parameters.

A mineral list for the FDC has previously been made in collaboration with Stefanie Lode, when adding new minerals their information is found from trusted databases (Barthelmy, 1997; Deer et al., 1996) and some leniency on the formulas are added while avoiding conflicting classifications. The results are then examined to check if the mineral classifications are seemingly accurate and match the backscatter image. To further increase the accuracy of the list the unclassified category is examined for any large gaps in the mineral list. Then some mineral classifications are adjusted and some mineral mixes are created to

better represent the acquired data based on these interactions. The mineral classification mixes were placed at the bottom of the list so that they only apply after all the known minerals have already been classified. Care is also being taken to not overfit the list and thereby creating an inaccurate result.

An overview map (OV) is created of the complete thin-sections, with the parameters as follows. Aperture at 120, counts per second at 275, the beam was sat at 20 W in high vacuum for the first round (specimen 3-6_2 – 6_4). The magnification was 178 x, with a 20 µm step-size, a working distance at 8.5 mm and a dwell time of 0.008 s. A required 1500 counts to register as a classification was set. There is also plotted in a field overlap of 5 %. For the second round (3_1 – 3-6_1 + the core thin-sections) the beam was reduced to 15 W while the other parameters remained the same.

To get the highest amount of detail on the Thorium, uranium containing minerals a “Bright phase search” (BPS) is conducted. This is done by adjusting the SEM parameters so that only the heaviest visible minerals are reported. This allows for a higher of resolution while still scanning the whole thin section in a reasonable timeframe. The SEM parameters remained the same as the OV for both rounds except the required counts was increased to 2000, the step-size was decreased to 3.5 µm and the magnification was set to 255 x.

For the detail map several small areas of interest found in the BPS were chosen to make a small map with a step-size of 0,5 µm, a dwell time of 0.009 s and magnification at 567 x.

The resulting AM data is presented in “area%” and “weight%” based on the analysed surface that is created based on the clasification list. This data is supported by an identical BSE map. By using outputed data, namely: the bulk mineralogy, element distribution and mineral associations for each specimen an assessment of the placement of thorium and uranium can be made.

2.2.4.1 Element distribution

Element distribution is created by adding up the total weight percentage of all pixels containing the selected element and then adding them together to find a total element percentage distribution. This is then put in a 100 % stacked column chart with the largest fractions at the top. This was done with the companion program mineralogic reporter.

To show how much of each thin-section thorium and uranium cover, an area table is created. Each pixel that registers the selected element is counted and the total is then multiplied by the

step-size to get an estimation of area covered. That area is then divided by the whole thin-section area (from the OV map), to show approximately how much of the thin-section is covered by the selected element.

2.2.4.2 Element grain size distribution

To show the grain size distribution of the selected mineral, a count is done based on the ferret max diameter from the mineralogic grain data. By counting every grain within several specified size ranges, a cumulative curve can be made to visualize the grain size distribution.

To view the element distribution for a specified element at differing ranges, a count is made. It counts every grain that has a trace of the specified element for each size range and represents this data as a pie chart. A distribution chart is also made to show the spread between the differing size ranges in each specimen.

3 Results

To find what main minerals the thorium, uranium, LREEs form and which analytical methods were effective to determine these results, a multitude of methods were applied. The 12 specimens from the Fen carbonatite complex were tested to determine placement, size, and relation to REEs of thorium and uranium. Note the tables and graphs uses the Norwegian "comma" to mark decimals.

3.1 Sorting

Sorting the material was done in two rounds. For both sorting rounds, there were a total of 284 hand specimens of varying sizes. The first sorting was based on radioactivity and resulted in 12 % being sorted in the >0.67 µSv/h category. 64 % and 24 % for the 0.3-0.67 µSv/h and <0.3 µSv/h category respectively (Figure 3-1). The 12 specimens chosen are pictured in Figure 3-2 and Figure 3-3.

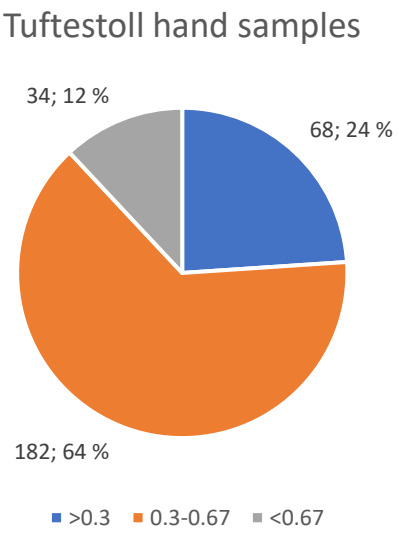

Figure 3-1 Shows the distribution of specimens based on measured radioactivity. First shown are counts and then the percentage of the whole. Blue represents the low category, orange the medium category, and grey the high category.

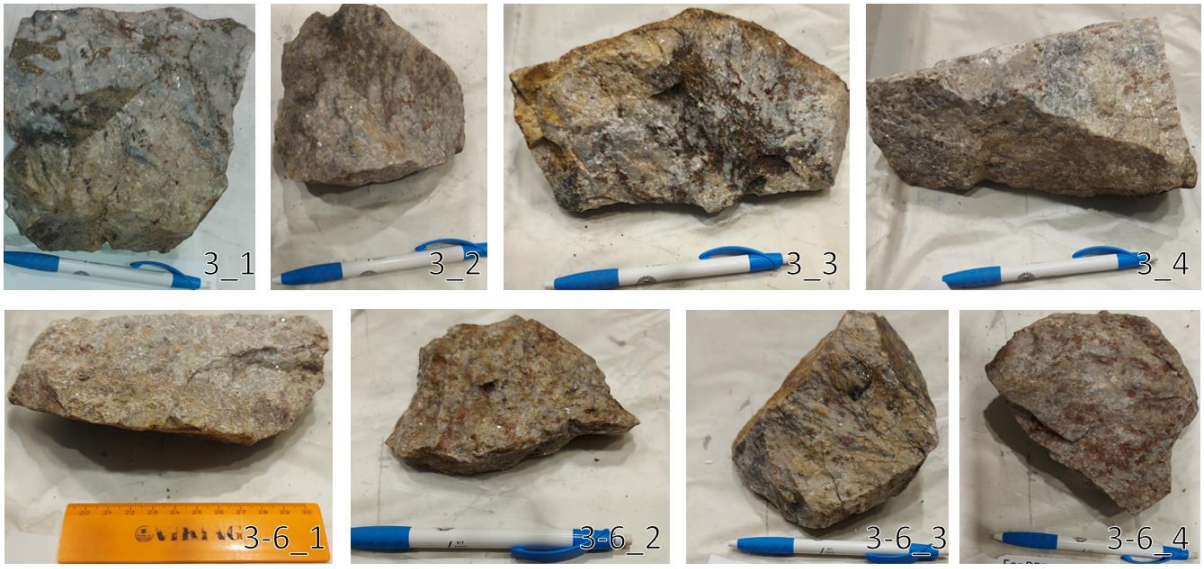

Figure 3-2 Shows the four specimens that were picked for the low radiation group, and the four specimens that were picked for the medium radiation group

Figure 3-3 Shows the four higher radioactive specimens and three different images of specimen 6_4 to illustrate the slight difference in measured µSv/h depending on where the detector is placed on the specimen.

The second sorting was based on the criteria set in Table 2-1 and each specimen was marked based on the previous category in the first sorting (Figure 3-4). The 12 specimens picked from the first sorting are shown in Figure 3-5, and the yellow numbers indicate what specimen was placed where. A representative specimen for each of the six categories is shown in Figure 3-6.

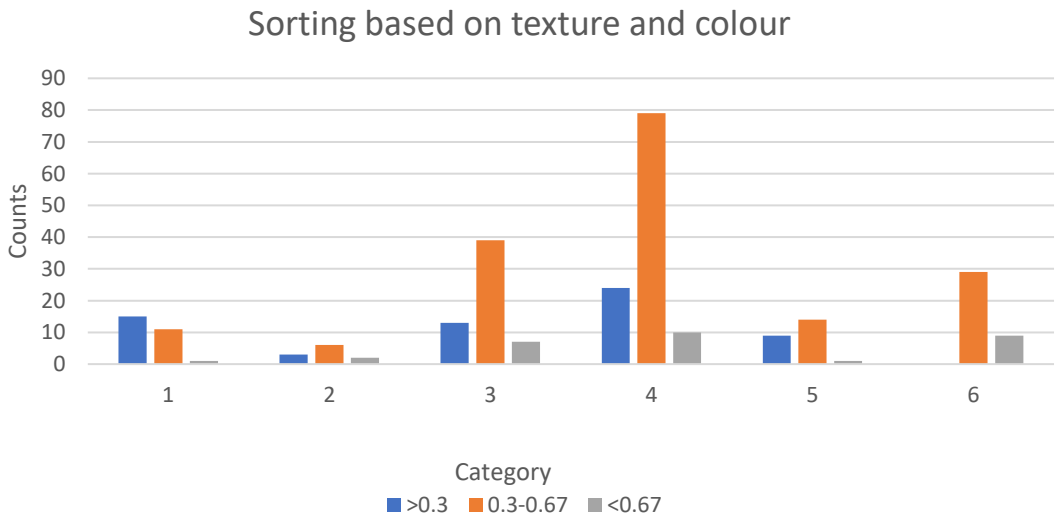

Figure 3-4 Shows sorting based on texture and from which radioactivity group the specimens came from. Description of the categories can be found in Table 2-1

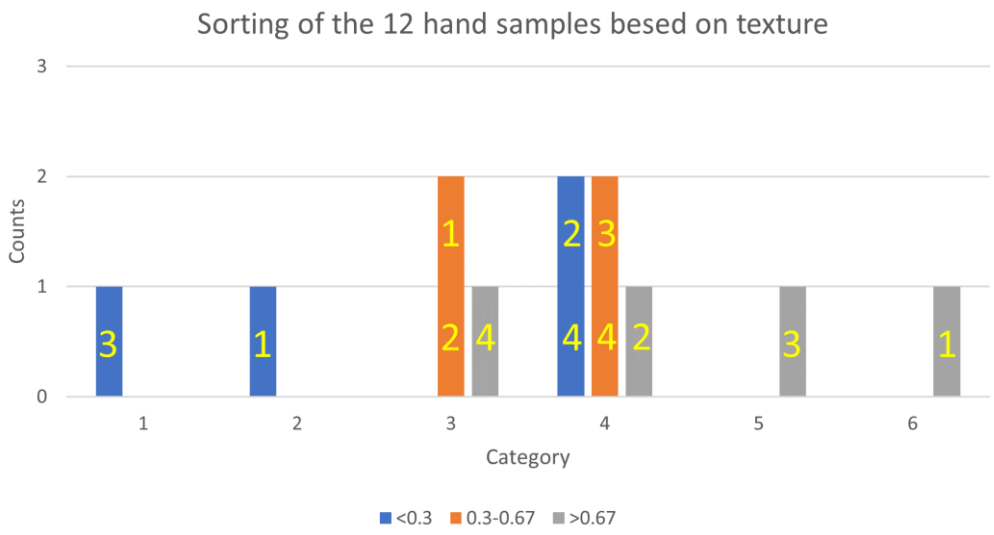

Figure 3-5 Shows where the 12 specimens chosen during the first sorting ended up in the second sorting. The yellow numbers denote what specimen within each category was sorted where.

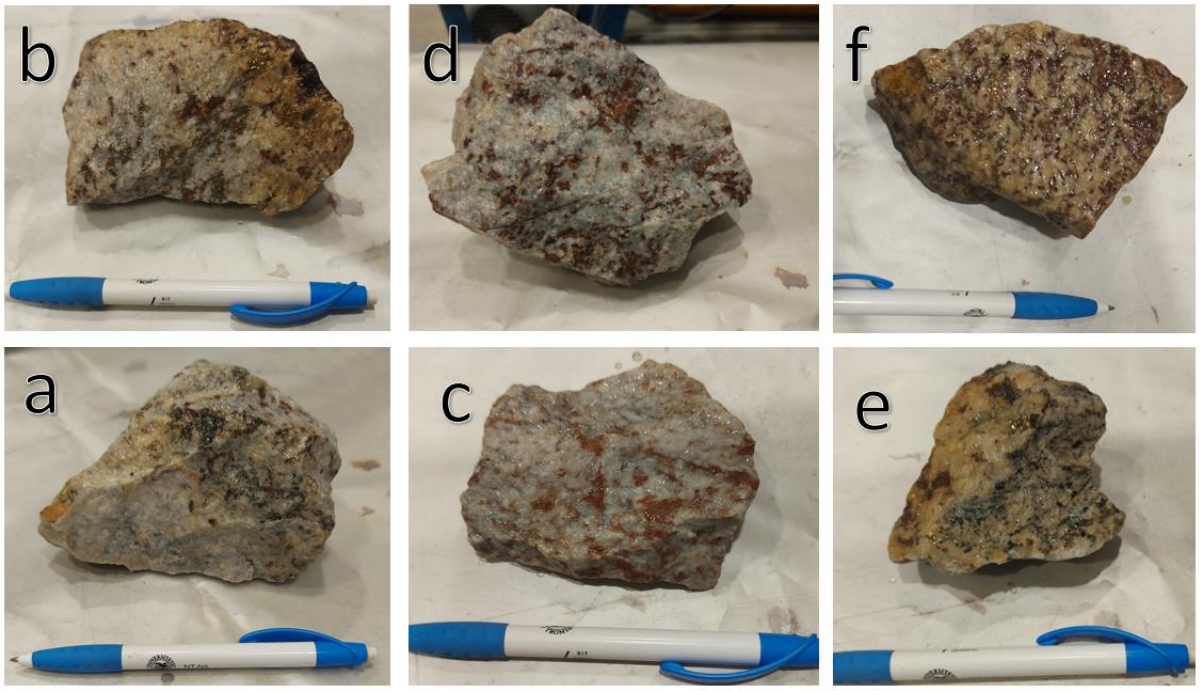

Figure 3-6 Shows representatives of the 6 texture categories from the second sorting. The specimens were wetted before the pictures were taken. The letters represent Table 2-1 in alphabetical order (a = 1, b = 2, c= 3, d = 4, e = 5, f = 6). (The marker in d is removed for space, but the mark on the table is visible in b and a.)

3.2 XRD & XRF

After crushing each specimen, a measurement was taken on the paper container with the Radeye B20. Table 3-1 shows that some of the crushed specimens measured lower than their hand specimen counterparts. Of these 6_1 and 6_4 showed the most drastic difference.

Table 3-1 Shows the difference in measurement compared to the previous classification class after grinding each specimen. Reading taken on specimen paper bag

Specimen	*Measurement*
<0,3_1	0
<0,3_2	0
<0,3_3	0
<0,3_4	+0,02
0,3-0,67_1	0
0,3-0,67_2	0
0,3-0,67_3	-0,05
0,3-0,67_4	-0,03
>0,67_1	-0,30
>0,67_2	0
>0,67_3	-0,01
>0,67_4	-0,32

The XRD is represented as bulk mineral and data picks up little to no thorium in most of the specimens (Table 3-2). Complete XRD spectra can be found in Appendix I.

Table 3-2 Bulk data for each specimen from the XRD. All values are percentages. Complete spectra in Appendix I.

Specimen	*3_1*	*3_2*	*3_3*	*3_4*	*3-6_1*	*3-6_2*	*3-6_3*	*3-6_4*	*6_1*	*6_2*	*6_3*	*6_4*
Calcite	1,78	47,88	1,23	30,44	43,47	6,45	18,55	53,78	14,72	7,05	28,87	4,08
Dolomite	68,6	30,23	69,57	42,11	25,50	70,94	68,89	25,91	75,90	86,64	61,81	81,14
Ankerite	22,98	8,43	23,92	11,66								
Bastnäsite	0,17	0,35	0,50	0,66	3,92	1,44		2,27	1,73	2,39	0,48	0,40
Parisite	0,95	1,71	0,49	2,74	4,45	0,47	1,15	1,76	1,96	1,31	1,09	0,51
Monazite	0,21	0,65	0,08	0,66	1,53			0,21	0,61	1,12	1,27	0,69
Allanite					3,61							
Quartz	0,66	9,14	2,52	10,85	2,46	16,79	10,34	11,81	2,70	0,75	1,19	3,88
Pyrite	4,64	0,21	0,24	0,06	0,13	0,07					0,60	4,78
Siderite		0,41	0,85		4,16	1,00		0,97	0,51	0,55	2,88	0,58
Talc		0,25					1,06					
Barite		0,74	0,60	0,20	10,79	2,83		3,28	1,88		1,65	3,94
Thorite										0,18	0,17	
Magnetite				0,64								

The results from the XRF are shown in Table 3-3. It was observed high levels of thorium and uranium in every specimen compared to the continental crust. There was an indicated increase in thorium related to placement in the radioactive sorting. The low category generally have lower thorium than the higher category. The uranium has a slight increase, but has a noticeably lower difference between the categories. Only the REEs lanthanum, cerium, neodymium, samarium, ytterbium was measured using XRD. The results show 3-6_1 having the highest REE in every category. Outside of outliers there seems to be a small uptick in REE toward the high radioactive category.

Table 3-3 Showing REE, thorium and uranium trace element results from the XRF. The full table can be found in the Appendix I

	La	*Ce*	*Nd*	*Sm*	*Th*	*U*
Specimen	(ppm)	(ppm)	(ppm)	(ppm)	(ppm)	(ppm)
3_1	6045,3	8525,7	2354,8	132,7	135,3	8,9
3_2	8710,5	12426,2	3561,7	215,2	175,3	11,7
3_3	4061	5886,6	1700,3	98,6	88,9	11,3
3_4	16066,2	19656	4830,8	280,1	234	12
3-6_1	43122,1	44127,2	10878,4	535,3	375,2	15,2
3-6_2	8624,3	11794,6	3729,5	226,9	216,7	12
3-6_3	5635,7	7762,3	2143,5	136	91,9	9,2
3-6_4	13546,5	16649	4183,2	187,8	127,2	10,9
6_1	18915,4	21768,5	5358,5	322,1	238,4	16
6_2	23161,3	27750,3	6988,3	500,8	894	18,1
6_3	13107,2	16132,3	3852,4	260,4	513,6	14,9
6_4	8559,9	11771,6	3664,6	198,6	202,8	11,7

1.1. Optical microscopy

Thorite and grains containing urainium have been identified using an optical microscope when larger grains were present in the specimen (Figure 3-7). Thorite is easy to spot because of the grey and red sputtered look. Small strands can be seen outside the main mineral grains. The coffinite has a distinct brown halo surrounding the grains, even on the smaller grains visible around the larger pyrite grain. Complete thin-sections in Appendix II.

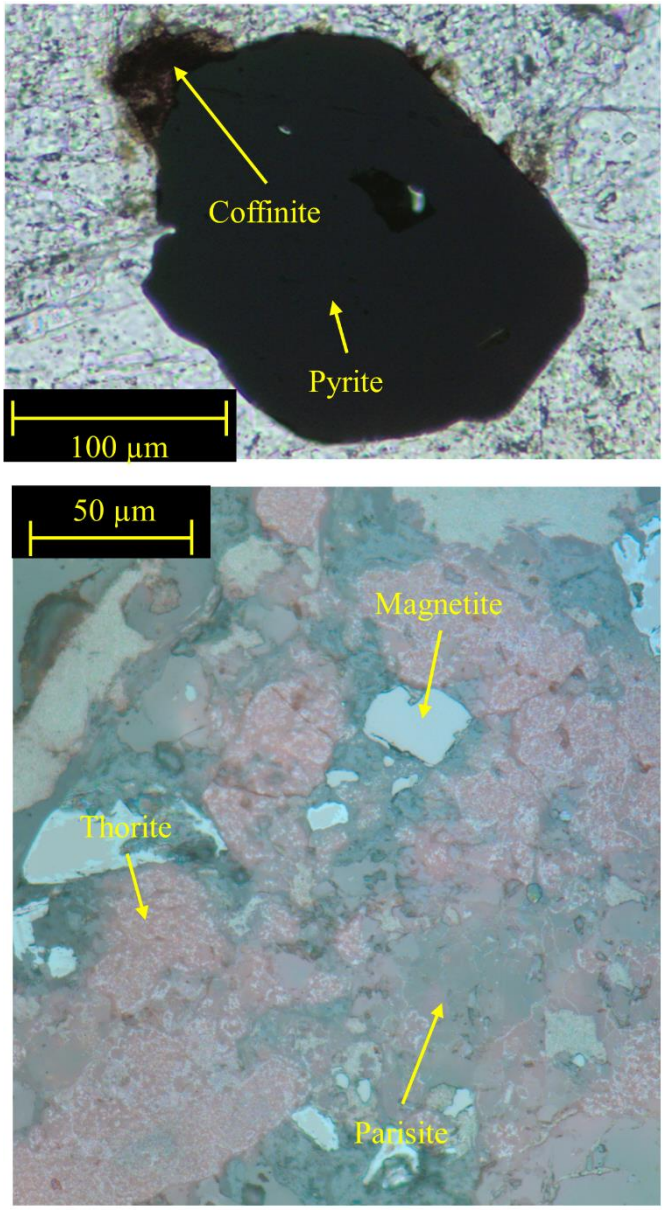

Figure 3-7 Top: view of a pyrite grain with several coffinite grains around it (top left) in specimen 6_1 in transmitted light and PPL at 20x magnification. Note the dark halo around the pyrite grain. Bottom: large thorite grain surrounded by various minerals from specimen 6_2, in reflected light PPL at 50x magnification. Note grey and red sputtered thorite with visible strands out into the surrounding mineral.

3.3 ICP-MS

Figure 3-8 shows chondrite-normalized data (Anders & Ebihara, 1982) for the five tested specimens. It shows an enrichment of REE with a considerable higher enrichment towards the LREE. The measured specimens indicate a general correlation towards the higher end data from Tuftestollen mine (Dahlgren, 2019). The top half of the Previous data corresponds to mineralised zones while the bottom half are mineralised adjacent. There is a light enrichment of Gd, Tb, Er that slightly deviate from the Tuftestollen data. Every specimen are within the Bayan obo range. There is a similar enrichment of Gd in the lower Bayan obo data as can be seen in the five specimens. Some of the HREE that are below the detection limit have been set to half the detection limit. Dataset with ppm values for each element can be found in Appendix I.

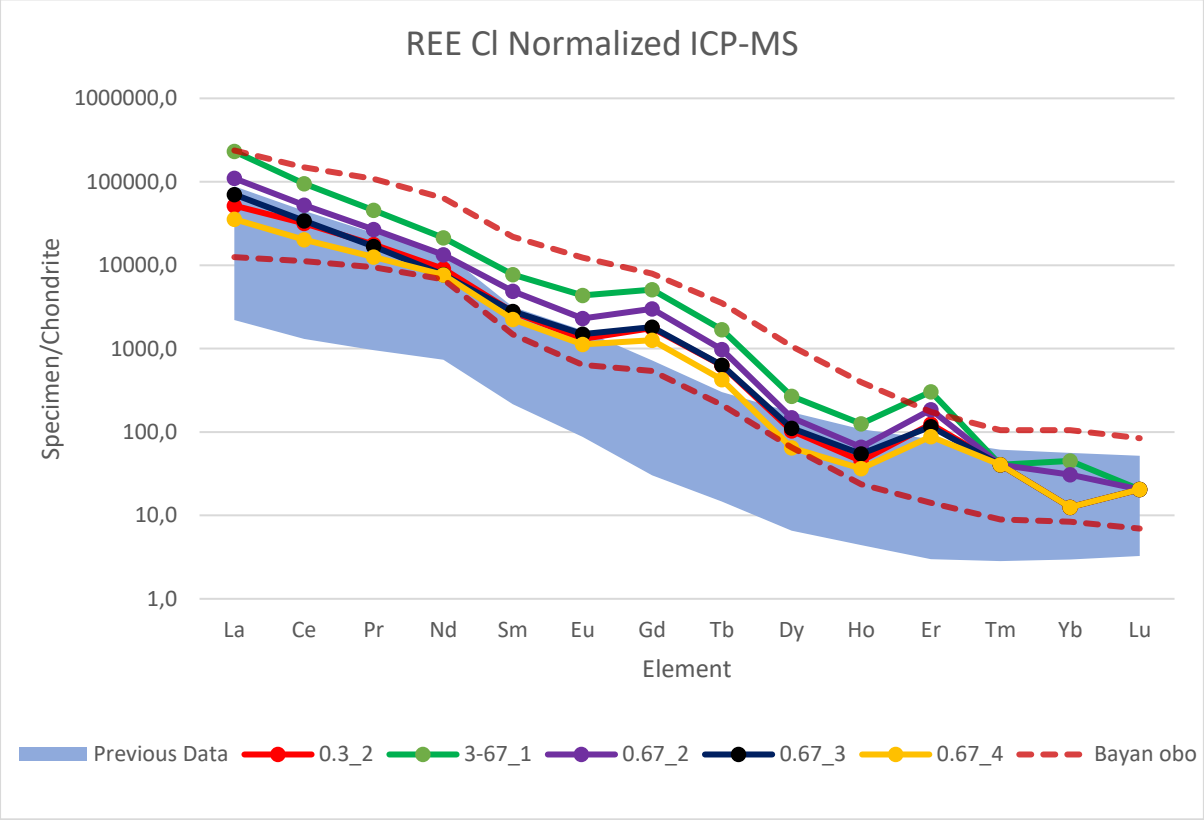

Figure 3-8 Shows normalized (Anders & Ebihara, 1982) ICP-MS results taken from five specimens put up against previous data from both mineralized zones and mineralized adjacent zones from Tuftestolen (Dahlgren, 2019). The dotted line is similar mineralised zones from Bayan obo ((K.-F. Yang et al., 2011). The specimens show a general correlating trend. Elements under the detection limit were included as half the detection limit, relevant for Tm, Yb, Lu. Dataset in Appendix II.

Figure 3-9 shows the correlation between the results from the trace element analysis and ICP-MS. There is a slight variation between the results, but they are internally consistent with each other.

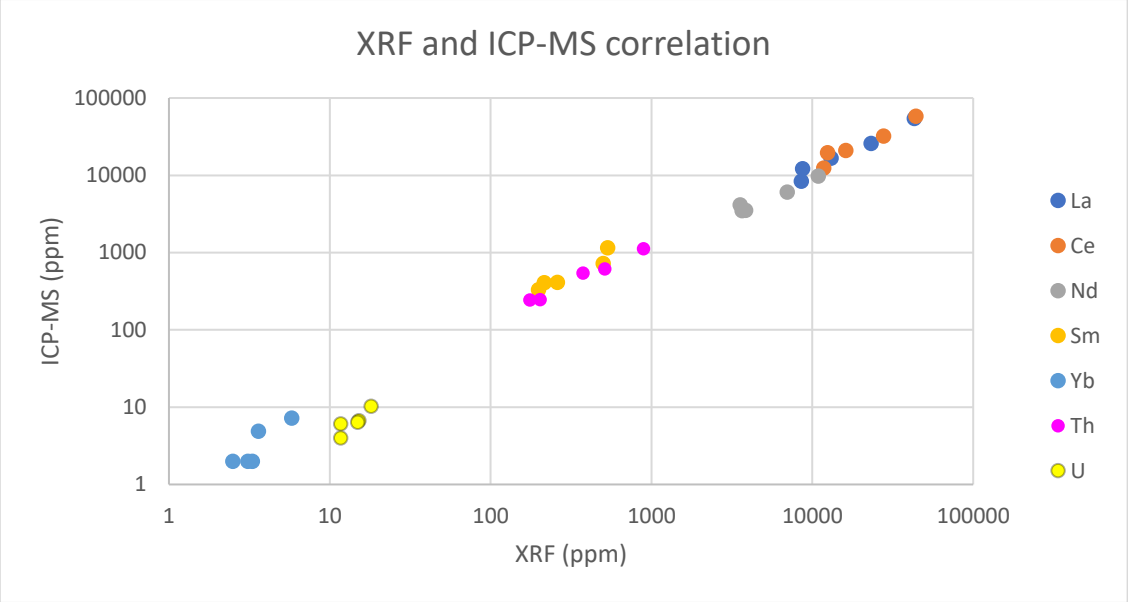

Figure 3-9 Shows the difference between the results obtained from the ICP-MS and XRF. ICP-MS is generally reported higher than XRF in every element except neodymium and uranium. They seem internally consistent.

Figure 3-10 and Figure 3-11 show the relationship between total rare earth elements (TREE), thorium and uranium, respectively. There is a possible low correlation at lower values for both elements. There seems to be no correlation at higher values.

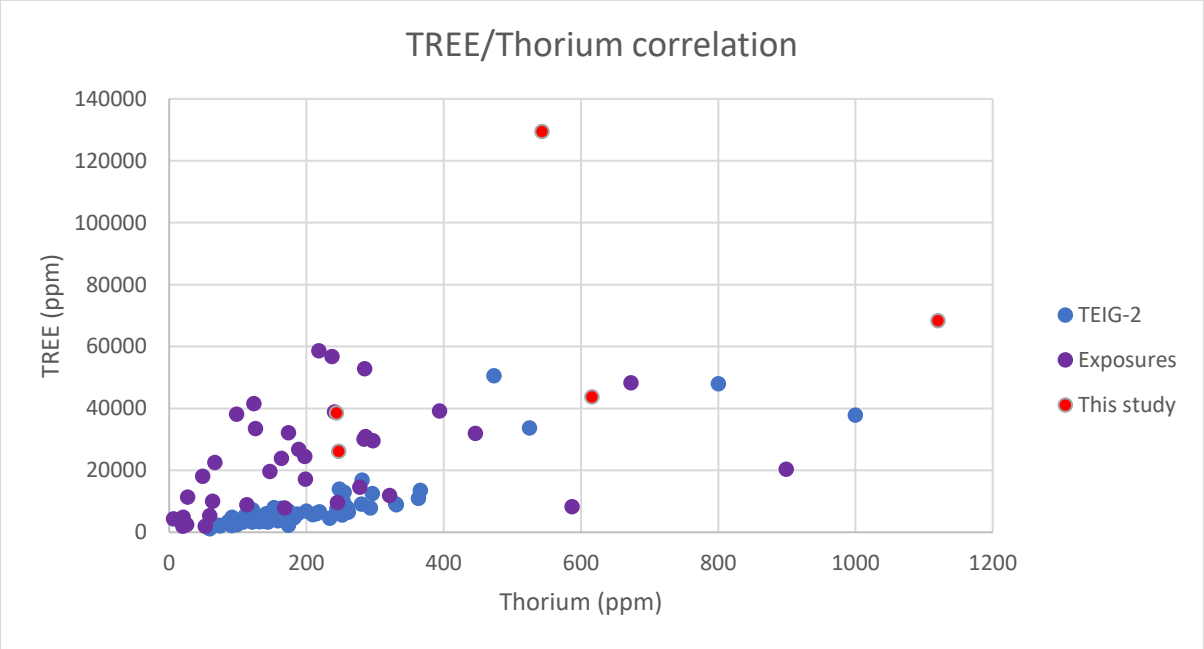

Figure 3-10 Shows total rare earth element (TREE) against thorium based on ICP-MS results. Both TEIG-2 and Exposures come from previous data (Dahlgren, 2019). TEIG-2 is a shallow drill core and Exposures are sampled exposed areas from Tuftestolen.

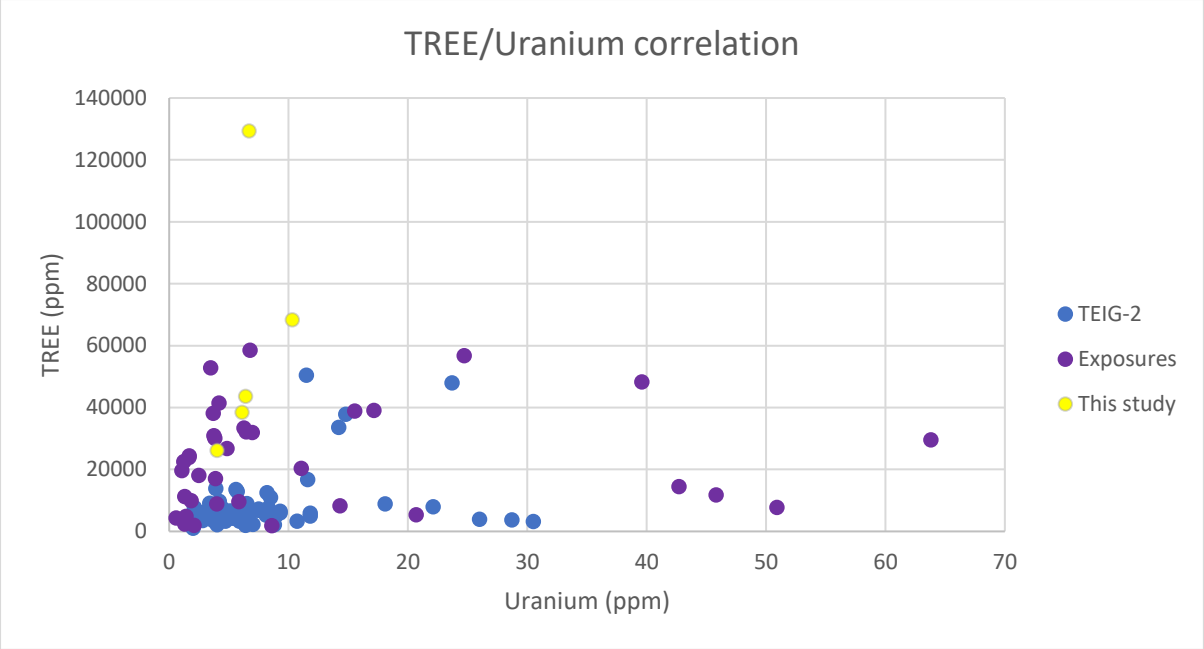

Figure 3-11 Shows the total rare earth element (TREE) against uranium based on ICP-MS results. Both TEIG-2 and Exposures come from previous data (Dahlgren, 2019). TEIG-2 is a shallow drill core, and Exposures are sampled from exposed areas from Tuftestolen.

3.4 µCT

The two thin-sections made from the core (Figure 3-12) were the basis for the four categories that approximately represent the differing mineral groups. Figure 3-13 shows the BSE of the Kjerne_H together with three chosen areas that are compared to the same area in the model (AM of Kjerne_H can be found in Appendix IV).

Figure 3-12 Two pictures of the 28 mm wide core made from specimen 6_4 (Figure 3-3) that was used for µCT. It was drilled down from the eroded side of the specimen.

Figure 3-14 is a full classification map that approximately represents the same area as the thin-section Kjerne_H with the four classifications. Light blue is the low-density minerals, mainly calcium carbonates. Light yellow is the mid-range minerals, including pyrite, barite,

and some REEs. The red ranges from the mid to the heavy minerals consisting mainly of REEs and some barite. There is considerable overlap between these mid-range category minerals (Table 2-4). Forth category is purple which represents the heaviest parts of REEs together with thorium and uranium.

Comparing the three areas in Figure 3-13 and Figure 3-15, show that the resolution in the 3D model is not high enough to capture the minute thorite grains. It also indicates that there are small differences between the model slice and the thin-section.

Figure 3-16 is a picture of the 3D modelled core with an overlay of the purple fraction. It shows clear textural differences between the top and the bottom of the core. Most of the purple fraction gather towards the top middle of the core.

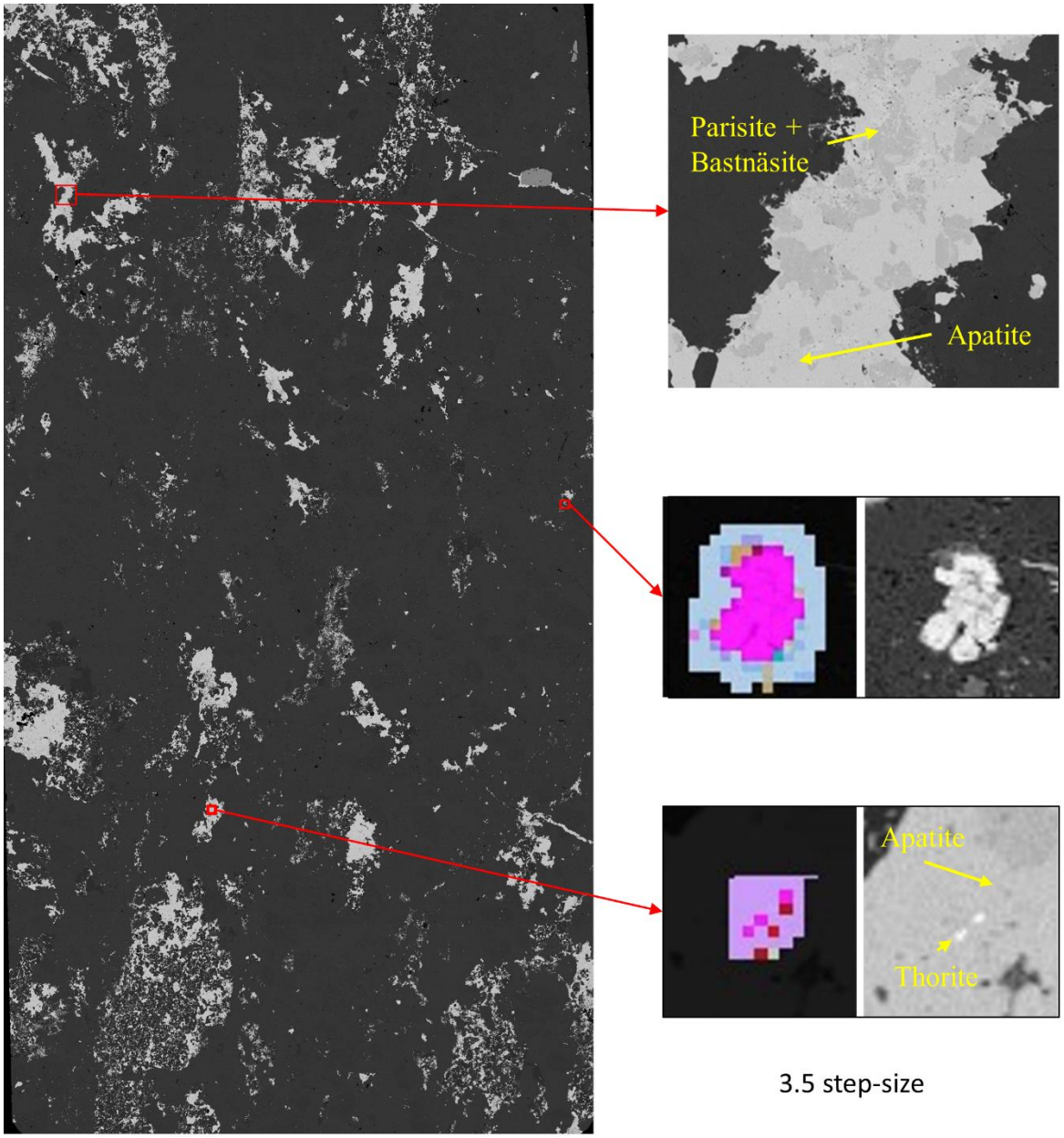

Figure 3-13 Shows the BSE image from the SEM of Kjerne_H. Outlined are three areas of interest, pictures two and three have AM images from the BPS map. no. one shows no signs of Thorite. No. two shows a relatively large thorite grain in both BSE and AM. No. three shows two small thorite grains in BSE.

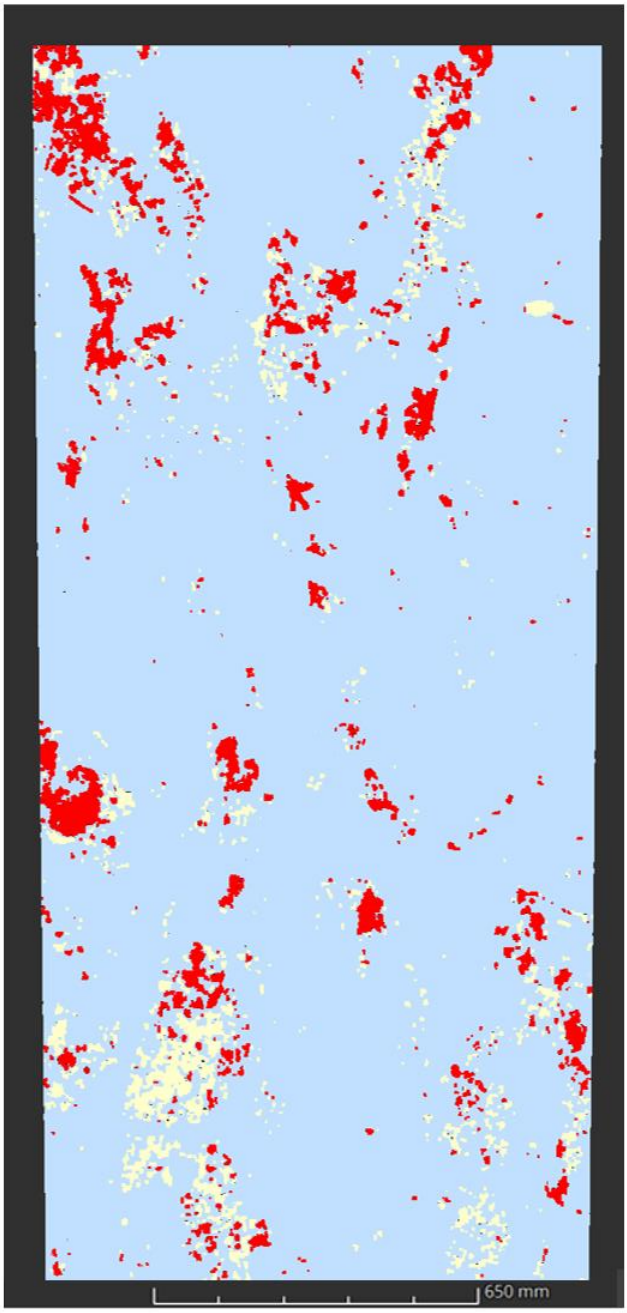

Figure 3-14 Shows a classification map made on approximately the same area as thin section Kjerne_H. Colours are based on density, with light blue being the lightest, light yellow the second lightest, red contains the majority of REE, and purple mainly represents thorium and uranium. (mm in legend refers to µm).

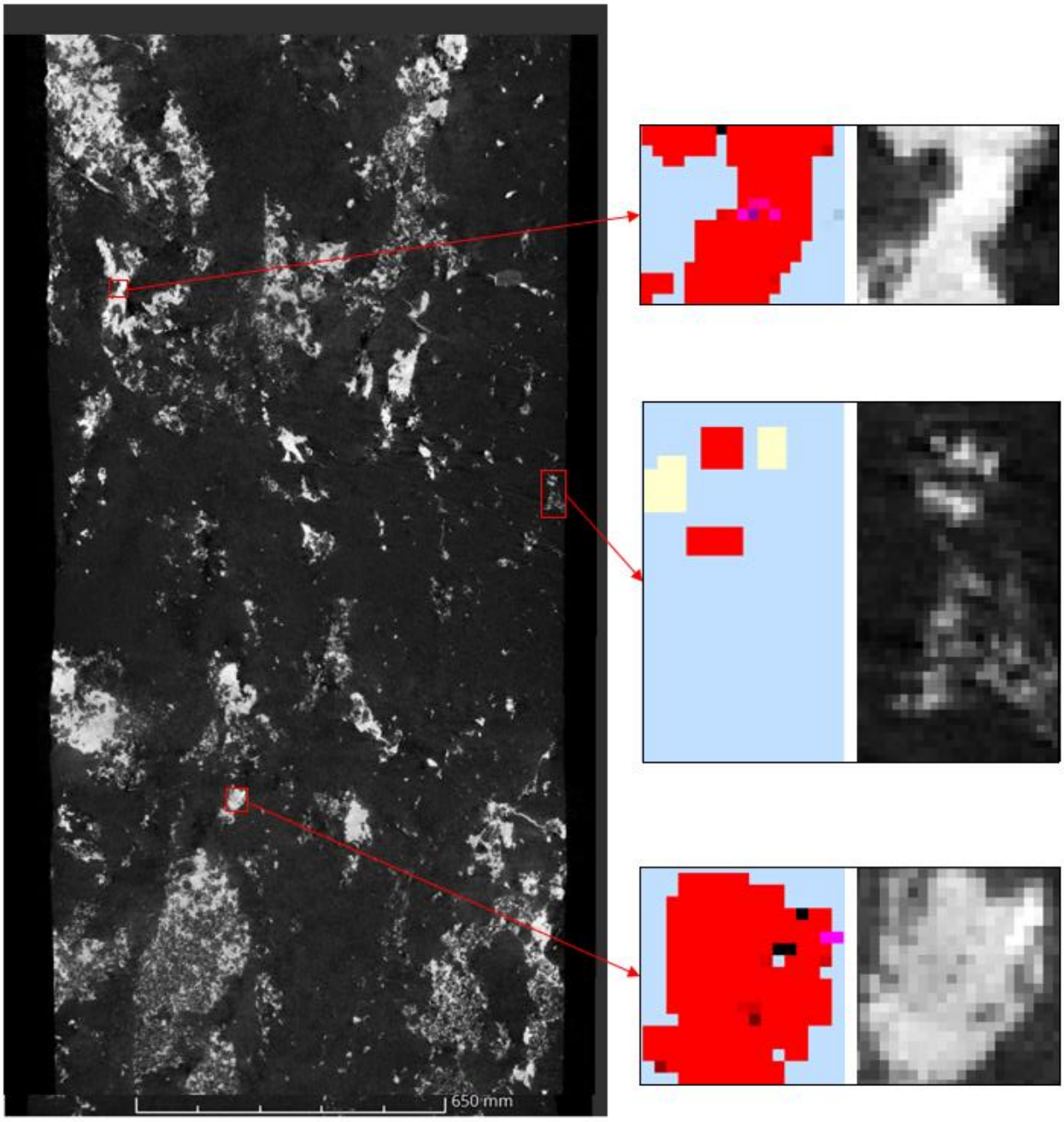

Figure 3-15 Shows a slice from the µCT model that approximates the respective Kjerne_H thin-section. The classification maps shows light blue carbonates, red REE minerals and purple thorite in the same three spots as Figure 3-13. The classification map comes from Figure 3-14. (mm in the legend refers to µm)

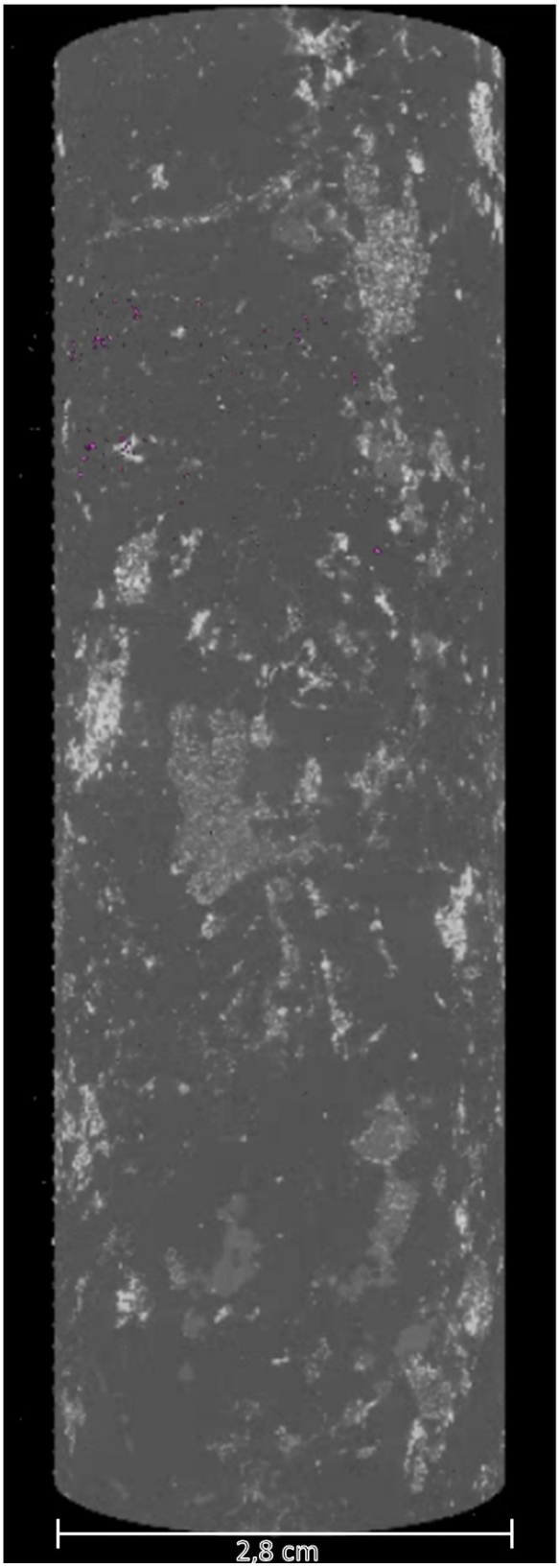

Figure 3-16 Shows the core model produced from the µCT scan with an overlay of the heaviest purple fraction from the entire core. The main concentration is visible in the top middle. The total width of the core is 2.8 cm.

3.5 SEM-base automated mineralogy (AM)

Figure 3-17 corresponds to the minerals found based on the mineral list made in mineralogic, with correct colours.

Figure 3-17 Legend for every classification made with the SEM, Note the multiple thorite and thorite-calcite mixes are combined into one in this legend.

Figure 3-18 Shows uraninite filling in cracks in pyrite (more specifics in 3.5.4 Detail map) and the two common forms of parisite/ bastnäsite intergrowth, and how the OV map classified it.

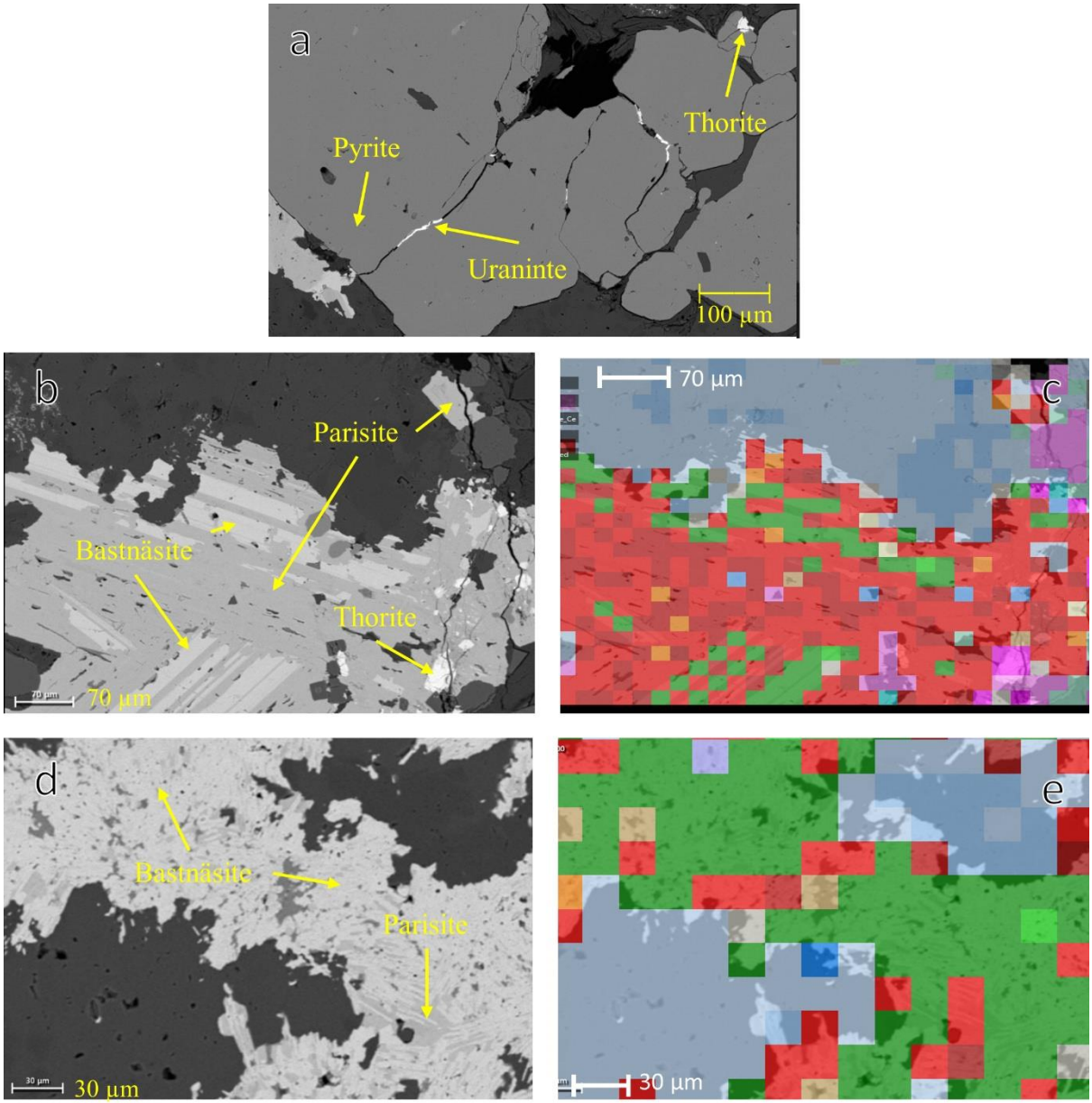

Figure 3-18 Shows BSE and AM pictures of uraninite and REE minerals. a) BSE of pyrite with uraninite filling in cracks, small thorite grain also visible. b) parisite intergrown with euhedral lath-shaped bastnäsite, AM (c) shows how the OV maps classified it. d) patchy irregular bastnäsite intergrown with parisite, AM (e) shows how the OV maps classified it. Figure 3-17 has the legend for the AM pictures.

3.5.1 Mineral associations

3.5.1.1 Thorite & Uranium Associations

The thorite associations that are shown in Table 3-4 shows combined association from the three thorite classification classes that were used during the BPS (Full table for both the raw data and the combined thorite in Appendix IV. It shows a larger variety in each specimen

with some common minerals that have a consistently higher association. Calcite and quarts are the ones with the highest general association throughout every specimen. The reason thorite appears to associate with itself is because the table is a composite of the three thorite classifications.

Full uraninite associations are shown in Table 3-5 and indicate a consistent association to pyrite and somewhat to quartz. Missing specimens in the table indicates that no uraninite was found in those specimen. Full coffinite associations are shown in Table 3-6 and show a general association with pyrite and quarts. It also has a slightly higher unclassified association compared to uraninite.

Table 3-4 Shows combined thorite associated minerals in a percentage (%) (only minerals with percentages above 5% are included. Full table can be found in Appendix IV).

	Ankerite	Apatite	Bastnäsite_Ce_La	Burbankite_Y	Calcite	Dolomite	Magnetite	Mg-Fe-chlorite	Monazite_Ce	Parisite_Ce	Parisite_Ce_La	Pyrite	Quartz	Siderite	Thorite2-Calcite mix	Thorite-Calcite mix	Thorite	Thorite2	Background	Unclassified
3_1	16,2	1,8	0,0	0,1	23,9	3,8	6,7	0,6	4,3	1,2	0,2	6,6	5,0	1,5	0,2	3,2	2,6	4,4	6,1	6,5
3_2	5,0	0,8	0,0	0,5	15,6	1,8	6,9	0,0	1,0	5,0	1,4	0,8	38,0	2,4	0,1	1,9	2,6	3,9	1,6	6,1
3_3	11,0	11,9	0,3	0,0	21,6	3,2	0,6	0,0	0,3	0,6	0,0	0,3	28,0	0,6	0,0	2,2	2,7	3,8	1,3	7,3
3_4	1,6	0,0	0,2	0,6	8,4	0,4	6,6	0,4	1,1	1,6	2,2	0,2	59,5	1,8	0,0	0,1	1,8	2,5	2,1	5,3
3-6_1	4,5	1,2	0,1	0,0	59,5	0,9	0,8	0,1	0,1	0,2	0,1	0,3	2,5	0,8	1,0	6,8	3,5	6,8	1,1	7,5
3-6_2	5,5	0,5	8,5	2,7	8,7	0,6	2,4	0,4	0,6	4,8	3,7	0,2	21,8	0,6	2,3	0,2	4,4	2,8	3,8	7,2
3-6_3	12,3	0,3	0,2	0,2	22,2	1,1	7,2	0,0	0,9	3,5	4,0	0,4	20,9	2,3	6,4	0,2	3,7	2,2	3,1	6,0
3-6_4	5,5	0,7	1,4	0,0	36,9	0,9	1,8	0,0	0,0	5,0	1,7	0,0	29,0	0,9	7,2	0,0	1,8	1,3	1,4	2,3
6_1	7,1	0,6	0,5	0,9	31,9	0,4	3,7	1,2	5,7	1,5	1,3	0,9	6,8	1,4	13,3	0,3	5,5	2,8	5,4	5,1
6_2	5,0	0,3	3,2	0,2	9,5	0,1	19,1	8,8	2,8	5,9	8,1	2,0	3,1	5,0	2,5	0,1	6,5	3,0	6,9	4,4
6_3	3,0	15,8	1,4	0,4	9,9	0,2	2,2	12,0	4,4	2,8	3,1	2,4	7,0	1,1	3,5	0,2	11,5	4,1	6,8	4,7
6_4	5,5	0,3	2,3	6,3	8,0	0,4	0,8	2,4	5,4	5,2	3,1	1,4	13,0	0,3	0,0	0,0	4,5	2,6	11,3	4,4
Kjerne_V	8,7	0,9	0,9	0,7	17,0	2,9	1,8	0,2	2,2	3,6	0,7	1,0	13,8	3,0	0,4	2,0	4,9	8,0	8,7	7,2
Kjerne_H	6,5	0,0	1,6	5,6	7,3	1,6	2,3	0,3	0,9	3,2	2,6	0,9	23,0	1,5	0,4	0,9	3,7	6,8	4,2	11,2
Legend	0		0-5		5-15		15-30			30-50			50-100							

Table 3-5 Shows Uraninite associations (%), missing specimens indicate that no uraninite was detected in that specimen.

	Ankerite	Apatite	Barite	Bastnäsite_Ce_La	Bastnäsite_sulph	Calcite	Calcite_w_Ce	Coffinite	Dolomite	Galena	Gypsum	Molybdenite	Monazite_Ce	Parisite_Ce	Parisite_Ce_La	Parisite_Ce_Nd	Pyrite	Pyrrhotite	Quartz	Synchysite_Ce	Background	Not Analysed	Not Classified	Unclassified
3_1	0,0	0,0	0,0	12,5	0,0	0,0	0,0	0,0	0,0	0,0	0,0	0,0	12,5	25,0	12,5	0,0	25,0	0,0	0,0	0,0	0,0	0,0	12,5	0,0
3_2	16,7	0,0	0,0	5,6	0,0	22,2	0,0	5,6	0,0	0,0	0,0	0,0	11,1	0,0	11,1	0,0	22,2	0,0	0,0	0,0	5,6	0,0	0,0	0,0
3_4	1,4	0,0	0,0	0,0	0,0	56,9	0,0	4,9	1,4	0,0	0,7	3,5	2,1	0,0	5,6	0,0	0,7	0,0	1,4	0,7	8,3	0,0	1,4	11,1
3-6_1	0,0	2,1	6,3	4,2	0,0	45,8	2,1	0,0	4,2	0,0	0,0	0,0	0,0	0,0	10,4	0,0	12,5	0,0	0,0	0,0	0,0	0,0	0,0	12,5
3-6_2	0,0	0,0	50,0	0,0	0,0	0,0	0,0	25,0	0,0	0,0	0,0	0,0	0,0	0,0	0,0	0,0	25,0	0,0	0,0	0,0	0,0	0,0	0,0	0,0
3-6_3	15,1	0,0	0,0	0,0	0,0	2,4	0,0	11,1	3,2	0,0	0,8	0,0	3,2	5,6	15,9	0,8	17,5	0,0	0,8	0,0	10,3	0,0	0,8	12,7
3-6_4	20,0	10,0	0,0	5,0	0,0	20,0	0,0	10,0	0,0	0,0	0,0	0,0	0,0	5,0	5,0	0,0	5,0	0,0	0,0	0,0	0,0	0,0	0,0	20,0
6_1	25,0	0,0	0,0	0,0	0,0	50,0	0,0	0,0	12,5	0,0	0,0	0,0	0,0	0,0	0,0	0,0	0,0	0,0	0,0	0,0	12,5	0,0	0,0	0,0
6_2	5,1	0,0	2,0	16,7	0,5	12,6	0,0	5,1	2,0	0,0	0,0	0,0	0,0	1,5	8,1	0,0	22,2	0,0	2,0	0,0	7,6	0,5	0,0	14,1
6_3	0,0	13,2	0,0	0,0	0,0	8,8	1,5	0,0	0,0	1,5	0,0	0,0	8,8	0,0	0,0	0,0	45,6	1,5	0,0	0,0	2,9	0,0	0,0	16,2
6_4	0,0	0,0	0,0	50,0	0,0	0,0	0,0	0,0	0,0	0,0	0,0	0,0	0,0	0,0	0,0	0,0	50,0	0,0	0,0	0,0	0,0	0,0	0,0	0,0
Legend	0			0-5			5-15			15-30			30-50				50-100							

Table 3-6 Shows coffinite associations (%), missing specimens indicates that no coffinite was found in that specimen.

	Actinolite	Ankerite	Apatite	Barite	Bastnäsite_Ce_La	Biotite	Burbankite_Y	Calcite	Calcite_w_Ce	Ce-quartz mix	Dolomite	Fe-Mg-chlorite	Gypsum	Mg-Fe-chlorite	Molybdenite	Monazite_Ce	Monazite_La	Nb_rutile	Parisite_Ce	Parisite_Ce_La	Parisite_Ce_Nd	Pyrite	Pyrrhotite	Quartz	REE-quartz mix	Talc	Thorite	Thorite2	Thorite3	Uraninite	Background	Not Classified	Unclassified
3_2	0,0	6,3	3,6	3,6	0,0	0,0	0,0	22,9	0,5	0,0	5,7	0,0	1,6	0,0	13,5	9,4	0,0	0,0	4,7	3,6	0,0	5,2	0,5	6,3	0,5	0,0	0,0	0,0	0,0	0,5	4,2	0,5	6,8
3_3	0,0	0,0	0,0	0,0	0,0	0,0	0,0	93,8	0,0	0,0	0,0	0,0	0,0	0,0	0,0	0,0	0,0	0,0	0,0	0,0	0,0	0,0	0,0	0,0	0,0	0,0	0,0	0,0	0,0	0,0	0,0	0,0	6,3
3_4	0,0	1,9	0,0	0,0	0,0	0,0	0,0	67,1	0,2	0,0	0,9	0,0	0,0	0,0	3,3	2,6	0,2	0,0	0,0	0,0	0,0	5,8	0,7	3,0	0,0	0,0	0,0	0,0	0,2	1,6	2,6	0,7	9,1
3-6_1	0,0	5,0	5,0	0,0	0,0	0,0	0,0	65,0	0,0	0,0	0,0	0,0	0,0	0,0	0,0	0,0	0,0	10,0	0,0	0,0	0,0	0,0	0,0	10,0	0,0	0,0	0,0	0,0	0,0	0,0	0,0	0,0	5,0
3-6_2	0,0	0,0	0,0	25,0	0,0	0,0	0,0	0,0	0,0	0,0	0,0	0,0	0,0	0,0	0,0	0,0	0,0	0,0	0,0	0,0	0,0	25,0	0,0	25,0	0,0	0,0	0,0	0,0	0,0	25,0	0,0	0,0	0,0
3-6_3	0,0	9,3	0,0	0,0	0,0	0,0	0,0	6,6	0,0	1,1	2,2	0,0	1,6	0,5	1,1	0,5	0,0	0,0	1,6	12,1	0,0	15,9	1,1	3,8	0,0	0,5	0,0	1,6	0,0	7,7	10,4	0,0	22,0
3-6_4	0,0	0,0	0,0	2,1	0,0	0,0	2,1	20,8	0,0	0,0	2,1	0,0	0,0	12,5	0,0	0,0	0,0	2,1	0,0	2,1	0,0	16,7	0,0	8,3	0,0	0,0	0,0	0,0	0,0	4,2	6,3	0,0	20,8
6_1	0,0	19,7	0,0	0,0	0,0	0,0	0,0	14,8	0,0	0,0	2,8	0,0	0,0	0,0	0,7	0,7	0,0	0,0	0,0	1,4	0,0	21,1	0,0	0,0	0,0	0,0	0,0	0,0	1,4	0,0	9,9	2,8	24,6
6_2	0,0	6,9	0,0	0,0	15,7	0,0	0,0	11,8	0,0	0,0	3,9	0,0	0,0	0,0	0,0	0,0	0,0	0,0	5,9	10,8	2,0	5,9	1,0	6,9	0,0	0,0	0,0	0,0	0,0	9,8	10,8	0,0	8,8
6_3	0,5	0,0	1,6	0,5	0,0	0,5	0,0	8,5	0,5	0,0	0,0	0,5	0,5	4,3	2,1	0,0	0,0	0,0	0,0	0,0	0,0	42,6	2,7	2,7	0,0	0,5	0,5	18,6	1,1	0,0	1,1	0,0	10,6
6_4	0,0	0,0	0,0	0,0	25,0	0,0	0,0	0,0	0,0	25,0	0,0	0,0	0,0	0,0	0,0	0,0	0,0	0,0	0,0	0,0	0,0	25,0	0,0	0,0	0,0	0,0	0,0	0,0	0,0	0,0	0,0	0,0	25,0

Legend: 0 | 0-5 | 5-15 | 15-30 | 30-50 | 50-100

3.5.2 Element distribution

3.5.2.1 Thorium & Uranium distribution

Distribution of thorium (Figure 3-19, Figure 3-21, Figure 3-20) indicates that thorium mainly occurs as thorite and only in trace amount in other minerals. Distribution was made by combining both thorium and silver to make up for a peak overlap.

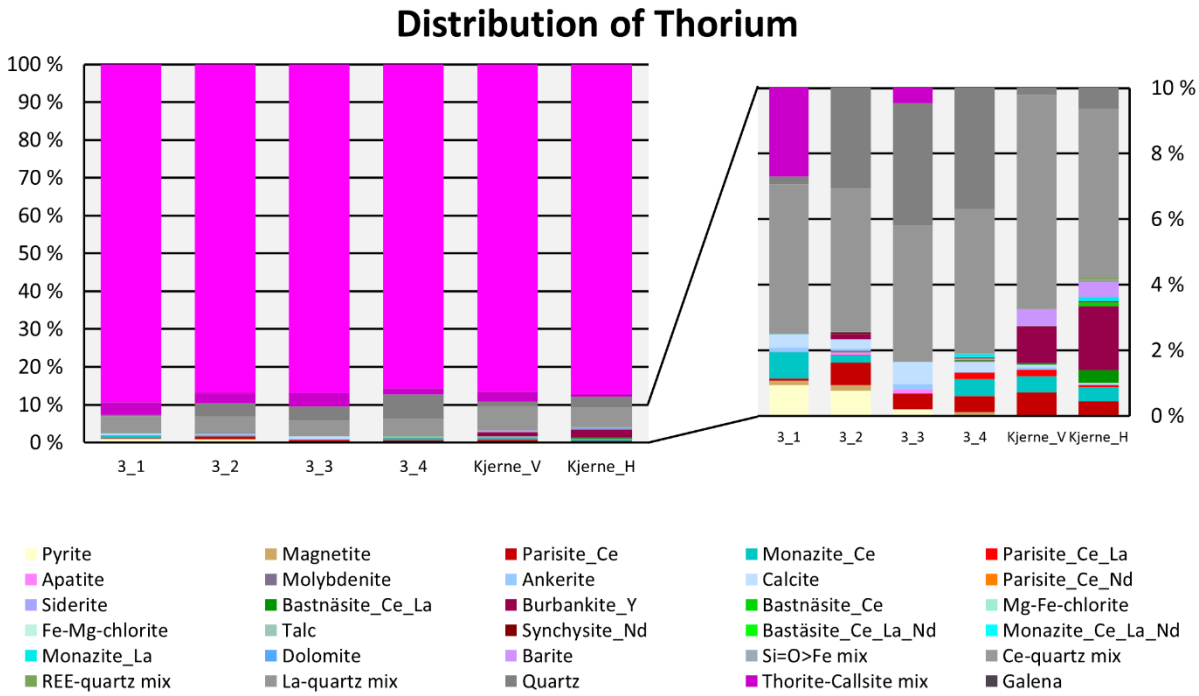

Figure 3-19 Shows distribution of thorium in the low radioactive group and the core specimens. Thorium occurs mainly in the form of thorite, with trace amounts in other minerals.

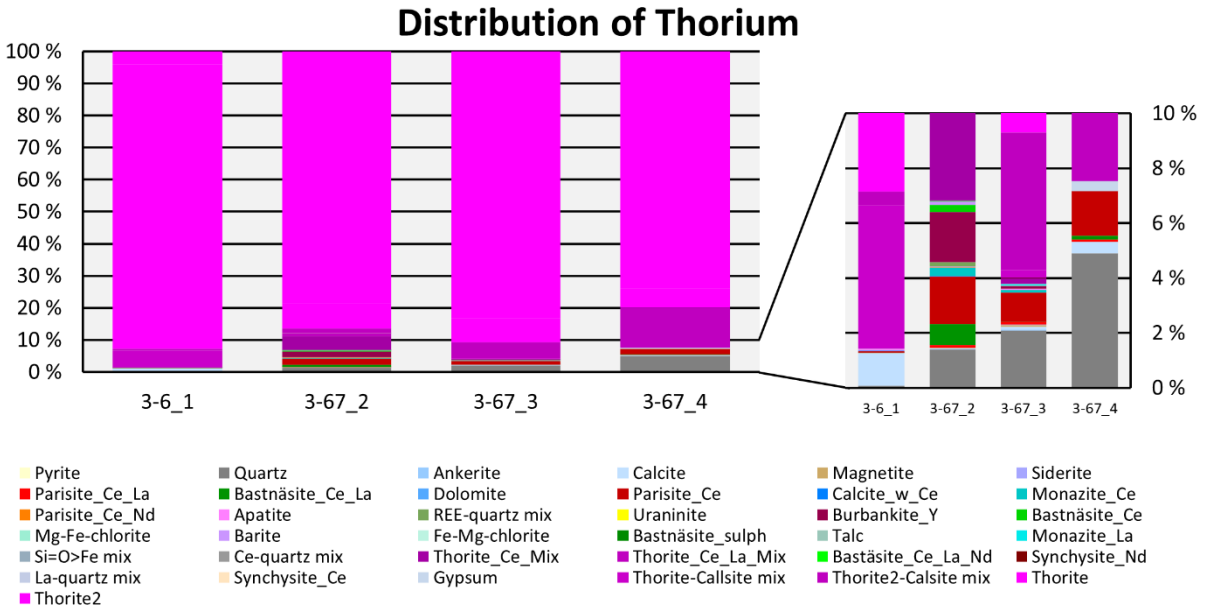

Figure 3-20 Shows distribution of thorium in the medium radioactive group. Thorium occurs mainly in the form of thorite, with small percentages in other minerals

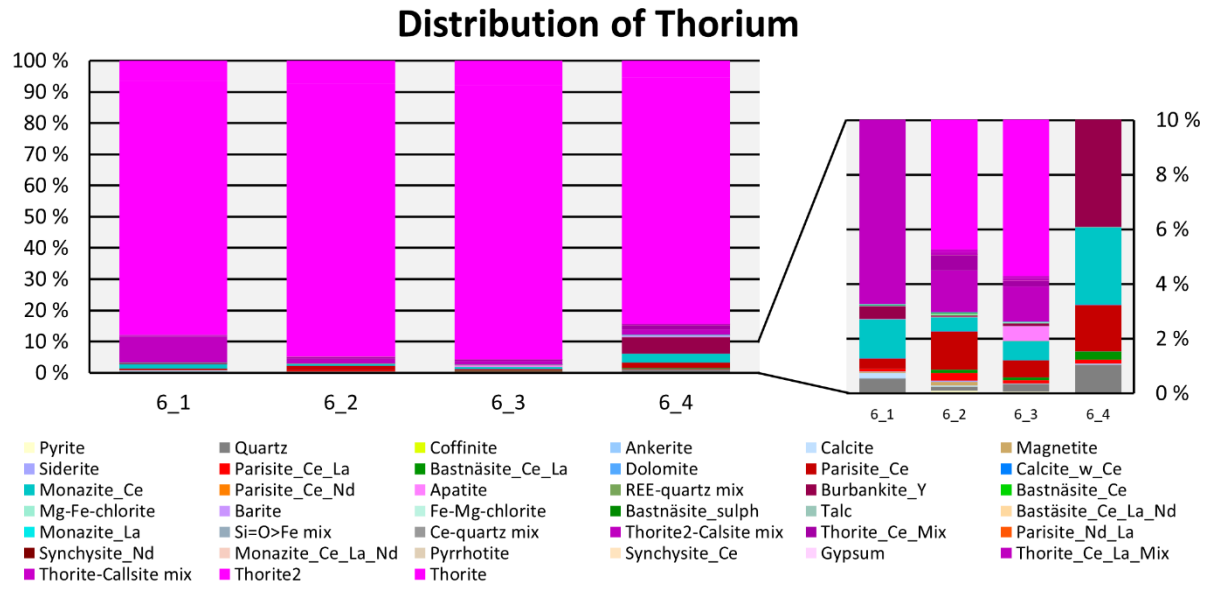

Figure 3-21 Shows distribution of thorium in the high radioactive group. Thorium occurs mainly in the form of thorite, with trace amounts in other minerals

The distribution of uranium (Figure 3-22, Figure 3-23, Figure 3-24) indicates that uranium occurs in uraninite and coffinite as main phases, there is some variation between specimens. It also appears to occur in some other minerals in lower percentages.

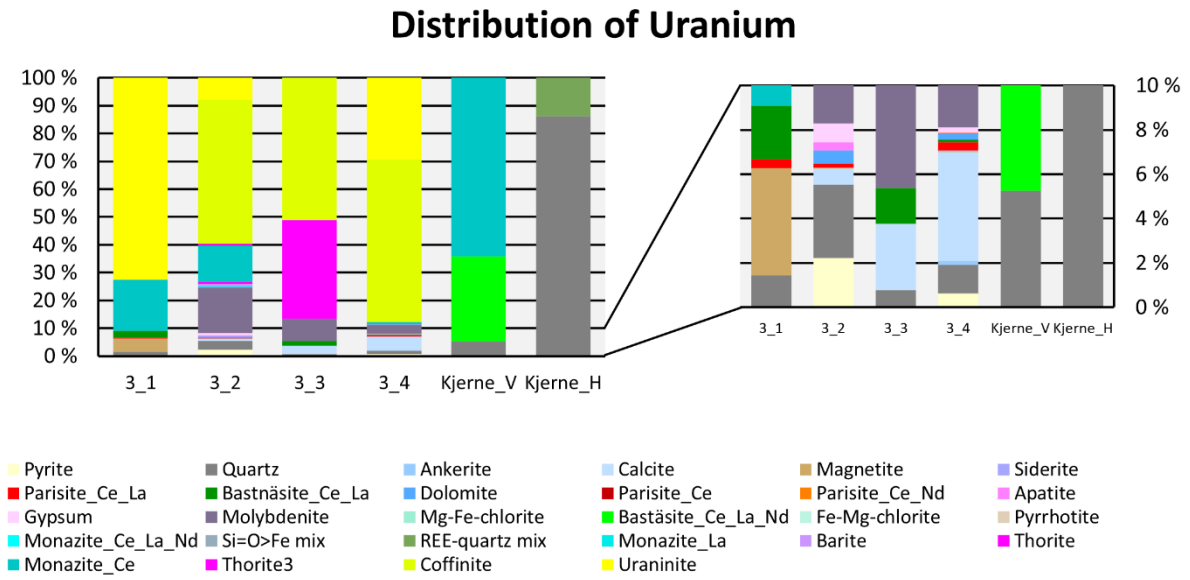

Figure 3-22 Shows the distribution of uranium in the low radioactive group and the core specimen. Uranium seems to occur in part in uraninite and coffinite, with small percentages in other minerals

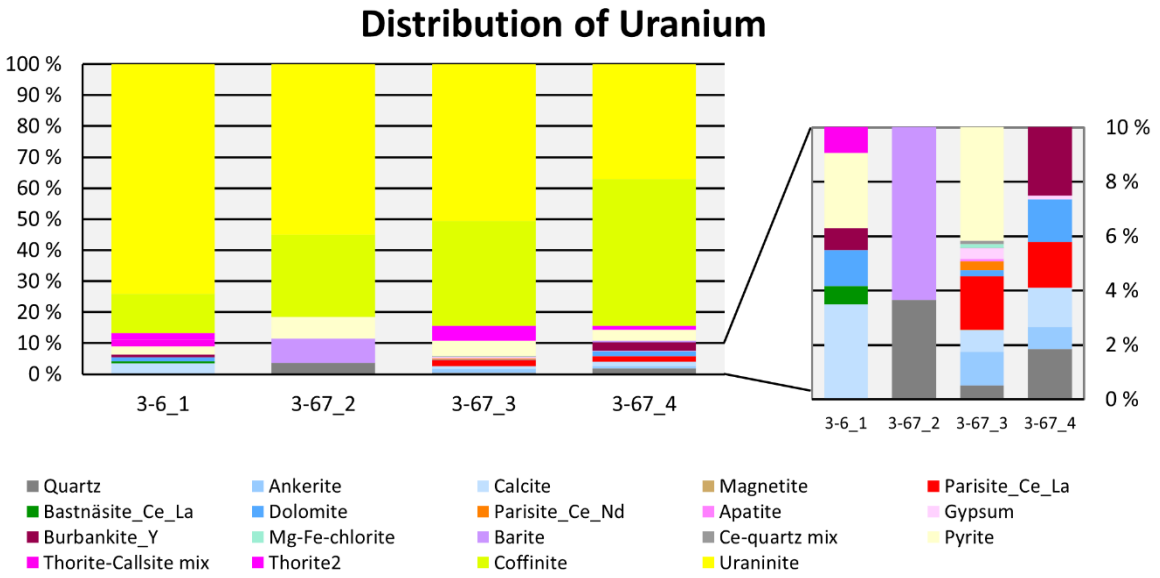

Figure 3-23 Shows the distribution of uranium in the medium radioactive group. Uranium seems to occur in part in uraninite and coffinite, with small percentages in other minerals

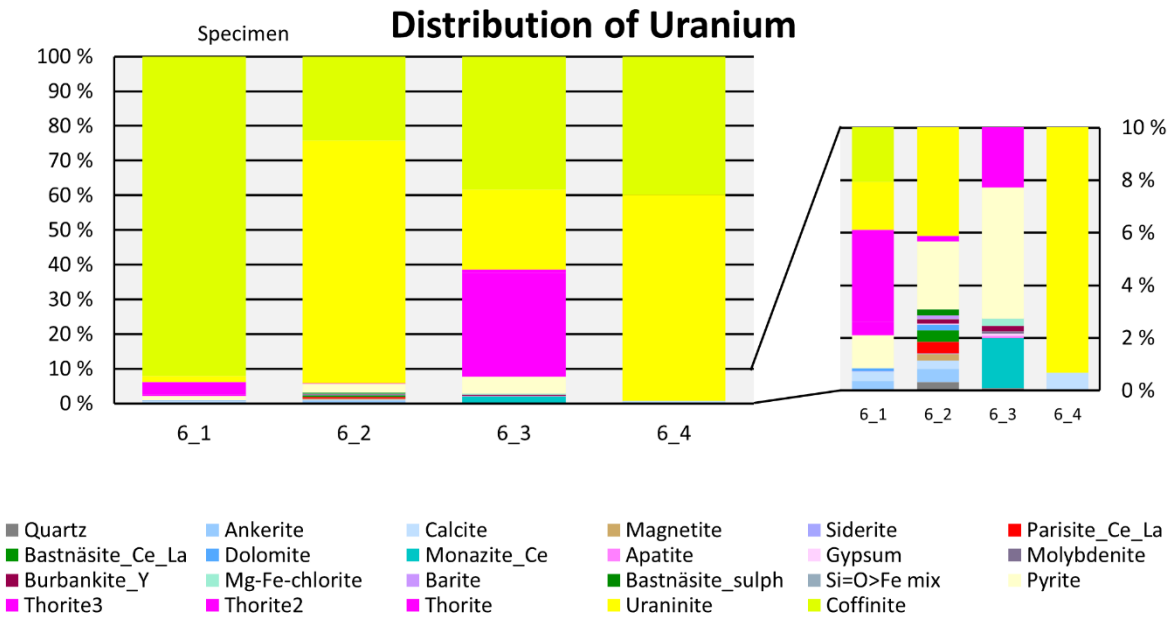

Figure 3-24 Shows the distribution of uranium in the high radioactive group. Uranium seems to occur in part in uraninite and coffinite, with small percentages in other minerals

Table 3-7 Shows the calculated estimated area for thorium and uranium for each specimen. Also, includes a percentage of the total areal of the thin-section the elements covers of.

	Th areal (µm)	*Total %*	*U areal (µm)*	*Total %*
3_1	5348	0,0007	59,5	0,000008
3_2	5887	0,0007	878,5	0,000107
3_3	605,5	0,0001	56	0,000007
3_4	7808,5	0,0010	1704,5	0,000223
3-6_1	4921	0,0007	154	0,000022
3-6_2	12404	0,0018	35	0,000005
3-6_3	10752	0,0016	861	0,000127
3-6_4	539	0,0001	185,5	0,000038
6_1	16481,5	0,0028	833	0,000143
6_2	103092,5	0,0157	749	0,000114
6_3	106330	0,0174	941,5	0,000154
6_4	5680,5	0,0011	14	0,000003
Kjerne_H	1200,5	0,0001	10,5	0,000001
Kjerne_V	4210,5	0,0011	49	0,000013

Table 3-7 gives an estimated area of total thorium and uranium in their respective specimen. Of note is small values in 6_4 and the core specimen.

3.5.2.2 REE distribution

The distribution of LREEs was made using the OV maps and consolidated into one graph (Figure 3-25). The full distribution for each specimen is in Appendix IV. Because of a software bug in the mineralogic reporter program it was not possible to make the same

distribution graphs for lanthanum, instead lanthanum distribution is interpreted from OV bulk data (Appendix IV). Lanthanum is consistently found in the REE minerals. Cerium and neodymium have a large occurrence in parisite. Cerium occurs almost exclusively in REE minerals, while neodymium also occurs in the surrounding minerals (carbonates and quartz). Both praseodymium and samarium occur mainly in carbonates and quartz, with samarium also appearing in apatite.

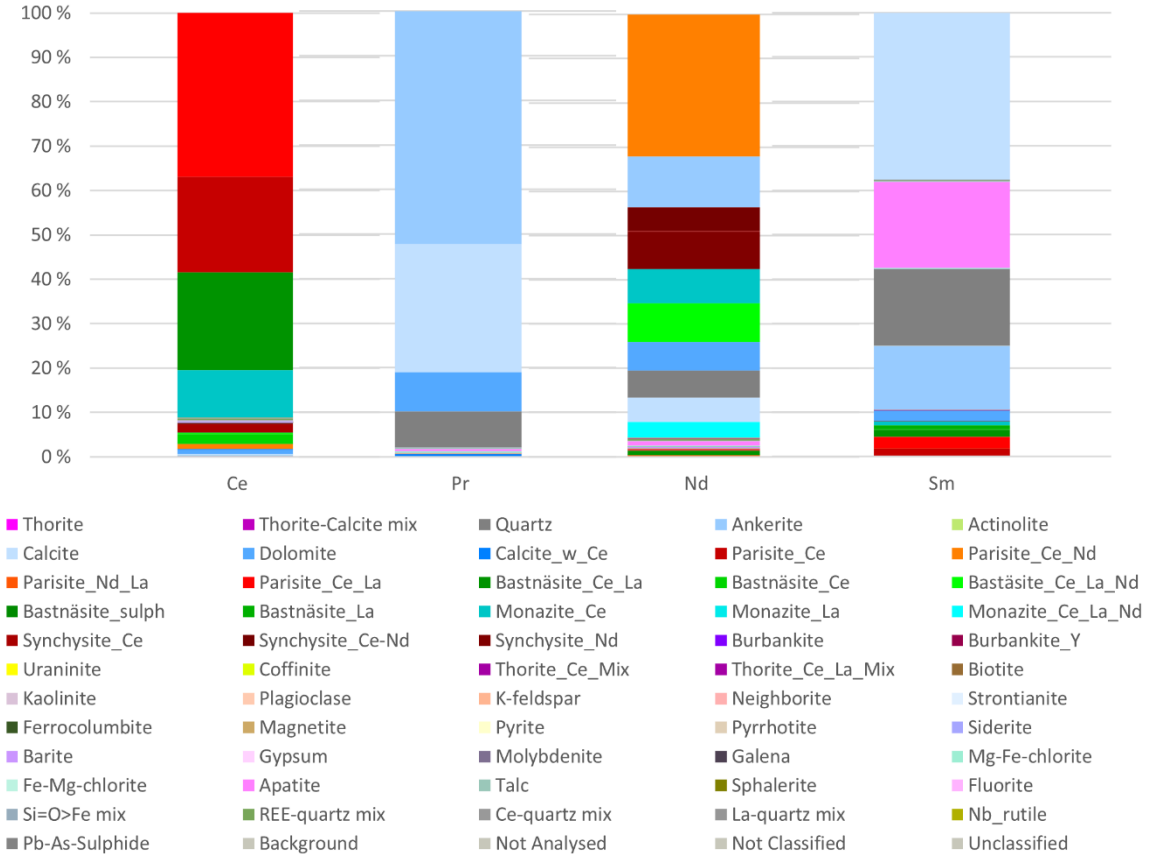

Figure 3-25 Consolidated distribution of available LREEs. Individual element distributions in Appendix IV..

3.5.3 Grain size distribution

Thorite grain size distribution (Figure 3-26) shows a consistent rise in grain size, with a large fraction being below 3.5 µm. The histogram (Figure 3-28) corroborates the result with the smallest fraction being the majority. Both figures indicate that most thorite grains are below 50 µm.

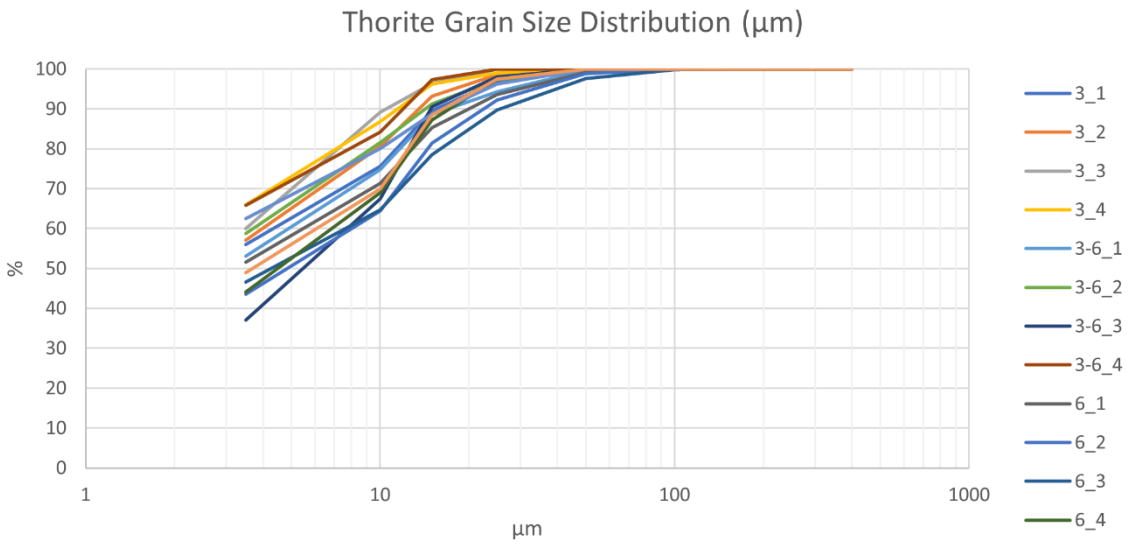

Figure 3-26 Shows thorite grain distribution for each specimen, based on ferret max diameter of each grain. Table available in Appendix IV

Both the uraninite and coffinite grain size distribution (Figure 3-27) shows larger variation between each specimen, but a significant fraction is under 3.5 µm in size. There are noticeably less uranium grains compared to thorite grains. The histogram (Figure 3-28) shows similar results as thorrite, but there is a larger split between the smallest fraction in uraninite compared to coffinite.

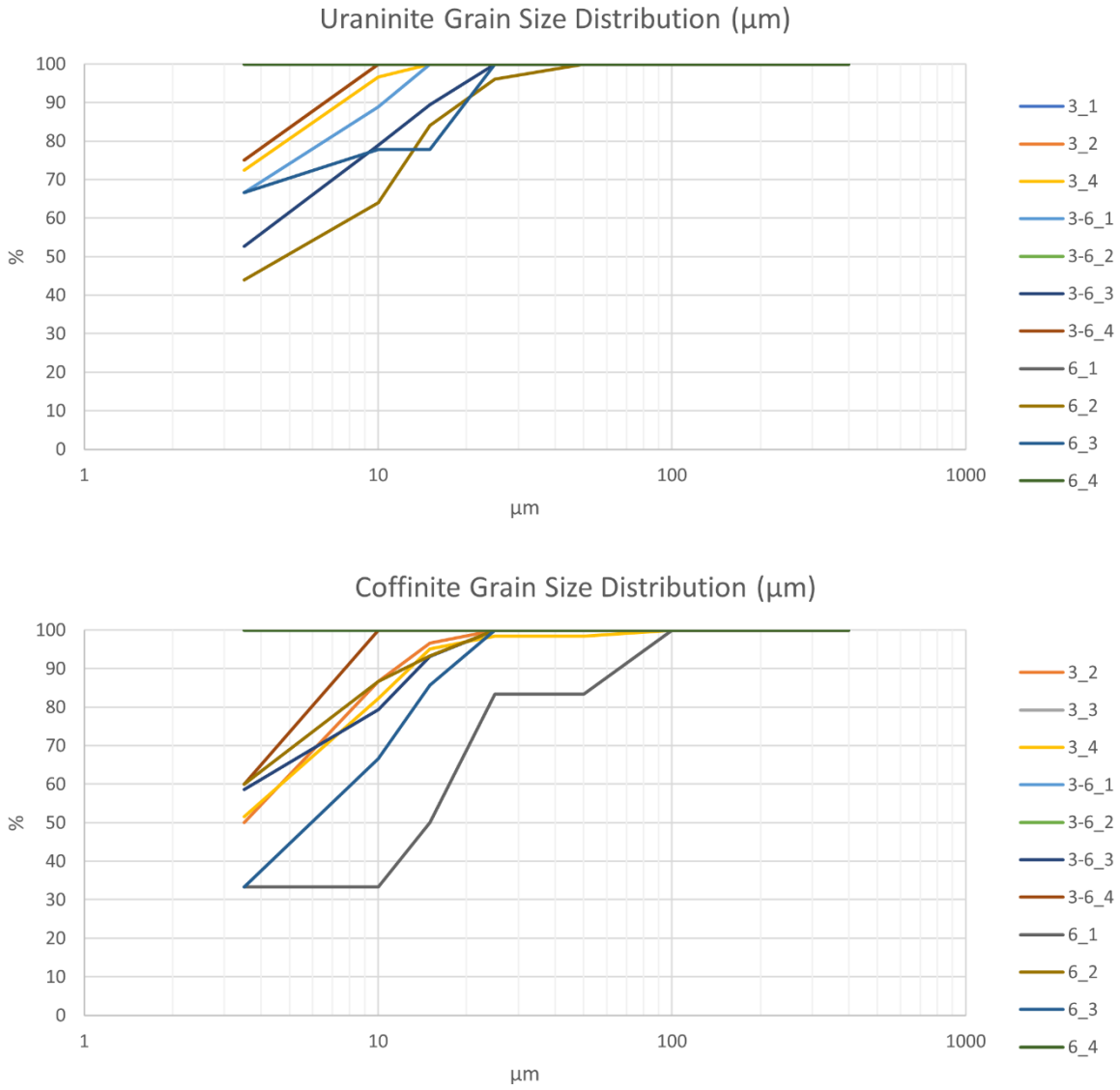

Figure 3-27 Shows uraninite (top) and coffinite (bottom) grain distribution for each specimen based on ferret max diameter. Specimens not included indicates that the mineral was not observed in specimen. Table available in Appendix IV.

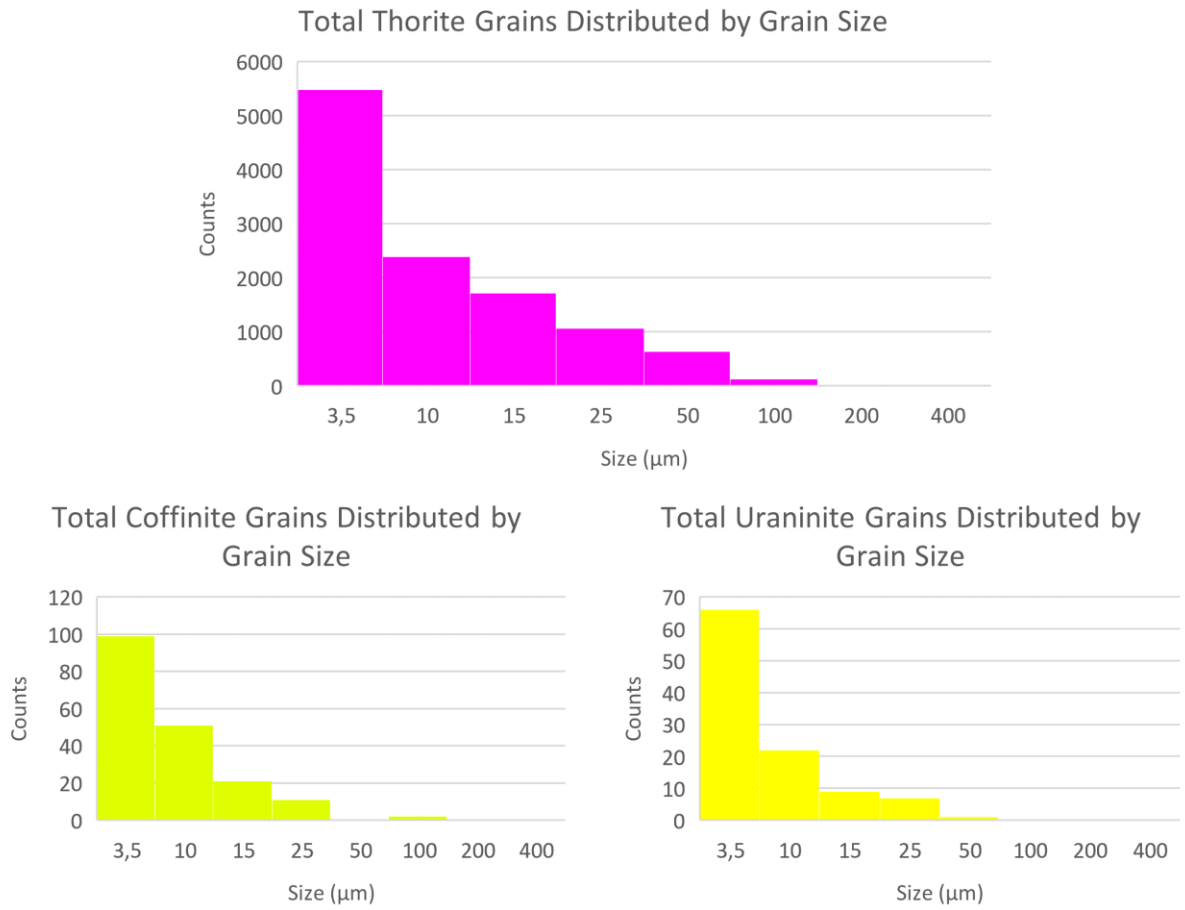

Figure 3-28 Shows the total spread of thorium (top), uraninite and coffinite (bottom) grains according to ferret max diameter.

3.5.3.1 Thorium & Uranium element distribution by grain size

The total thorium distribution based on grain size (Figure 3-29). The three top charts show distribution based on 0-5 µm, 5–25 µm, and 25+ µm grain size. The final pie chart shows fractions for each size. The charts are combined from every specimen. Separate graphs for each specimen are in Appendix IV.

Thorium occurs as thorite around 50 % of the time in the smaller fractions and seems to occur less in thorite as grain size increases. Uranium shows occurrence in uraninite and coffinite in the smaller fractions but does not occur in the largest fraction. The largest fraction is composed of mainly quartz. In the two smaller sizes is a significant amount that is unclassified.

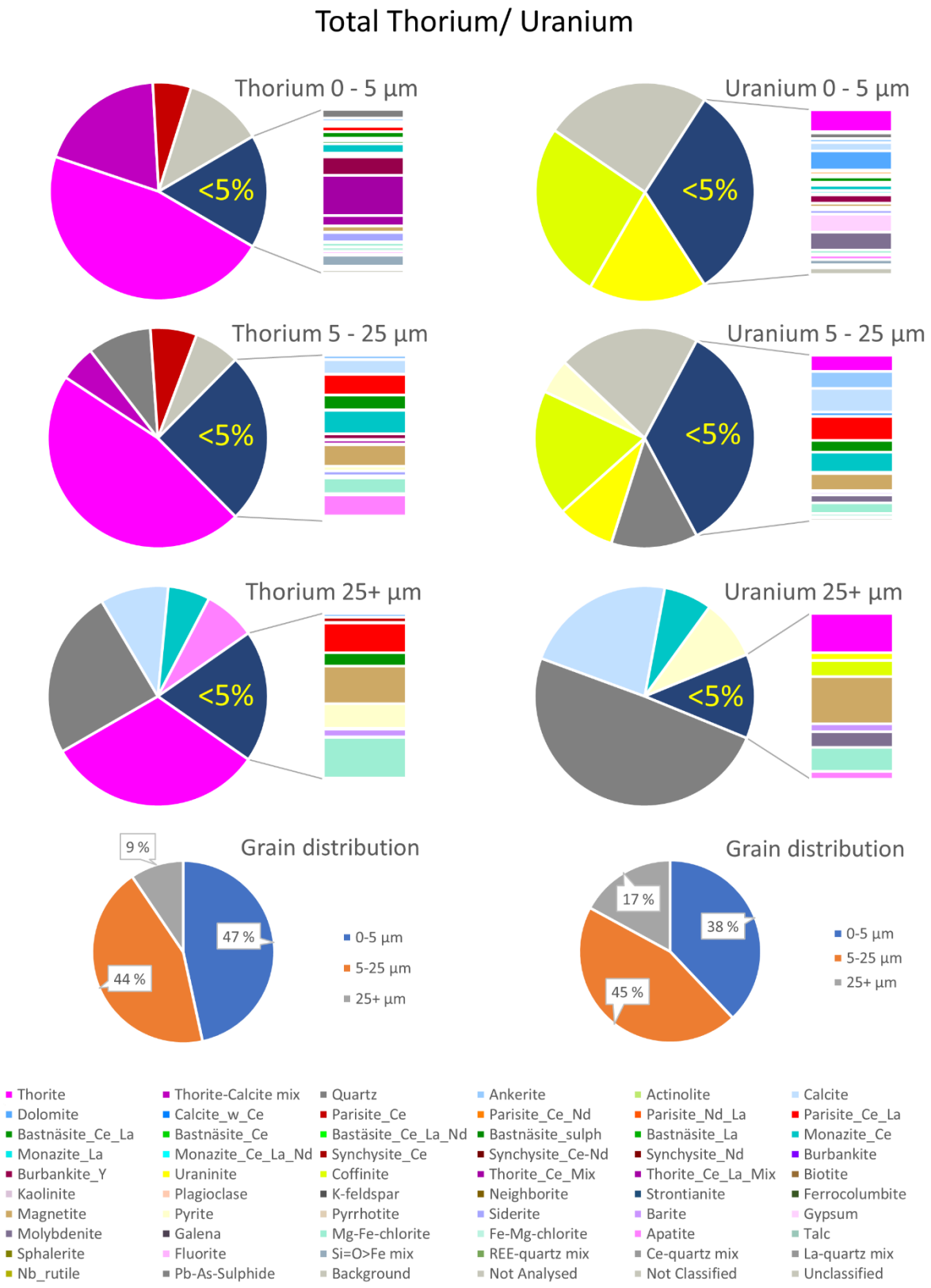

Figure 3-29 Shows total distribution of thorium and uranium based on measured grain size. Minerals under 5 % are taken out into the column graph. Bottom graph shows the distribution between the three sizes. Distribution for each specimen separate can be found in Appendix IV.

3.5.4 Detail maps

Figure 3-30 shows a coffinite grain with two phases surrounding large parts of a pyrite grain. Figure 3-31a shows the surrounding carbonatite in an optical microscope. Comparing BPS results (Figure 3-31b) to the detail map shows that the BPS has not picked up the smallest uranium grains. The uranium heat map (Figure 3-31c-d) shows that the uranium is not within the pyrite, and a small low concentration halo appears around the coffinite grain. Two REEs are included within the coffinite grain (Figure 3-31e, f), that being cerium and neodymium. The distinction between the two visible coffinite phases seems to be inclusions of phosphorus (*Figure 3-31g)* in the phase closest to the pyrite grain.

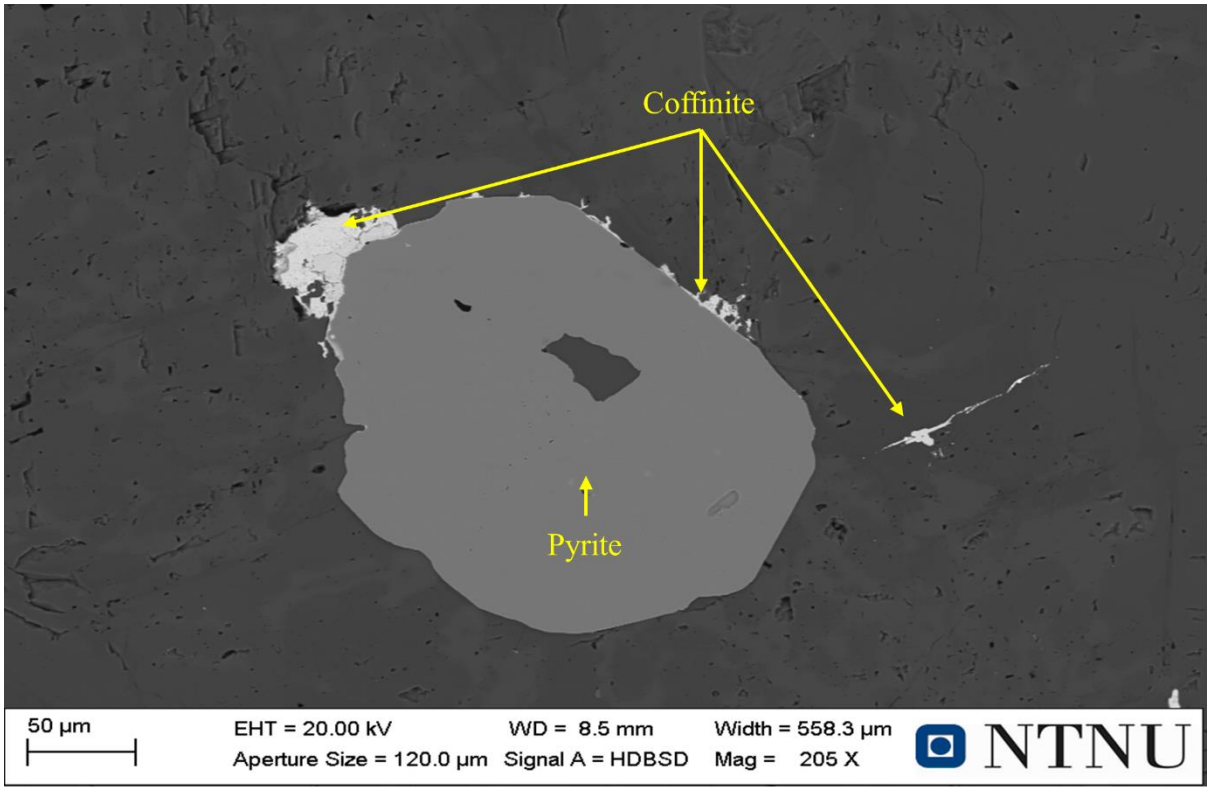

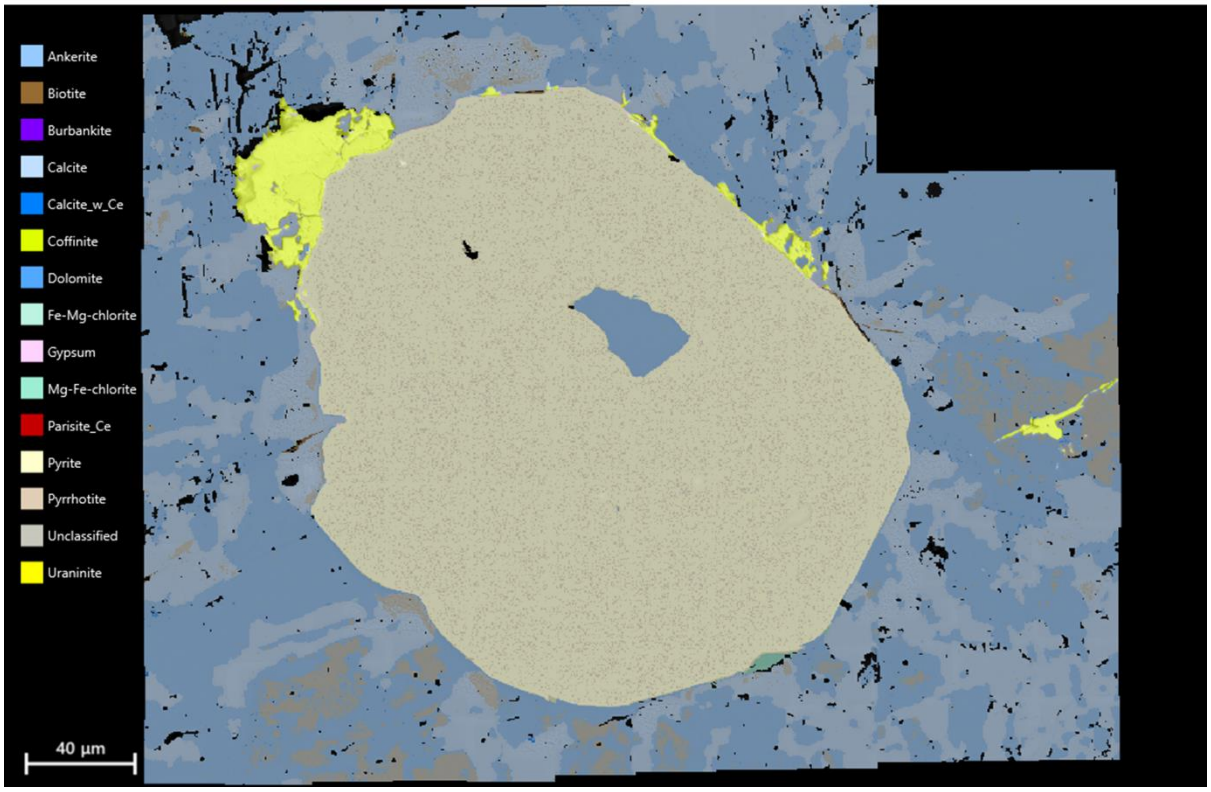

Figure 3-30 Shows EBS (top) and AM (bottom). It shows a pyrite grain with coffinite surrounding the edges, all surrounded by carbonates. The grey unclassified areas are a result of degradation caused by the long scanning time.

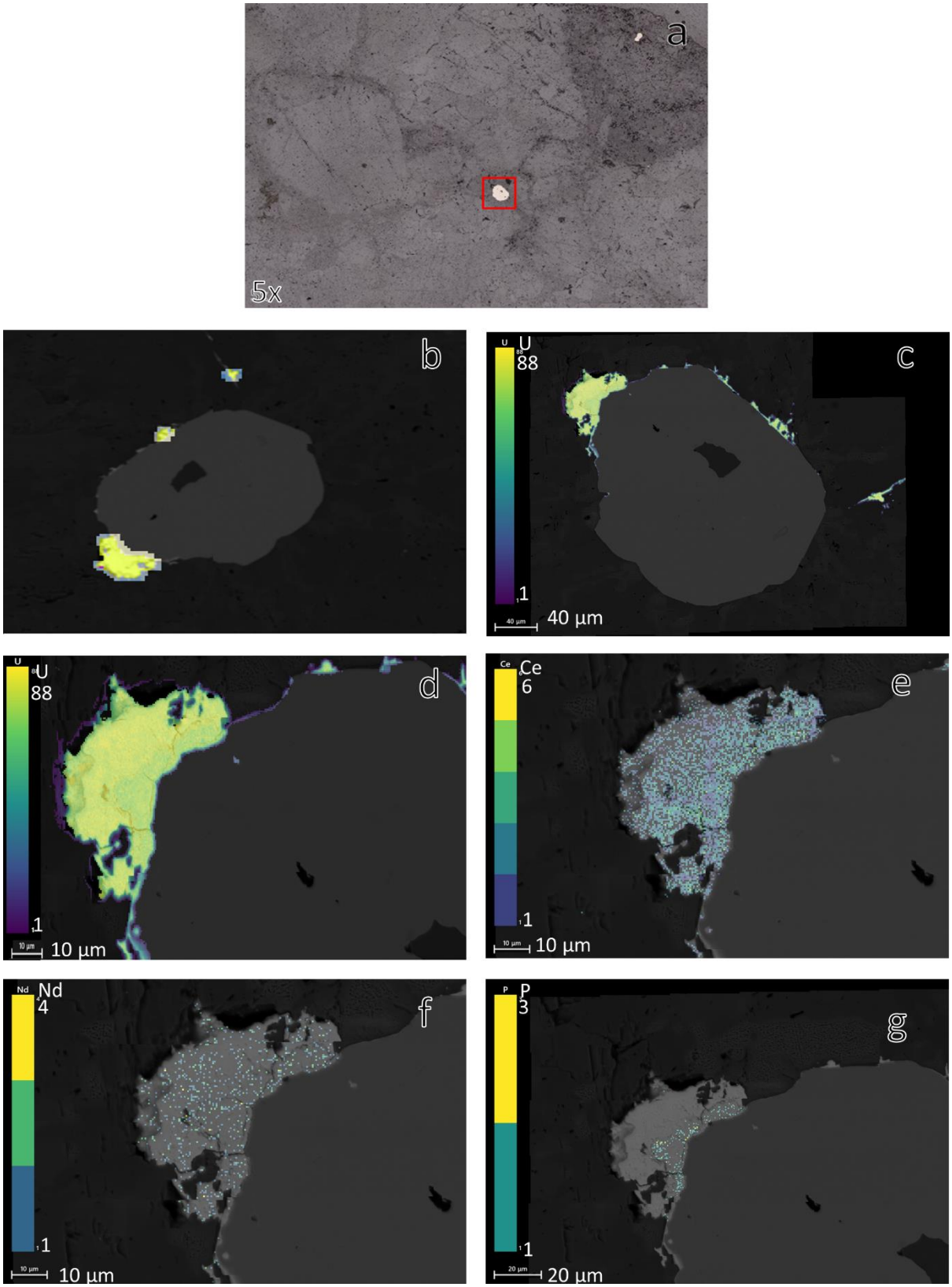

Figure 3-31 Taken from specimen 6_1. a) Reflected light (PPL), red marks the pyrite grain. b) The result of the same area in the BPS map. c) Heat map of uranium distribution. d) Closeup of the large coffinite grain, two distinct phases visible and a weak halo around the uranium grain. e) Heatmap for cerium showing a closeup that cerium only appears within the uranium grain. f) Heat map of neodymium only registering within the uranium grain. g) showing a phosphorus difference in the two visible phases.

Two areas in specimen 6_2 were scanned, one large thorite grain and one smaller uranium grain, respectively. The thorium EBS and AM (Figure 3-32) shows multiple interconnected thorite grains surrounded by magnetite, chlorite, and a spread of REE minerals. The same grain is also shown in an optical microscope (Figure 3-7). There are several smaller thorite grains included within the surrounding minerals (mainly in the REE minerals). Thorium occurs in large concentrations as thorite, but outside of the thorite are low concentrations of possible remobilised thorium within the REE minerals (Figure 3-33a and Figure 3-34b). These low concentrations match up with the cracks and grain boundaries found in the REE minerals (Figure 3-34a) and some of them match the treads seen in optical microscope (Figure 3-7). The BPS (Figure 3-33e) shows little of these low concentration inclusions because they are outside the map's detection range. The low concentrations do not show up on the OV map. The detected REEs are shown in Figure 3-33b-d and Figure 3-34c-e. Lanthanum seems to only appear within the REE minerals, while cerium and neodymium show some low consentrations within thorite, with cerium being significantly more present.

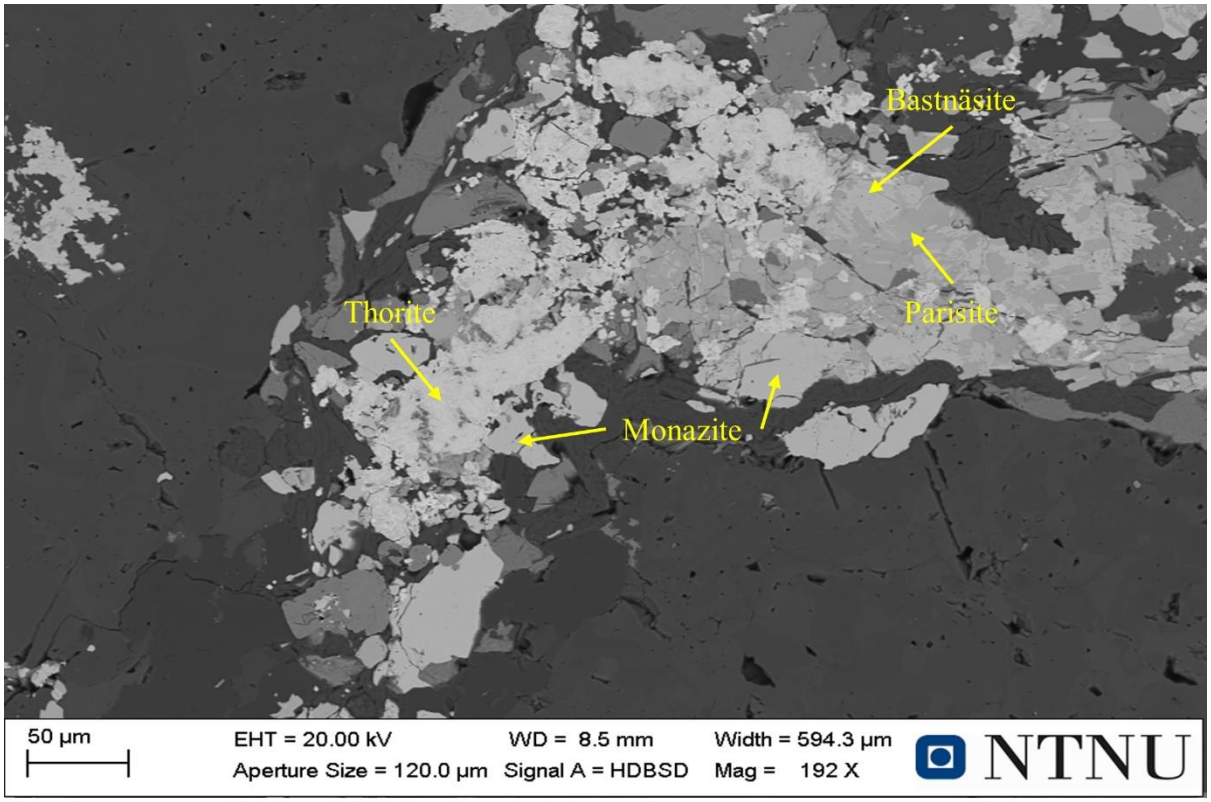

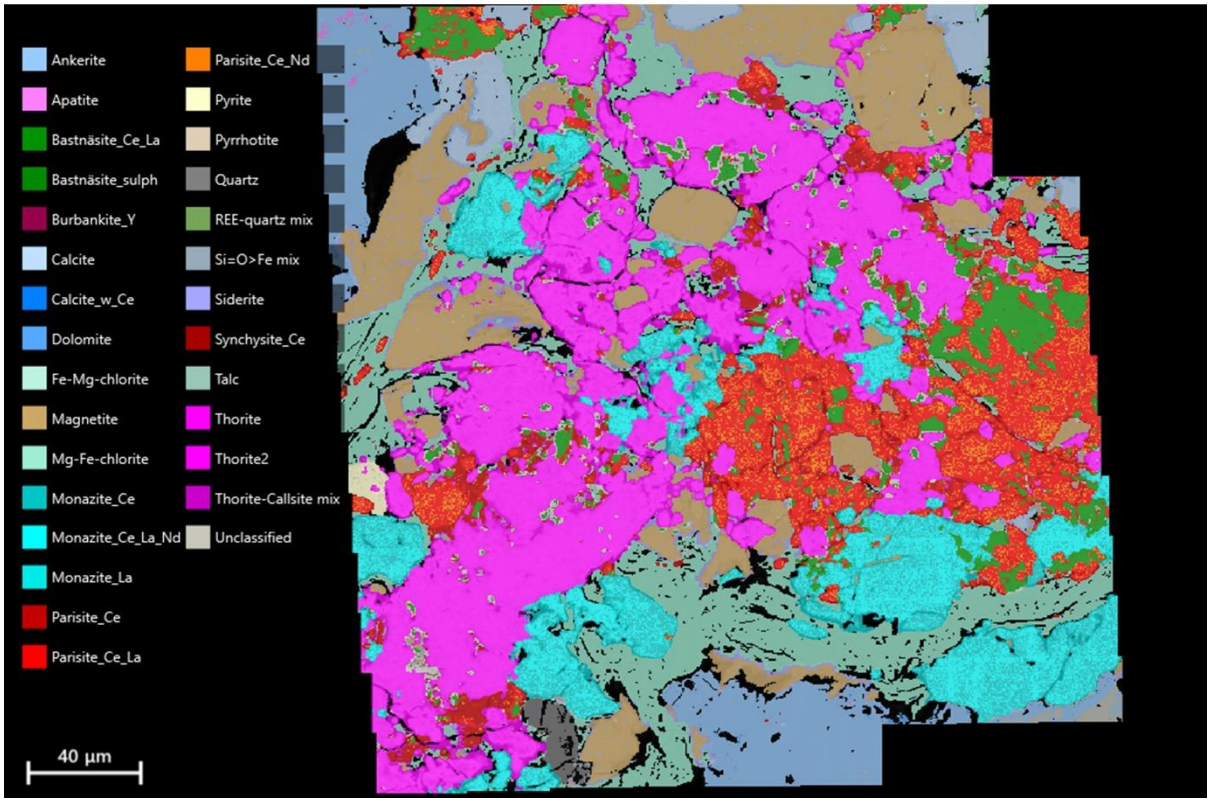

Figure 3-32 Shows the first detail map for specimen 6_2 in EBS (top) and AM (bottom).

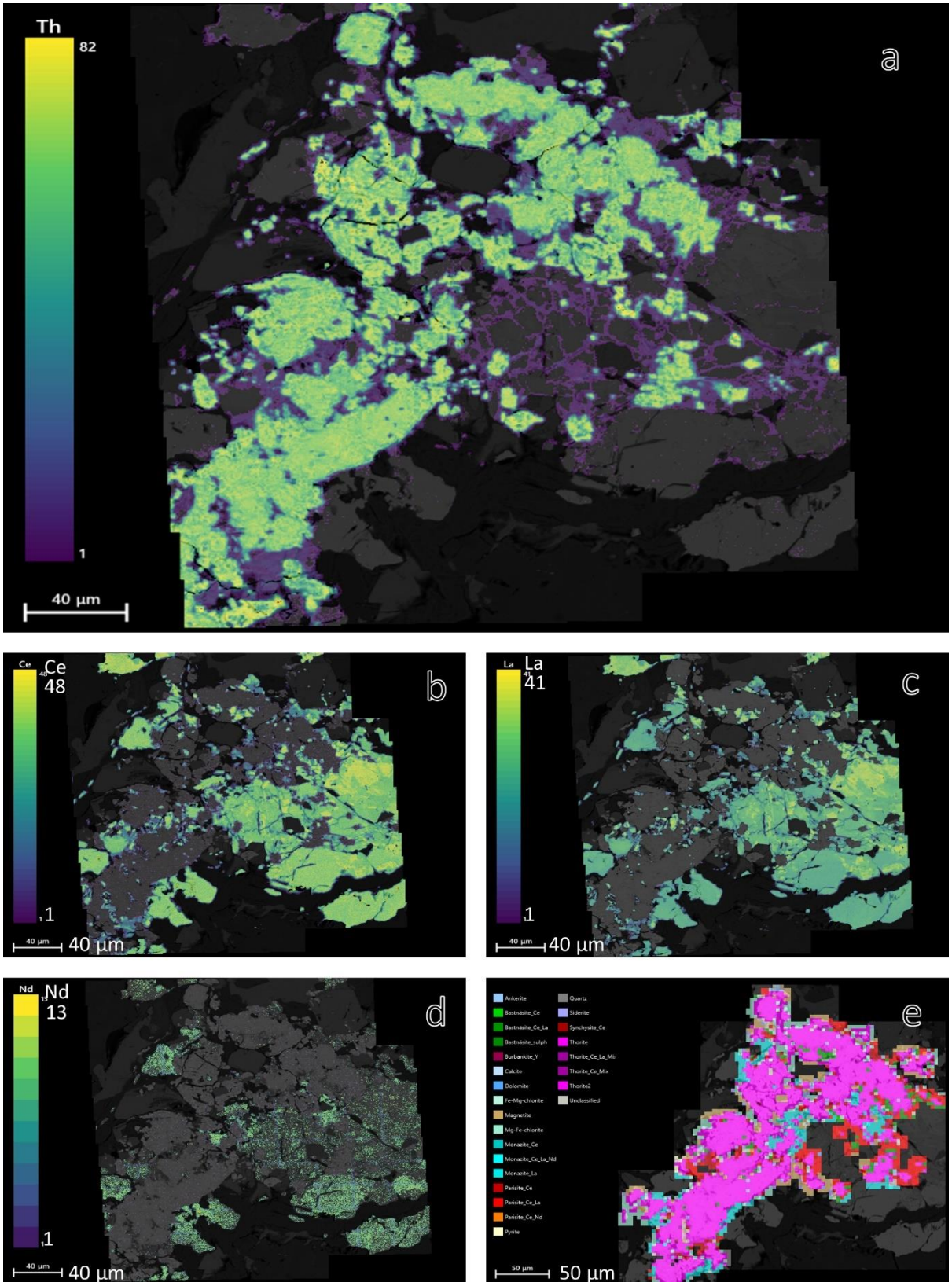

Figure 3-33 Shows heat maps from specimen 6_2 and one BPS map of the same area. a) Heat map of thorium, bright parts are thorite, while the dark parts are thorium in other minerals. b) Heat map of cerium. c) Heat map of lanthanum. d) Heat map for neodymium. e) BPS map showing the same area as covered by the detail map.

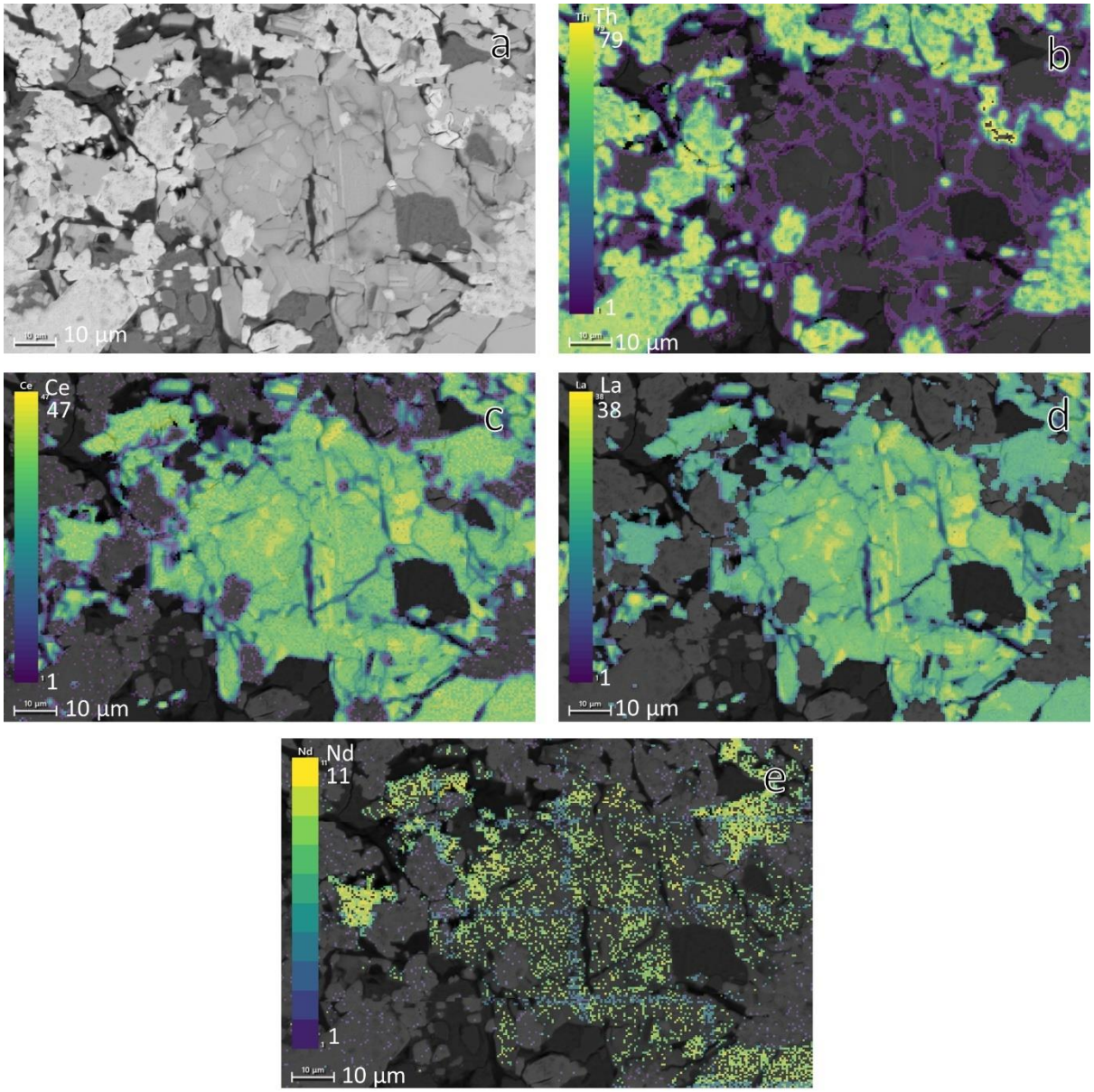

Figure 3-34 A zoomed in look at the detail heat maps from Figure 3-33. a) BSE of the smaller area. b) Heat map of thorium, bright parts are thorite, while the dark parts are thorium inclusions in other minerals. c) Heat map of cerium. d) Heat map of lanthanum. e) Heat map of neodymium.

The uranium grain scanned from specimen 6_2 (Figure 3-35) has both coffinite and uraninite appearing interlocked in the grain boundaries around the pyrite grain and filling in cracks in the surrounding bastnäsite/ parisite. The uranium heat map (Figure 3-36a-b) shows that uranium almost surrounds the pyrite grain but does not appear within the pyrite other than as a weak halo. The halo can also be seen on every mineral that comes into contact with the uraninite/ coffinite, this remains consistent with the uranium shown in 6_1. The three REEs acts similarly here as in the other 6_2 detail map by having lanthanum not interacting with the surrounding minerals and cerium being a consistent inclusion in the uranium minerals. Neodymium has some overlap but is nowhere near the level of cerium. Similar areas

distinguish uranium throughout each specimen, it often fills in cracks in between pyrite grains exactly as seen in Figure 3-18a.

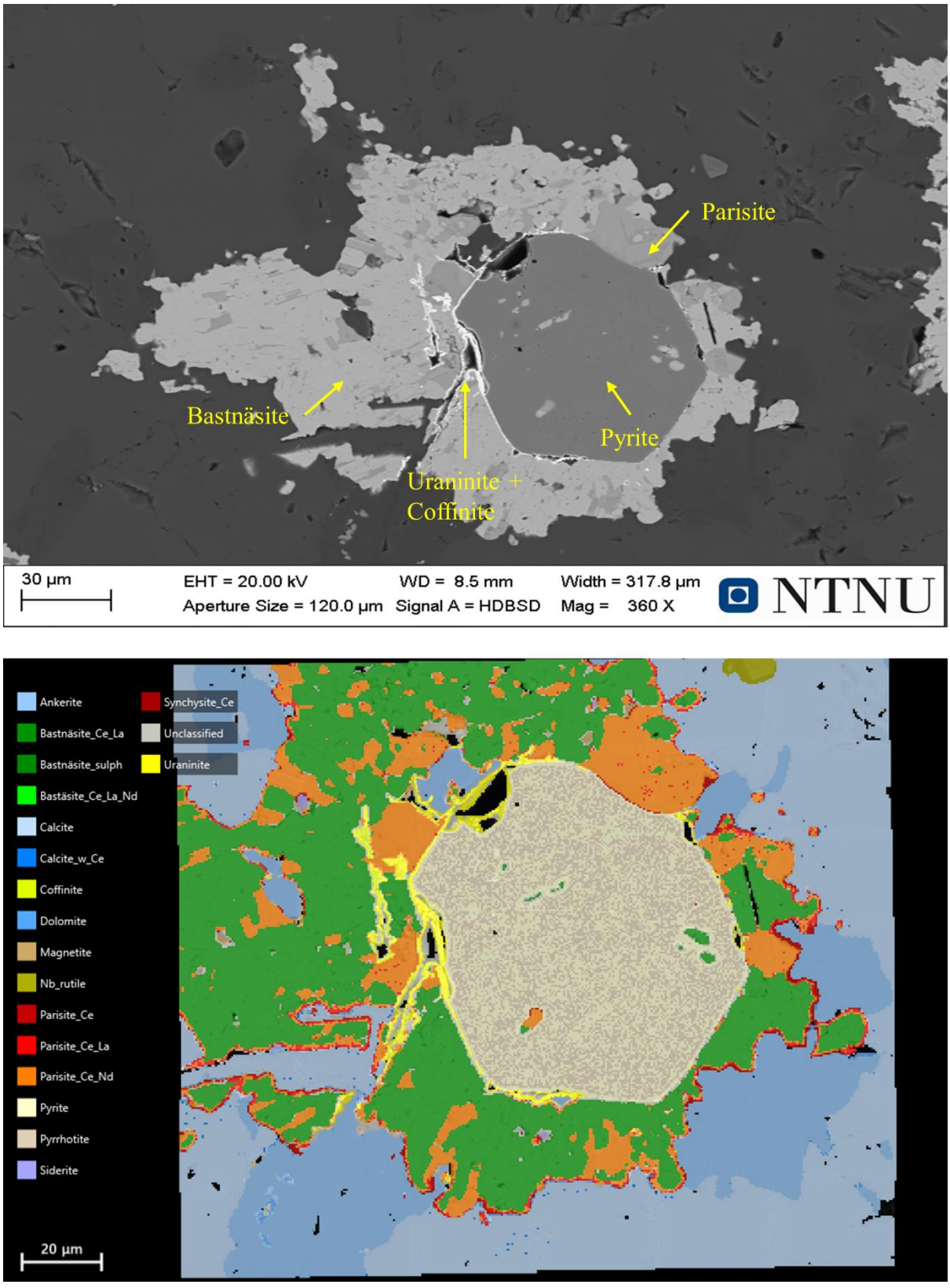

Figure 3-35 Shows the second detail map for specimen 6_2 in EBS (top) and AM (bottom). It shows uranium minerals covering the surface of a pyrite grain, while also covering the boundaries of REE mineral grains.

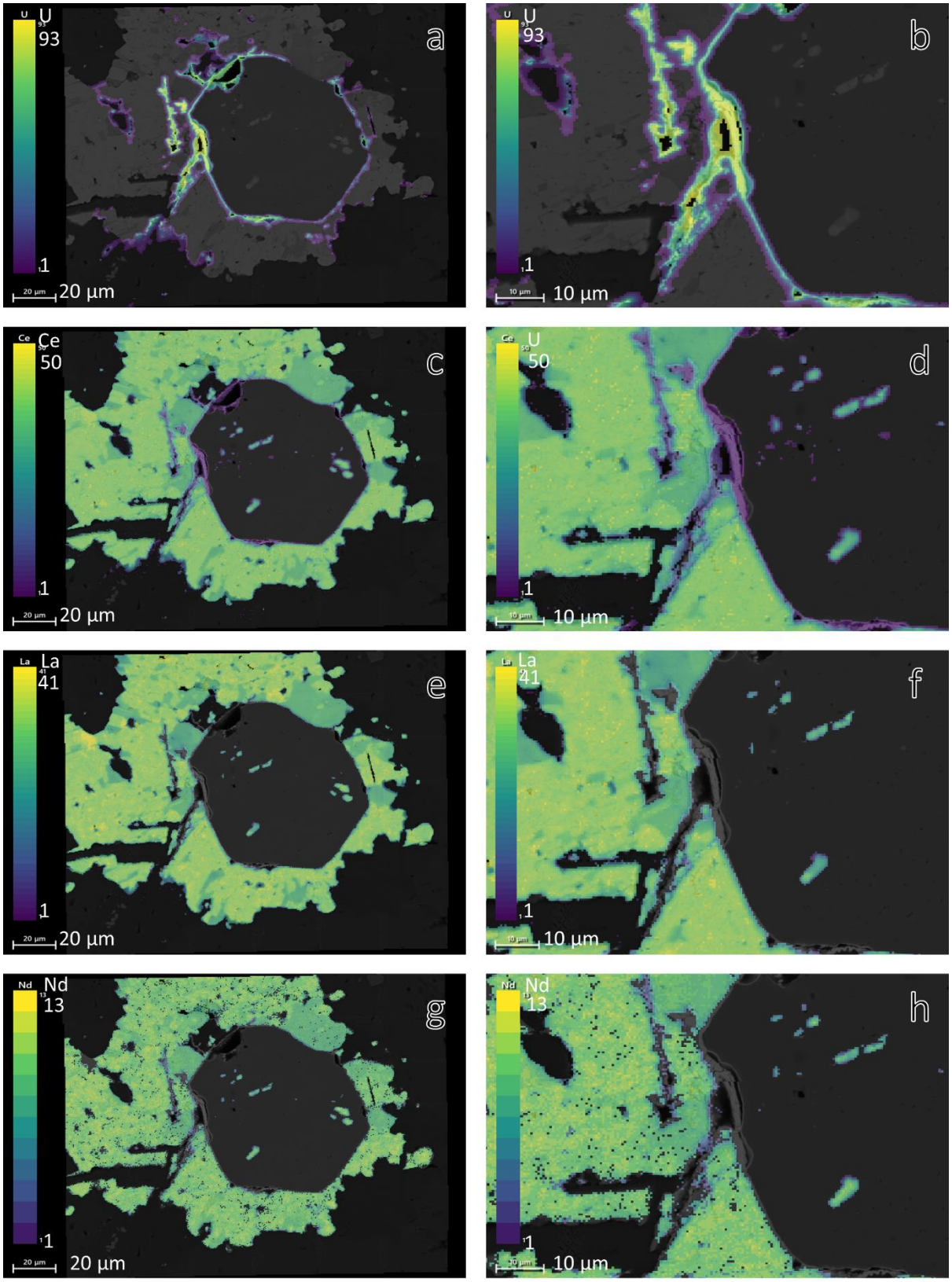

Figure 3-36 Shows four different heat maps from the uranium 6_2 detail map. a) Heat map for uranium and a closer look at the grain boundaries (b). c) Heat map for cerium and with a closer view (d), shows some cerium in the uranium minerals. e) Heat map for lanthanum with a closer look at the grain boundaries (f). g) Heat map for neodymium with a closer look at the grain boundaries (h).

In specimen 6_3 (Figure 3-37) there were less thorite and more of the surrounding area covered, consisting of chlorite, apatite, and monazite with grains within apatite. Thorium is still in high concentrations in thorite and low concentrations along grain boundaries of monazite (Figure 3-38a-b). The REEs (Figure 3-38c-h) continue to show a consistent occurrence compared to the previous detail maps. Cerium appears in the surrounding minerals to the monazite grains, including in thorite. There is significantly less neodymium present, it is within the monazite and low concentrations in the thorite. Lanthanum remains the same of only appearing within a REE mineral.

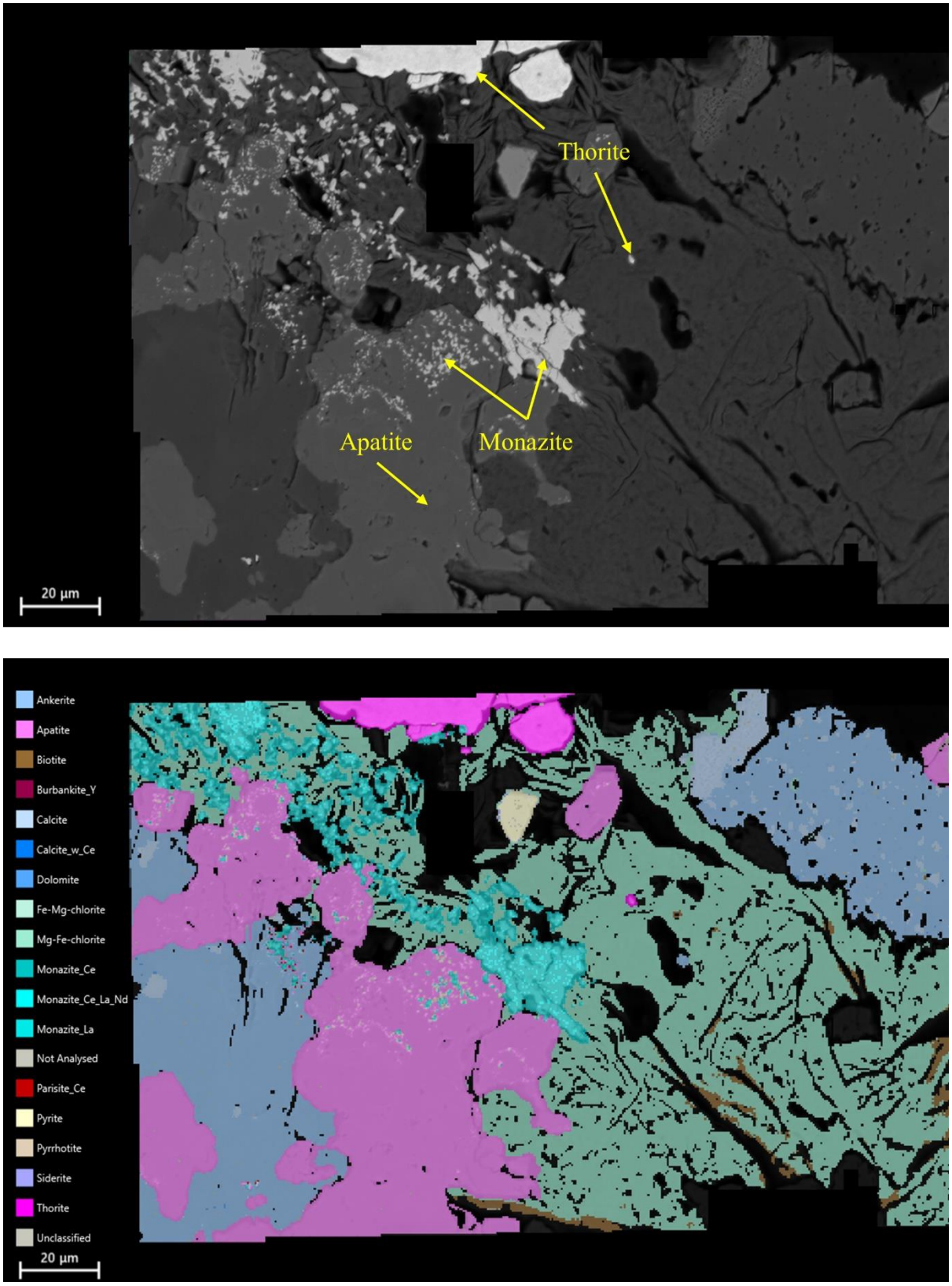

Figure 3-37 Shows the detail map for specimen 6_3 in EBS (top) and AM (bottom). The thorite grain is located top middle, and the surroundings shows monazite, chlorite, and apatite.

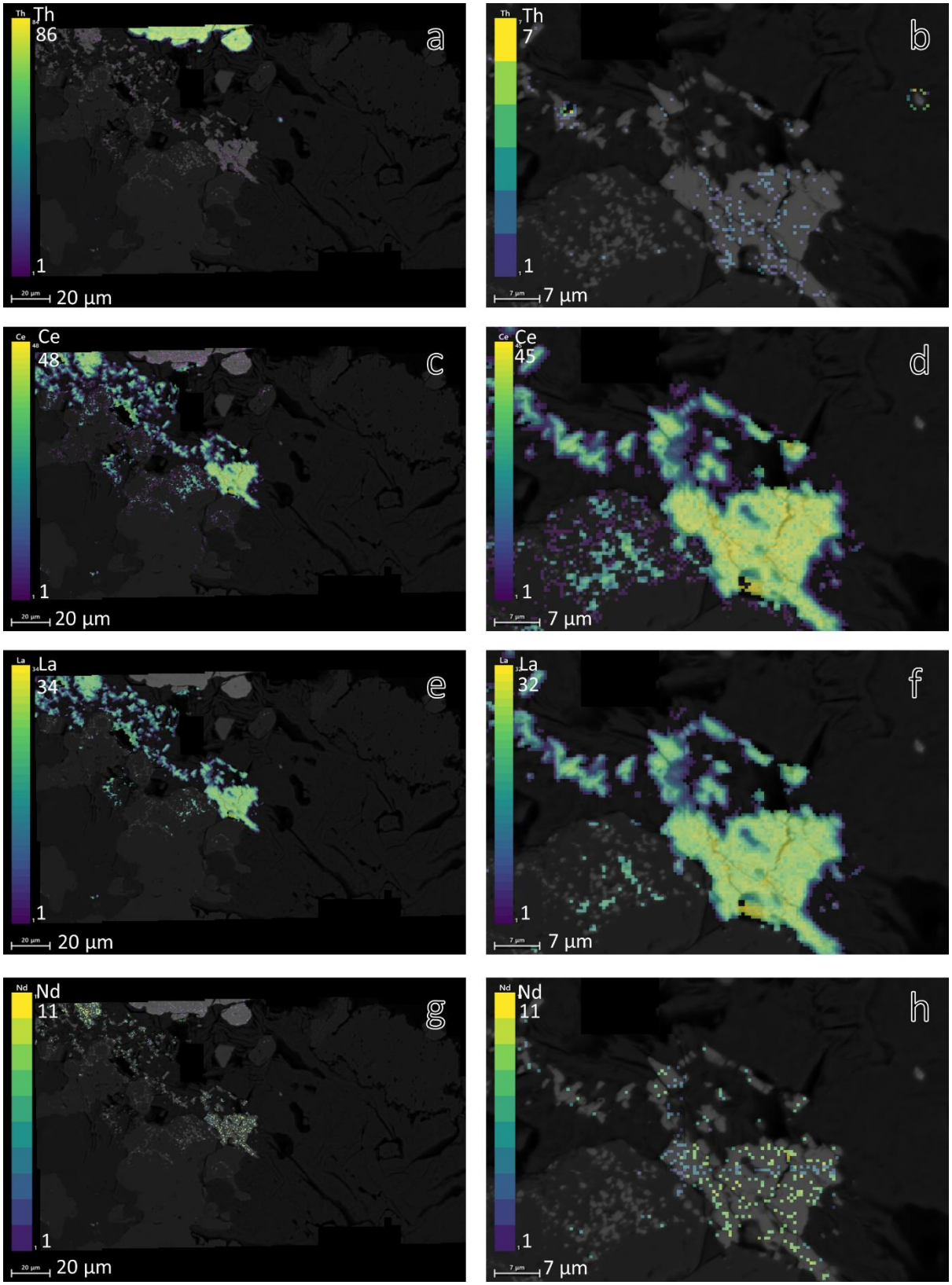

Figure 3-38 Shows four different heat maps from the 6_3 detail map. a) Heat map for thorium and a detailed view of the monazite (b). c) Heat map for cerium with a detailed view around the monazite (d). e) Heat map for lanthanum and a detailed view around a monazite grain (f). g) Heat map for neodymium and view around a monazite (h).

4 Discussion

4.1 Sorting

The sorting shows that specimens with more red mineralized grains (Figure 3-5) might contain higher amounts of thorium. The pyrite rich specimen does not seem to contain higher amounts of uranium. Textural category 3 and 4 seems to give specimens with higher REE content, likely because more mineralisation means more possible REE. It is hard to say with only the 12 specimens if light or dark red can be used to indicate thorium content. Based on the thorium content in the specimens (Table 3-3) it can be concluded that sorting based on radioactivity does indicate thorium content to a certain degree.

4.2 Optical microscopy

Only using optical microscopy will not be suitable to characterise thorium and uranium in the future. It is possible to find the larger thorite, uraninite and coffinite grains (Figure 3-7), but Figure 3-28 shows that a large amount of grains are smaller than 3.5 µm, which would make it exceedingly difficult to find in specimens with only such small grains. Therefore, is optical microscopy not an effective way to characterise the thorium and uranium minerals. Optical microscopy does give a rough idea about minerals and textural characteristics present, but it fails to give a detailed overview of the variations present in each specimen.

4.3 XRD & XRF

The XRD (Table 3-2) shows little to no thorite, but in the two specimens where it was picked up do correlate with the two specimens with the highest amount of thorium in the XRF (Table 3-3). It seems that specimen with somewhere less than 500 ppm thorium might not be detected. No uranium minerals were identified. This might be because of how little uranium there is in each specimen. Therefore, should XRD be considered a poor method for detecting thorium and uranium minerals.

The XRF (Table 3-3) shows that there is a general increase in thorium and uranium according to sorting class placement. This is further supported when combining class and radioactive measurements taken on the crushed specimen (Table 3-1). Most of the lower radioactive readings correlate to a lower thorium and uranium content. This method does not give any kind of textural information, but it seems to identify both thorium and uranium well.

4.4 ICP-MS

The normalized ICP-MS results (Figure 3-8) show a trend that corresponds to previous data from the Fen area. There are a few outliers in gadolinium, terbium, and erbium that do not appear in previous Fen data. Comparing it to mineralized Bayan obo zones does show that most of the results are within that zone. The lower Bayan obo results also show a small trend towards an increase in gadolinium, but the increase in erbium does not seem to appear anywhere else.

Comparing the trace element analysis with available elements in the ICP-MS (Figure 3-9) indicates that both methods give consistent results on the available element and are likely reliable to detect these elements.

The correlation between TREE and thorium (Figure 3-10)/ uranium (Figure 3-11) does show that the five specimens contained high amounts of REEs compared to samples taken in the surrounding area. The correlation data shows the same result as presented in previous works (Dahlgren, 2019). There seem to be a weak correlation between REE and thorium/ uranium in lower concentrations. The correlation fades with increasingly higher concentrations of both groups. This indicates that the possible texture sorting correlation might not be indicative to increased thorium content. More specimens would have to be sampled to further confirm or deny the texture and colour correlation to thorium and uranium.

4.5 µCT

Direct comparison between µCT and automated mineralogy proved difficult with the current data because the core was not cut exactly along the 3D model axis. That is why the model had to be carefully adjusted to match the thin-section visually. Because the slice was not an exact match, it proved hard to make detailed distinctions. The low amount of large thorite, uraninite and coffinite grains (Figure 3-26, Figure 3-27) combined with the low amount of thorite in the specimen (Table 3-3) made it difficult to make distinct mineral classes. Also because thorite density is not too distinct from the surrounding minerals (Table 2-4) made it hard to narrow down without any large grains to go by.

Comparatively, uranium has a much higher density which theoretically makes it easier to separate. This was not possible because of the lack of identified grains in both core thin-sections (Figure 3-27, or size distribution (Appendix IV)).

µCT does not show the distinction of REEs accurately because of the low distinction between REE minerals and some of the surrounding minerals (Table 2-4). It is also hard to distinguish because of the densities vary depending on what REE is included in each mineral.

The result proves that the method can be used to give a general indication of abundance in the core for the radioactive minerals (Figure 3-16), but an understanding of the specimen analysed is required to decide what resolution the model will need to accurately depict the grain size. More research with a specimen containing higher amounts of thorium, uranium would need to be done to decide if µCT is viable to separate the exact radioactive minerals.

4.6 SEM-base automated mineralogy (AM)

In total three different step-sizes were used, each covering progressively less of each specimen. The OV maps did not depict the complicated intergrowth between REE minerals and the small thorite, uraninite and coffinite grains, which is corroborated by the total grain size histograms (Figure 3-28) being much smaller than 20 µm. It presents an approximate image of the REE minerals, but some inaccuracies are expected (Figure 3-18). The BPS maps were the backbone of this thesis, the step-size of 3.5 µm seems to have been adequate to identify most grains while still covering the entire specimen. The smallest radioactive grains did not get included (Figure 3-31 and Figure 3-33), this unnoticed fraction likely to makes up a tiny fraction of total uranium minerals. Considering how little the total fraction of thorium and uranium are in each specimen, (Table 3-7) it likely does not present any considerable inaccuracies. The detail maps depict the complicated mineralogy very well, and the heat maps for each element indicate where they are found. The same heat map was tried on the larger sized maps but did not produce any significant information.

4.6.1 Associations

The associations of Thorite (Table 3-4) show great variation between each specimen, but there is a visible increase in certain minerals compared to others, mainly quartz and calcite. Uraninite (Table 3-5) and coffinite (Table 3-6) are both consistently associated with pyrite and calcite, with uraninite having a higher REE mineral association.

There is a noticeable unclassified category and is likely the result of the step-size. The surrounding pixels are made up of grain boundaries between the radioactive minerals and the surroundings. This also correlates with the radioactive minerals having a very fine grain size.

4.6.2 Element distribution

The total area covered by each element (Table 3-7) is based on a few assumptions, first that every particle of said element should have been detected properly, and secondly that the area scanned for BPS and OV are identical. Otherwise, the estimate will be inaccurate, based on comparisons between BPS and the detail maps it can be surmised that not every small grain was accounted for in the BPS. This is again likely a very small fraction and would not have changed the area percentages by any significant margin. It might even out the estimate anyway because this will always be an overestimation. This is a result of using pixel data and counting every pixel with thorium or uranium. If the pixel only contains small grains of trace amounts of thorium or uranium, then it will still be registered as the full pixel size. This is corroborated by the grain size distribution (Figure 3-26, Figure 3-27), as a significant portion registers as the step-size. The calculated area should therefore only be taken as an estimation. Combining the estimation (Table 3-7) with the XRF and ICP-MS results shows a somewhat similar thorium correlation between the specimens, this implies it can be used to represent the specimens.

Element distribution for thorium and uranium is based on the BPS maps and is therefore only representing the bright thorite, uraninite and coffinite minerals. This might lead to an inaccurate element distribution as thorite inclusions in other minerals might not have been registered, this in turn, would present a distribution favouring thorite, uraninite and coffinite.

4.6.3 Grain size distribution

Grain size distribution presents a differing image in comparison to the element distribution. This is because it counts grains and not pixels, so larger grains of thorite would still only be one count and grains of other minerals with only a fraction of thorium would count the same as that thorite. Therefore, it leads itself to show more of the surrounding minerals. It is likely that the large 3.5 fraction is overrepresented in thorium because of the already mentioned peak overlap error. If there are two different thorite classifications within the same grain, then it would report as two separate smaller grains. The smallest grain size in Figure 3-28 is therefore likely overrepresented.

4.7 Thorium, uranium & REE occurrence

4.7.1 Thorium

The thorium distribution graphs (Figure 3-19, Figure 3-20, Figure 3-21) indicate that the majority of thorium is thorite, and only small traces in other elements. Notably, there is

reported more quartz and unclassified in the lower categories. It is likely that this is because the grains are smaller in those specimens and would therefore be easier included within other pixels and not be properly registered.

The most consistently associated mineral between the specimens is calcium carbonates and quartz (Table 3-4), but they seem to decrease with an increase in thorite. The associations do show that there is great variation between specimens. A general decrease in unclassified pixels is likely because there are more sizable thorite grains that better match the step-size and more thorite to calculate associations for. Additionally, the thorium correlation towards the TREE (Figure 3-10) shows little correlation in higher TREE concentrations. The results place every specimen that were tested in ICP-MS to be higher than the majority of similar specimen taken in the Fen area. It is unknow if this is because preparation errors or simply that the concentration in the five are higher than their surroundings.

Thorite grain sizes (Figure 3-28) vary from 3.5 µm up to 100 µm, with the main fraction being under 50 µm and a very small fraction of outliers between 200 and 400 µm. Thorium distribution based on grain size (Figure 3-29) indicates that the smallest fraction consists of a large part thorite with a small fraction as parisite inclusions. While thorite still makes up most of the thorium, it likely can be found as small inclusions in the surrounding minerals.

The two detail maps (Figure 3-32 and Figure 3-37) indicate that thorium shows up as mainly thorite and in very low concentrations along the REE minerals boundaries and cracks. That means that the thorium distribution would likely pick this up in some areas, and that is why it might sometimes be seen as inclusions in the REE minerals. Based on the heat map of specimen 6_2 (Figure 3-33) and specimen 6_3 (Figure 3-38), it can be concluded that the thorium content in the cracks along the REE minerals is variable and could possibly coincide with the size of the thorite grains. It might be possible to see the thorium in the cracks when it occurs in some areas, this is likely the some of the strands visible in optical microscope (Figure 3-7).

The same heat maps also show small inclusions of cerium and neodymium in the thorite minerals. This might corroborate the theory that thorium came from the REE enriched fluid observed in the area.

Therefore, can SEM-base automated mineralogy be a useful tool when classifying thorium and viewing overview and textural information when the step-size fits to the grain size.

4.7.2 Uranium

Uranium distribution (Figure 3-22, Figure 3-23, Figure 3-24) indicates that the majority of uranium occurs as uraninite and coffinite and a small minority in other minerals. Some specimens show larger variety, but it is likely that these are small grains not correctly identified or possibly the halo surrounding some larger uranium grains seen in the detail maps (Figure 3-31 and Figure 3-36). Grain size distribution (Figure 3-27) shows a more inconsistent spread that indicates variation between specimens. Total grain distribution (Figure 3-28) shows a similar proportion to thorium with coffinite consisting of more large grains and more grains in general. It seems that no grains except a few outliers are over 50 µm in size.

The detail maps show that there is no uranium within the pyrite grains they coat around (Figure 3-31d-e, Figure 3-36a-b). The coffinite in 6_3 also coats cracks in the surrounding REE minerals while showing no uranium in these minerals except the small low concentration halo, indicating that it came after both the sulphide rich fluid and presumedly late in the REE enriched fluid. Similarly, it also forms in cracks in the pyrite grains (Figure 3-18).

The halo seen in the heat maps is likely the reason for the brown halo seen in the optical microscope (Figure 3-7). Other than the low concentration halo, there seems to be no uranium in the surrounding minerals. Because the BPS map does not pick up every small grain (Figure 3-31b), it is likely that most minerals containing uranium are tiny uraninite and/or coffinite grains not correctly classified because of grain size or grain boundaries. In 6_1 there are two visible phases of coffinite separated by phosphorus content (Figure 3-31h) and a slight difference in uranium content.

Distribution by grain size (Figure 3-29) shows that uranium is detected largely in surrounding minerals with under half being detected as uranium minerals. This is likely because of the small grain size observed in each specimen. There are small fragments within or along the edges of the larger grains that are picked up as an inclusion rather than its own mineral because of the step-size. This could be the reason for how few uraninite and coffinite are found in the largest fraction, not to mention that the surrounding minerals are likely larger, thus “crowding” in the larger fraction.

There are less uranium minerals observed in each specimen compared to thorite (Figure 3-28), and this might negatively affect the associations. A smaller sample size means less

certain results. There are similar associations between uraninite (Table 3-5) and coffinite (Table 3-6), pyrite and calcite are consistently high throughout every specimen, with only a few outliers. Ankerite also has a higher association, more so in uraninite. The REE minerals, mainly parisite/ bastnäsite, a small fraction of monazite, also have a higher association with uraninite and significantly less with coffinite. There are consistently more unclassified associations for coffinite, but it is still present for uraninite. Because the general grain size is so low that the surrounding pixels often contain the grain boundaries and end up as unclassified.

Figure 3-11 indicates that there is a large variation between uranium and the REEs, and there might be a connection at lower TREE and uranium concentrations, but it does not seem to correlate with higher concentrations.

This indicates that SEM-based automated mineralogy is usable for detecting uranium when combined with some previous general knowledge of the material.

4.7.3 REEs

The OV maps are the basis of the REE distribution and will therefore not be able to fully represent the tightly intergrown network of parisite and bastnäsite and small grains because of the large step-size (Figure 3-18). The large step-size should be taken into consideration when viewing the REE distribution results.

Because of a bug in the mineralogic reporter program it was not possible to create the same graphs for lanthanum as the rest of the REEs. Instead, an assumption is made based on bulk data from each specimen (Appendix IV), it shows that most of the lanthanum is within bastnäsite, monazite and parisite. It also shows a small fraction in the quarts REE mixes, a grain boundary mix meaning that it is picking up pixels containing multiple grains. It is not possible to identify which of these minerals it mainly occurs in from the bulk data. From the detail maps it is observed no lanthanum within the thorite, uraninite and coffinite grains.

Total cerium distribution (Figure 3-25) indicates that cerium is mainly within parisite. It is also in smaller quantities in bastnäsite and monazite. This is consistent with some variation between each specimen. In the high radioactive specimens, there seems to be more lanthanum in the associated parisite. Otherwise, it only occurs in very small percentages in other minerals, which may be because of step-size considering how there is no traceable cerium in the surrounding minerals of the detail maps (Figure 3-31 and Figure 3-33), except contrary to lanthanum there is low concentrations of cerium in the thorite, uraninite and coffinite.

Praseodymium is distributed (Figure 3-25) almost exclusively in the carbonates (mainly ankerite) but also a small percentage in quartz. It is consistent between each specimen with some variation in what carbonates are strongly represented. It is possible that this is not entirely accurate because of the large step-size.

Total neodymium distribution (Figure 3-25) indicates that it is found firstly in parisite, this remains constant in every specimen. In low radioactive specimens, it is found in synchisite and calcium carbonates, with only a small fraction being in bastnäsite/ monazite. Every other specimen shows the second highest mineral to be calcium carbonates or bastnäsite and monazite. From the detail maps (Figure 3-33 and Figure 3-36) it is observed that neodymium can be included within the radioactive minerals but in even smaller concentrations than cerium.

Samarium is distributed (Figure 3-25) mainly in the calcium carbonates (calcite and ankerite), apatite and quartz. There is larger variation between the specimens in the lower radioactive category and lower measured thorium, they also show less apatite. The medium and large radioactive groups shown an increase in apatite. Only a small fraction samarium is found within any REE minerals namely parisite and bastnäsite. These REE minerals occur in nearly every specimen with some variation in concentration.

4.8 Errors, inaccuracies & improvements

Sorting had variations in the measuring of each specimen because of several reasons. First, is the time it took to reach a stable reading. If taken too early, it could misrepresent the specimen. Second, not every specimen had an even surface meaning radiation might not be picked up in its entirety. Third, specimen size makes a difference because more material to emit radiation. Most of the specimens were of similar size, there were outliers like specimen 6_4. Forth is different measuring areas. Some specimens could produce different results depending on where the detector was placed (Figure 3-3). To reduce the uncertainties, some guidelines should be made, including a specific wait time before writing a result and multiple readings per specimen. This would significantly increase work time, so a balance will have to be struck. The radioactive sorting criteria were created early on in this thesis and should likely be revaluated by increasing the high category to further differentiate and represent each category better.

The XRD (Table 3-2) gave poor results, possibly a result of preparation errors when preparing the material for the differing tests. If this is the case, then it is likely to be in the

final steps for XRD because the XRF (Table 3-3) and other methods that used the crushed material gave viable results. The only specimens that picked up any thorite were the two specimens with the highest amount of thorium in them. This suggests that there might be too little thorium in the other specimen to properly identify. There is the possibility that the material used in the chemical tests was not indicative for the entire specimen. This is unlikely as the BPS area estimation (Table 3-7) also shows similar results for the thorium, uranium does not show the same correlation.

The ICP-MS outliers could have been a result of not dissolving the material completely in the preparation stages. This is unlikely because the solution used with the material has previously been used on Fen material. The µCT would need a proper setup to precisely cut the core adjusted based on the 3D model axis. This should increase accuracy and, therefore the viability of µCT.

In SEM-base automated mineralogy (AM), every mineral classification is based on a list made by the operator based on normalized weight percentage for each mineral. Most mineral assemblages have minute differences that can affect the results presented. To get the most accurate result, the list is edited to fit that source. This creates some uncertainties because of operator bias and the risk of overfitting the list. To reduce the risk of wrongfully classifying minerals, the list is reiterated after observing the results to improve the accuracy.

Step-size compared to mineral grain size is important. If the grains are significantly smaller than the step-size, then they might not be analysed correctly and could appear as inclusions or not at all. This could misrepresent an element and make it appear to occur within another mineral, as can likely be seen in the element distribution results; otherwise, they can be classified as unclassified. To reduce the unclassified category, multiple mineral mixes were made with the intent to represent these unclassified areas. Reducing the step-size will also reduce inaccuracies and the need for mix classifications at the cost of massively increased time. Therefore it would not be feasible to fully classify every specimen at the smallest step-size. This is the reason that each AM map covers less area than the maps before it and works as a compromise.

The misidentification of thorium as silver and much lesser degree cadmium was caused because of a peak overlap. This resulted in low concentrations of thorium would be misclassified. Extra thorite classes were made to catch the wrongfully classified pixels where thorite was replaced with the other elements. The peak overlap was heavily reduced in the

second round when the electron beam was lowered to 15 W. This reduced the error but did not fix it. The thorium and uranium mineral associations have a notable unclassified category, which could have been reduced by reducing the step-size or make other mineral mixes. This was not done because of the size of the majority of the grains was so low that there was a considerable risk of overfitting the list, it was also not done because of time constraints and the unclassified group being comparatively small in every specimen.

5 Conclusion

Thorite makes up a large fraction of all thorium with only very low thorium concentrations along REE mineral cracks and grain boundaries. The majority of thorite grains are below 50 µm except a few outliers with sizes no larger than 400 µm. There seems to only be a low correlation between TREE and thorium at low concentrations of both. The thorite grains are mainly associated with the calcium carbonates (calcite and ankerite) and quartz.

Uranium occurs as two main minerals, uraninite and coffinite, and is not seen in any large capacity outside of these. Most uranium grains are below 25 µm, with few outliers that can reach 100 µm. The uranium grains are consistently associated with pyrite and calcite but are not included in those minerals. The same trend as thorium when correlated towards the TREEs, there is an even lower correlation at low concentrations, and it is shaky at best.

The specimens have high LREEs, mainly lanthanum, cerium, and neodymium. These three are found in the known REE minerals of parisite, bastnäsite, monazite, and to a lesser degree, synchysite. The remaining praseodymium and samarium are mainly found in calcium carbonates, quartz, and apatite for the latter.

The radioactive minerals were identified in an optical microscope when larger grains were present. XRD proved insufficient to measure the thorium and uranium minerals. XRF did properly detect both thorium and uranium but did not include every REE. ICP-MS did sufficiently pick up the REEs, thorium and uranium. µCT might be a viable way to gain textural knowledge of thorite, uraninite and coffinite minerals if most grains are within the resolution size. It does require thin-section that depicts such grains to create such an accurate depiction or another way to accurately reference these grains. It is less effective to classify the REE minerals because there are density variations within the group and the surrounding minerals have densities that closely match these variations. Sem AM proved useful at detecting thorium, uranium and providing an overview of associations, element distribution and textural information when it matched closely to the grains in step-size. Some previous knowledge is therefore required to present an accurate result from this method.

6 References

Alstad, J., & Bjørnstad, T. (2020). Thorium. In *Store norske leksikon*. http://snl.no/thorium

Anders, E., & Ebihara, M. (1982). *Solar-system abundances of the elements*. 18.

Andersen, T. (1986). Magmatic fluids in the Fen carbonatite complex, S.E. Norway. *Contributions to Mineralogy and Petrology*, *93*(4), 491–503. https://doi.org/10.1007/BF00371719

Barthelmy, D. (1997). *Mineralogy Database*. Mineralogy Database. http://webmineral.com/

Brøgger, W. C. (1921). Die Eruptivgesteine des Kristianiagebietes. IV: Das Fengebiet in Telemark, Norwegen. By W. C. Brøgger. Vid. Selsk. Skrifter I.M.N.Kl. No. 9, pp. 1–408. 1920. *Geological Magazine*, *58*(12), 549–554. https://doi.org/10.1017/S0016756800105217

Chakhmouradian, A., & Wall, F. (2012). Rare Earth Elements: Minerals, Mines, Magnets (and More). *Elements*, *8*, 333–340. https://doi.org/10.2113/gselements.8.5.333

Chen, X.-A., Cheng, Y.-E., & Rong, Z. (2005). Recent results from a study of thorium lung burdens and health effects among miners in China. *Journal of Radiological Protection*, *25*(4), 451–460. https://doi.org/10.1088/0952-4746/25/4/007

Coint, N., & Dahlgren, S. (2019). *Rare earth elements (REE) in two long drill-cores from the Fen Carbonatite (2019)* (2019.008). NGU.

Dahlgren, S. (2012). *Thorium i fensfeltet—Ressursanslag.pdf* (p. 23). https://www.nome.kommune.no/_f/p9/i701ace19-9fb2-4e41-bab2-7b69c6f7f5c2/ressursanslag_thorium_i_fensfeltet.pdf

Dahlgren, S. (2016). *Fensfeltet. Kjerneboringer Tufte 2016.* (p. 20p) [Regiongeolograpport 1-2016].

Dahlgren, S. (2019). *REE mineralization in the Fen Carbonatite Complex*. Buskerud Telemark Vestfold County Councils.

Deer, W. A., Howie, R. A., & Zussman, J. (1996). *An Introduction to the Rock-Forming Minerals* (2nd edition). Pearson.

Dietzel, C. A. F., Kristandt, T., Dahlgren, S., Giebel, R. J., Marks, M. A. W., Wenzel, T., & Markl, G. (2019). Hydrothermal processes in the Fen alkaline-carbonatite complex, southern Norway. *Ore Geology Reviews, 111*, 102969. https://doi.org/10.1016/j.oregeorev.2019.102969

Duchemin, C., Guertin, A., Haddad, F., Michel, N., & Métivier, V. (2015). Production of medical isotopes from a thorium target irradiated by light charged particles up to 70 MeV. *Physics in Medicine and Biology*, *60*(3), 931–946. https://doi.org/10.1088/0031-9155/60/3/931

Dushyantha, N., Batapola, N., Ilankoon, I. M. S. K., Rohitha, S., Premasiri, R., Abeysinghe, B., Ratnayake, N., & Dissanayake, K. (2020). The story of rare earth elements (REEs): Occurrences, global distribution, genesis, geology, mineralogy and global production. *Ore Geology Reviews*, *122*, 103521. https://doi.org/10.1016/j.oregeorev.2020.103521

Gauß, R., Burkhardt, C., Carencotte, F., Gasparon, M., Gutfleisch, O., Higgins, I., Karajić, M., Klossek, A., Mäkinen, M., Schäfer, B., Schindler, R., & Veluri, B. (2021). *Rare Earth Magnets and Motors: A European Call for Action. A report by the Rare Earth Magnets and Motors Cluster of the European Raw Materials Alliance*. 38.

Geiger, H., & Müller, W. (1928). “Das Elektronenzählrohr” [The electron counting tube]. *Physikalische Zeitschrift (in German)*, 839–841.

Goodge, J. (2016, October 11). *Back-scatter detector (BSE)*. Geochemical Instrumentation and Analysis. https://serc.carleton.edu/research_education/geochemsheets/bse.html

Guyonnet, D., Planchon, M., Rollat, A., Escalon, V., Tuduri, J., Charles, N., Vaxelaire, S., Dubois, D., & Fargier, H. (2015). Material flow analysis applied to rare earth

elements in Europe. *Journal of Cleaner Production*, *107*, 215–228. https://doi.org/10.1016/j.jclepro.2015.04.123

Jordens, A., Cheng, Y. P., & Waters, K. E. (2013). A review of the beneficiation of rare earth element bearing minerals. *Minerals Engineering*, *41*, 97–114. https://doi.org/10.1016/j.mineng.2012.10.017

JoVE Science Education Database. (2022). *X-Ray Diffraction for Determining Atomic and Molecular Structure*. X-Ray Diffraction. https://www.jove.com/v/10446/x-ray-diffraction

Ketcham, R., & Carlson, W. (2001). Acquisition, optimization and interpretation of X-ray computed tomographic imagery: Applications to the geosciences. *Computers & Geosciences*, *27*, 381–400. https://doi.org/10.1016/S0098-3004(00)00116-3

Kofstad, P. K., Bjørnstad, T., & Alstad, J. (2019). Uran. In *Store norske leksikon*. http://snl.no/uran

Liao, Y. (2007). Energy Peak Overlapping in EDS Spectrum. In *Practical Electron Microscopy and Database* (Second). Nortwestern University. https://www.globalsino.com/EM/

Mees, F., Swennen, R., Geet, M. V., & Jacobs, P. (2003). Applications of X-ray computed tomography in the geosciences. *Geological Society, London, Special Publications*, *215*(1), 1–6. https://doi.org/10.1144/GSL.SP.2003.215.01.01

Radiation Dosimetry. (2019, December 14). *What is Geiger-Müller tube—Geiger Chamber—Definition*. Radiation Dosimetry. https://www.radiation-dosimetry.org/what-is-geiger-muller-tube-geiger-chamber-definition/

Reimer, L. (1998). *Scanning electron microscopy: Physics of image formation and microanalysis* (p. 527). Springer.

Reisman, D., Weber, R., Mckernan, J., & Northeim, C. (2013). Rare Earth Elements: A review of production, processing, recycling, and associated enviromental issues. *U.S. Enviromental Protection Agency*. https://cfpub.epa.gov/si/si_public_record_report.cfm?dirEntryId=251706&Lab=NRMRL

Schulz, B., Sandmann, D., & Gilbricht, S. (2020). SEM-Based Automated Mineralogy and Its Application in Geo- and Material Sciences. *Minerals*, *10*(11), 1004. https://doi.org/10.3390/min10111004

Sæther, E. (1957). *The alkaline rock province of the Fen area in southern Norway*. Bruns Bokhandel i kommisjon.

Swapp, S. (2017, May 26). *Scanning Electron Microscopy (SEM)*. Techniques. https://serc.carleton.edu/research_education/geochemsheets/techniques/SEM.html

Thermoscientific. (2017). *RadEye B20 Operating Instructions Manual*. Thermo Fisher Scientific Messtechnik GmbH.

Thomas, R. (2008). *Practical Guide to ICP-MS: A Tutorial for Beginners, Second Edition* (2nd ed.). CRC Press. https://doi.org/10.1201/9781420067873

Wall, F. (2021). Rare Earth Elements. In D. Alderton & S. A. Elias (Eds.), *Encyclopedia of Geology (Second Edition)* (pp. 680–693). Academic Press. https://doi.org/10.1016/B978-0-08-102908-4.00101-6

Wibetoe, G. (2019). ICP – induktivt koblet plasma. In *Store norske leksikon*. http://snl.no/ICP_-_induktivt_koblet_plasma

Wirth, K., & Barth, A. (2020, January 21). *X-Ray Fluorescence (XRF)*. Techniques. https://serc.carleton.edu/research_education/geochemsheets/techniques/XRF.html

Yang, K., Fan, H., Pirajno, F., & Li, X. (2019). The bayan Obo (China) giant REE accumulation conundrum elucidated by intense magmatic differentiation of carbonatite. *Geology*, *47*(12), 1198–1202. Scopus. https://doi.org/10.1130/G46674.1

Yang, K.-F., Fan, H.-R., Santosh, M., Hu, F.-F., & Wang, K.-Y. (2011). Mesoproterozoic carbonatitic magmatism in the Bayan Obo deposit, Inner Mongolia, North China: Constraints for the mechanism of super accumulation of rare earth elements. *Ore Geology Reviews*, *40*(1), 122–131. https://doi.org/10.1016/j.oregeorev.2011.05.008

Appendix I – XRD & XRF

3_1

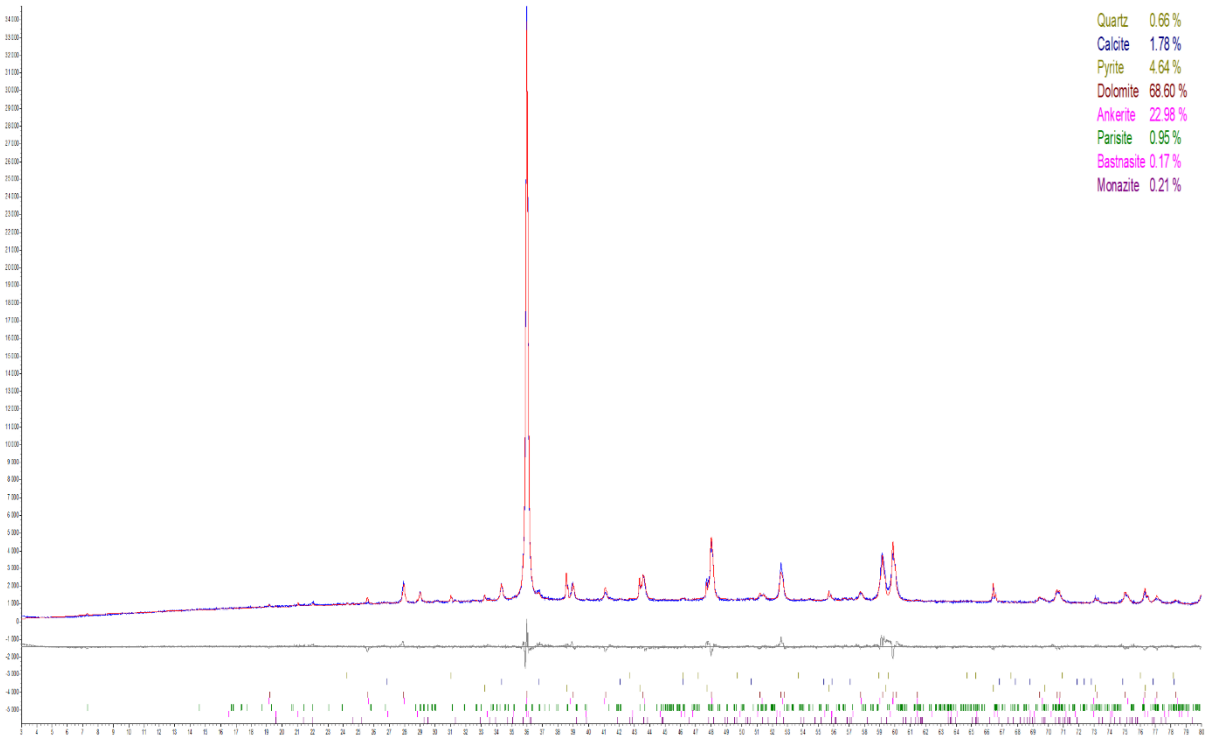

3_2

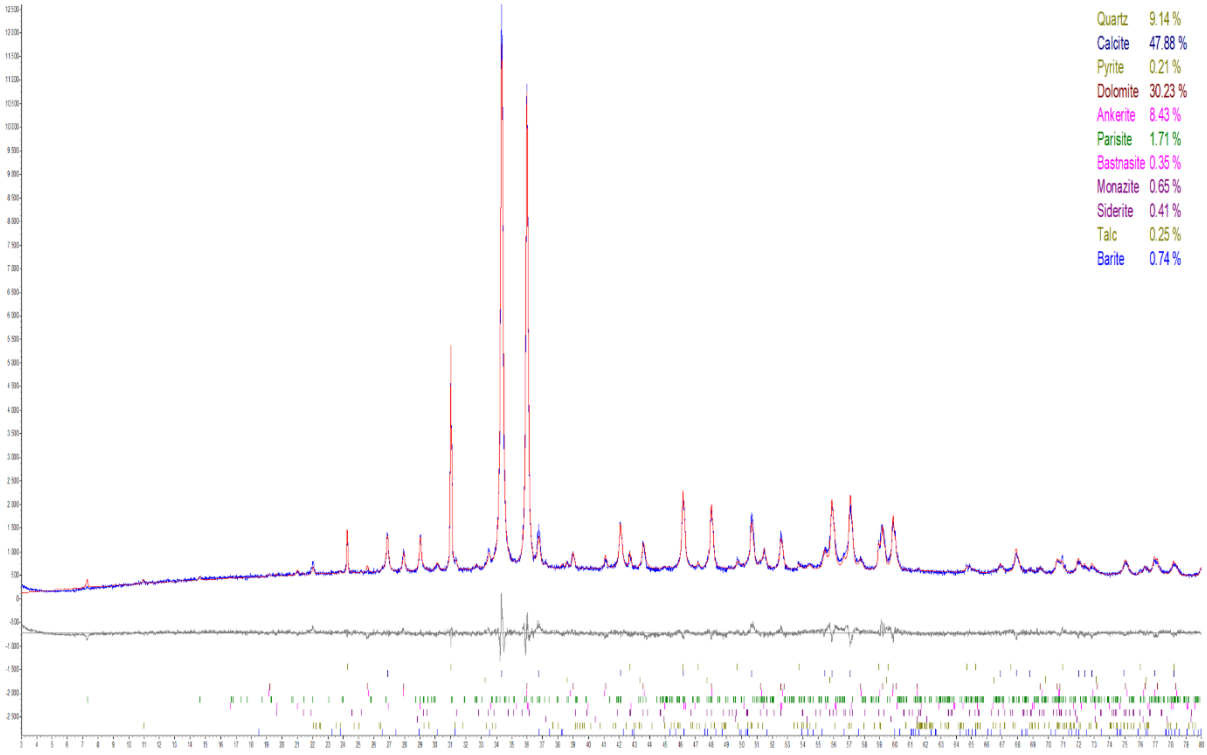

XRD results for specimen 3_1 and 3_2

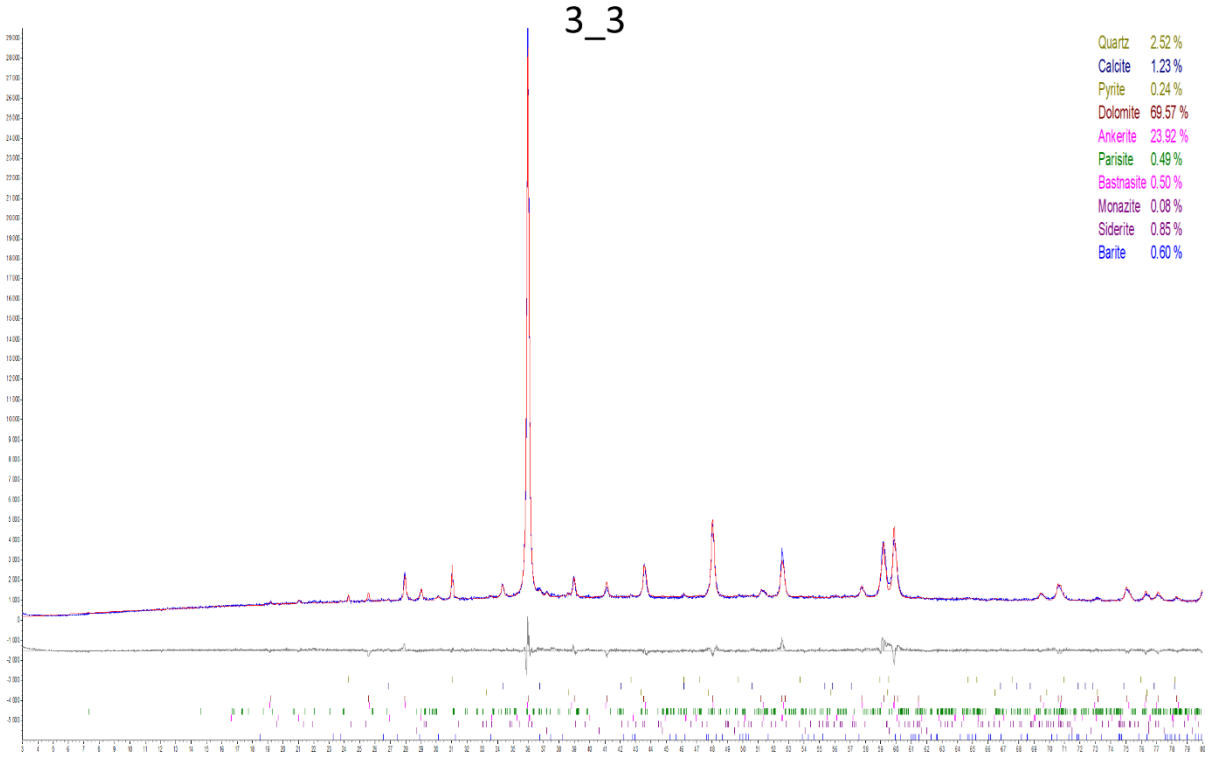

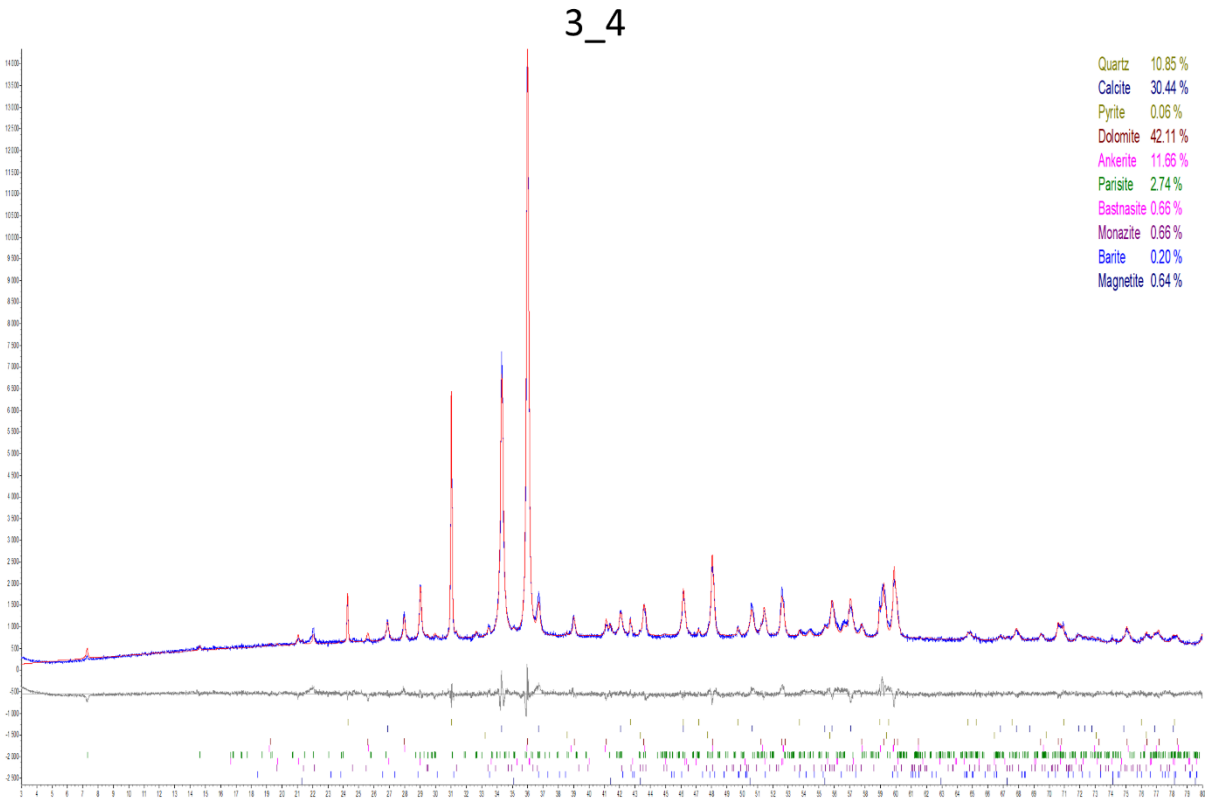

XRD results for specimen 3_3 and 3_4

3-6_1

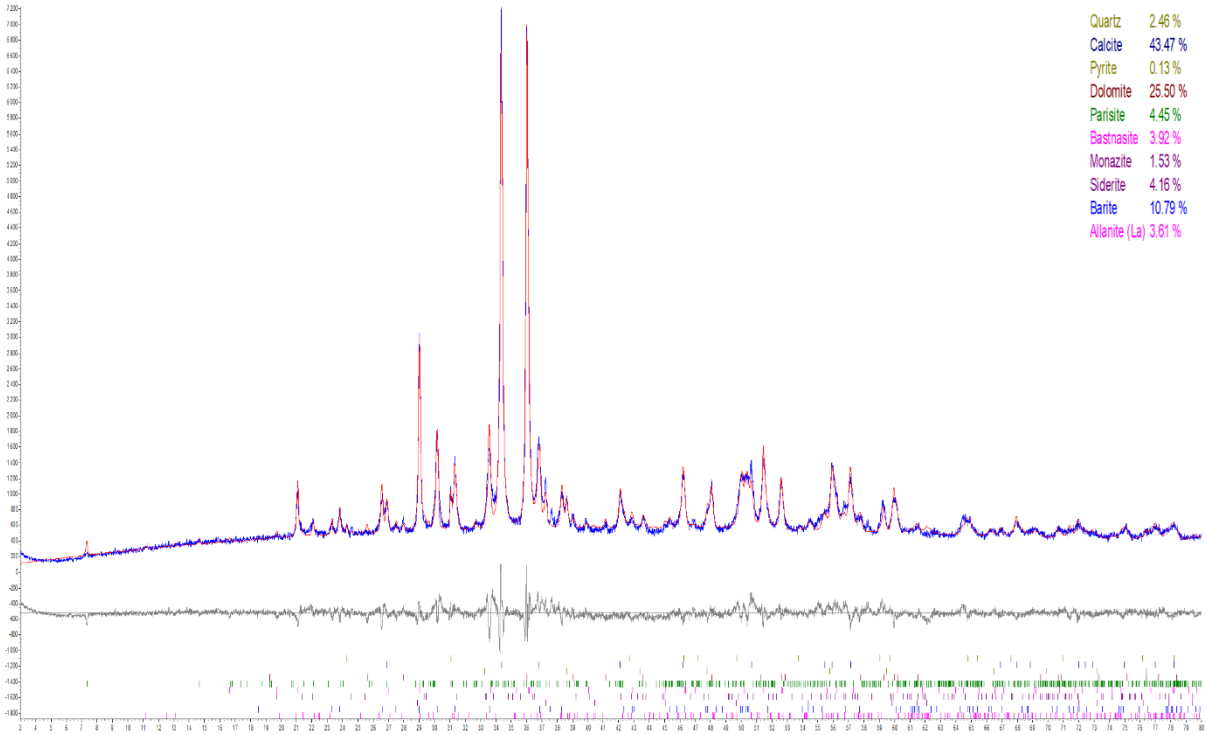

3-6_2

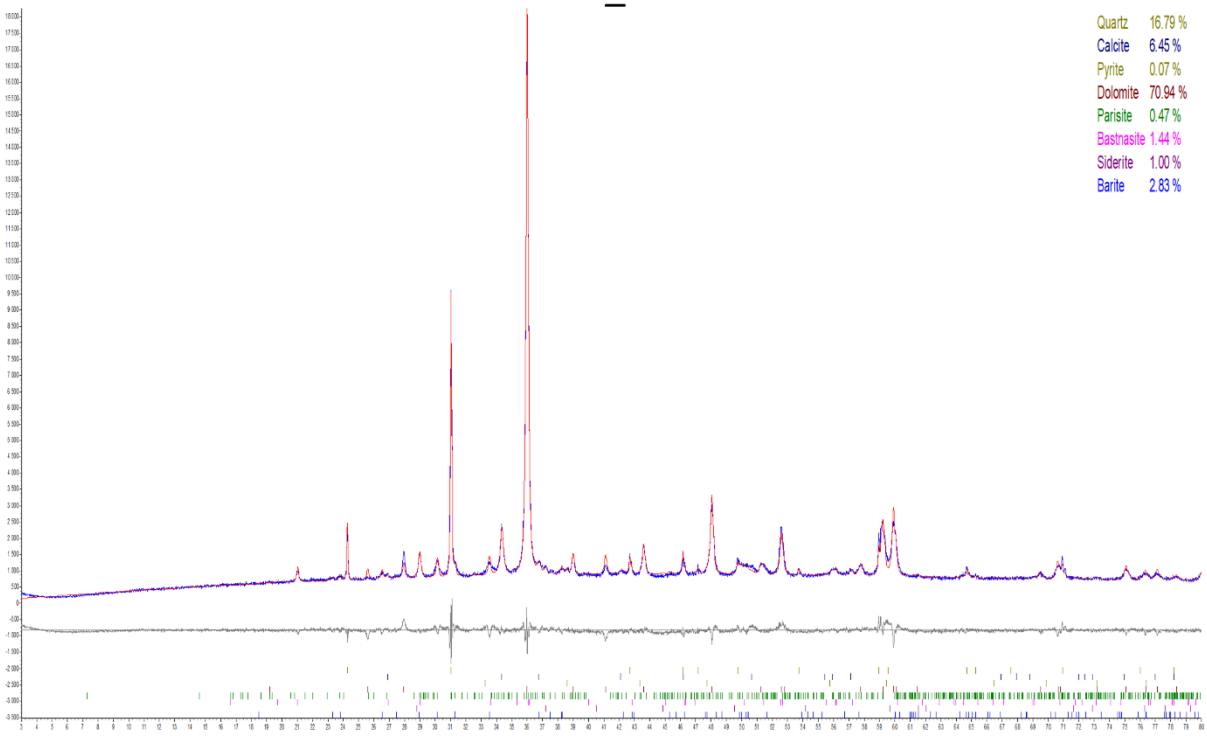

XRD results for specimen 3-6_1 and 3-6_2

3-6_3

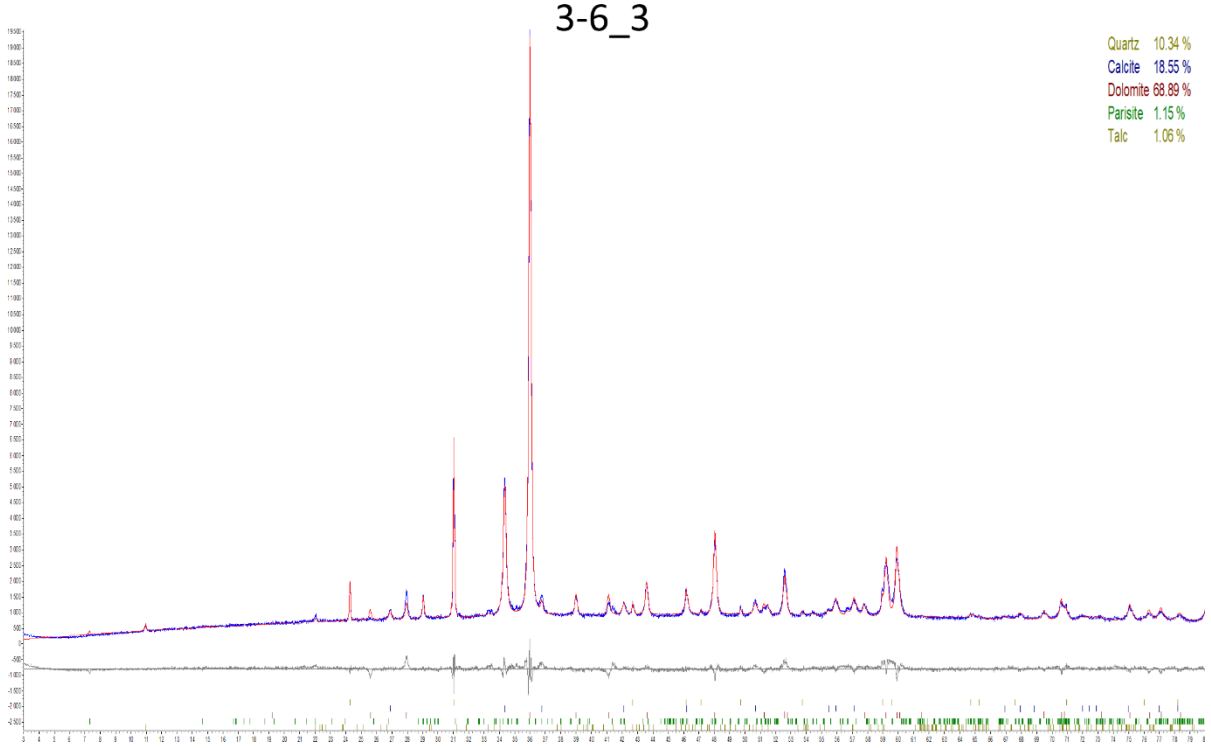

3-6_4

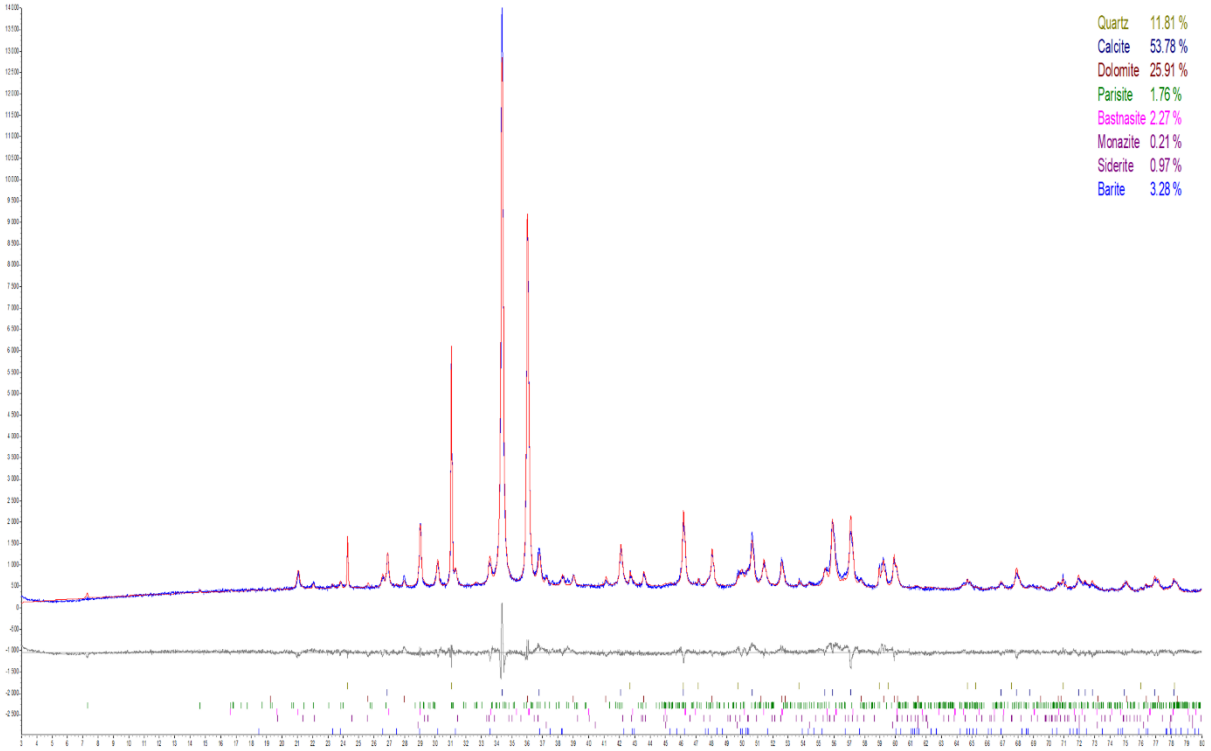

XRD results for specimen 3-6_3 and 3-6_4

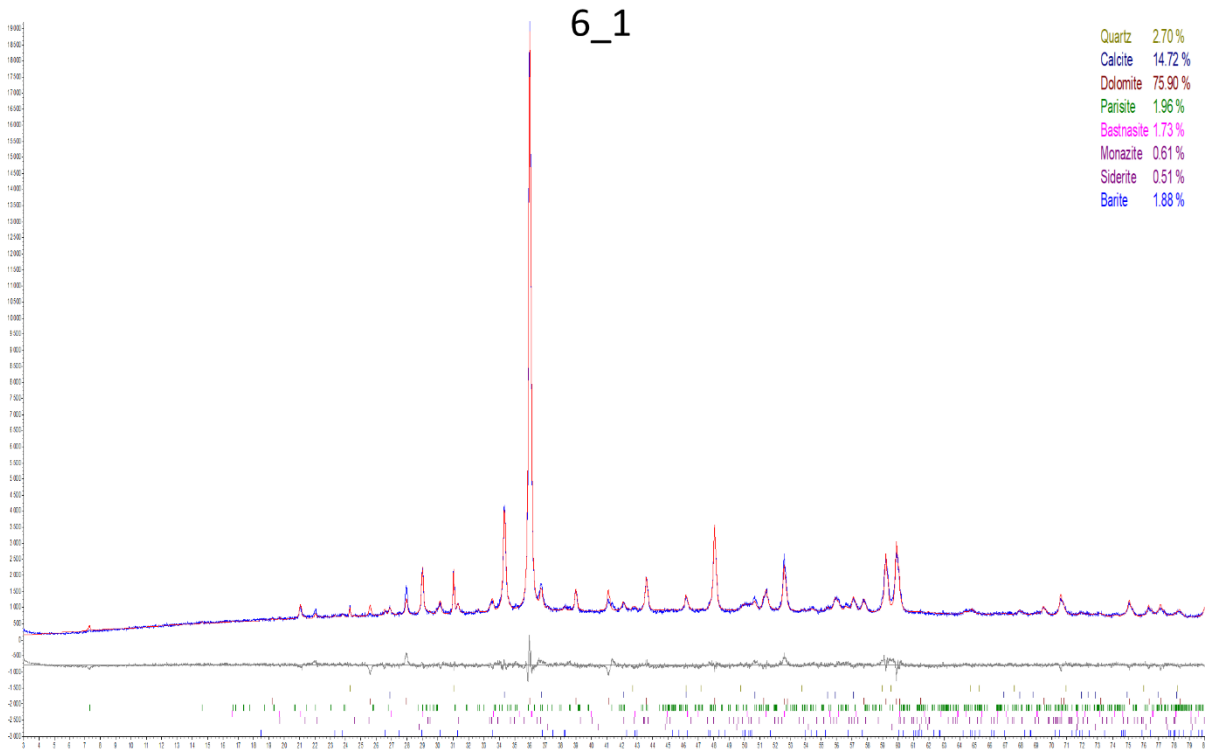

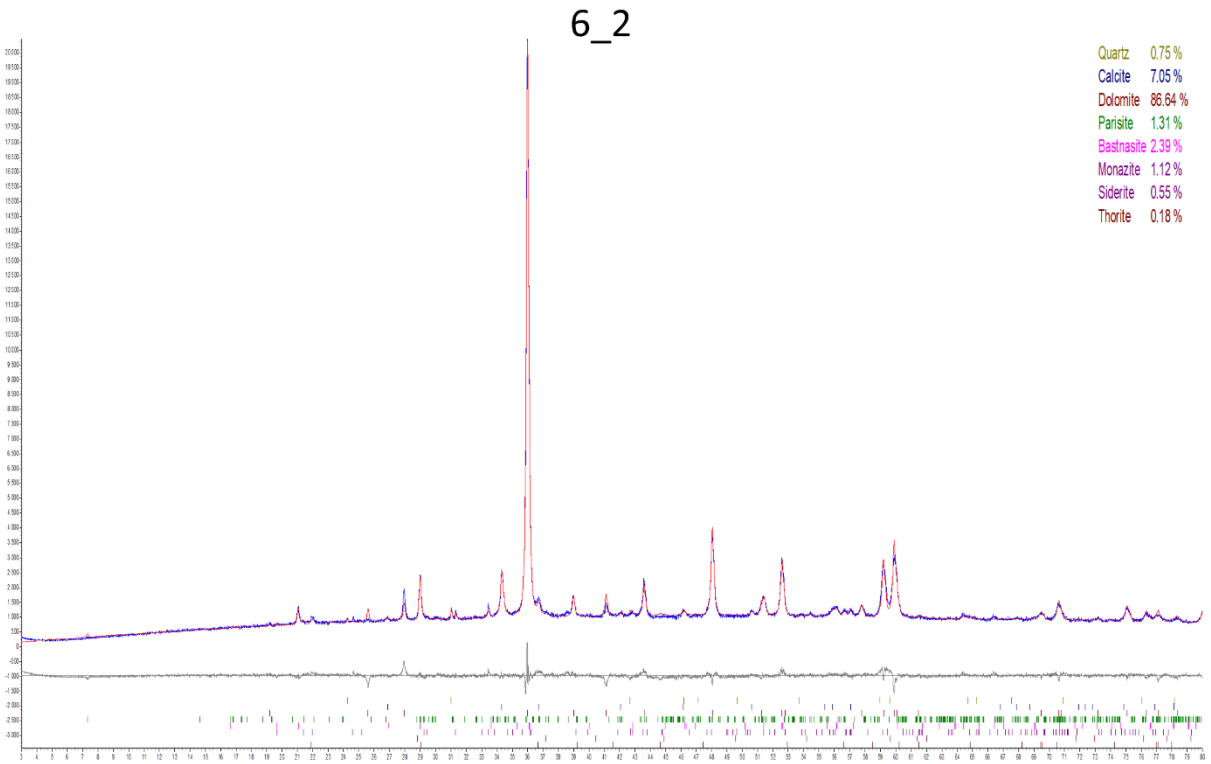

XRD results for specimen 6_1 and 6_2

6_3

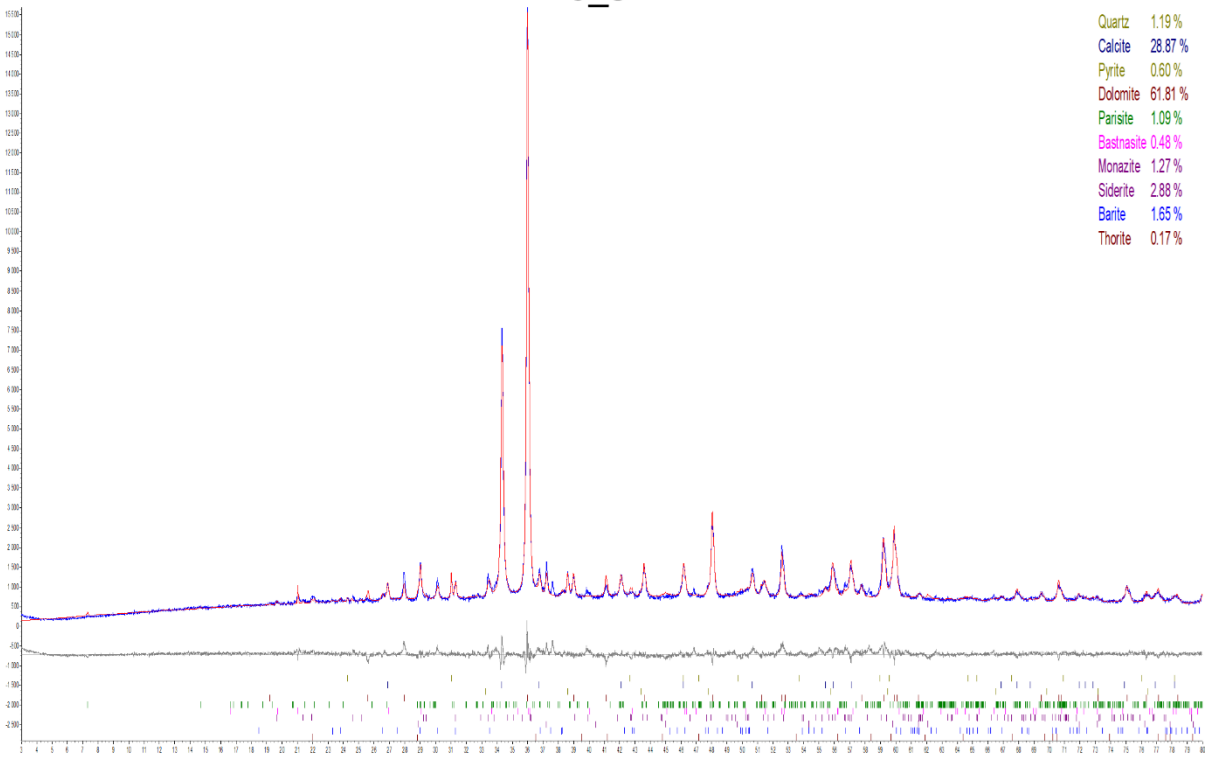

6_4

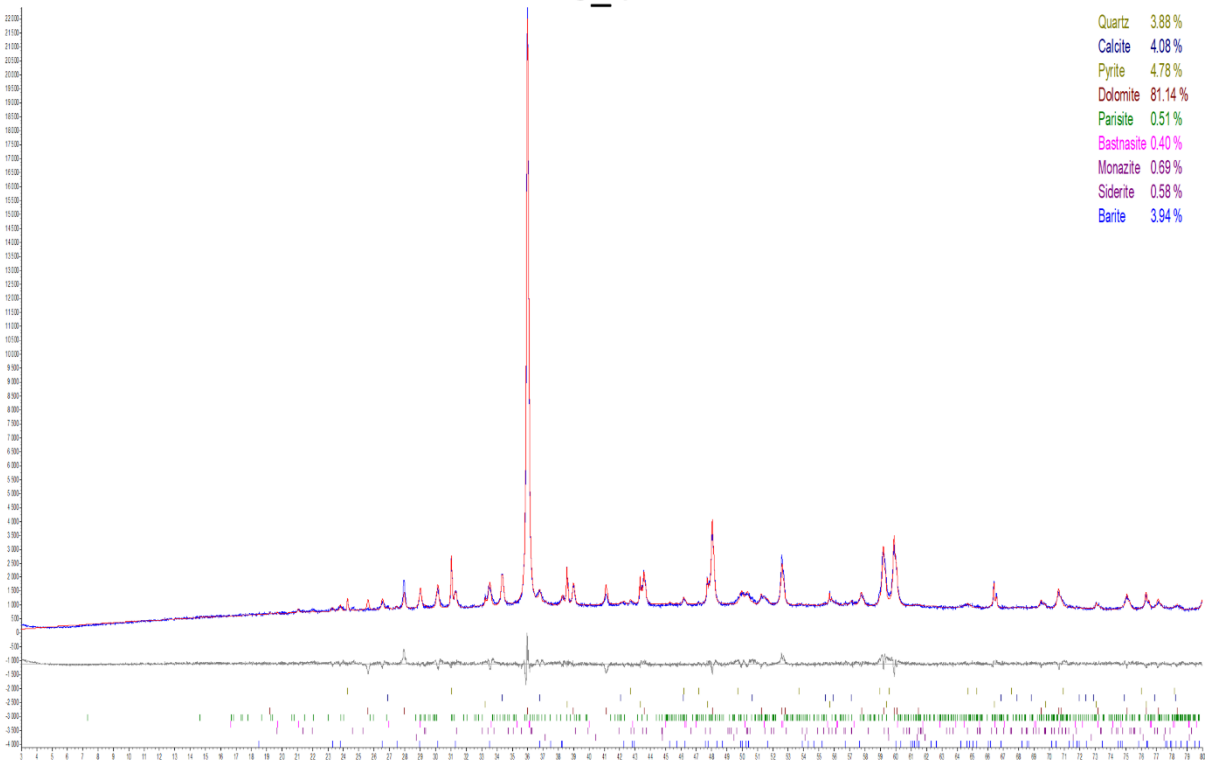

XRD results for specimen 6_1 and 6_2

Full XRF trace elements analysis made from the 12 specimen. Elements under detection limit is marked with "<", Na is not applicable for that specimen. (on next page)

	Sc	*V*	*Cr*	*Mn*	*Co*	*Ni*	*Cu*	*Zn*	*Ga*	*Ge*	*As*	*Se*	*Br*	*Rb*	*Sr*	*Y*	*Zr*	*Nb*	*Mo*	*Ag*
Specimen	(ppm)	(ppm)	(ppm)	(ppm)	(ppm)	(ppm)	(ppm)	(ppm)	(ppm)	(ppm)	(ppm)	(ppm)	(ppm)	(ppm)	(ppm)	(ppm)	(ppm)	(ppm)	(ppm)	(ppm)
3_1	<3.8	<3.2	7,5	15667,3	30,7	3,7	11,8	74,6	<0.4	<0.4	11,8	1,5	1,7	6,8	2479,3	19,4	30,6	2,8	57,7	5,5
3_2	<4.5	<3.6	13,2	9461	3,5	1,3	10,5	46,1	<0.4	<0.4	17,1	1,5	0,6	4,5	1530,8	34,2	22,3	2,3	43,2	4,3
3_3	<3.5	<3.0	5	15701	6,7	1,1	8,5	71,1	<0.4	<0.3	7,6	1,3	1,3	7,5	2775,5	18,9	36,7	3,6	18,9	4,6
3_4	<4.4	<3.8	22,1	9977	2	1,5	10,9	46,3	0,6	<0.4	12,7	1,2	<0.7	4,8	1606,4	33	19,5	6,4	79,4	5,1
3-6_1	<7.0	<9.1	59,5	6257	Na	3,6	23,8	25	0,7	<0.5	14,6	3	1,2	8,8	3046,2	116,4	46,7	5,6	19,9	6,6
3-6_2	<3.9	<4.1	7,1	11331,5	6,4	1	14,6	56	<0.4	<0.4	9,1	2,7	1,6	8,4	2864,9	21,5	41,6	4,8	63	4,3
3-6_3	<3.6	<2.9	7,9	12458,7	5,5	1,3	8	73,4	<0.4	<0.3	9,8	1,3	<0.6	5,9	2160,8	19,9	25,8	0,7	90,4	4,5
3-6_4	<5.1	<4.8	19,4	6401,2	3,3	<1.0	12	18,4	<0.4	<0.4	7,1	1,6	1,4	5,2	1645,9	29,6	30,1	10,6	109	6,2
6_1	<4.7	<4.8	23,4	12924,5	0,1	2,8	15	51,1	<0.5	<0.4	14,6	2,2	2	10	2828,4	34,8	41,4	7,1	32,5	5,2
6_2	<4.6	<4.4	28,6	14818,4	Na	1,6	15,3	88,1	<0.5	<0.4	38,6	2,7	1,9	8	2552,7	61,7	55,8	14,2	35,9	6,1
6_3	<4.7	<4.1	15,6	10812,8	1,6	1,3	13,7	50,9	0,7	<0.4	19,3	2,3	1,5	7,5	2395,2	54,2	44,3	6	88	5
6_4	<4.4	<5.0	10,2	14177,4	26,2	2,5	16,8	66,3	<0.5	<0.4	18,7	2,1	1,7	8	2668,8	20,5	40,3	4,8	37	6

	Cd	Sn	Sb	Te	I	Cs	Ba	La	Ce	Nd	Sm	Yb	Hf	Ta	W	Tl	Pb	Bi	Th	U
Specimen	(ppm)	(ppm)	(ppm)	(ppm)	(ppm)	(ppm)	(ppm)	(ppm)	(ppm)	(ppm)	(ppm)	(ppm)	(ppm)	(ppm)	(ppm)	(ppm)	(ppm)	(ppm)	(ppm)	(ppm)
3_1	6,8	<2.6	<2.9	<3.3	<3.7	167,3	4014,4	6045,3	8525,7	2354,8	132,7	<2.6	<3.0	<2.4	46,2	2,1	3,8	2,2	135,3	8,9
3_2	4,9	4,9	<3.0	<3.5	<3.9	233,8	5571,8	8710,5	12426,2	3561,7	215,2	2,5	<2.8	<2.1	34,9	1,7	<1.2	2,8	175,3	11,7
3_3	8,2	3,4	1,2	<3.2	<3.5	118	7123,1	4061	5886,6	1700,3	98,6	<2.3	<2.7	2,2	22,3	2,7	<1.2	2,2	88,9	11,3
3_4	5,5	6,3	3,8	<3.6	<3.9	367,4	630,9	16066,2	19656	4830,8	280,1	3	<2.8	<2.2	24,1	1,3	<1.2	2,6	234	12
3-6_1	16,3	26,2	17,7	<6.8	<7.5	946,5	136435,8	43122,1	44127,2	10878,4	535,3	5,8	<3.9	<3.2	19,8	2,5	<1.7	6,5	375,2	15,2
3-6_2	7,8	9,3	6,8	<4.0	<4.6	250	34970,7	8624,3	11794,6	3729,5	226,9	3,2	<2.8	<2.2	61,8	2,4	<1.3	4,3	216,7	12
3-6_3	4,3	<2.3	<2.6	<2.9	<3.2	143,5	197,9	5635,7	7762,3	2143,5	136	<2.0	<2.6	<1.9	41,1	2,3	<1.2	1,6	91,9	9,2
3-6_4	9,3	11,5	7,8	<4.4	<5.0	325,3	34523,4	13546,5	16649	4183,2	187,8	2,6	<2.9	<2.3	32	2,8	<1.2	3,8	127,2	10,9
6_1	9,6	10,7	7	<4.4	<4.0	463,8	27777,6	18915,4	21768,5	5358,5	322,1	3,5	<3.1	<2.4	8,8	4,4	<1.4	4,2	238,4	16
6_2	7,6	7,5	6,5	<4.1	<4.5	540,7	2541	23161,3	27750,3	6988,3	500,8	3,6	<3.2	<2.5	21,3	2,4	16,8	3,5	894	18,1
6_3	6,5	6,7	5,4	<4.0	<4.5	323,4	15223,9	13107,2	16132,3	3852,4	260,4	3,3	<3.0	<2.3	17,7	<2.3	7,8	3,9	513,6	14,9
6_4	11,8	13,2	8,6	<4.8	<5.4	266,2	58996,4	8559,9	11771,6	3664,6	198,6	3,1	<3.2	<3.2	33,4	2,1	3,7	4,3	202,8	11,7

Appendix II – ICP-MS

Shows ICP-MS results done on five specimens in ppm (results with "<" were under the detection limit).

Element	*Det. Lim.*	*0.3_2*	*3-67_1*	*0.67_2*	*0.67_3*	*0.67_4*
Y	0,3	43,6	157	71,1	62,1	22,9
La	0,06	12200	54400	25900	16600	8390
Ce	0,3	19600	58300	32200	21000	12400
Pr	0,08	1640	4230	2490	1560	1160
Nd	2	4120	9730	6090	3510	3480
Sm	2	406	1150	725	414	332
Eu	2	72,9	243	129	83,2	62,7
Gd	7	349	1000	592	357	248
Tb	1	22,2	59,7	34,5	22,5	15,1
Dy	3	25,3	65,6	36,5	27,1	15,9
Ho	2	2,45	6,89	3,60	2,99	< 2
Er	3	19,9	48,8	29,7	18,7	14,1
Tm	2	< 2	< 2	< 2	< 2	< 2
Yb	4	< 4	7,19	4,90	< 4	< 4
Lu	1	< 1	< 1	< 1	< 1	< 1
Th	2	244	543	1120	616	247
U	0,001	6,10	6,70	10,3	6,40	4,00

Appendix III – Optical microscope

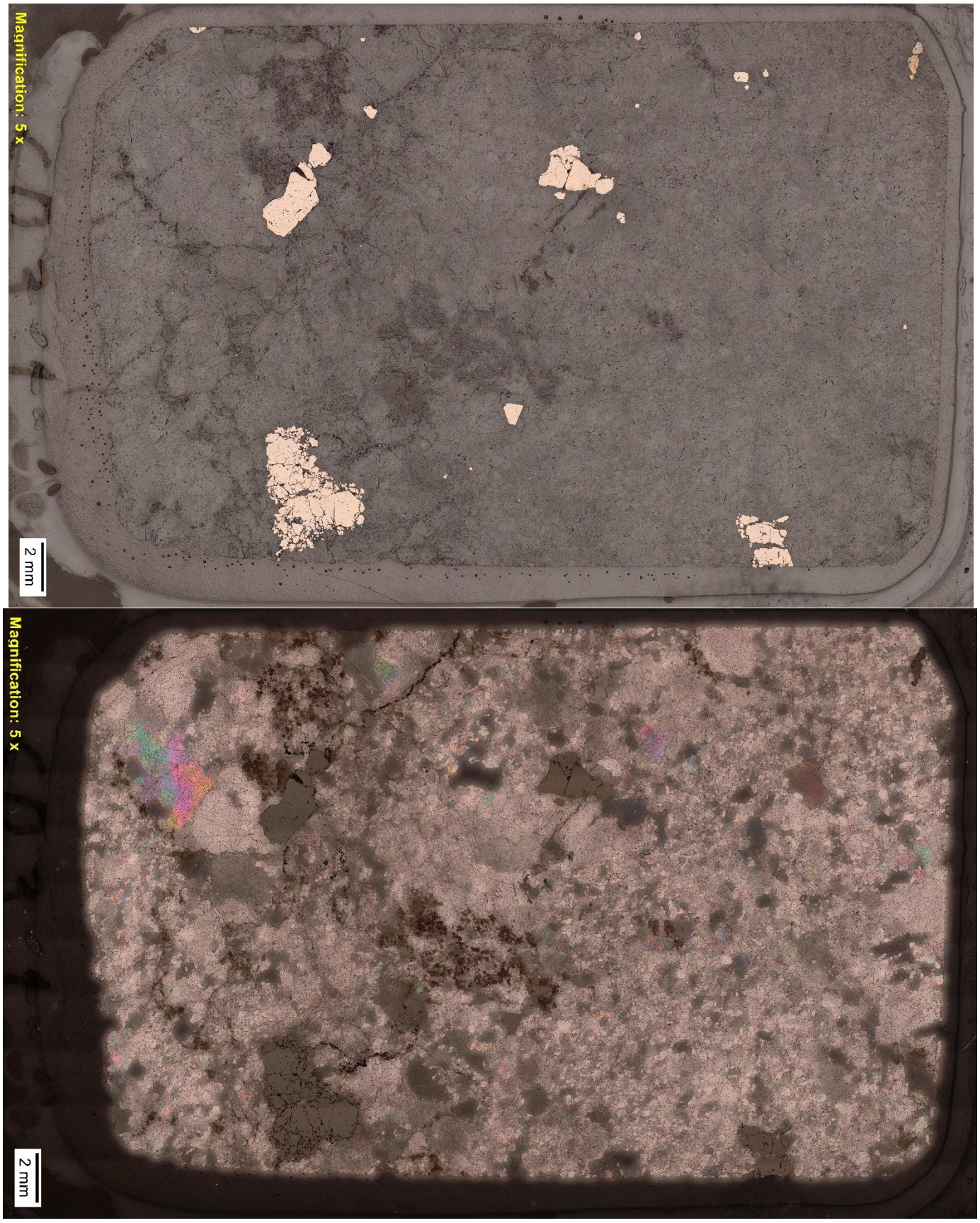

Shows an optical microscopy scan of thin-section 3_1. Top: reflected light PPL, Bottom: reflected light XPL

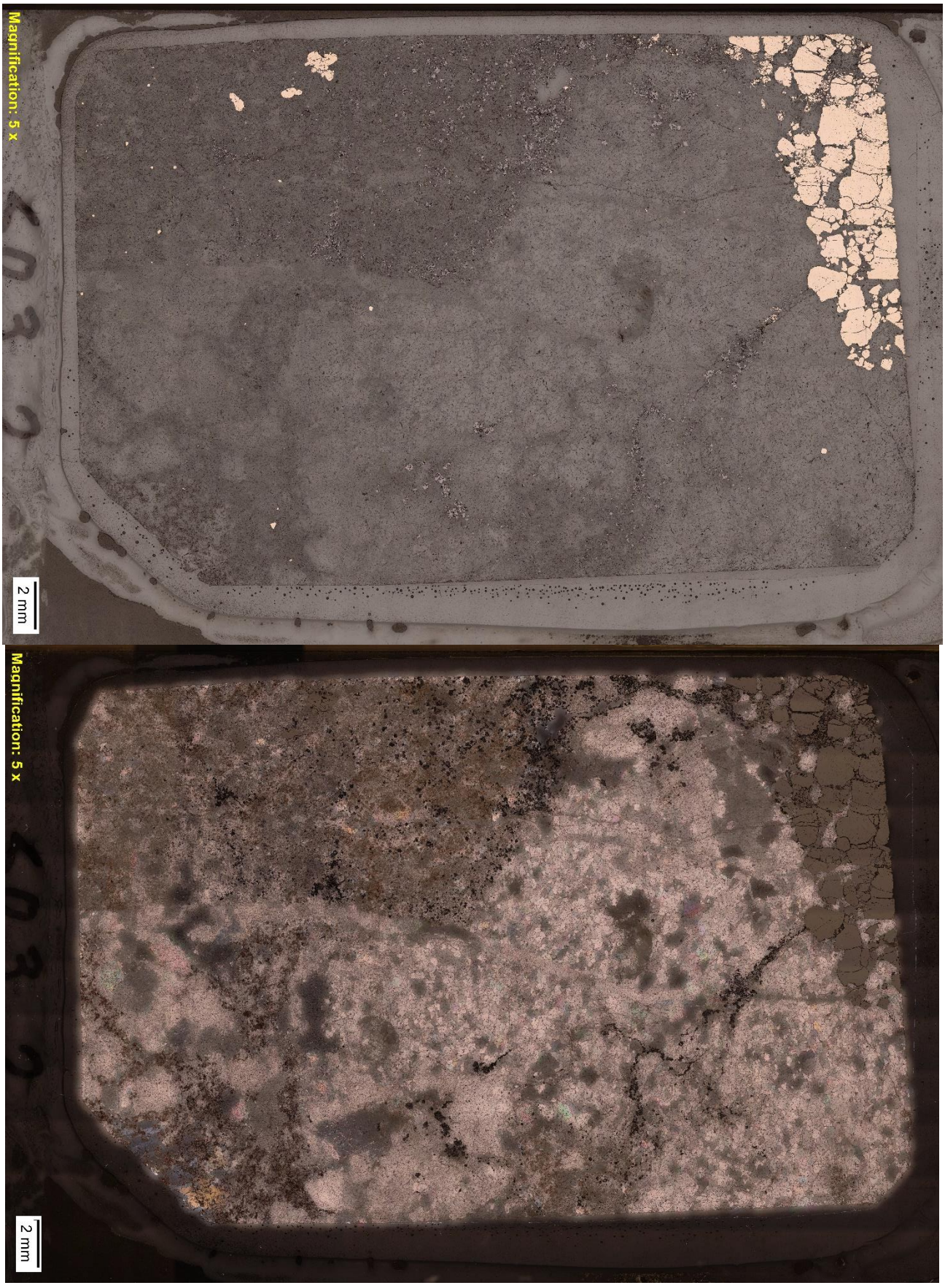

Shows optical microscopy scan of thin-sections 3_2. Top: Reflected light PPL, Bottom: reflected light XPL

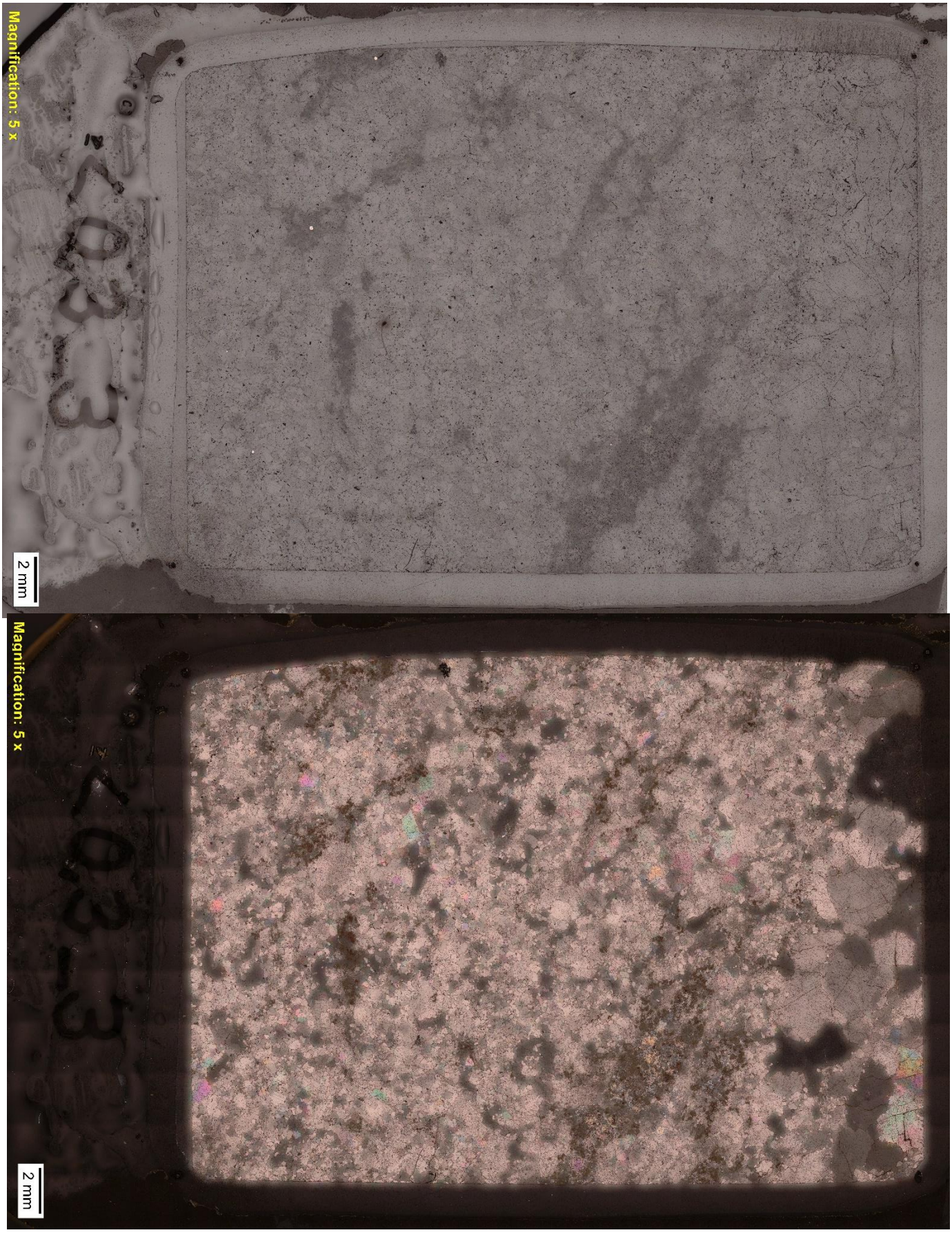

Shows optical microscopy scan of thin-sections 3_3. Top: Reflected light PPL, Bottom: reflected light XPL

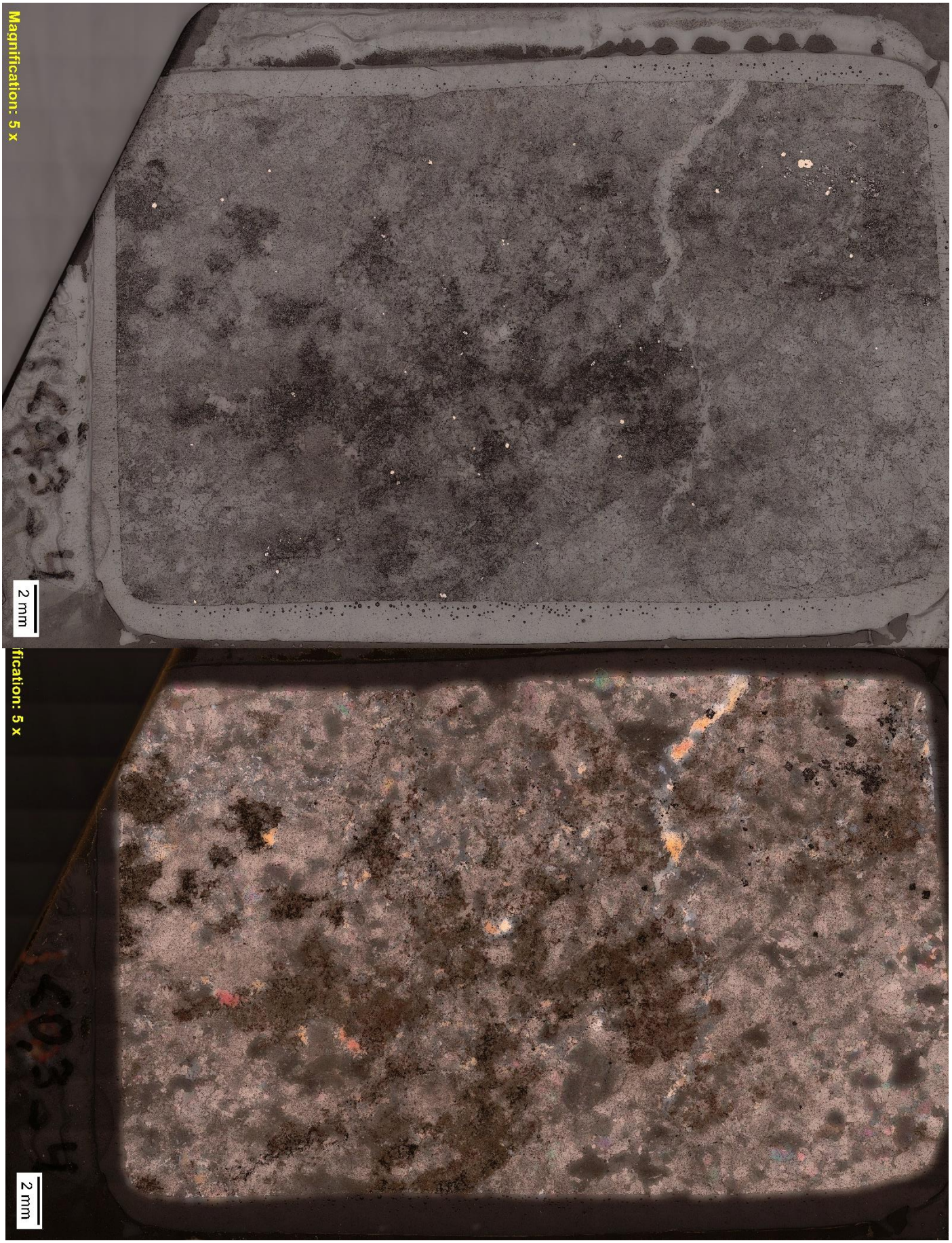

Shows optical microscopy scan of thin-sections 3_4. Top: Reflected light PPL, Bottom: reflected light XPL

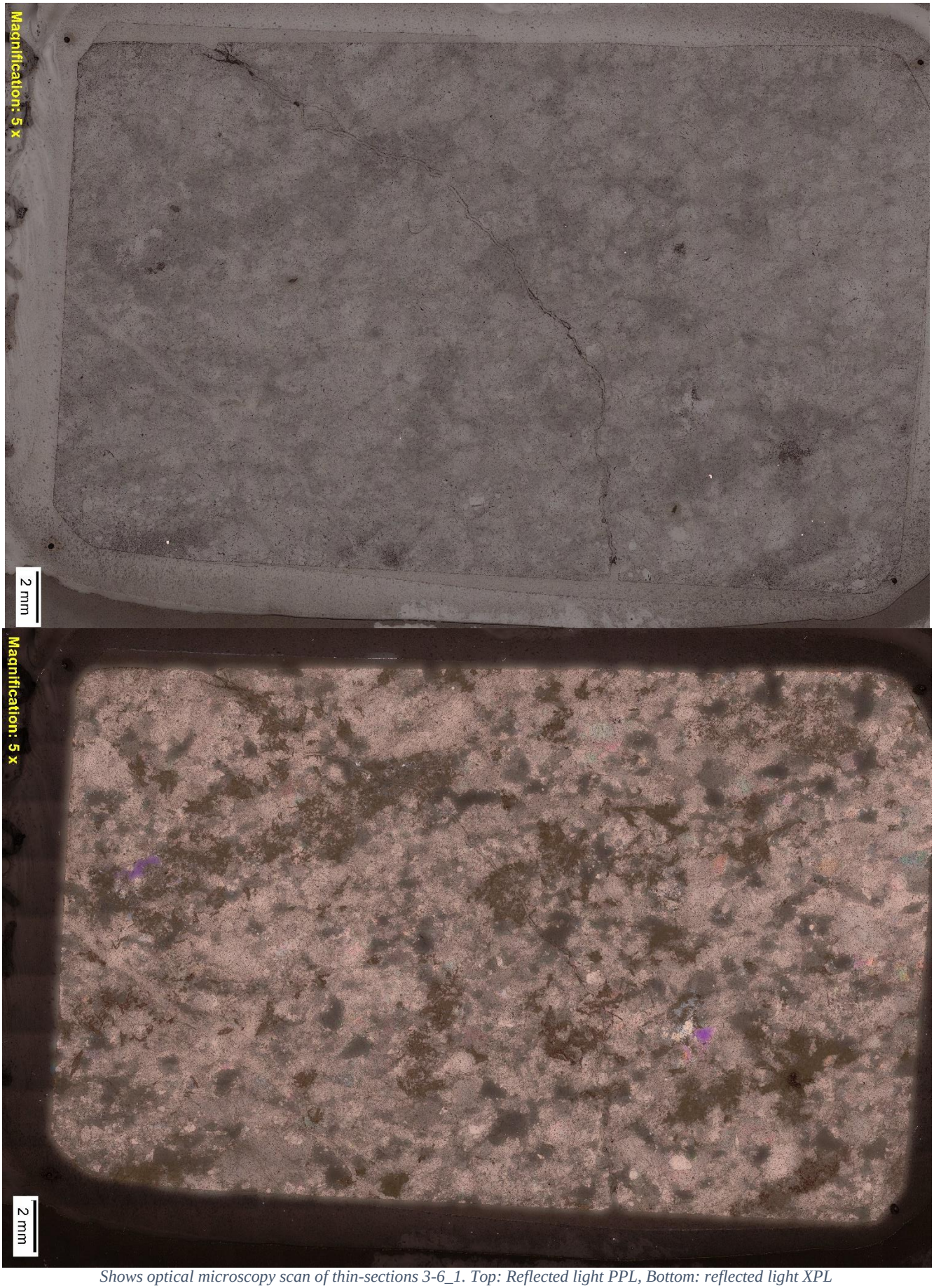

Shows optical microscopy scan of thin-sections 3-6_1. Top: Reflected light PPL, Bottom: reflected light XPL

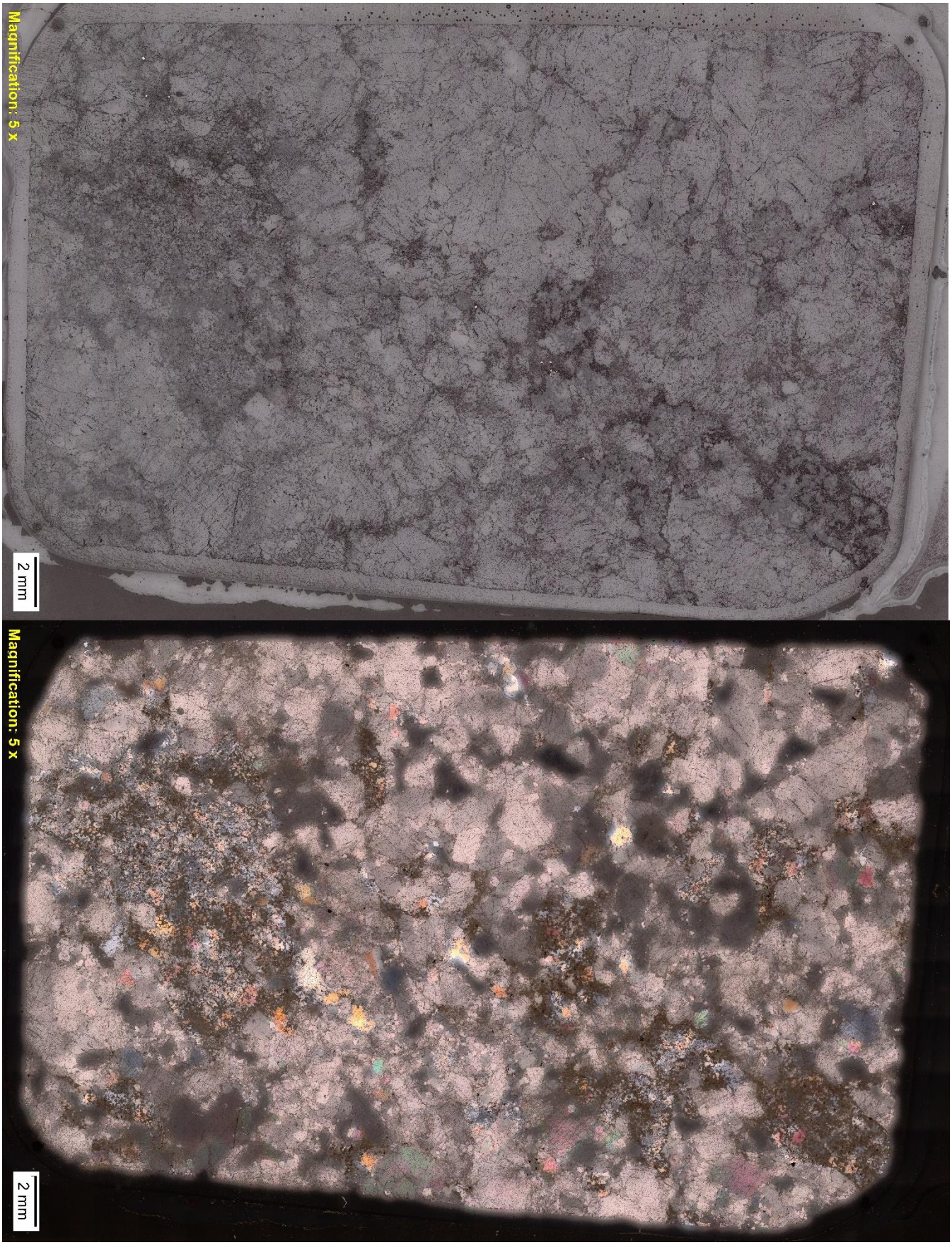

Shows optical microscopy scan of thin-sections 3-6_2. Top: Reflected light PPL, Bottom: reflected light XPL

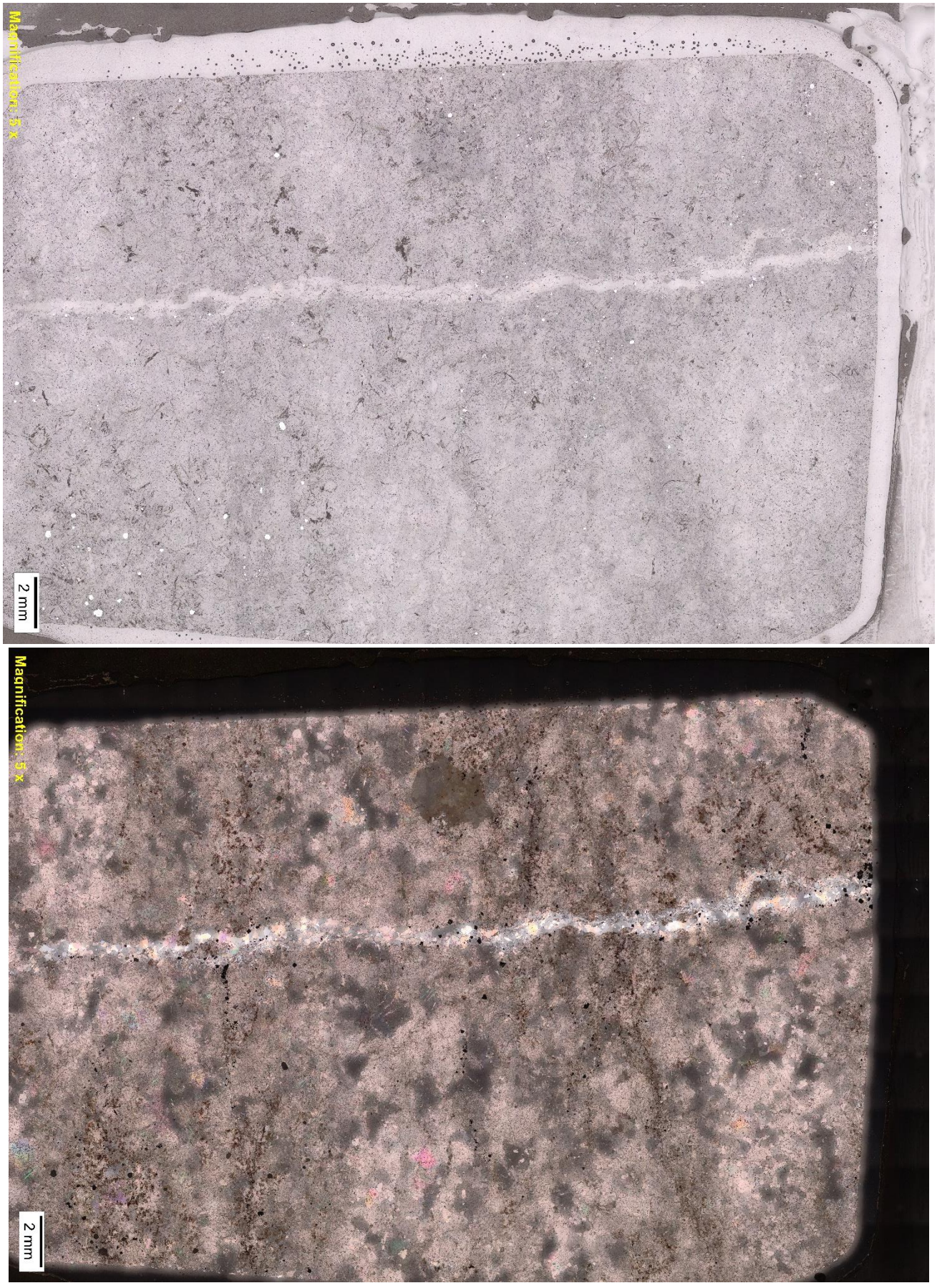

Shows optical microscopy scan of thin-sections 3-6_3. Top: Reflected light PPL, Bottom: reflected light XPL

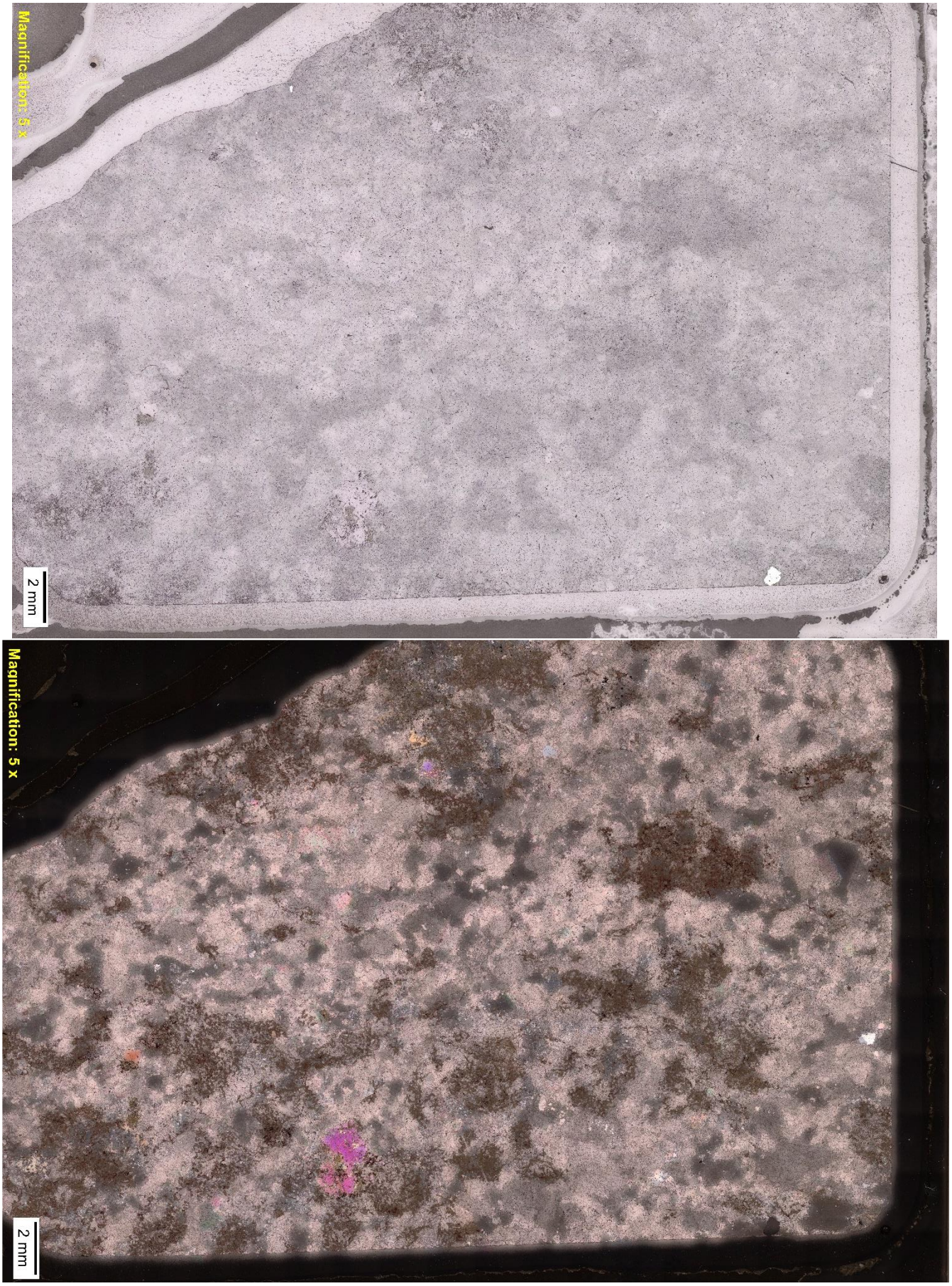

Shows optical microscopy scan of thin-sections 3-6_4. Top: Reflected light PPL, Bottom: reflected light XPL

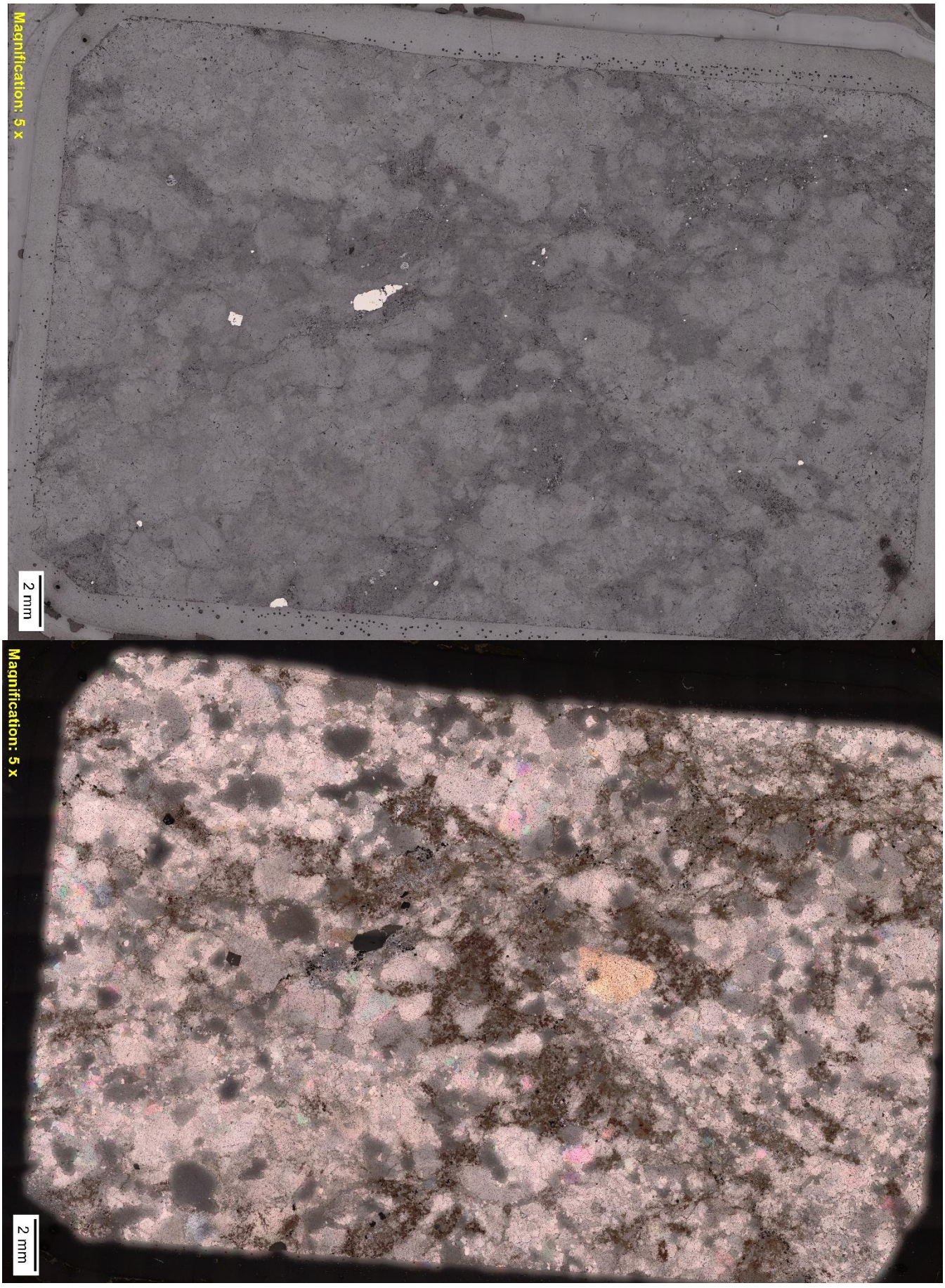

Shows optical microscopy scan of thin-sections 6_1. Top: Reflected light PPL, Bottom: reflected light XPL

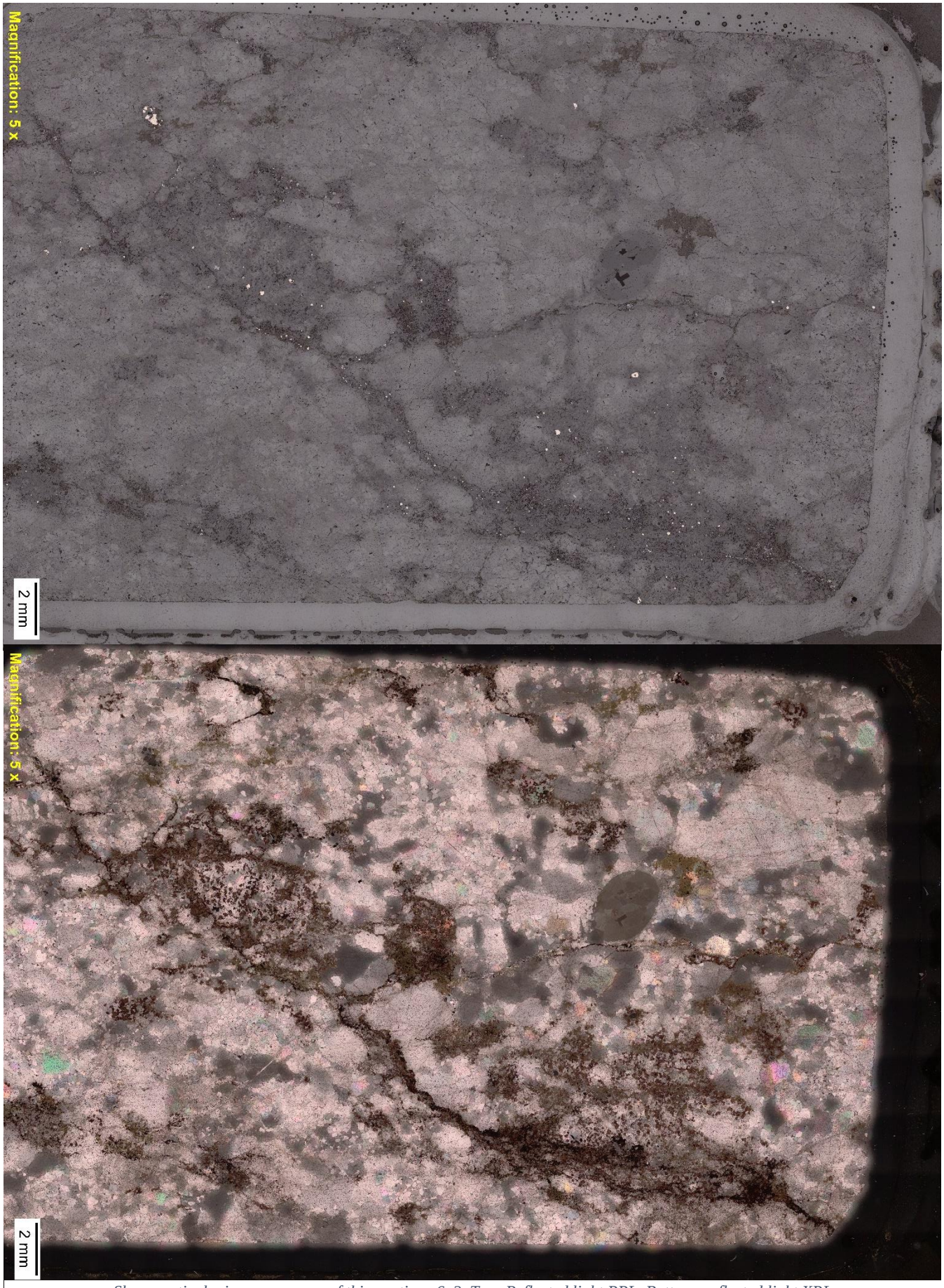

Shows optical microscopy scan of thin-sections 6_2. Top: Reflected light PPL, Bottom: reflected light XPL

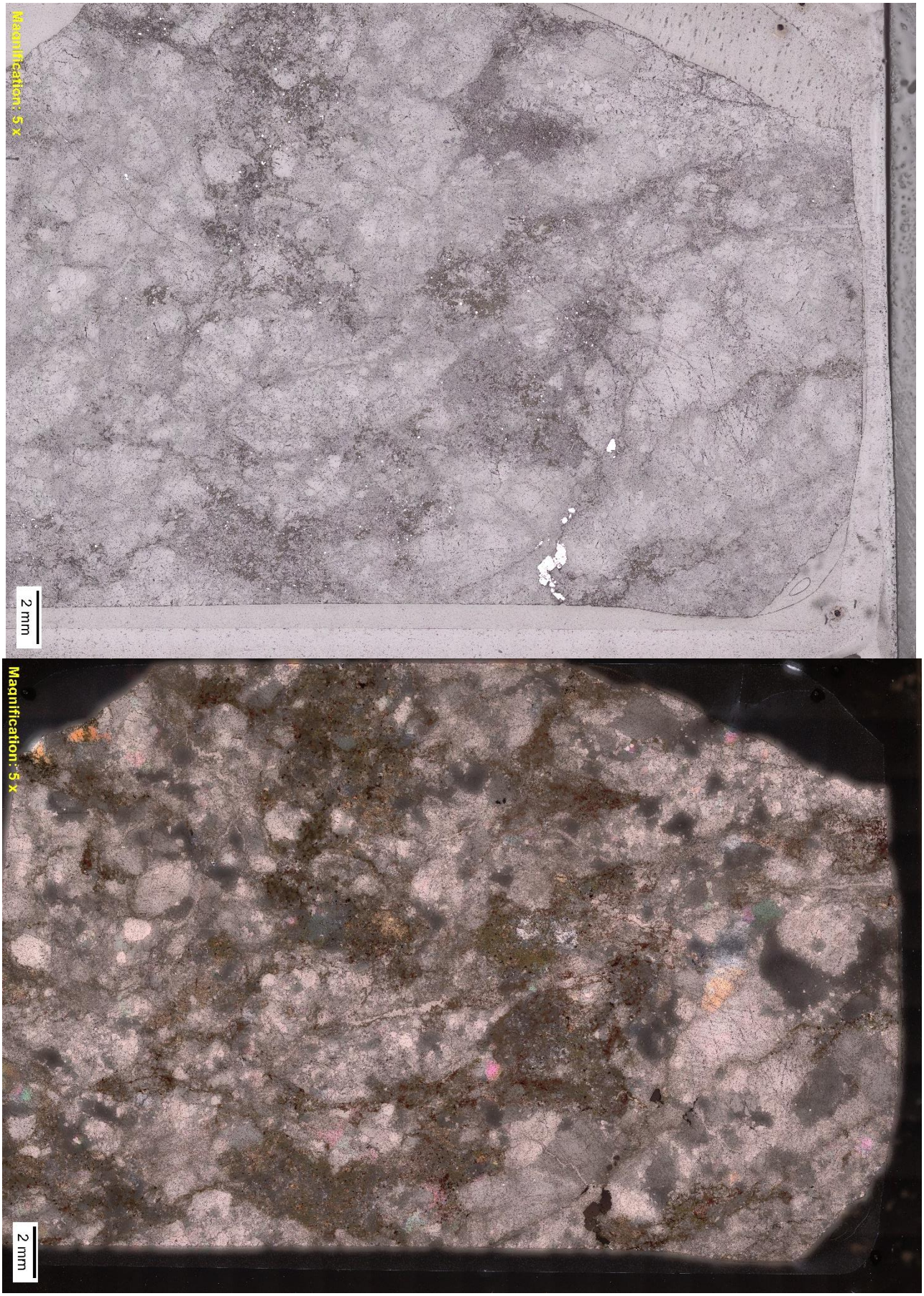

Shows optical microscopy scan of thin-sections 6_3. Top: Reflected light PPL, Bottom: reflected light XPL

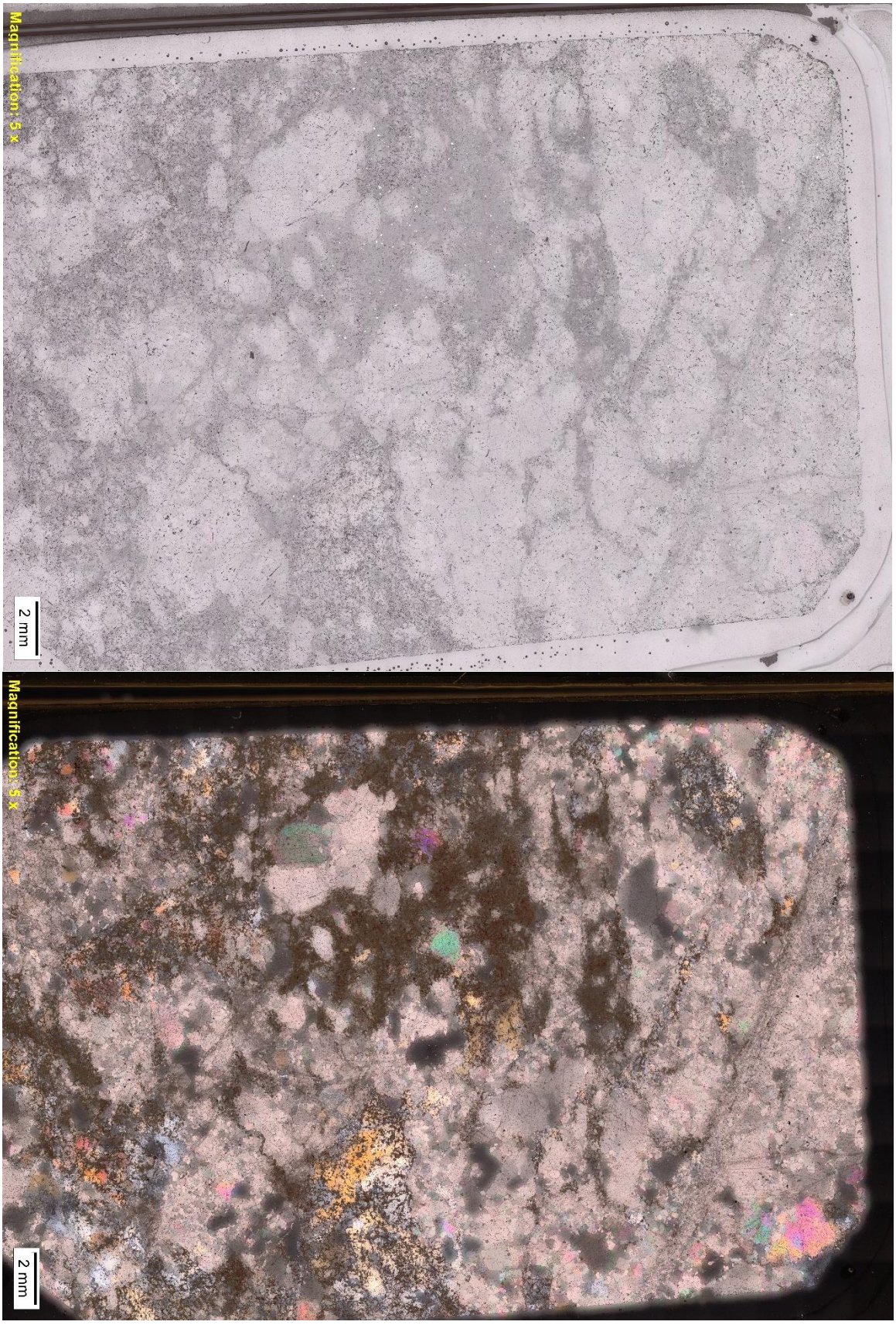

Shows optical microscopy scan of thin-sections 6_4. Top: Reflected light PPL, Bottom: reflected light XPL

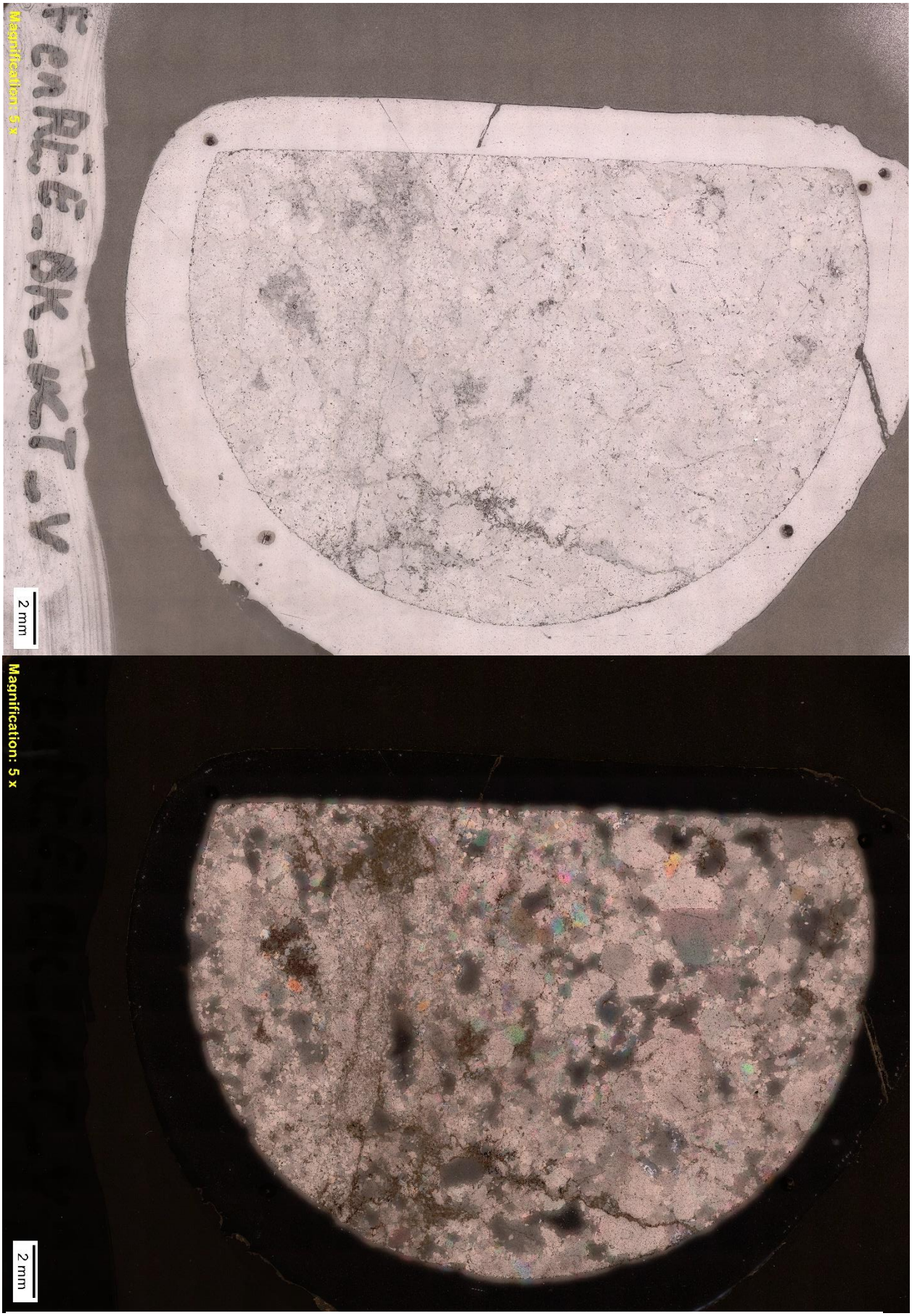

Shows optical microscopy scan of thin-sections Kjerne_V. Top: Reflected light PPL, Bottom: reflected light XPL

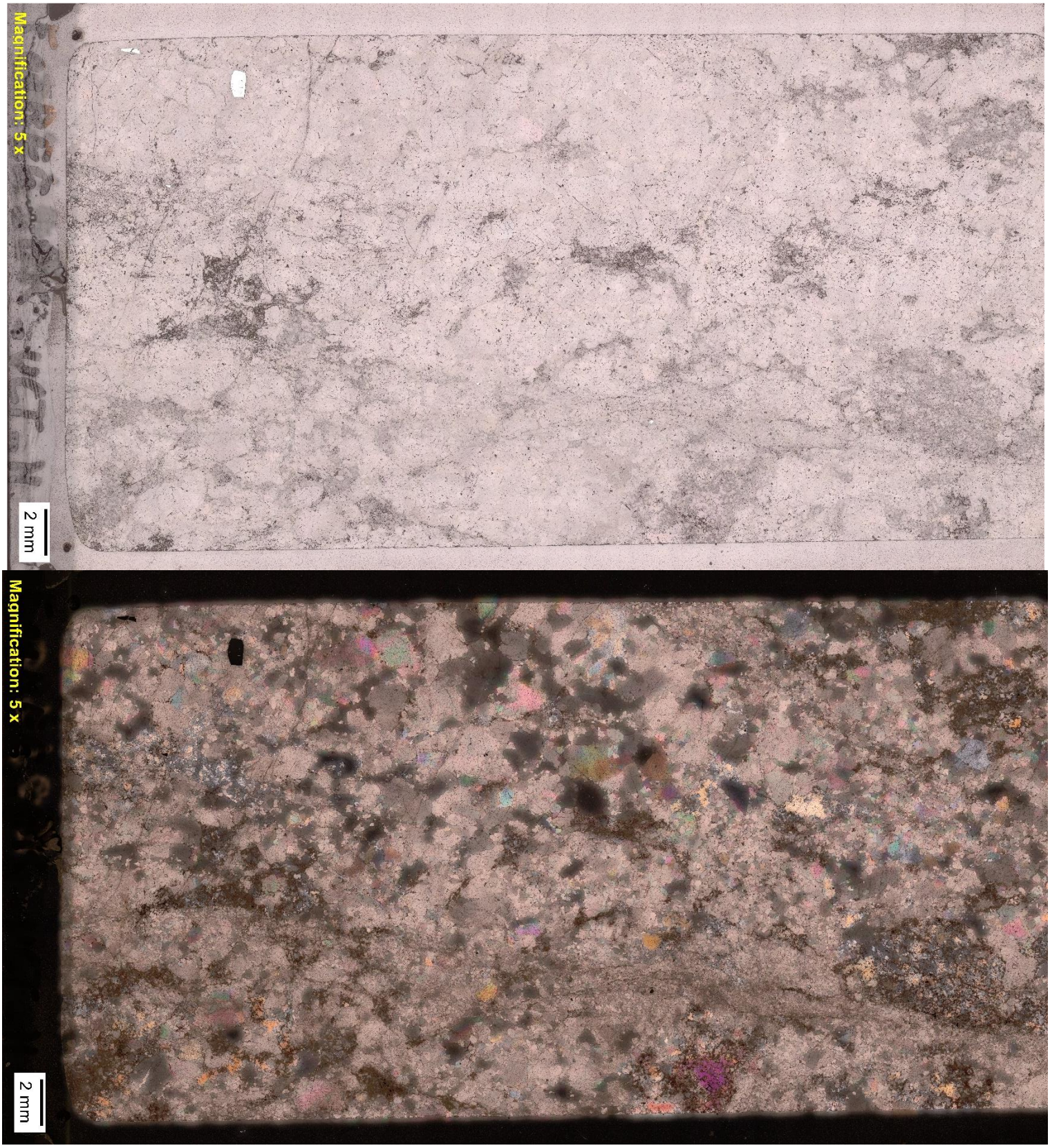

Shows optical microscopy scan of thin-sections Kjerne_V. Top: Reflected light PPL, Bottom: reflected light XPL

Appendix IV – SEM

OV Bulk data

Bulk data for the OV maps for the 12 specimens + the two cores (on the following pages). The results show every classification that was picked up in the specimen (not the complete mineral list), except for classifications with zeros in every category, these are only included because of a quirk in the cluster classification of mineralogic (every element under 1 % is removed for the unclassified and not classified category for readability).

3_1	Number	Area %	Weight %	Grain Size (µm)	Grain Size Std Dev (µm)	Average Composition
Allanite_Ce	0	0	0	0	0	
Allanite_La	0	0	0	0	0	
Allanite_Y	0	0	0	0	0	
Ankerite	555	21,2815	17,76772	11,40903	9,388174	O 46,98; Ca 30,66; Fe 11,51; Mg 10,68; Mn 0,1; Th 0,05; P 0,01; Ag 0,01; Sr 0;
Apatite	76	2,07995	1,758581	9,452053	7,827581	Ca 48,33; O 36,69; P 14,26; F 0,58; Ce 0,08; Ag 0,04; Nd 0,02;
Bastnäsite_Ce	76	0,482003	0,641317	4,247553	1,918228	Ce 74,6; O 20,21; F 5; Ca 0,12; La 0,08;
Bastnäsite_Ce_La	166	2,577671	3,443317	8,225612	5,651966	Ce 46,92; La 33,52; O 15,92; F 3,11; Ca 0,39; Nd 0,13; P 0,01;
Bastnäsite_La	0	0	0	0	0	
Bastnäsite_sulph	1	0,005239	0,006999	3,5	0	La 39,52; Ce 34,99; O 19,31; F 6,18;
Bastnäsite_Y	0	0	0	0	0	
Bastäsite_Ce_La_Nd	24	0,12574	0,167967	3,5	2,37E-07	Ce 37,59; La 29,44; Nd 15,51; O 13,73; F 2,5; Ca 1,24;
Burbankite_Y	11	0,057631	0,057586	3,5	2,44E-07	O 94,23; Ba 5,77;
Calcite	373	20,3856	14,64239	13,93712	15,39309	Ca 52,14; O 46,59; Mg 0,68; Fe 0,37; Th 0,2; P 0,01; Nd 0,01; Ce 0; La 0; Y 0; Ag 0;
Calcite_w_Ce	42	0,225284	0,238841	3,617851	0,763763	Ca 52,68; O 43,18; Ce 3,74; Mg 0,4;
Thorite_Ce_La_Mix	0	0	0	0	0	
Thorite_Ce_Mix	0	0	0	0	0	
Thorite2-Calsite mix	7	0,036674	0,065612	3,5	0	O 40,05; Ca 39,23; Ag 16,75; Si 3,96;
Thorite-Callsite mix	78	0,461047	0,824836	3,978192	1,355191	Ca 44,53; Th 30,65; O 20,19; Si 4,43; Sm 0,08; Ce 0,08; La 0,03;
Dolomite	435	4,123225	3,103662	5,757643	4,017821	O 53,03; Ca 33,91; Mg 12,53; Fe 0,43; Mn 0,1;
Fe-Mg-chlorite	9	0,073348	0,051518	5,118369	3,726918	O 48,69; Fe 19,94; Si 16,08; Mg 9,18; Al 6,1;
Galena	36	0,518678	1,044793	7,211371	6,047942	Pb 100;
Gypsum	5	0,026196	0,016038	3,5	2,54E-07	Ca 41,82; O 30,43; S 27,74;
Magnetite	138	3,106827	4,290162	8,747213	7,708678	Fe 77,87; O 22,13;
Mg-Fe-chlorite	24	0,560591	0,393741	8,592126	7,413699	O 41,15; Si 18,87; Fe 16,15; Mg 15,76; Al 8,07;
Molybdenite	6	0,104783	0,138861	8,57885	3,946995	S 98,15; Ca 1,85;
Monazite_Ce	46	3,766962	5,331525	18,87523	11,98998	Ce 49,12; O 20,65; P 17,48; La 10,93; Ca 0,99; Nd 0,83;
Monazite_Ce_La_Nd	21	0,110023	0,155719	3,5	2,27E-07	Ce 33,89; La 24,55; O 16,19; Nd 13,38; P 11,99;
Monazite_La	0	0	0	0	0	
Nb_rutile	2	0,015718	0,020829	5,249999	2,474873	O 53,1; Ti 30,52; Fe 11,64; Nb 4,74;
Parisite_Ce	241	2,420496	2,784281	6,047472	4,411535	Ce 47,33; O 28,28; Ca 19,94; La 2,44; F 2,01; P 0,01;
Parisite_Ce_La	216	2,389061	2,748121	6,503602	4,419591	Ce 40,26; La 29,16; O 18,8; Ca 10,2; F 1,57; Nd 0,01;
Parisite_Ce_Nd	35	0,18861	0,216957	3,6	0,591608	Ce 38,27; O 20,28; Nd 14,47; Ca 13,68; La 11,43; F 1,87;
Parisite_Nd_La	0	0	0	0	0	
Pyrite	142	17,55645	23,31275	23,45345	11,92835	Fe 52,98; S 47,02;
Pyrrhotite	263	1,812752	2,210117	4,602596	2,387196	Fe 60,32; S 39,68;
Quartz	68	3,950333	2,743178	15,83455	10,52818	Si 57,03; O 42,61; Fe 0,3; La 0,03; Ce 0,03;
Ce-quartz mix	1	0,005239	0,00368	3,5	0	Si 50,6; O 40,55; Ce 8,85;
La-quartz mix	0	0	0	0	0	
REE-quartz mix	0	0	0	0	0	
Si=O>Fe mix	17	0,094305	0,024995	3,705882	0,848875	Si 44,16; O 41,93; Fe 13,92;
Siderite	70	0,429612	0,447495	4,182842	1,650036	Fe 56,2; O 36,83; Ca 6; Mg 0,92; Th 0,05;
Sphalerite	2	0,010478	0,011248	3,5	0	Zn 72,42; S 27,58;
Synchysite_Ce	73	0,461047	0,485126	4,253737	1,872676	Ce 64,78; O 20,86; Ca 12,57; F 1,8;
Synchysite_Ce-Nd	10	0,052392	0,055545	3,5	1,14E-07	Ce 50,16; Nd 19,05; O 18,02; Ca 10,72; F 2,05;
Synchysite_Nd	3	0,015718	0,017538	3,5	2,57E-07	O 46,47; Ca 26,37; Nd 19,72; F 5,9; P 1,54;
Synchysite_Y	0	0	0	0	0	
Talc	14	0,094305	0,070486	4,54038	3,032364	O 54,33; Si 36,32; Mg 9,36;
Thorite	284	5,522083	9,879289	8,734264	7,620201	Th 72,19; O 12; Si 10,19; Ca 5,52; Ce 0,06; Nd 0,02; La 0,01; Sm 0,01;
Thorite2	80	0,445329	0,796717	3,773115	1,079338	Ag 46,27; O 34,91; Si 10,53; Ca 8,14; Nd 0,07; Sm 0,07; La 0,02;
Thorite3	0	0	0	0	0	
Coffinite	0	0	0	0	0	
Uraninite	2	0,010478	0,030466	3,5	0	U 80,03; O 19,97;
Uranothorite	0	0	0	0	0	
Not Analysed	5	0,0261958	0	3,4999996	0	
Not Classified	0	1,7865563	0	0	0	O 31,48; Ca 31,39; Fe 11,81; Ce 8,52; Mg 5,04; La 2,95; Th 2,82; S 1,9; Si 1,07;
Unclassified	360	2,6038665	0	4,8300129	2,5860524	O 34,24; Ca 23,53; Fe 9,68; Ce 7,39; Th 6,7; S 4,99; Si 4,28; Mg 3,06; La 1,77; P 1,44

3_2	Number	Area %	Weight %	Grain Size (µm)	Grain Size Std Dev (µm)	Average Composition
Allanite_Ce	0	0	0	0	0	
Allanite_La	0	0	0	0	0	
Allanite_Y	0	0	0	0	0	
Ankerite	663	4,045823	3,204675	7,434851	6,314151	O 46,31; Ca 31,79; Fe 12,42; Mg 9,35; Mn 0,08; Th 0,03; P 0,02; Sr 0;
Apatite	399	3,114438	2,498256	8,397382	6,888011	Ca 49,16; O 35,13; P 14,59; F 0,6; Ce 0,43; Th 0,05; Nd 0,03; Ag 0,01;
Barite	17	0,400849	0,45157	18,15298	7,823755	Ba 66,21; O 19,71; S 14,08;
Bastnäsite_Ce	5	0,01179	0,014882	4,2	1,565247	Ce 72,46; O 21,18; F 6,37;
Bastnäsite_Ce_La	18	0,039299	0,049806	3,888889	1,131833	Ce 45,89; La 31,69; O 17,55; F 2,58; P 1,06; Ca 0,65; Nd 0,59;
Bastnäsite_La	0	0	0	0	0	
Bastnäsite_sulph	0	0	0	0	0	
Bastnäsite_Y	0	0	0	0	0	
Bastäsite_Ce_La_Nd	3	0,005895	0,007471	3,5	0	Ce 41,26; La 29,27; Nd 15,05; O 14,42;
Burbankite_Y	80	0,176845	0,167649	3,967102	2,141498	O 85,42; Ba 11,56; Ca 2,89; Ce 0,13;
Calcite	1015	16,14792	11,00405	13,35554	8,979954	Ca 52,08; O 47,15; Mg 0,38; Fe 0,22; Th 0,06; P 0,05; Ce 0,04; Nd 0,01; La 0; Y 0; Sr 0;
Calcite_w_Ce	115	0,229899	0,23124	3,586082	0,649884	Ca 51,52; O 44,18; Ce 4,03; Mg 0,16; Fe 0,11;
Thorite_Ce_La_Mix	0	0	0	0	0	
Thorite_Ce_Mix	0	0	0	0	0	
Thorite2-Calsite mix	6	0,01179	0,020011	3,5	2,27E-07	Ca 39,92; O 32,82; Ag 22,11; Si 5,14;
Thorite-Callsite mix	55	0,123792	0,210117	4,129515	1,731649	Ca 44,75; Th 29,36; O 21,63; Si 4,26;
Dolomite	550	1,683958	1,202586	4,950925	3,407486	O 57,05; Ca 33,51; Mg 9,01; Fe 0,33; Mn 0,09;
Fe-Mg-chlorite	55	0,155231	0,10344	4,94523	2,591954	O 40,33; Fe 29,68; Si 15,34; Al 7,76; Mg 6,89;
Galena	94	0,253478	0,484418	4,564941	2,275076	Pb 99,99; As 0,01;
Gypsum	33	0,064843	0,037665	3,5	1,89E-07	Ca 39,87; S 32,94; O 27,19;
Magnetite	232	2,302916	3,017049	9,389505	7,375816	Fe 77,41; O 22,59;
Mg-Fe-chlorite	10	0,076633	0,051065	7,934286	7,37307	O 40,14; Si 19,06; Fe 18,45; Mg 14,7; Al 7,65;
Molybdenite	43	0,34976	0,439751	6,732307	8,052388	S 99,71; Ca 0,27; Ti 0,02;
Monazite_Ce	538	17,38584	23,34551	19,55028	11,6154	Ce 47,91; O 20,42; P 17,06; La 12,77; Ca 1,13; Nd 0,7; F 0; Pr 0;
Monazite_Ce_La_Nd	318	0,695591	0,934032	3,938743	1,34769	Ce 33,78; La 24,44; O 16,02; Nd 13,25; P 12,42; Ca 0,09;
Monazite_La	5	0,009825	0,013193	3,5	1,97E-07	O 56,35; P 18,23; La 16,6; Nd 5,83; Ce 2,99;
Nb_rutile	1	0,001965	0,002471	3,5	0	Ti 59,13; O 37; Nb 3,88;
Parisite_Ce	398	2,627132	2,867069	8,65233	6,600885	Ce 45,81; O 30,18; Ca 21,21; F 1,83; La 0,95; P 0,02; Nd 0,01;
Parisite_Ce_La	366	1,680028	1,833466	6,978723	4,739426	Ce 37,02; La 27,6; O 20,78; Ca 13,38; F 1,2; P 0,02;
Parisite_Ce_Nd	66	0,139511	0,152253	3,809083	1,105544	Ce 37,66; O 24,34; Ca 15,66; Nd 15,31; La 5,93; F 1,03; P 0,07;
Parisite_Nd_La	0	0	0	0	0	
Pyrite	547	24,64042	31,04219	23,31194	10,80621	Fe 52,87; S 47,13;
Pyrrhotite	975	2,542639	2,941096	4,682438	2,453524	Fe 60,4; S 39,6;
Quartz	398	14,29694	9,419136	20,50029	11,4201	Si 57,3; O 42,28; Fe 0,35; Ce 0,04; La 0,03; Al 0;
Ce-quartz mix	24	0,047159	0,031425	3,5	2,17E-07	Si 50,48; O 37,81; Ce 11,72;
La-quartz mix	3	0,005895	0,003928	3,5	2,64E-07	Si 44,44; O 44,31; La 11,24;
REE-quartz mix	4	0,00786	0,007906	3,5	0	Si 45,38; O 30,17; Ce 12,69; La 10,72; Ca 1,04;
Si=O>Fe mix	107	0,241688	0,060775	4,071716	1,563127	Si 44,89; O 40,45; Fe 14,67;
Siderite	163	0,363515	0,359237	4,009342	1,469197	Fe 57,66; O 38,02; Ca 3,93; Mg 0,32; Th 0,04; Ag 0,03;
Sphalerite	7	0,037334	0,038021	8,471067	5,867904	Zn 71,75; S 28,25;
Synchysite_Ce	27	0,055018	0,054924	3,629629	0,673575	Ce 62,35; O 20,62; Ca 17,02;
Synchysite_Ce-Nd	6	0,01179	0,011858	3,5	2,38E-07	Ce 41,79; O 20,75; Nd 19,81; Ca 16,66; F 0,99;
Synchysite_Nd	16	0,031439	0,033283	3,5	2,24E-07	O 38,61; Nd 31,07; Ca 22,01; F 4,24; Ce 4,06;
Synchysite_Y	0	0	0	0	0	
Talc	45	0,096282	0,068275	3,811111	1,007297	O 52,48; Si 36,79; Mg 10,73;
Thorite	341	1,831329	3,108399	7,384122	5,276988	Th 68,35; Si 15,06; O 13,12; Ca 3,41; Ce 0,03; La 0,02; Nd 0,01;
Thorite2	81	0,168985	0,286827	3,733947	0,929158	Ag 39,97; O 37,37; Si 18,86; Ca 3,64; Nd 0,1; La 0,06;
Thorite3	1	0,001965	0,003335	3,5	0	O 38,03; Cd 22,59; Si 15,74; Ce 14,02; Ca 9,62;
Coffinite	30	0,115932	0,158587	6,37154	3,54804	U 78,49; O 12,05; Si 9,46;
Uraninite	4	0,009825	0,027102	4,375	1,75	U 80,04; O 19,96;
Uranothorite	0	0	0	0	0	
Not Analysed	5	0,009825	0	3,5	2,48E-07	
Not Classified	0	1,505148	0	0	0	O 41,71; Ca 24,6; Fe 11,49; Ce 8,51; S 3,83; Mg 2,73; P 2,67
Unclassified	831	2,243968	0	4,796291	2,510223	O 34,75; Ca 19,86; Ce 13,22; Fe 7,83; P 6,69; Si 6,65; S 2,56; Th 2,27; Mg 1,04

3_3	Number	Area %	Weight %	Grain Size (µm)	Grain Size Std Dev (µm)	Average Composition
Allanite_Ce	0	0	0	0	0	
Allanite_La	0	0	0	0	0	
Allanite_Y	0	0	0	0	0	
Ankerite	92	18,93143	18,155	14,21041	9,470845	O 46,8; Ca 30,79; Fe 11,25; Mg 10,95; Mn 0,17; Th 0,03; P 0,01;
Apatite	27	3,912495	3,799679	12,02688	9,819216	Ca 48,44; O 35,84; P 14,71; F 0,68; Ce 0,19; Ag 0,11; Nd 0,02; La 0;
Barite	20	9,002945	12,27906	21,9599	7,72557	Ba 67,2; O 18,77; S 14,03;
Bastnäsite_Ce	27	0,778292	1,189457	4,897402	3,197211	Ce 74,54; O 19,61; F 5,85;
Bastnäsite_Ce_La	49	3,029028	4,647681	7,244261	7,088526	Ce 48,02; La 33,07; O 16,02; F 2,58; Ca 0,23; Nd 0,08;
Bastnäsite_La	0	0	0	0	0	
Bastnäsite_sulph	0	0	0	0	0	
Bastnäsite_Y	0	0	0	0	0	
Bastäsite_Ce_La_Nd	9	0,189314	0,29048	3,5	1,33E-07	Ce 36,44; La 29,42; Nd 16,31; O 14,09; F 2,9; Ca 0,84;
Burbankite_Y	9	0,210349	0,241426	4,049972	1,649916	O 70,61; Ba 21,41; Ca 7,97;
Calcite	126	26,88262	22,17907	13,62992	9,980096	Ca 52,87; O 46,26; Mg 0,46; Fe 0,19; Th 0,1; Ce 0,08; La 0,01; P 0,01; Nd 0,01; Sr 0;
Calcite_w_Ce	16	0,357594	0,435464	3,71875	0,875	Ca 52,49; O 42,14; Ce 4,9; Mg 0,46;
Thorite_Ce_La_Mix	0	0	0	0	0	
Thorite_Ce_Mix	0	0	0	0	0	
Thorite2-Calsite mix	1	0,021035	0,043226	3,5	0	O 52,08; Ca 39,51; Ag 6,58; Si 1,83;
Thorite-Callsite mix	9	0,210349	0,432262	3,888889	1,166667	Ca 48,32; Th 28,43; O 18,21; Si 5,03;
Dolomite	108	3,93353	3,400973	5,636871	4,167816	O 52,75; Ca 36; Mg 10,64; Mn 0,33; Fe 0,28;
Galena	3	0,105175	0,243347	5,149915	2,857738	Pb 100;
Magnetite	5	0,126209	0,200185	4,489949	2,213594	Fe 69,41; O 30,59;
Molybdenite	3	0,105175	0,160097	6,799831	2,857738	S 94,41; Ca 4,34; Fe 1,25;
Monazite_Ce	6	0,946571	1,538853	12,86803	10,61708	Ce 46,42; O 20,17; P 16,78; La 12,16; Ca 2,61; Nd 1,86;
Monazite_Ce_La_Nd	0	0	0	0	0	
Monazite_La	0	0	0	0	0	
Parisite_Ce	102	4,669752	6,170011	6,406213	4,719562	Ce 46,04; O 28,58; Ca 21,57; F 2,22; La 1,6;
Parisite_Ce_La	85	2,902819	3,835412	5,413989	3,184919	Ce 40,1; La 28,12; O 18,81; Ca 11,17; F 1,77; P 0,02;
Parisite_Ce_Nd	7	0,147244	0,19455	3,5	2,23E-07	Ce 40,7; O 20,89; Nd 15,41; Ca 15,13; La 7,86;
Parisite_Nd_La	0	0	0	0	0	
Pyrite	4	1,346235	2,05334	16,45459	11,28505	Fe 52,5; S 47,5;
Pyrrhotite	6	0,126209	0,176747	3,5	0	Fe 59,28; S 40,72;
Quartz	34	15,08204	12,02995	22,0195	10,99932	Si 58,02; O 41,73; Fe 0,17; La 0,03; Ce 0,03;
Ce-quartz mix	2	0,04207	0,033941	3,5	0	Si 43,35; O 38,82; Ce 17,84;
La-quartz mix	1	0,021035	0,01697	3,5	0	O 51,23; Si 36,03; La 12,75;
REE-quartz mix	4	0,105175	0,128078	4,737436	2,474873	Si 37,6; O 28,65; Ce 18,75; La 15,01;
Si=O>Fe mix	2	0,04207	0,012808	3,5	0	Si 45,75; O 42; Fe 12,25;
Siderite	9	0,210349	0,251673	3,888889	1,166666	Fe 58,52; O 36,49; Ca 4,99;
Synchysite_Ce	19	0,483803	0,584738	4,356532	2,160651	Ce 65,32; O 21,05; Ca 11,16; F 2,47;
Synchysite_Ce-Nd	3	0,063105	0,076847	3,5	2,57E-07	Ce 51,18; Nd 21,01; O 16,21; Ca 10,36; F 1,24;
Synchysite_Nd	5	0,105175	0,134802	3,5	2,41E-07	O 44,8; Ca 30,22; Nd 21,2; F 3,78;
Synchysite_Y	0	0	0	0	0	
Talc	6	0,147244	0,126413	4,083333	1,428869	O 58,33; Si 33,56; Mg 8,11;
Thorite	47	2,166597	4,452299	6,281305	3,587097	Th 66,97; Si 13,97; O 12,2; Ca 6,75; Ce 0,1;
Thorite2	8	0,168279	0,34581	3,5	2,31E-07	Ag 39,8; O 34,13; Ca 17,1; Si 8,97;
Thorite3	0	0	0	0	0	
Coffinite	4	0,08414	0,139348	3,5	0	U 73,36; O 16,4; Si 10,23;
Uraninite	0	0	0	0	0	
Uranothorite	0	0	0	0	0	
Not Analysed	1	0,021035	0	3,5	0	
Not Classified	0	0,988641	0	0	0	Ca 36,1; Ce 24,04; O 21,25; Fe 5,78; La 5,29; Mg 3,32; Ba 2,33
Unclassified	87	2,334876	0	4,568073	2,261207	O 36,27; Ca 29,41; Ce 10,92; Si 5,04; Fe 3,47; Th 3,08; S 2,12; Mg 2,01; F 2,01; P 1,63; La 1,15; Nd 1,07

3_4	Number	Area %	Weight %	Grain Size (µm)	Grain Size Std Dev (µm)	Average Composition
Actinolite	2	0,00281	0,002447	3,5	0	O 55,7; Si 16,77; Fe 12,04; Mg 7,19; Ca 5,26; Al 3,04;
Allanite_Ce	0	0	0	0	0	
Allanite_La	0	0	0	0	0	
Allanite_Y	0	0	0	0	0	
Ankerite	362	0,923207	0,814324	5,315073	3,888512	O 46,12; Ca 32,44; Fe 15,16; Mg 6,21; Mn 0,06; Ag 0,01; P 0;
Apatite	182	0,390641	0,348945	4,9808	2,970653	Ca 45,45; O 41,29; P 11,73; Ce 1,09; F 0,37; Nd 0,08;
Barite	5	0,030914	0,038781	7,269335	8,42849	Ba 65,97; O 19,55; S 14,48;
Bastnäsite_Ce	95	0,140519	0,197526	3,692888	1,124846	Ce 74,02; O 22,29; F 3,55; P 0,09; Ca 0,05;
Bastnäsite_Ce_La	1243	4,505024	6,357926	7,142126	5,23382	Ce 44,13; La 36,68; O 15,86; F 2,66; Ca 0,42; P 0,19; Nd 0,06;
Bastnäsite_La	69	0,099768	0,141641	3,601449	0,591482	La 57,57; O 32,99; F 9,44;
Bastnäsite_sulph	16	0,022483	0,03173	3,5	2,27E-07	Ce 33,54; La 31,57; O 26,28; F 4,71; Fe 3,89;
Bastnäsite_Y	0	0	0	0	0	
Bastäsite_Ce_La_Nd	31	0,044966	0,06346	3,612903	0,628618	Ce 36,07; La 31,42; Nd 15,95; O 13,58; F 2,19; Ca 0,79;
Burbankite_Y	186	0,271201	0,286299	3,662898	0,913308	O 94,31; Ba 5,41; Ca 0,27;
Calcite	1329	18,37701	13,94543	14,62857	9,541144	Ca 53,09; O 46,49; Mg 0,16; Fe 0,14; Ce 0,04; Th 0,04; P 0,02; Nd 0,01; La 0,01; Ag 0; Sr 0; Y 0;
Calcite_w_Ce	178	0,258554	0,2896	3,642411	0,776199	Ca 52,48; O 43,56; Ce 3,89; Mg 0,04; Fe 0,01; Nd 0,01; P 0,01;
Thorite_Ce_La_Mix	0	0	0	0	0	
Thorite_Ce_Mix	0	0	0	0	0	
Thorite2-Calsite mix	6	0,008431	0,015936	3,5	2,33E-07	Ca 37,85; O 37,72; Ag 20,02; Si 4,41;
Thorite-Callsite mix	28	0,042156	0,079679	3,801776	1,125464	Ca 46,27; Th 29,97; O 19,06; Si 4,71;
Dolomite	1220	2,106373	1,675103	4,310983	2,072535	O 66,49; Ca 32,12; Mg 1,3; Fe 0,08; Mn 0,01; Th 0; Ag 0;
Fe-Mg-chlorite	742	2,031898	1,507772	6,141012	3,889949	O 39,84; Fe 27,4; Si 16,19; Mg 8,56; Al 8,01; K 0;
Fluorite	2	0,026699	0,023774	16,82661	18,84667	Ca 57,75; F 42,25;
Galena	1	0,00281	0,005981	6,999999	0	Pb 100;
Gypsum	3	0,004216	0,002727	3,5	2,64E-07	Ca 47,13; S 34,52; O 18,35;
Kaolinite	3	0,004216	0,003093	3,5	2,57E-07	O 47,98; Si 40,01; Al 12,01;
K-feldspar	2	0,00281	0,002007	3,5	0	O 51,71; Si 28,87; K 10,46; Al 7,95; Na 1,01;
Magnetite	403	1,735404	2,531781	7,494957	5,908682	Fe 75,57; O 24,43;
Mg-Fe-chlorite	828	2,445022	1,814331	6,501017	4,276967	O 39,32; Fe 22,47; Si 16,92; Mg 12,2; Al 9,1;
Molybdenite	23	0,051992	0,072794	4,980447	3,940409	S 98,18; Ca 1,82;
Monazite_Ce	812	17,91611	26,79001	19,68907	9,804042	Ce 42,85; La 21,93; O 19,27; P 15,19; Ca 0,58; Nd 0,18; F 0,01; Pr 0;
Monazite_Ce_La_Nd	327	0,503056	0,752221	3,865359	1,306626	Ce 32,92; La 26,55; O 16,29; Nd 12,13; P 12,07; Ca 0,05;
Monazite_La	47	0,067449	0,100857	3,605313	0,721995	O 48,49; La 28,75; P 16,91; Nd 5,07; Ce 0,78;
Nb_rutile	2	0,00281	0,003935	3,5	0	O 50,31; Ti 23,07; Nb 15,99; Fe 10,64;
Parisite_Ce	1735	3,949975	4,80034	5,444339	3,416471	Ce 46,56; O 29,41; Ca 20,2; La 1,91; F 1,89; P 0,02; Nd 0; U 0;
Parisite_Ce_La	2018	11,06162	13,443	9,387737	6,702336	Ce 37,35; La 30,84; O 19,18; Ca 11,21; F 1,38; P 0,02; Nd 0,01;
Parisite_Ce_Nd	113	0,163001	0,198093	3,60575	0,652853	Ce 34,98; O 19,77; La 18,84; Nd 13,68; Ca 10,6; F 2,07; P 0,05;
Parisite_Nd_La	2	0,00281	0,003533	3,5	0	O 32,61; Ce 21,87; La 21,4; Nd 12,65; Ca 11,47;
Plagioclase	7	0,009836	0,007382	3,5	1,54E-07	O 60,19; Si 17,94; Ca 12,97; Al 8,9;
Pyrite	28	0,422961	0,59337	16,73141	13,94723	Fe 53,3; S 46,7;
Pyrrhotite	21	0,03794	0,04887	4,608291	2,198593	Fe 60,57; S 39,43;
Quartz	852	25,23431	18,51316	21,11348	14,49487	Si 57,24; O 42,36; Fe 0,33; La 0,03; Ce 0,03; Al 0,01;
Ce-quartz mix	34	0,047776	0,035452	3,5	2,20E-07	Si 51,65; O 36,1; Ce 12,25;
La-quartz mix	32	0,044966	0,033367	3,5	2,04E-07	Si 46,5; O 42,17; La 11,33;
REE-quartz mix	31	0,043561	0,048791	3,5	2,16E-07	Si 36,83; O 28,38; Ce 18,92; La 15,45; F 0,23; Ca 0,2;
Si=O>Fe mix	227	0,33865	0,094828	3,725877	1,016216	Si 44,5; O 41,05; Fe 14,46;
Siderite	307	0,500246	0,550508	4,090994	1,688704	Fe 59,2; O 37,13; Ca 2,29; Mg 1,33; Ag 0,03; Th 0,01;
Synchysite_Ce	153	0,216399	0,240565	3,522876	0,282958	Ce 62,85; O 22,4; Ca 14,08; F 0,64; P 0,02;
Synchysite_Ce-Nd	10	0,014052	0,015739	3,5	1,97E-07	Ce 47,12; Nd 21,2; O 18,02; Ca 13,66;
Synchysite_Nd	25	0,03513	0,041414	3,5	1,67E-07	O 39,71; Nd 29,65; Ca 22,97; F 7,67;
Synchysite_Y	0	0	0	0	0	
Talc	44	0,061828	0,048823	3,5	1,70E-07	O 50,58; Si 38,23; Mg 11,19;
Thorite	463	1,377081	2,602863	6,186091	4,600261	Th 67,25; Si 17,5; O 13,93; Ca 1,25; Ce 0,04; La 0,02; Nd 0,02;
Thorite2	85	0,136303	0,25763	4,03822	1,527046	O 38,95; Ag 37,98; Si 22,35; Ca 0,62; Ce 0,09;
Thorite3	1	0,001405	0,002656	3,5	0	O 44,12; Ca 31,96; Cd 19,79; Si 4,12;
Coffinite	62	0,222019	0,338203	7,076766	6,988774	U 80,58; O 11,01; Si 8,42;
Uraninite	29	0,059018	0,181291	4,764607	2,214748	U 87,69; O 12,31;
Uranothorite	0	0	0	0	0	
Not Analysed	15	0,022483	0	3,733333	0,903696	
Not Classified	0	1,59067	0	0	0	O 33,69; Ca 21,96; Ce 14,95; La 8,03; Fe 7,24; Si 4,67; Mg 2,14; P 1,94; Al 1,35
Unclassified	1324	2,38741	0	4,538081	2,253526	O 36,23; Ca 16,32; Ce 10,26; Si 9,88; Fe 7,65; La 6,64; P 3,19; Th 1,99; S 1,87; U 1,64; F 1,6

3-6_1	Number	Area %	Weight %	Grain Size (µm)	Grain Size Std Dev (µm)	Average Composition
Allanite_Ce	0	0	0	0	0	
Allanite_La	0	0	0	0	0	
Allanite_Y	0	0	0	0	0	
Ankerite	275	4,309207	4,212768	7,117672	5,201092	O 46,33; Ca 32,49; Fe 12,72; Mg 8,35; Mn 0,11; P 0,01;
Apatite	78	2,010563	1,990527	9,292257	7,115741	Ca 49,68; O 36,04; P 13,21; F 0,54; Ce 0,27; Th 0,12; Ag 0,1; Nd 0,04;
Barite	57	7,616132	10,58942	23,93564	4,849558	Ba 67,78; O 18,33; S 13,89;
Bastnäsite_Ce	3	0,018005	0,028052	3,5	0	Ce 76,27; O 23,73;
Bastnäsite_Ce_La	115	1,662465	2,600416	7,276979	5,131346	Ce 42,6; La 37,7; O 15,96; F 2,87; Ca 0,86;
Bastnäsite_La	11	0,07202	0,113324	3,949977	1,492405	La 53,42; O 29,7; F 16,88;
Bastnäsite_sulph	0	0	0	0	0	
Bastnäsite_Y	0	0	0	0	0	
Bastäsite_Ce_La_Nd	1	0,006002	0,009388	3,5	0	Ce 40,49; La 33,9; Nd 13,66; O 11,95;
Burbankite_Y	19	0,120034	0,140444	3,760513	1,13555	O 62,75; Ba 22,36; Ca 14,89;
Calcite	422	63,41976	53,34007	24,1637	12,02858	Ca 53,31; O 46,13; Th 0,21; Mg 0,16; Fe 0,13; P 0,02; Ce 0,02; Nd 0,01; Ag 0; La 0; Y 0; Sr 0;
Calcite_w_Ce	123	0,756212	0,938778	3,597152	0,626197	Ca 52,4; O 44,58; Ce 2,95; Mg 0,07; P 0,01;
Thorite_Ce_La_Mix	0	0	0	0	0	
Thorite_Ce_Mix	0	0	0	0	0	
Thorite2-Calsite mix	18	0,114032	0,238886	3,694444	0,824958	Ca 40,74; O 36,08; Ag 18,99; Si 4,11; Sm 0,08;
Thorite-Callsite mix	111	0,82223	1,722491	4,394791	2,156066	Ca 46,35; Th 28,94; O 20,5; Si 4,19; Sm 0,02;
Dolomite	168	1,254351	1,105598	4,371639	2,125148	O 60,09; Ca 34,33; Mg 5,35; Fe 0,14; Mn 0,06; Ag 0,03;
Fe-Mg-chlorite	8	0,060017	0,04936	4,478045	2,766331	O 49,89; Fe 17,82; Si 15,95; Mg 9,1; Al 7,25;
Fluorite	2	0,018005	0,01777	5,249999	2,474873	Ca 57,93; F 42,07;
Galena	4	0,024007	0,056625	3,5	0	Pb 100;
Kaolinite	3	0,024007	0,019521	4,666666	2,020726	O 41,67; Si 36,64; Al 21,68;
Magnetite	13	0,156044	0,252315	5,142043	4,964018	Fe 73,02; O 26,98;
Mg-Fe-chlorite	10	0,102029	0,083913	5,334924	2,405561	O 41,7; Si 18,41; Fe 16,74; Mg 13,49; Al 9,65;
Monazite_Ce	18	0,114032	0,188985	3,694444	0,824958	Ce 29,85; O 28,68; Ca 19,11; P 12,37; La 9,99;
Monazite_Ce_La_Nd	0	0	0	0	0	
Monazite_La	0	0	0	0	0	
Nb_rutile	1	0,006002	0,009313	3,5	0	O 47,06; Nb 40,64; Ti 12,3;
Parisite_Ce	79	0,582163	0,784141	4,257188	2,321047	Ce 41,68; O 30,64; Ca 22,41; La 3,55; F 1,69; P 0,03;
Parisite_Ce_La	124	4,405234	5,933601	12,02773	7,51317	Ce 37,3; La 33,18; O 18,19; Ca 9,34; F 1,99; P 0,01;
Parisite_Ce_Nd	4	0,024007	0,032336	3,5	2,58E-07	Ce 32,61; La 29,91; O 16,14; Nd 12,69; Ca 6,3; F 2,35;
Parisite_Nd_La	0	0	0	0	0	
Pyrite	9	0,324091	0,503923	10,00073	7,821023	Fe 52,97; S 47,03;
Pyrrhotite	2	0,012003	0,017136	3,5	0	Fe 58,6; S 41,4;
Quartz	34	2,016565	1,639733	14,03067	10,59004	Si 57,03; O 42,6; Ce 0,18; Fe 0,14; La 0,05;
Ce-quartz mix	1	0,006002	0,004936	3,5	0	Si 51,57; O 39,34; Ce 9,09;
La-quartz mix	0	0	0	0	0	
REE-quartz mix	3	0,024007	0,029802	5,149915	2,857738	Si 37,49; O 33,4; Ce 13,49; La 12,59; F 3,02;
Si=O>Fe mix	3	0,018005	0,005588	3,5	2,64E-07	Si 42,52; O 41,99; Fe 15,49;
Siderite	18	0,126035	0,153725	4,163875	1,554251	Fe 53,54; O 38,73; Ca 7,73;
Synchysite_Ce	14	0,084024	0,103526	3,5	2,09E-07	Ce 63,65; O 22,99; Ca 12,23; F 1,12;
Synchysite_Ce-Nd	0	0	0	0	0	
Synchysite_Nd	1	0,006002	0,007842	3,5	0	Nd 35,61; O 35,04; F 19,37; Ca 9,97;
Synchysite_Y	0	0	0	0	0	
Talc	2	0,012003	0,010505	3,5	3,22E-07	O 54,98; Si 32,03; Mg 12,99;
Thorite	198	5,665586	11,86884	9,630434	8,566886	Th 73,68; O 10,05; Si 9,82; Ca 6,41; Ce 0,02; Sm 0,01; La 0,01;
Thorite2	64	0,420118	0,880105	3,850777	1,111806	Ag 46,73; O 33,26; Ca 10,13; Si 9,89;
Thorite3	0	0	0	0	0	
Coffinite	5	0,030008	0,050664	3,5	1,97E-07	U 73,06; O 14,33; Si 12,61;
Uraninite	9	0,078022	0,265633	5,055555	2,542691	U 88,32; O 11,68;
Uranothorite	0	0	0	0	0	
Not Analysed	4	0,024007	0	3,5	0	
Not Classified	0	1,344376	0	0	0	O 39,07; Ca 34,64; Ba 11,32; Ce 2,58; Si 2,2; La 1,99; Fe 1,86; Mg 1,59; Th 1,41; S 1,36
Unclassified	261	2,112592	0	4,840876	2,384398	Ca 38,02; O 36,86; Th 10,66; La 2,67; Si 2,09; Ce 1,72; Fe 1,71; P 1,04;

3-6_2	Number	Area %	Weight %	Grain Size (µm)	Grain Size Std Dev (µm)	Average Composition
Actinolite	1	0,004775	0,003933	3,5	0	Si 33,01; O 29,17; Mg 18,01; Fe 13,09; Ca 6,72;
Allanite_Ce	0	0	0	0	0	
Allanite_La	0	0	0	0	0	
Allanite_Y	0	0	0	0	0	
Ankerite	301	4,731891	3,9477	7,587206	5,75578	O 44,87; Ca 33,87; Fe 12,31; Mg 8,65; Mn 0,27; Ag 0,02; P 0,02; Th 0; Y 0;
Apatite	53	0,53956	0,455857	6,266583	3,594991	Ca 44,25; O 40,7; P 13,6; Ce 0,55; Ag 0,49; F 0,32; La 0,04; Nd 0,04;
Barite	233	8,699804	10,32253	13,72131	7,612221	Ba 68,42; O 17,11; S 14,47;
Bastnäsite_Ce	148	0,749654	0,996697	3,732429	0,928588	Ce 72,8; O 24,22; F 2,66; Ca 0,25; La 0,07;
Bastnäsite_Ce_La	567	9,669102	12,90671	8,659861	6,238426	Ce 48,22; La 33,58; O 15,91; F 2,06; Ca 0,13; Nd 0,09; P 0,01;
Bastnäsite_La	0	0	0	0	0	
Bastnäsite_sulph	7	0,033424	0,044616	3,5	2,02E-07	Ce 36,88; La 31,28; O 25,08; F 6,76;
Bastnäsite_Y	0	0	0	0	0	
Bastäsite_Ce_La_Nd	61	0,300817	0,401542	3,614754	0,628447	Ce 39,13; La 29,61; Nd 16,14; O 12,87; F 1,84; Ca 0,41;
Biotite	12	0,062073	0,04932	3,791667	1,010363	O 40,05; Si 21,6; Mg 16,95; Fe 9,75; K 6,25; Al 5,39;
Burbankite	2	0,00955	0,009535	3,5	0	O 51,3; Sr 25,34; Ba 23,36;
Burbankite_Y	235	1,618679	1,616222	4,970586	2,778554	O 67,46; Ba 30,82; Ca 1,23; Ce 0,34; Sr 0,15;
Calcite	398	9,349186	6,710299	10,80277	7,252608	Ca 51,85; O 46,54; Fe 0,89; Mg 0,65; Ag 0,03; Ce 0,02; P 0,01; Th 0; Nd 0; Y 0; Sr 0;
Calcite_w_Ce	98	0,506136	0,536199	3,823713	1,239185	Ca 51,6; O 41,24; Ce 6,55; Fe 0,42; Mg 0,18; P 0,01;
Thorite_Ce_La_Mix	48	0,243518	0,279911	3,748953	1,224963	Ag 32,92; Ce 25,51; O 23,87; La 17,7;
Thorite_Ce_Mix	175	1,06002	1,218436	4,398254	2,011365	Ag 44,21; O 31,18; Ce 24,62;
Thorite2-Calsite mix	94	0,563434	1,00727	4,423102	1,969858	Ca 41,68; O 38; Ag 16,88; Si 3,39; Nd 0,05;
Thorite-Callsite mix	6	0,033424	0,059753	4,324958	2,020726	Ca 49,25; Th 30,31; O 16,86; Si 3,58;
Dolomite	150	0,821277	0,617741	4,010988	1,369205	O 54,91; Ca 41,25; Mg 2,87; Fe 0,97; Mn 0;
Fe-Mg-chlorite	11	0,062073	0,043566	4,268158	1,739518	O 45,21; Si 21,73; Fe 21,31; Mg 7,09; Al 4,66;
Galena	16	0,095497	0,192222	4,246859	1,634528	Pb 97,78; As 2,22;
Magnetite	111	1,093444	1,508805	6,303744	4,296099	Fe 77,91; O 22,09;
Mg-Fe-chlorite	22	0,138471	0,097186	4,652238	2,488465	O 39,1; Si 27,65; Mg 17,48; Fe 11,78; Al 3,99;
Molybdenite	3	0,014325	0,018969	3,5	0	S 97,88; Ca 2,12;
Monazite_Ce	53	0,635057	0,898158	6,975593	4,545851	Ce 45,76; O 25,11; P 16,01; La 8,92; Ca 2,9; Nd 1,29;
Monazite_Ce_La_Nd	5	0,023874	0,033765	3,5	2,48E-07	Ce 34,12; La 23,08; Nd 15,56; O 13,96; P 13,28;
Monazite_La	0	0	0	0	0	
Parisite_Ce	594	5,228477	6,009852	5,849336	3,748512	Ce 40,84; O 33,09; Ca 19,29; La 5,64; F 1,14; P 0,01;
Parisite_Ce_La	529	5,047032	5,801291	6,092924	4,099887	Ce 39,95; La 27,4; O 19,14; Ca 12,39; F 1,09; P 0,03;
Parisite_Ce_Nd	115	0,759204	0,872663	4,507107	3,317842	Ce 33,34; O 23,28; Ca 18,08; Nd 15,38; La 9,25; F 0,67;
Parisite_Nd_La	9	0,042974	0,051103	3,5	2,38E-07	Ce 27,53; O 23,07; La 18,72; Nd 15,67; Ca 14,5; F 0,51;
Plagioclase	1	0,004775	0,003389	3,5	0	O 61,84; Si 20,14; Al 9,19; Ca 6,01; Na 2,83;
Pyrite	11	0,224419	0,29778	10,29511	6,780769	Fe 52,2; S 47,8;
Pyrrhotite	4	0,023874	0,029086	4,737437	2,474874	Fe 62,03; S 37,97;
Quartz	944	27,36953	18,99186	11,7556	7,058769	Si 57,77; O 41,74; Fe 0,27; Ce 0,15; La 0,05; Al 0,02;
Ce-quartz mix	302	1,695077	1,189691	4,131028	1,64116	Si 51,55; O 35,24; Ce 13,18; Ag 0,03;
La-quartz mix	43	0,210094	0,147455	3,581395	0,533745	Si 47,42; O 42,45; La 10,08; Ag 0,05;
REE-quartz mix	343	2,048417	2,170087	4,397137	2,094255	Si 37,8; O 27,33; Ce 19,7; La 14,7; Nd 0,25; F 0,15; Ca 0,07;
Si=O>Fe mix	41	0,214869	0,056908	3,876823	1,177159	Si 44,41; O 41,2; Fe 14,39;
Siderite	53	0,286492	0,298197	3,978287	1,535639	Fe 59,89; O 35; Ca 3,21; Mg 1,84; Mn 0,06;
Synchysite_Ce	78	0,386764	0,406664	3,671788	0,874963	Ce 58,2; O 30,02; Ca 10,07; F 1,47; Nd 0,24;
Synchysite_Ce-Nd	22	0,17667	0,187164	5,644254	4,022664	Ce 39,16; Nd 21,73; O 20,54; Ca 18,35; F 0,22;
Synchysite_Nd	10	0,066848	0,074537	5,127411	2,818314	O 28,61; Ce 24,81; Ca 24,19; Nd 22,06; F 0,32;
Synchysite_Y	0	0	0	0	0	
Talc	64	0,587308	0,438646	5,750452	3,780978	O 45,77; Si 36,88; Mg 17,35;
Thorite	116	0,630282	1,126776	3,936841	1,429759	Th 74,6; Si 11,63; O 11,47; Ca 1,78; Ce 0,4; La 0,09; Nd 0,04;
Thorite2	644	9,979468	17,84062	7,603037	6,790749	Ag 50,66; O 33; Si 13,11; Ca 2,75; Ce 0,37; La 0,07; Nd 0,04; Sm 0;
Thorite3	1	0,004775	0,008536	3,5	0	O 77,39; Cd 17,59; Si 5,03;
Coffinite	1	0,004775	0,00688	3,5	0	U 83,33; O 12,32; Si 4,35;
Uraninite	1	0,004775	0,013873	3,5	0	U 89,29; O 10,71;
Uranothorite	0	0	0	0	0	
Not Analysed	3	0,014325	0	3,5	0	
Not Classified	0	0,095497	0	0	0	Ba 53,41; O 16,35; Si 10,14; Ce 9,81; S 7,41; Ti 1,23; Fe 1,09
Unclassified	626	3,834217	0	4,532022	2,255431	O 31,36; Si 18,66; Ce 14,73; Ca 12,4; Fe 7,45; Ag 5,83; La 3,52; Th 1,12

3-6_3	Number	Area %	Weight %	Grain Size (µm)	Grain Size Std Dev (µm)	Average Composition
Actinolite	1	0,006687	0,005798	3,5	0	Si 33,78; O 32,45; Mg 18,64; Fe 9,48; Ca 5,66;
Allanite_Ce	0	0	0	0	0	
Allanite_La	0	0	0	0	0	
Allanite_Y	0	0	0	0	0	
Ankerite	576	9,041059	7,939708	6,784789	4,609762	O 43,94; Ca 35,35; Fe 14,16; Mg 6,34; Mn 0,13; Ag 0,05; P 0,01; Th 0; Sr 0;
Apatite	16	0,220677	0,196256	5,031234	4,42136	Ca 45,24; O 40,05; P 10,02; Ce 2,45; Ag 2,02; F 0,22;
Barite	1	0,133743	0,167042	20,99975	0	Ba 69,44; O 16,17; S 14,39;
Bastnäsite_Ce	0	0	0	0	0	
Bastnäsite_Ce_La	9	0,086933	0,122149	4,82775	2,035121	Ce 46,55; La 33,34; O 18,1; F 1,37; Ca 0,64;
Bastnäsite_La	0	0	0	0	0	
Bastnäsite_sulph	0	0	0	0	0	
Bastnäsite_Y	0	0	0	0	0	
Bastäsite_Ce_La_Nd	0	0	0	0	0	
Burbankite_Y	23	0,153805	0,161654	3,5	6,86E-08	O 91,74; Ba 6,55; Ca 1,72;
Calcite	609	27,67821	20,91135	13,05099	7,93322	Ca 52,54; O 46,07; Fe 0,86; Mg 0,47; Ag 0,04; Th 0,01; P 0,01; Sr 0; Ce 0; Y 0; Nd 0;
Calcite_w_Ce	48	0,334359	0,372861	3,676036	0,866179	Ca 52,08; O 41,28; Ce 5,25; Fe 0,78; Mg 0,62;
Thorite_Ce_La_Mix	0	0	0	0	0	
Thorite_Ce_Mix	7	0,04681	0,056638	3,5	4,64E-08	Ag 46,76; O 32,18; Ce 21,06;
Thorite2-Calsite mix	216	2,006152	3,775221	4,777092	2,562255	Ca 41,87; O 39,43; Ag 15,63; Si 3,07;
Thorite-Callsite mix	9	0,060185	0,113257	3,5	6,96E-08	Ca 45,61; Th 29,46; O 21,04; Si 3,88;
Dolomite	190	1,511301	1,196586	4,214456	1,819425	O 56,03; Ca 34,36; Mg 7,54; Fe 2,06; Mn 0,01;
Fe-Mg-chlorite	9	0,066872	0,049404	4,049972	1,649916	O 46,02; Si 24,12; Fe 20,75; Mg 5; Al 4,11;
Galena	1	0,006687	0,014169	3,5	0	Pb 100;
Gypsum	4	0,040123	0,025839	4,737437	2,474874	Ca 39,69; S 31,71; O 28,6;
Magnetite	203	3,744817	5,439301	7,582929	5,559178	Fe 76,73; O 23,27;
Mg-Fe-chlorite	7	0,060185	0,044464	4,5	2,645751	O 38,82; Si 20,75; Mg 17,37; Fe 17,08; Al 5,98;
Molybdenite	2	0,020062	0,027965	5,25	2,474874	S 95,58; Ca 4,42;
Monazite_Ce	41	0,96964	1,443532	9,345873	4,843631	Ce 44,04; O 21,69; P 15,82; La 14,76; Ca 3,57; Nd 0,13;
Monazite_Ce_La_Nd	2	0,013374	0,019911	3,5	0	Ce 33,2; La 24,42; O 15,12; P 13,66; Nd 13,6;
Monazite_La	1	0,006687	0,009955	3,5	0	O 74,44; P 12,78; La 12,78;
Parisite_Ce	217	2,253578	2,726697	5,253902	3,225787	Ce 37,54; O 34,74; Ca 19,9; La 7,04; F 0,72; P 0,06;
Parisite_Ce_La	196	5,396549	6,52951	9,183666	6,7202	Ce 37,72; La 27,88; O 19,6; Ca 13,95; F 0,84;
Parisite_Ce_Nd	16	0,113682	0,137549	3,809359	1,237437	Ce 32,95; O 22,83; La 15,19; Ca 14,72; Nd 13,38; F 0,93;
Parisite_Nd_La	0	0	0	0	0	
Pyrite	27	1,725291	2,409765	17,16371	7,047514	Fe 51,98; S 48,02;
Pyrrhotite	6	0,040123	0,051455	3,5	5,08E-08	Fe 59,44; S 40,56;
Quartz	324	22,5224	16,45094	15,90907	7,858907	Si 57,35; O 41,83; Fe 0,73; Al 0,04; La 0,03; Ce 0,02;
Ce-quartz mix	15	0,106995	0,079047	3,733333	0,903696	Si 51,2; O 38,5; Ce 10,3;
La-quartz mix	2	0,013374	0,009881	3,5	0	Si 45,23; O 44,53; La 10,24;
REE-quartz mix	6	0,040123	0,044743	3,5	5,08E-08	Si 38,25; O 31,91; Ce 16,83; La 12,48; Ca 0,53;
Si=O>Fe mix	101	0,722215	0,201345	3,785636	1,068923	Si 45,18; O 40,34; Fe 14,48;
Siderite	136	1,069948	1,172276	4,131782	1,637945	Fe 58,1; O 35,03; Ca 6,01; Mg 0,67; Ag 0,15; Th 0,03; P 0,01;
Sphalerite	3	0,033436	0,037752	5,833333	2,020726	Zn 68,3; S 27,41; Fe 4,29;
Synchysite_Ce	6	0,040123	0,044408	3,5	5,08E-08	O 56,44; Ce 35,24; Ca 8,32;
Synchysite_Ce-Nd	0	0	0	0	0	
Synchysite_Nd	1	0,006687	0,007849	3,5	0	O 49,57; F 19,4; Nd 19,4; Ca 11,64;
Synchysite_Y	0	0	0	0	0	
Talc	75	0,815835	0,641396	5,22528	3,6563	O 48,21; Si 35,55; Mg 16,25;
Thorite	92	0,702153	1,321327	3,981511	1,524235	Th 71,37; O 12,27; Si 10,97; Ca 5,32; Ce 0,08;
Thorite2	529	13,07343	24,60185	9,120911	5,579914	Ag 44,33; O 36,54; Si 12,34; Ca 6,7; Ce 0,07; La 0,02; Nd 0;
Thorite3	1	0,006687	0,012584	3,5	0	O 47,18; Cd 26,76; Si 26,06;
Coffinite	29	0,40123	0,60851	6,29969	4,205589	U 77,94; O 13,8; Si 8,26;
Uraninite	19	0,267487	0,818058	6,875909	4,690013	U 87,95; O 11,35; Si 0,6; Th 0,1;
Uranothorite	0	0	0	0	0	
Not Classified	0	0,695466	0	0	0	O 83,64; K 6,28; Cl 2,51
Unclassified	431	3,744817	0	4,496874	2,18772	O 35,06; Ca 21,12; Fe 18,9; Si 11,01; U 4,19; Ce 1,95; S 1,94; Ag 1,61; Mg 1,43

3-6_4

	Number	Area %	Weight %	Grain Size (µm)	Grain Size Std Dev (µm)	Average Composition
Allanite_Ce	0	0	0	0	0	
Allanite_La	0	0	0	0	0	
Allanite_Y	0	0	0	0	0	
Ankerite	36	3,464567	3,27039	5,586201	3,888346	O 45,96; Ca 34,63; Fe 12,91; Mg 6,3; Mn 0,16; P 0,03;
Apatite	5	0,734908	0,702528	9,554822	3,926395	Ca 49,98; O 35,7; P 13,11; F 1,21;
Barite	2	0,839895	1,127569	17,95594	4,795054	Ba 68,98; O 16,29; S 14,74;
Bastnäsite_Ce	6	0,419948	0,631741	4,666667	1,807392	Ce 63,52; O 25,55; F 10,3; Ca 0,63;
Bastnäsite_Ce_La	16	9,291339	14,03295	11,90583	21,62092	Ce 43,32; La 32,76; O 19,37; F 3,84; Ca 0,71;
Bastnäsite_La	0	0	0	0	0	
Bastnäsite_sulph	0	0	0	0	0	
Bastnäsite_Y	0	0	0	0	0	
Bastäsite_Ce_La_Nd	1	0,104987	0,158564	7	0	Ce 35,55; La 26,03; O 17,88; Nd 13,66; F 6,88;
Burbankite_Y	3	0,209974	0,237217	4,666666	2,020726	O 53,54; Ba 46,46;
Calcite	82	38,53018	31,29035	14,37883	8,525224	Ca 52,89; O 46,58; Fe 0,27; Mg 0,17; Ag 0,04; P 0,02; Th 0,02; Nd 0,01; Ce 0; Y 0;
Calcite_w_Ce	10	0,524934	0,629224	3,5	2,21E-07	O 46,99; Ca 46,01; Ce 6,49; Fe 0,5;
Thorite_Ce_La_Mix	0	0	0	0	0	
Thorite_Ce_Mix	0	0	0	0	0	
Thorite2-Calsite mix	19	1,364829	2,760719	4,64996	2,012106	Ca 41,53; O 36,78; Ag 17,72; Si 3,69; La 0,27;
Thorite-Callsite mix	0	0	0	0	0	
Dolomite	29	1,994751	1,697645	4,554496	2,9844	O 59,23; Ca 36,92; Mg 3,16; Fe 0,69;
Fluorite	1	0,052493	0,050023	3,5	0	Ca 56,83; F 43,17;
Galena	2	0,104987	0,239105	3,5	3,22E-07	Pb 100;
Gypsum	2	0,104987	0,072675	3,5	0	Ca 39,86; O 32,65; S 27,49;
Magnetite	5	0,367454	0,573695	4,489949	2,213594	Fe 76,27; O 23,73;
Mg-Fe-chlorite	2	1,469816	1,16721	21,17315	0,245232	O 38,76; Fe 19,49; Mg 16,39; Si 14,92; Al 10,44;
Molybdenite	1	0,052493	0,078653	3,5	0	S 100;
Monazite_Ce	3	0,419947	0,672011	8,716244	9,034801	Ce 47,19; O 27,69; P 16,18; La 8,94;
Monazite_Ce_La_Nd	0	0	0	0	0	
Monazite_La	0	0	0	0	0	
Nb_rutile	1	0,052493	0,078653	3,5	0	O 49,89; Ti 37,36; Nb 12,75;
Parisite_Ce	27	1,784777	2,321206	4,286069	2,017112	O 37,3; Ce 35,24; Ca 20,58; La 4,46; F 2,42;
Parisite_Ce_La	44	4,934383	6,417452	5,876191	5,083353	Ce 38,07; La 28,99; O 20,22; Ca 11,11; F 1,61;
Parisite_Ce_Nd	4	0,262467	0,341354	4,375	1,75	Ce 34,12; O 24,06; Ca 18,41; La 11,82; Nd 9,7; F 1,88;
Parisite_Nd_La	0	0	0	0	0	
Pb-As-Sulphide	1	0,052493	0,083844	3,5	0	Pb 82,58; As 17,42;
Pyrite	8	1,994751	2,99479	10,78266	7,405126	Fe 52,62; S 47,38;
Quartz	35	22,09974	17,35116	16,08611	9,168146	Si 57,86; O 41,84; Fe 0,22; Ce 0,05; La 0,02; Al 0,01;
Ce-quartz mix	2	0,104987	0,083372	3,5	0	Si 44,89; O 39,21; Ce 15,9;
La-quartz mix	2	0,104987	0,083372	3,5	3,22E-07	O 46,72; Si 38,24; La 15,05;
REE-quartz mix	2	0,104987	0,125845	3,5	0	Si 39,5; O 29,39; Ce 17,29; La 13,82;
Si=O>Fe mix	1	0,104987	0,031461	7	0	Si 48,52; O 39,39; Fe 12,1;
Siderite	3	0,262467	0,309106	6,108122	4,5174	Fe 58,02; O 34,98; Ca 6,58; Mg 0,42;
Sphalerite	1	0,052493	0,063709	3,5	0	Zn 70,09; S 29,91;
Synchysite_Ce	1	0,052493	0,06245	3,5	0	Ce 61,83; O 28,63; Ca 9,54;
Synchysite_Ce-Nd	1	0,052493	0,062922	3,5	0	Ce 47,03; Nd 20; O 17,36; Ca 15,6;
Synchysite_Nd	0	0	0	0	0	
Synchysite_Y	0	0	0	0	0	
Thorite	4	0,209974	0,424726	3,5	2,32E-07	Th 58,55; Ca 14,08; Si 13,62; O 11,69; Ce 2,06;
Thorite2	34	3,727034	7,538886	6,169176	4,051045	Ag 40,73; O 35,11; Si 14,11; Ca 9,85; Ce 0,21;
Thorite3	0	0	0	0	0	
Coffinite	10	0,734908	1,198042	4,899999	1,807392	U 81,73; O 10,86; Si 7,41;
Uraninite	4	0,314961	1,035388	4,737437	2,474873	U 87,02; O 12,21; Si 0,77;
Uranothorite	0	0	0	0	0	
Unclassified	38	2,939632	0	4,963772	3,06374	O 32,03; Ca 29,19; Si 9,66; U 9,43; Ce 4,42; Fe 3,83; Zn 3,16; S 2,33; La 1,59

6_1	Number	Area %	Weight %	Grain Size (µm)	Grain Size Std Dev (µm)	Average Composition
Allanite_Ce	0	0	0	0	0	
Allanite_La	0	0	0	0	0	
Allanite_Y	0	0	0	0	0	
Ankerite	478	8,409643	6,615104	6,691754	5,186279	O 45,04; Ca 33,99; Fe 12,42; Mg 8,25; Mn 0,25; Ag 0,03; P 0,01; Th 0; Y 0; Sr 0;
Apatite	48	0,454744	0,362248	4,954632	2,588215	Ca 46,93; O 39,95; P 9,32; Ce 2,23; Ag 1,38; F 0,2;
Barite	18	1,102598	1,233513	15,54124	16,26014	Ba 68,31; O 17,26; S 14,43;
Bastnäsite_Ce	1	0,006229	0,007809	3,5	0	Ce 90,58; O 9,42;
Bastnäsite_Ce_La	27	0,361303	0,454727	5,562686	3,97997	Ce 44,96; La 37,45; O 14,53; F 2,07; P 0,45; Ca 0,33; Nd 0,21;
Bastnäsite_La	0	0	0	0	0	
Bastnäsite_sulph	3	0,018688	0,02352	3,5	0	Ce 37,02; La 31,7; O 20,39; Fe 9,51; F 1,38;
Bastnäsite_Y	0	0	0	0	0	
Bastäsite_Ce_La_Nd	0	0	0	0	0	
Burbankite	2	0,012459	0,011729	3,5	3,22E-07	O 61,93; Sr 22,78; Ba 15,29;
Burbankite_Y	42	0,460973	0,433976	5,85234	3,7479	O 69,72; Ba 30,07; Ca 0,11; Sr 0,11;
Calcite	521	37,82471	25,59726	18,1312	14,54684	Ca 52,62; O 46,16; Fe 0,66; Mg 0,42; Ag 0,09; Th 0,03; P 0,01; La 0; Ce 0; Nd 0; Y 0; Sr 0;
Calcite_w_Ce	43	0,274092	0,273782	3,61511	0,754829	Ca 52,64; O 42,68; Ce 3,66; Mg 0,57; Fe 0,46;
Thorite_Ce_La_Mix	1	0,006229	0,006751	3,5	0	Ag 36,46; Ce 23,83; O 23,1; La 16,61;
Thorite_Ce_Mix	9	0,062294	0,067512	3,888889	1,166667	Ag 43,56; O 31,34; Ce 25,11;
Thorite2-Calsite mix	511	4,90251	8,26363	5,328511	3,00309	Ca 41,56; O 39,12; Ag 16,25; Si 3,07; La 0;
Thorite-Callsite mix	19	0,118358	0,199503	3,5	1,47E-07	Ca 48,22; Th 26,26; O 21,57; Si 3,95;
Dolomite	97	0,716377	0,508052	4,169046	1,802117	O 55,47; Ca 35,5; Mg 6,72; Fe 2,1; Mn 0,11; Ag 0,08; Y 0,01;
Fe-Mg-chlorite	59	0,598019	0,39574	5,441219	3,17873	O 45,51; Fe 26,18; Si 13,7; Mg 8,43; Al 6,17;
Galena	15	0,124587	0,236448	4,626633	1,972317	Pb 99,15; As 0,85;
Gypsum	7	0,043606	0,025154	3,5	1,61E-07	Ca 42,61; O 38,66; S 18,73;
Magnetite	92	2,136672	2,779868	8,541194	6,695865	Fe 78,51; O 21,49;
Mg-Fe-chlorite	41	0,610478	0,403984	7,383287	4,744604	O 38,19; Fe 23,31; Si 16,35; Mg 13,12; Al 9,03;
Molybdenite	5	0,037376	0,046667	4,2	1,565247	S 98,93; Fe 1,07;
Monazite_Ce	82	5,762163	7,683788	17,84401	10,96109	Ce 40,97; La 23,22; O 19,01; P 15,28; Ca 1,4; Nd 0,12;
Monazite_Ce_La_Nd	9	0,056064	0,074761	3,5	1,93E-07	Ce 33,77; La 25,46; O 16,64; P 13,56; Nd 10,57;
Monazite_La	3	0,018688	0,02492	3,5	0	O 65,53; La 19,25; P 8,28; Ce 6,94;
Parisite_Ce	76	0,635395	0,688624	4,639041	2,423049	O 36,92; Ce 29,74; Ca 21,79; La 10,96; F 0,4; P 0,19;
Parisite_Ce_La	94	1,588488	1,72156	7,092951	5,850538	Ce 35,21; La 28,98; O 20,85; Ca 14,48; F 0,47; P 0,02;
Parisite_Ce_Nd	5	0,031147	0,033756	3,5	2,41E-07	Ce 32,29; La 22,36; O 19,01; Ca 14,12; Nd 12,23;
Parisite_Nd_La	0	0	0	0	0	
Pb-As-Sulphide	1	0,006229	0,008291	3,5	0	Pb 68,44; As 31,56;
Pyrite	22	1,532424	1,91719	17,12786	16,52837	Fe 52,19; S 47,81;
Pyrrhotite	13	0,09967	0,114491	4,14998	1,613945	Fe 62,91; S 37,09;
Quartz	125	7,319504	4,788853	15,33181	8,913505	Si 57,12; O 41,84; Fe 0,94; Al 0,05; Ce 0,03; La 0,02;
Ce-quartz mix	3	0,018688	0,012367	3,5	2,64E-07	Si 50,53; O 38,87; Ce 10,6;
La-quartz mix	1	0,006229	0,004122	3,5	0	O 48,95; Si 39,34; La 11,71;
REE-quartz mix	5	0,031147	0,031112	3,5	1,97E-07	Si 42,27; O 32,94; Ce 11,98; La 10,46; Ca 1,83; F 0,51;
Si=O>Fe mix	36	0,242945	0,060668	3,791666	0,981071	Si 44,43; O 41,23; Fe 14,34;
Siderite	79	0,660313	0,648024	4,652483	2,358709	Fe 57,7; O 35,58; Ca 4,67; Mg 1,76; Ag 0,3;
Synchysite_Ce	1	0,006229	0,006176	3,5	0	O 60,78; Ce 30,59; P 4,31; Ca 4,31;
Synchysite_Ce-Nd	0	0	0	0	0	
Synchysite_Nd	0	0	0	0	0	
Synchysite_Y	0	0	0	0	0	
Talc	14	0,09967	0,070188	4,103553	1,560329	O 55,52; Si 37,81; Mg 6,67;
Thorite	134	0,915717	1,543524	3,915285	1,427154	Th 70,32; O 13,05; Si 9,63; Ca 6,97; Ce 0,03;
Thorite2	544	18,45761	31,11199	10,23369	9,918	Ag 46,56; O 35,38; Si 10,04; Ca 7,92; Ce 0,05; La 0,03; Nd 0,02; Sm 0;
Thorite3	1	0,006229	0,0105	3,5	0	Ca 38,06; Cd 26,87; O 24,25; Si 10,82;
Coffinite	6	1,07768	1,463987	21,20796	24,21784	U 83,56; O 8,91; Si 7,53;
Uraninite	2	0,012459	0,034129	3,5	0	U 87,02; O 12,98;
Uranothorite	0	0	0	0	0	
Not Classified	0	0,09967	0	0	0	O 15,78; Si 15,42; Ca 15,22; Fe 12,74; Ce 12,71; La 9,79; U 6,18; S 3,13; Mg 2,72; Ba 2,56; Ag 1,44
Unclassified	376	3,033701	0	4,599984	2,227129	O 35,29; Ca 31,63; Fe 10,19; Si 5,86; Ag 4,42; Ce 3,04; U 1,92; Th 1,68; S 1,41; La 1,37

6_2	Number	Area %	Weight %	Grain Size (µm)	Grain Size Std Dev (µm)	Average Composition
Allanite_Ce	0	0	0	0	0	
Allanite_La	0	0	0	0	0	
Allanite_Y	0	0	0	0	0	
Ankerite	2100	4,758702	3,264983	5,832052	4,072848	O 42,6; Ca 35,74; Fe 16,99; Mg 4,43; Mn 0,16; Ag 0,05; P 0,01; Th 0,01; Sr 0; Y 0;
Apatite	72	0,312028	0,216803	9,66507	6,932334	Ca 47,4; O 37,51; P 13,55; Ag 0,92; F 0,33; Ce 0,24; Th 0,03; La 0,02; Nd 0,01;
Barite	20	0,200668	0,195812	14,76927	6,84287	Ba 68,63; O 16,99; S 14,38;
Bastnäsite_Ce	30	0,033077	0,036167	3,5	5,97E-08	Ce 71,69; O 26,75; F 0,81; Ca 0,74;
Bastnäsite_Ce_La	1295	3,466487	3,805415	6,987952	5,512685	Ce 45,14; La 36,51; O 15,93; F 1,83; Ca 0,52; P 0,04; Nd 0,02;
Bastnäsite_La	1	0,001103	0,001218	3,5	0	La 61,63; O 38,37;
Bastnäsite_sulph	48	0,052923	0,058098	3,5	0	Ce 35,38; La 32,07; O 21,16; Fe 8,63; F 2,06; Nd 0,47; S 0,23;
Bastnäsite_Y	0	0	0	0	0	
Bastäsite_Ce_La_Nd	13	0,014333	0,015735	3,5	6,56E-08	Ce 37,62; La 32,23; Nd 14,65; O 13,66; Ca 0,97; F 0,88;
Burbankite_Y	97	0,114668	0,094159	3,782469	1,150229	O 81,16; Ba 16,42; Ca 2,18; Ce 0,24;
Calcite	1947	13,48887	7,962084	13,26549	9,007086	Ca 53,41; O 45,38; Fe 0,94; Mg 0,19; Ag 0,04; Th 0,02; P 0,01; Ce 0; Nd 0; Y 0; Sr 0; La 0;
Calcite_w_Ce	139	0,15877	0,138328	3,646759	0,774392	Ca 52,7; O 41,06; Ce 5,17; Fe 1; Mg 0,07;
Thorite_Ce_La_Mix	47	0,058436	0,05524	3,934032	1,292924	Ag 31,6; Ce 24,52; O 24; La 19,88;
Thorite_Ce_Mix	238	0,288874	0,273074	3,890535	1,402155	Ag 40,34; O 33,53; Ce 26,11; P 0,02;
Thorite2-Calsite mix	741	1,083829	1,593479	4,646521	2,405114	Ca 42,08; O 39,42; Ag 15,67; Si 2,79; Ce 0,02; La 0,01; Nd 0,01; Sm 0;
Thorite-Callsite mix	43	0,047411	0,069705	3,5	0	Ca 47,65; Th 26,19; O 22,78; Si 3,37;
Dolomite	170	0,212796	0,131633	3,839455	1,853608	O 55,22; Ca 39,01; Mg 4,31; Fe 1,42; Mn 0,02; Th 0,01;
Fe-Mg-chlorite	427	0,522619	0,301657	3,918374	1,279129	O 41,94; Fe 30,9; Si 12,64; Mg 8,67; Al 5,84;
Galena	15	0,019846	0,032853	4,2	1,449138	Pb 97,43; As 2,57;
Gypsum	5	0,005513	0,002774	3,5	5,68E-08	Ca 41,68; O 29,72; S 28,6;
Magnetite	2694	12,9872	14,73788	9,936038	8,396932	Fe 76,86; O 23,14;
Mg-Fe-chlorite	1520	6,2152	3,587426	9,096204	7,57451	O 36,79; Fe 22,56; Si 16,45; Mg 15,19; Al 9,01; K 0;
Molybdenite	1	0,001103	0,001201	3,5	0	S 81,66; Ca 18,34;
Monazite_Ce	347	2,701302	3,141929	13,3223	9,746749	Ce 41,89; La 21,83; O 20,64; P 15,07; Ca 0,44; Nd 0,12; F 0;
Monazite_Ce_La_Nd	31	0,03418	0,039755	3,5	5,87E-08	Ce 32,77; La 25,88; O 15,6; Nd 13,09; P 12,66;
Monazite_La	19	0,022051	0,025648	3,760513	1,13555	O 63,55; La 20,49; P 11,96; Ce 3,52; Nd 0,48;
Nb_rutile	16	0,049616	0,054035	7,905936	4,39301	Ti 52,25; O 35,08; Nb 7,93; Fe 4,73;
Parisite_Ce	2392	4,092748	3,868893	5,245061	3,279338	Ce 36,7; O 36,61; Ca 16,44; La 9,58; F 0,64; P 0,02; Nd 0,01;
Parisite_Ce_La	2518	10,52957	9,953644	9,275347	7,284444	Ce 37,56; La 29,82; O 19,64; Ca 12,13; F 0,84; P 0,01; Nd 0;
Parisite_Ce_Nd	130	0,14554	0,137579	3,553846	0,432436	Ce 32,08; La 22,86; O 20,34; Nd 12,78; Ca 11,18; F 0,76;
Parisite_Nd_La	5	0,005513	0,005391	3,5	5,68E-08	Ce 28,3; La 22,73; O 21,96; Nd 13,83; Ca 13,18;
Pb-As-Sulphide	4	0,00441	0,00512	3,5	0	Pb 78,2; As 21,8;
Pyrite	266	2,083862	2,27399	13,92906	9,905086	Fe 53,01; S 46,99;
Pyrrhotite	117	0,14995	0,15024	4,137377	1,812765	Fe 64,82; S 35,18;
Quartz	495	3,01774	1,722127	11,34849	8,09079	Si 56,38; O 41,86; Fe 1,56; Al 0,11; La 0,04; Ce 0,04;
Ce-quartz mix	29	0,033077	0,019092	3,62069	0,649934	Si 50,71; O 37,11; Ce 12,18;
La-quartz mix	23	0,025359	0,014637	3,5	6,86E-08	O 44,78; Si 44,01; La 11,21;
REE-quartz mix	34	0,045205	0,039385	4,124231	1,819275	Si 36,7; O 26,55; Ce 19,62; La 16,13; Ca 0,49; F 0,3; Nd 0,21;
Si=O>Fe mix	193	0,244771	0,053314	4,017604	1,531755	Si 45,22; O 40,18; Fe 14,6;
Siderite	2078	3,195255	2,735142	4,82177	2,891313	Fe 57,9; O 33,75; Mg 5,38; Ca 2,78; Ag 0,19; Th 0,01; Sr 0;
Synchysite_Ce	69	0,076077	0,065785	3,5	0	Ce 50,08; O 39,84; Ca 9,67; F 0,41;
Synchysite_Ce-Nd	1	0,001103	0,000961	3,5	0	Ce 42,15; Nd 20; O 19,38; Ca 18,46;
Synchysite_Nd	5	0,005513	0,005055	3,5	5,68E-08	O 62,89; Nd 25,29; Ca 11,82;
Synchysite_Y	0	0	0	0	0	
Talc	30	0,040795	0,025058	4,275804	2,108395	O 52,52; Si 40,15; Mg 7,32;
Thorite	1069	1,315369	1,933896	3,94849	1,426591	Th 72,13; O 16; Si 9,84; Ca 1,86; Ce 0,08; La 0,07; Nd 0,01;
Thorite2	2975	25,09455	36,89479	12,67962	12,9056	Ag 47,11; O 39,82; Si 10,38; Ca 2,46; Ce 0,15; La 0,08; Nd 0,01; Sm 0;
Thorite3	8	0,008821	0,012968	3,5	4,30E-08	O 58,25; Si 24,84; Cd 12,16; Ca 4,76;
Coffinite	15	0,049616	0,05879	6,374042	5,602448	U 82,39; O 10,08; Si 7,53; Th 0;
Uraninite	25	0,078283	0,187048	8,542267	6,433665	U 89,15; O 10,52; Si 0,33;
Uranothorite	0	0	0	0	0	
Not Analysed	5	0,005513	0	3,5	5,68E-08	
Not Classified	0	0,084898	0	0	0	O 48,87; Fe 19,45; S 5,57; Si 3,51; Ce 3,43; Ca 2,96; Mg 2,85; Ag 1,89; Cl 1,65; Ni 1,33; Al 1,3; Co 1,3
Unclassified	2084	2,814867	0	4,370183	1,985143	O 30,07; Fe 25,39; Ca 13,43; Ce 8,25; Si 7,37; La 6,19; Ag 3,75; Mg 1,69

6_3	Number	Area %	Weight %	Grain Size (µm)	Grain Size Std Dev (µm)	Average Composition
Actinolite	1	0,001261	0,000891	3,5	0	O 50,56; Si 17,98; Ca 12,92; Fe 8,43; Mg 7,3; Al 2,81;
Allanite_Ce	0	0	0	0	0	
Allanite_La	0	0	0	0	0	
Allanite_Y	0	0	0	0	0	
Ankerite	1100	2,301561	1,646463	5,274793	3,398138	O 43,22; Ca 36,56; Fe 16,08; Mg 3,75; P 0,26; Ag 0,08; Mn 0,04; Sr 0; Th 0; Y 0;
Apatite	1451	14,21797	10,30024	13,90605	11,62626	Ca 47; O 35,24; P 15,44; Ag 1,25; F 0,52; Ce 0,48; Nd 0,03; Th 0,03; La 0,01; Cl 0;
Barite	46	0,454007	0,461912	14,26658	12,12997	Ba 68,89; O 16,17; S 14,94;
Bastnäsite_Ce	34	0,046662	0,053197	3,83307	1,453303	Ce 72,14; O 23,66; F 3,75; Ca 0,28; P 0,17;
Bastnäsite_Ce_La	384	2,432719	2,784462	10,45677	8,490985	Ce 45,97; La 36,59; O 14,93; F 2,11; Ca 0,19; P 0,18; Nd 0,02;
Bastnäsite_La	1	0,001261	0,001452	3,5	0	La 61,25; O 22,22; F 16,52;
Bastnäsite_sulph	9	0,01135	0,012991	3,5	6,96E-08	Ce 39,8; La 34,55; O 25,64;
Bastnäsite_Y	0	0	0	0	0	
Bastäsite_Ce_La_Nd	4	0,005045	0,005774	3,5	0	Ce 39,58; La 30,1; Nd 15,26; O 13,2; F 1,86;
Biotite	11	0,021439	0,014607	5,165852	2,597019	O 37,12; Si 21,32; Mg 16,45; Fe 12,62; Al 7,58; K 4,91;
Burbankite	2	0,002522	0,002159	3,5	0	O 67,4; Sr 30,12; Ba 2,49;
Burbankite_Y	128	0,176558	0,151164	3,823434	1,158196	O 78,6; Ba 18,45; Ca 2,93; Na 0,02;
Calcite	1687	13,23934	8,148062	12,82054	9,915602	Ca 53,04; O 45,79; Fe 0,69; Mg 0,3; P 0,11; Ag 0,05; Th 0,01; Ce 0,01; Nd 0; La 0; Sr 0; Y 0;
Calcite_w_Ce	163	0,210609	0,191318	3,603678	0,665499	Ca 52,25; O 42,31; Ce 4,37; Fe 0,77; Mg 0,3; P 0,01;
Thorite_Ce_La_Mix	41	0,07819	0,077065	5,072774	3,260648	Ag 33,02; Ce 24,23; O 22,95; La 19,77; P 0,03;
Thorite_Ce_Mix	89	0,126113	0,124299	4,039583	1,745313	Ag 45,43; O 31,48; Ce 23,09;
Thorite2-Calsite mix	725	1,112316	1,705104	4,290731	2,010792	Ca 40,52; O 37,22; Ag 18,81; Si 3,39; Ce 0,04; Nd 0,01; La 0,01;
Thorite-Callsite mix	36	0,045401	0,069596	3,5	7,69E-08	Ca 46,9; Th 28,26; O 20,3; Si 4,5; Sm 0,03;
Dolomite	190	0,266098	0,171624	3,899989	1,579956	O 66,08; Ca 30,69; Mg 2,15; Fe 1,03; Ag 0,03; Mn 0,01;
Fe-Mg-chlorite	230	0,325371	0,195814	3,980398	1,613454	O 43,72; Fe 24,04; Si 16,48; Mg 9,28; Al 6,48;
Galena	46	0,157641	0,272083	7,383085	5,771594	Pb 98,8; As 1,2;
Gypsum	18	0,0227	0,011909	3,5	7,80E-08	Ca 39,64; O 33,53; S 26,83;
Kaolinite	2	0,002522	0,001501	3,5	0	O 58,48; Si 30,08; Al 11,43;
Magnetite	399	1,182939	1,399649	6,948539	6,257991	Fe 75,93; O 24,07;
Mg-Fe-chlorite	1000	8,406689	5,059291	13,41788	10,76119	O 37,83; Fe 18,48; Si 17,81; Mg 16,41; Al 9,48; K 0;
Molybdenite	19	0,046662	0,052985	6,21042	4,254421	S 97,84; Ca 1,66; Fe 0,51;
Monazite_Ce	863	3,623225	4,393952	7,941295	7,47925	Ce 39,19; O 24,06; La 18; P 14,44; Ca 4,19; Nd 0,1; F 0,02;
Monazite_Ce_La_Nd	20	0,025223	0,030588	3,5	7,38E-08	Ce 32,45; La 24,98; O 18,11; P 12,19; Nd 11,75; Ca 0,37; F 0,15;
Monazite_La	31	0,040356	0,048941	3,612903	0,628619	O 66; La 15,85; P 10,72; Ce 6,78; Nd 0,47; Ca 0,18;
Nb_rutile	1	0,007567	0,008592	19,14874	0	O 50,36; Ti 37,7; Nb 8,12; Fe 3,83;
Parisite_Ce	803	1,903044	1,875674	6,05731	4,322165	Ce 39,82; O 33,6; Ca 19,97; La 5,45; F 0,76; P 0,38; Nd 0;
Parisite_Ce_La	712	4,917144	4,846424	10,95183	9,453264	Ce 37,53; La 28,79; O 19,29; Ca 13,55; F 0,74; P 0,1;
Parisite_Ce_Nd	44	0,059273	0,058421	3,771585	1,031533	Ce 34,56; O 20,7; La 15,86; Ca 15,31; Nd 13,26; F 0,22; P 0,09;
Parisite_Nd_La	1	0,001261	0,001286	3,5	0	O 40,6; Ce 22,74; La 16,01; Nd 10,44; Ca 10,21;
Pb-As-Sulphide	9	0,01135	0,013739	3,5	6,96E-08	Pb 77,08; As 22,92;
Pyrite	280	2,763135	3,143826	14,408	12,35432	Fe 52,4; S 47,6;
Pyrrhotite	109	0,148813	0,15546	3,815592	1,071058	Fe 61,86; S 38,14;
Quartz	820	5,72805	3,408214	11,82333	8,495013	Si 56,74; O 41,85; Fe 1,2; Al 0,14; Ce 0,05; La 0,03;
Ce-quartz mix	90	0,139985	0,084246	4,285329	2,081198	Si 51,55; O 36,18; Ce 12,26; Ag 0,01;
La-quartz mix	2	0,002522	0,001518	3,5	0	Si 50,45; O 40,15; La 9,4;
REE-quartz mix	26	0,035312	0,032077	3,690375	0,970725	Si 43,75; O 29,34; Ce 15,22; La 11,59; F 0,09;
Si=O>Fe mix	236	0,351855	0,079907	4,164875	1,76068	Si 44,98; O 40,52; Fe 14,49;
Siderite	322	0,530936	0,473863	4,556491	2,429195	Fe 58,05; O 34,86; Ca 3,77; Mg 3,19; Ag 0,12; Th 0,01; Sr 0;
Synchysite_Ce	23	0,029006	0,026152	3,5	6,86E-08	Ce 59,65; O 26,22; Ca 12,77; F 1,36;
Synchysite_Ce-Nd	1	0,001261	0,001146	3,5	0	Ce 39,28; O 23,13; Nd 20,48; Ca 17,11;
Synchysite_Nd	4	0,005045	0,004823	3,5	0	O 49,39; Nd 27,45; Ca 20,02; P 3,14;
Synchysite_Y	0	0	0	0	0	
Talc	63	0,080712	0,05169	3,578567	0,62361	O 50,32; Si 41; Mg 8,68;
Thorite	1169	1,751709	2,685248	4,218863	1,850922	Th 75,73; O 11,85; Si 9,72; Ca 2,64; Ce 0,04; Nd 0,02;
Thorite2	1895	29,65041	45,45204	15,59921	15,18499	Ag 52,23; O 33,68; Si 10,77; Ca 3,24; Ce 0,06; Nd 0,02; La 0,01; Sm 0;
Thorite3	5	0,006306	0,009666	3,5	5,68E-08	O 58,05; Cd 21,75; Si 20,2;
Coffinite	21	0,10089	0,124643	8,956863	5,956861	U 77,75; Si 11,2; O 11,05;
Uraninite	9	0,029006	0,072262	7,303318	6,354752	U 91,25; O 8,69; Si 0,06;
Uranothorite	0	0	0	0	0	
Not Analysed	1	0,001261	0	3,5	0	
Not Classified	0	0,103413	0	0	0	O 22,33; Ca 21,84; Fe 14,87; Ag 7,4; Ce 6,03; Si 5,91; Pb 3,49; S 2,96; Mg 2,83; Th 2,37; Ba 2,33; P 2,24; Cl 2
Unclassified	1809	3,056978	0	4,694197	2,468423	O 32,73; Ca 25,69; Fe 12,08; Si 9,22; Ce 5,39; Ag 4,26; P 3,31; La 1,61; S 1,58

6_4	Number	Area %	Weight %	Grain Size (µm)	Grain Size Std Dev (µm)	Average Composition
Allanite_Ce	0	0	0	0	0	
Allanite_La	0	0	0	0	0	
Allanite_Y	0	0	0	0	0	
Ankerite	124	10,99404	8,469449	10,47996	6,839941	O 45,4; Ca 32,7; Fe 10,81; Mg 10,76; Mn 0,28; P 0,03; Ag 0,01; Y 0; Th 0;
Apatite	11	0,351199	0,273987	6,833965	3,323435	Ca 42,09; O 40,84; P 11,56; Ce 5,1; Ag 0,42;
Barite	136	21,66743	23,73955	15,86222	8,514424	Ba 68,45; O 16,87; S 14,68;
Bastnäsite_Ce	10	0,152695	0,187463	3,5	1,97E-07	Ce 78,3; O 21,19; Ca 0,51;
Bastnäsite_Ce_La	75	3,511987	4,32883	7,598859	5,740842	Ce 47,26; La 33,84; O 16,17; F 2,04; P 0,38; Ca 0,31;
Bastnäsite_La	1	0,01527	0,018933	3,5	0	La 46,75; O 31,95; F 21,3;
Bastnäsite_sulph	4	0,061078	0,075284	3,5	2,23E-07	Ce 40,04; La 34,9; O 25,06;
Bastnäsite_Y	0	0	0	0	0	
Bastäsite_Ce_La_Nd	5	0,076348	0,094105	3,5	2,05E-07	Ce 38,91; La 28,77; Nd 15,53; O 13,8; F 2,11; Ca 0,88;
Biotite	1	0,045809	0,033609	11,32437	0	O 36,33; Si 25,43; Mg 19,35; K 9,17; Al 5,96; Fe 3,75;
Burbankite	1	0,01527	0,014078	3,5	0	O 42,91; Ba 39,83; Sr 17,26;
Burbankite_Y	132	3,114979	2,871995	5,158467	3,182862	O 64,18; Ba 33,29; Ca 2,02; Ce 0,34; Sr 0,1; Na 0,06;
Calcite	133	8,535654	5,657092	10,07358	6,120851	Ca 49,98; O 47,02; Mg 1,51; Fe 1,4; P 0,04; Ag 0,03; Th 0,01; Ce 0;
Calcite_w_Ce	19	0,351199	0,343558	4,389447	1,802295	Ca 51,15; O 41,69; Ce 6,3; Fe 0,68; Mg 0,13; P 0,04;
Thorite_Ce_La_Mix	5	0,106887	0,113449	4,9	1,917029	Ag 31,85; Ce 26,78; O 21,3; La 20,07;
Thorite_Ce_Mix	27	0,473355	0,502416	4,049972	1,585188	Ag 44,88; O 32,73; Ce 22,39;
Thorite2-Calsite mix	42	0,900901	1,487195	4,867013	2,480189	Ca 40,21; O 39,72; Ag 16,57; Si 3,5;
Thorite-Callsite mix	1	0,01527	0,025207	3,5	0	Ca 46,17; Th 33,77; O 16,31; Si 3,75;
Dolomite	32	0,549702	0,381797	4,028109	1,443285	O 58,27; Ca 34,64; Mg 4,97; Fe 1,95; Ag 0,17;
Fe-Mg-chlorite	7	0,122156	0,079168	4	1,322876	O 40,37; Si 23,45; Fe 21,87; Mg 8,12; Al 6,19;
Galena	16	0,274851	0,510856	3,9375	1,195477	Pb 97,82; As 2,18;
Gypsum	2	0,030539	0,017253	3,5	0	O 45,47; Ca 28,36; S 26,18;
Magnetite	13	0,61078	0,778233	7,78352	5,935936	Fe 78,85; O 21,15;
Mg-Fe-chlorite	12	0,839823	0,544278	9,882408	12,6677	O 37,83; Fe 18,17; Si 17,47; Mg 16,75; Al 9,78;
Molybdenite	4	0,061078	0,074686	3,5	2,67E-07	S 90,07; Ca 9,93;
Monazite_Ce	88	4,107497	5,364209	7,728534	6,044476	Ce 44,84; O 28,71; P 15,61; La 7,77; Ca 2,59; Nd 0,44; F 0,03;
Monazite_Ce_La_Nd	6	0,091617	0,119648	3,5	1,83E-07	Ce 34,51; La 25,49; O 14,46; Nd 13,85; P 10,88; Ca 0,81;
Monazite_La	1	0,01527	0,019941	3,5	0	O 72,28; Ce 13,25; La 8,56; P 5,91;
Parisite_Ce	138	3,450909	3,662776	5,376521	3,426634	Ce 38,67; O 35,57; Ca 18,71; La 6,09; F 0,76; P 0,18; Nd 0,02;
Parisite_Ce_La	107	3,71049	3,938294	7,21223	4,790608	Ce 39,55; La 28,39; O 18,86; Ca 11,9; F 1,13; P 0,16;
Parisite_Ce_Nd	15	0,259582	0,275519	4,063316	1,511624	Ce 33,05; O 21,29; La 17,7; Nd 14,19; Ca 12,3; F 1,24; P 0,24;
Parisite_Nd_La	2	0,030539	0,033534	3,5	0	Ce 29,75; La 21,4; O 21,34; Ca 14,92; Nd 12,6;
Pyrite	24	0,778745	0,954157	6,510336	4,3318	Fe 51,33; S 48,67;
Quartz	162	11,51321	7,377085	10,29152	7,03682	Si 56,84; O 42,09; Fe 0,82; Ce 0,13; Al 0,09; La 0,04;
Ce-quartz mix	44	0,763475	0,494798	4,04317	1,40612	Si 51,02; O 36,46; Ce 12,52;
La-quartz mix	3	0,061078	0,039584	4,666667	2,020726	Si 48,61; O 40,39; La 11;
REE-quartz mix	33	0,564972	0,55268	3,968174	1,29924	Si 37,3; O 27,9; Ce 19,18; La 14,87; Nd 0,48; Ca 0,28;
Si=O>Fe mix	23	0,412277	0,100827	4,019554	1,394656	Si 45,35; O 40,95; Fe 13,7;
Siderite	14	0,213773	0,205463	3,5	1,34E-07	Fe 62,79; O 34,55; Ca 1,72; Mg 0,56; Ag 0,38;
Synchysite	19	0,30539	0,29841	3,684211	0,802955	Ce 54,8; O 28,43; Ca 12,02; Nd 2,89; F 1,86;
Talc	14	0,244312	0,168493	4,103553	1,560328	O 54,76; Si 36,11; Mg 9,13;
Thorite	39	0,656589	1,083888	3,858974	1,075742	Th 73,48; O 12,53; Si 10,16; Ca 3,83;
Thorite2	235	14,91831	24,62694	9,060563	6,538448	Ag 48,66; O 34,67; Si 12,74; Ca 3,78; Ce 0,1; La 0,04; Nd 0,01;
Thorite3	0	0	0	0	0	
Coffinite	1	0,01527	0,020315	3,5	0	U 85,46; O 8,93; Si 5,61;
Uraninite	1	0,01527	0,040966	3,5	0	U 92,73; O 7,27;
Uranothorite	0	0	0	0	0	
Not Classified	0	2,091923	0	0	0	O 53,97; Ca 40,22
Unclassified	150	2,901206	0	4,348976	2,486038	O 32,68; Si 15,13; Ca 13,04; Ce 9,73; Fe 6,83; Ag 4,61; Ba 3,74; S 3,21; La 2,68; Mg 2,49; Th 1,69

Kjerne_V	Number	Area %	Weight %	Grain Size (µm)	Grain Size Std Dev (µm)	Average Composition
Allanite_Ce	0	0	0	0	0	
Allanite_La	0	0	0	0	0	
Allanite_Y	0	0	0	0	0	
Ankerite	228	16,80217	14,85767	11,19747	8,203079	O 47,35; Ca 30,39; Fe 11,07; Mg 11,02; Mn 0,12; P 0,03; Th 0,02; Sr 0;
Apatite	45	1,235772	1,106634	5,528581	4,861116	Ca 44,09; O 40,61; P 12,65; Ce 1,55; F 0,95; La 0,14; Nd 0,01;
Barite	81	15,49051	19,48134	19,66588	10,01204	Ba 67,62; O 18,39; S 13,98;
Bastnäsite_Ce	63	0,834688	1,176259	4,294811	1,819128	Ce 74,55; O 20,87; F 4,43; La 0,15;
Bastnäsite_Ce_La	143	3,338753	4,723781	6,420507	4,389783	Ce 46,41; La 32,96; O 16,6; F 3,32; Ca 0,39; P 0,18; Nd 0,15;
Bastnäsite_La	2	0,02168	0,030856	3,5	0	La 48,55; O 41,64; F 9,81;
Bastnäsite_sulph	1	0,01084	0,015337	3,5	0	Ce 38,22; La 30,31; O 26,06; F 5,41;
Bastnäsite_Y	0	0	0	0	0	
Bastäsite_Ce_La_Nd	18	0,205962	0,291402	3,774986	1,166667	Ce 36,49; La 28,82; Nd 17,23; O 15,1; F 1,49; Ca 0,87;
Biotite	8	0,097561	0,082162	3,9375	1,237437	O 41,66; Si 24,72; Mg 15,53; K 6,17; Fe 5,96; Al 5,95;
Burbankite_Y	43	0,596206	0,630976	4,48195	2,679326	O 66,34; Ba 28,94; Ca 4,64; Ce 0,08;
Calcite	212	15,55556	11,83395	11,12025	10,72842	Ca 51,4; O 47,3; Mg 0,72; Fe 0,35; Ce 0,15; P 0,04; Th 0,02; La 0,01; Nd 0,01; Ag 0;
Calcite_w_Ce	25	0,271003	0,304305	3,5	2,02E-07	Ca 50,98; O 43,67; Ce 4,78; Mg 0,57;
Thorite_Ce_La_Mix	0	0	0	0	0	
Thorite_Ce_Mix	0	0	0	0	0	
Thorite2-Calsite mix	1	0,01084	0,020541	3,5	0	Ca 38,44; Ag 37,07; O 20,59; Si 3,89;
Thorite-Callsite mix	12	0,140921	0,267027	3,791666	1,010363	Ca 44,58; Th 33,86; O 16,95; Si 4,62;
Dolomite	216	3,121951	2,488968	4,655648	2,767433	O 55,22; Ca 34,91; Mg 9,58; Fe 0,25; Mn 0,05;
Fe-Mg-chlorite	24	0,401084	0,298371	5,345791	2,762193	O 41,22; Fe 20,79; Si 19,46; Al 9,74; Mg 8,79;
Galena	6	0,097561	0,208144	5,25	1,917029	Pb 100;
Kaolinite	61	1,116531	0,821196	5,605983	3,583663	O 46,37; Si 38,23; Al 14,82; Ca 0,3; Mg 0,28;
Magnetite	20	0,422764	0,618317	5,796142	4,498001	Fe 74,28; O 25,72;
Mg-Fe-chlorite	35	0,834688	0,620934	6,914341	4,675761	O 40,74; Fe 18,44; Si 18,22; Mg 12,86; Al 9,74;
Molybdenite	1	0,01084	0,015215	3,5	0	S 87,65; Ca 12,35;
Monazite_Ce	154	9,420054	14,12113	10,79673	7,975786	Ce 48,55; O 24,33; P 16,89; La 6,6; Ca 2,42; Nd 1,21; F 0;
Monazite_Ce_La_Nd	17	0,184282	0,276248	3,5	2,24E-07	Ce 32,89; La 23,4; O 16,57; Nd 14,22; P 12,63; Ca 0,29;
Monazite_La	0	0	0	0	0	
Parisite_Ce	224	5,04065	6,141171	6,339565	4,607627	Ce 44,78; O 29,9; Ca 22,23; F 1,6; La 1,41; P 0,08;
Parisite_Ce_La	204	3,837398	4,675214	5,800772	3,666679	Ce 39,86; La 28,81; O 19,54; Ca 10,25; F 1,51; P 0,04;
Parisite_Ce_Nd	43	0,520325	0,633927	3,974406	1,345825	Ce 36,51; O 21,87; Nd 15,06; Ca 14,67; La 10,01; F 1,82; P 0,08;
Parisite_Nd_La	2	0,02168	0,027327	3,5	3,22E-07	O 31,81; Ce 24,88; La 19,13; Nd 15,76; Ca 8,42;
Plagioclase	9	0,097561	0,073398	3,5	2,13E-07	O 49,79; Si 31,07; Al 11,93; Ca 7,21;
Pyrite	4	0,260163	0,365896	9,987373	7,629921	Fe 51,61; S 48,39;
Pyrrhotite	2	0,03252	0,041994	5,249999	2,474873	Fe 60,89; S 39,11;
Quartz	95	9,084011	6,68119	13,31644	9,157488	Si 56,84; O 42,84; Fe 0,21; Ce 0,06; La 0,04; Al 0,01;
Ce-quartz mix	13	0,151762	0,112897	3,76923	0,970725	Si 48,04; O 38,33; Ce 13,63;
La-quartz mix	4	0,04336	0,032256	3,5	2,67E-07	Si 45,46; O 42,5; La 12,04;
REE-quartz mix	5	0,054201	0,060861	3,5	2,41E-07	Si 39,6; O 32,66; Ce 15,36; La 12,37;
Si=O>Fe mix	6	0,065041	0,018258	3,5	0	Si 42,9; O 41,55; Fe 15,55;
Siderite	15	0,292683	0,322898	4,983682	4,109666	Fe 58,06; O 38,7; Ca 2,67; Mg 0,34; Mn 0,24;
Sphalerite	1	0,03252	0,036973	8,449746	0	Zn 71,54; S 23,45; Fe 5,01;
Synchysite_Ce	55	0,682927	0,761096	3,987254	1,712925	Ce 64,6; O 21,61; Ca 11,91; F 1,88;
Synchysite_Ce-Nd	12	0,140921	0,158238	3,912479	1,428869	Ce 47,23; Nd 20,47; O 17,66; Ca 12,73; F 1,91;
Synchysite_Nd	5	0,054201	0,064056	3,5	2,34E-07	O 35,92; Nd 35,2; Ca 21,33; F 7,55;
Synchysite_Y	0	0	0	0	0	
Talc	58	0,878049	0,695093	4,941777	3,045405	O 53,41; Si 39,98; Mg 6,61;
Thorite	59	2,287263	4,334058	8,453791	7,781769	Th 71,81; Si 12,59; O 12,08; Ca 3,51; Sm 0,01;
Thorite2	21	0,249322	0,472433	3,833333	1,052774	Ag 49,14; O 32,35; Si 16,21; Ca 1,93; Ce 0,37;
Thorite3	0	0	0	0	0	
Coffinite	0	0	0	0	0	
Uraninite	0	0	0	0	0	
Uranothorite	0	0	0	0	0	
Not Analysed	3	0,03252	0	3,5	2,64E-07	
Not Classified	0	2,092141	0	0	0	O 36,16; Ca 24,97; Ce 8,01; Si 7,21; Fe 5,72; Ba 5,46; Mg 3,65; Al 2,02; P 1,51; Th 1,17
Unclassified	253	3,826558	0	4,863066	2,741332	O 38,43; Ca 17,81; Ce 12,4; Si 10,37; Mg 3,65; Fe 3,13; Al 2,6; P 2,47; Th 2,16; La 2,11; Nd 1,34; F 1,1

Kjerne_H	Number	Area %	Weight %	Grain Size (µm)	Grain Size Std Dev (µm)	Average Composition
Allanite_Ce	0	0	0	0	0	
Allanite_La	0	0	0	0	0	
Allanite_Y	0	0	0	0	0	
Ankerite	237	15,03144	13,21919	12,79525	9,481844	O 47,51; Ca 30,38; Fe 11,12; Mg 10,88; Mn 0,08; P 0,01; Th 0,01; Ag 0,01;
Apatite	29	0,233952	0,208359	3,91206	1,254648	O 46,02; Ca 42,07; P 6,48; Ce 5,19; Nd 0,25;
Barite	199	23,6365	29,56342	19,26494	9,283304	Ba 67,16; O 19,05; S 13,79;
Bastnäsite_Ce	49	0,402106	0,563556	3,873966	1,377785	Ce 73,68; O 23,66; F 2,66;
Bastnäsite_Ce_La	99	1,856997	2,612975	7,007894	5,414185	Ce 46,03; La 32,93; O 17,86; F 2,66; Ca 0,25; P 0,14; Nd 0,12;
Bastnäsite_La	3	0,021933	0,031046	3,5	2,57E-07	La 52,94; O 47,06;
Bastnäsite_sulph	6	0,043866	0,061724	3,5	1,76E-07	Ce 36,63; La 34,15; O 25,61; F 3,61;
Bastnäsite_Y	0	0	0	0	0	
Bastäsite_Ce_La_Nd	13	0,095043	0,133735	3,5	2,32E-07	Ce 37,57; La 27,57; Nd 16,09; O 15,77; F 2,07; Ca 0,92;
Biotite	5	0,036555	0,030617	3,5	0	O 40,24; Si 24,13; Mg 12,75; Fe 12,05; Al 6,84; K 3,98;
Burbankite_Y	141	1,345226	1,415892	4,644288	2,131509	O 66,85; Ba 30,08; Ca 2,62; Ce 0,45;
Calcite	180	7,347565	5,559124	9,854348	9,573366	Ca 50,28; O 47,8; Mg 1,18; Fe 0,52; Ce 0,1; P 0,08; Th 0,03; Nd 0,02;
Calcite_w_Ce	14	0,109665	0,122468	3,75	0,935414	Ca 52,39; O 43,72; Ce 3,87; Mg 0,03;
Thorite_Ce_La_Mix	0	0	0	0	0	
Thorite_Ce_Mix	3	0,021933	0,026576	3,5	4,02E-08	Ag 44,09; O 32,42; Ce 23,49;
Thorite2-Calsite mix	4	0,029244	0,055111	3,5	0	O 36,8; Ca 35,33; Ag 23,92; Si 3,94;
Thorite-Callsite mix	9	0,087732	0,165332	4,758263	2,720792	Ca 43,66; Th 29,85; O 21,76; Si 4,73;
Dolomite	243	2,639275	2,09265	4,988134	3,276293	O 54,95; Ca 33,47; Mg 11,06; Fe 0,41; Mn 0,12;
Fe-Mg-chlorite	11	0,087732	0,064908	3,818181	1,05529	O 44,62; Si 20,6; Fe 18,02; Mg 8,4; Al 8,36;
Galena	11	0,102354	0,217176	4,268158	1,739519	Pb 100;
Gypsum	3	0,021933	0,014145	3,5	0	Ca 46,85; O 27,9; S 25,25;
Kaolinite	15	0,131598	0,09626	3,966666	1,807392	O 46,23; Si 37,84; Al 15,82; Ca 0,11;
Magnetite	38	0,606814	0,882647	6,384929	4,716057	Fe 72,9; O 27,1;
Mg-Fe-chlorite	11	0,380173	0,281268	8,750522	7,766425	O 40,59; Si 18,85; Fe 16,86; Mg 14,19; Al 9,51;
Monazite_Ce	133	2,697763	4,021968	7,701493	5,814045	Ce 48,46; O 24,84; P 16,54; Ca 5,06; La 4,22; Nd 0,89;
Monazite_Ce_La_Nd	4	0,029244	0,043599	3,5	0	Ce 29,53; La 21,32; O 18,79; Nd 16,85; P 13,51;
Monazite_La	0	0	0	0	0	
Parisite_Ce	273	5,022664	6,085797	7,203152	5,08539	Ce 45,98; O 30,97; Ca 19,86; F 1,67; La 1,44; P 0,07; Nd 0,02;
Parisite_Ce_La	202	2,471122	2,994177	5,549523	3,418031	Ce 39; La 28,36; O 19,99; Ca 11,14; F 1,46; P 0,06;
Parisite_Ce_Nd	40	0,35824	0,434067	4,432474	1,954414	Ce 38,51; O 22,89; Nd 14,21; Ca 12,36; La 10,03; F 2;
Parisite_Nd_La	2	0,014622	0,018329	3,5	3,22E-07	O 29; Ce 27,18; La 24,03; Nd 15,25; Ca 4,54;
Plagioclase	5	0,036555	0,027351	3,5	2,48E-07	O 52,31; Si 28,05; Ca 10,02; Al 9,62;
Pyrite	5	0,109665	0,153391	7,977938	4,890104	Fe 55,93; S 44,07;
Pyrrhotite	1	0,007311	0,009389	3,5	0	Fe 58,32; S 41,68;
Quartz	243	22,41556	16,39625	17,03688	9,82265	Si 57,1; O 42,64; Fe 0,14; Ce 0,07; La 0,04; Al 0;
Ce-quartz mix	76	0,679924	0,503037	4,284715	2,327948	Si 48,75; O 36,64; Ce 14,61;
La-quartz mix	21	0,153531	0,113589	3,5	2,27E-07	Si 44,15; O 43,53; La 12,32;
REE-quartz mix	33	0,248574	0,277594	3,60606	0,609272	Si 35,99; O 28,62; Ce 19,41; La 15,44; Ca 0,19; F 0,18; Nd 0,17;
Si=O>Fe mix	24	0,21933	0,061234	4,349979	1,72464	Si 44,18; O 41,18; Fe 14,64;
Siderite	39	0,307062	0,336909	3,806403	1,0923	Fe 58,39; O 37,42; Ca 3,79; Mg 0,4;
Synchysite_Ce	42	0,35824	0,397061	4,054145	1,634786	Ce 61,99; O 25,61; Ca 12,1; F 0,3;
Synchysite_Ce-Nd	14	0,109665	0,122468	3,853553	1,322875	Ce 41,88; O 21,74; Nd 21,02; Ca 14,35; F 1;
Synchysite_Nd	11	0,080421	0,094525	3,5	2,03E-07	O 44,93; Nd 29,95; Ca 19,49; F 5,1; P 0,52;
Synchysite_Y	0	0	0	0	0	
Talc	31	0,270507	0,212972	4,250778	1,870802	O 54,22; Si 37,58; Mg 8,19;
Thorite	147	5,000731	9,423905	9,579743	6,977639	Th 72,07; Si 12,95; O 12,68; Ca 2,05; Ce 0,19; Sm 0,03; La 0,02; Nd 0,01;
Thorite2	53	0,453283	0,854214	4,125917	1,702412	Ag 47,41; O 35,6; Si 14,93; Ca 2,06;
Thorite3	0	0	0	0	0	
Coffinite	0	0	0	0	0	
Uraninite	0	0	0	0	0	
Uranothorite	0	0	0	0	0	
Not Analysed	2	0,014622	0	3,5	3,22E-07	
Not Classified	0	1,659599	0	0	0	O 42,24; Ba 17,89; Ca 17,81; Si 4,53; Ce 3,58; Mg 3,38; Fe 3,36; S 2,5
Unclassified	285	3,012136	0	4,882535	2,955344	O 33,94; Si 13,82; Ce 12,23; Ca 11,08; Th 10,05; Fe 4,76; La 2,56; Ba 2,28; Mg 2,24; Nd 1,21; Ag 1,08; P 1,02

Associations

Shows associations for each of the three thorite classifications in every specimen.

3_1

	Thorite	Thorite2
Ankerite	16,6	11,6
Apatite	1,8	1,5
Bastnäsite_Ce_La	0,0	0,0
Burbankite_Y	0,1	0,0
Calcite	24,6	15,2
Calcite_w_Ce	0,2	0,0
Dolomite	3,9	3,3
Fe-Mg-chlorite	0,2	0,0
Magnetite	6,6	8,0
Mg-Fe-chlorite	0,6	0,0
Molybdenite	0,0	0,0
Monazite_Ce	4,4	3,3
Monazite_Ce_La_Nd	0,2	0,0
Nb_rutile	0,1	0,0
Parisite_Ce	1,2	0,0
Parisite_Ce_La	0,2	0,0
Pyrite	7,1	0,9
Pyrrhotite	1,5	0,0
Quartz	5,1	4,5
Si=O>Fe mix	0,1	0,3
Siderite	1,6	1,2
Talc	0,1	0,0
Thorite	0,0	34,2
Thorite2	4,8	0,0
Thorite2-Calcite mix	0,2	0,0
Thorite-Calcite mix	3,2	3,0
Background	6,2	4,5
Not Analysed	0,0	0,0
Not Classified	2,8	2,4
Unclassified	6,5	6,3

3_2

	Thorite	Thorite2	Thorite3
Ankerite	5,2	3,3	0,0
Apatite	0,9	0,6	0,0
Barite	1,1	0,3	0,0
Bastnäsite_Ce_La	0,0	0,0	0,0
Burbankite_Y	0,5	0,0	0,0
Calcite	16,2	10,1	0,0
Calcite_w_Ce	0,2	0,0	0,0
Ce-quartz mix	0,2	0,3	0,0
Coffinite	0,0	0,0	0,0
Dolomite	1,9	1,2	0,0
Fe-Mg-chlorite	0,3	0,0	0,0
Gypsum	0,0	0,0	0,0
Magnetite	6,9	6,8	0,0
Molybdenite	0,6	0,0	0,0
Monazite_Ce	0,9	1,5	100,0
Parisite_Ce	5,2	3,3	0,0
Parisite_Ce_La	1,4	1,5	0,0
Parisite_Ce_Nd	0,2	0,0	0,0
Pyrite	0,8	0,0	0,0
Pyrrhotite	0,5	0,0	0,0
Quartz	39,1	26,8	0,0
REE-quartz mix	0,0	0,0	0,0
Si=O>Fe mix	1,2	1,8	0,0
Siderite	2,4	2,4	0,0
Synchysite_Nd	0,2	0,0	0,0
Talc	0,0	0,0	0,0
Thorite	0,0	30,4	0,0
Thorite2	4,2	0,0	0,0
Thorite2-Calcite mix	0,1	0,0	0,0
Thorite-Calcite mix	2,0	0,3	0,0
Uraninite	0,0	0,0	0,0
Background	1,5	2,1	0,0
Not Analysed	0,0	0,0	0,0
Not Classified	0,2	0,6	0,0
Unclassified	6,1	6,8	0,0

3_3

	Thorite	Thorite2
Ankerite	9,9	25,0
Apatite	12,3	6,3
Barite	2,1	0,0
Bastnäsite_Ce_La	0,3	0,0
Burbankite_Y	0,7	0,0
Calcite	21,6	21,9
Dolomite	3,4	0,0
Magnetite	0,7	0,0
Molybdenite	0,3	0,0
Monazite_Ce	0,3	0,0
Parisite_Ce	0,7	0,0
Pyrite	0,3	0,0
Quartz	29,5	9,4
REE-quartz mix	0,3	0,0
Si=O>Fe mix	0,3	0,0
Siderite	0,7	0,0
Thorite	0,0	37,5
Thorite2	4,1	0,0
Thorite-Calcite mix	2,4	0,0
Background	1,4	0,0
Not Classified	0,7	0,0
Unclassified	7,9	0,0

3_4

	Thorite	Thorite2	Thorite3
Ankerite	1,5	1,9	50,0
Apatite	0,0	0,0	0,0
Bastnäsite_Ce_La	0,2	0,3	0,0
Burbankite_Y	0,5	1,1	0,0
Calcite	8,5	6,4	25,0
Calcite_w_Ce	0,0	0,0	0,0
Ce-quartz mix	0,1	0,0	0,0
Coffinite	0,0	0,0	25,0
Dolomite	0,5	0,3	0,0
Fe-Mg-chlorite	0,8	2,1	0,0
Fluorite	0,1	0,0	0,0
Gypsum	0,0	0,0	0,0
La-quartz mix	0,1	0,0	0,0
Magnetite	6,6	6,4	0,0
Mg-Fe-chlorite	0,4	0,5	0,0
Molybdenite	0,0	0,0	0,0
Monazite	0,0	0,0	0,0
Monazite_Ce	1,1	1,6	0,0
Monazite_La	0,1	0,0	0,0
Parisite_Ce	1,6	1,1	0,0
Parisite_Ce_La	2,3	1,1	0,0
Parisite_Ce_Nd	0,0	0,0	0,0
Pyrite	0,2	0,0	0,0
Pyrrhotite	0,0	0,0	0,0
Quartz	60,9	45,5	0,0
Si=O>Fe mix	1,9	2,1	0,0
Siderite	1,7	2,1	0,0
Synchysite_Ce	0,0	0,0	0,0
Synchysite_Nd	0,0	0,0	0,0
Talc	0,1	0,0	0,0
Thorite	0,0	20,5	0,0
Thorite2	2,7	0,0	0,0
Thorite2-Calcite mix	0,0	0,0	0,0
Thorite3	0,0	0,0	0,0
Thorite-Calcite mix	0,1	0,0	0,0
Uraninite	0,0	0,0	0,0
Background	2,1	1,3	0,0
Not Classified	0,2	0,0	0,0
Unclassified	5,3	5,9	0,0

3-6_1

	Thorite	Thorite2
Ankerite	4,6	4,4
Apatite	1,3	0,7
Barite	0,0	0,0
Bastnäsite_Ce_La	0,1	0,4
Calcite	61,5	32,6
Calcite_w_Ce	0,9	0,7
Dolomite	1,0	0,0
Galena	0,1	0,0
Magnetite	0,9	0,0
Mg-Fe-chlorite	0,1	0,7
Monazite_Ce	0,1	0,0
Nb_rutile	0,0	0,0
Parisite_Ce	0,3	0,0
Parisite_Ce_La	0,1	0,4
Pyrite	0,4	0,0
Quartz	2,6	1,1
REE-quartz mix	0,1	0,0
Siderite	0,9	0,0
Thorite	0,0	50,7
Thorite2	7,3	0,0
Thorite2-Calcite mix	1,1	0,0
Thorite-Calcite mix	7,1	2,2
Background	1,0	1,9
Not Classified	1,0	0,4
Unclassified	7,8	3,7

3-6_2

	Thorite	Thorite2	Thorite3
Ankerite	1,8	5,7	0,0
Apatite	0,6	0,5	0,0
Barite	2,6	6,6	0,0
Bastnäsite_Ce	0,4	0,9	0,0
Bastnäsite_Ce_La	6,2	8,7	0,0
Bastnäsite_sulph	0,0	0,0	0,0
Bastäsite_Ce_La_Nd	0,0	0,1	0,0
Biotite	0,0	0,0	0,0
Burbankite	0,0	0,0	0,0
Burbankite_Y	2,2	2,7	0,0
Calcite	3,0	9,1	0,0
Calcite_w_Ce	0,4	0,5	0,0
Ce-quartz mix	0,6	1,2	0,0
Coffinite	0,0	0,0	0,0
Dolomite	0,0	0,6	0,0
Fe-Mg-chlorite	0,2	0,2	0,0
La-quartz mix	0,0	0,2	0,0
Magnetite	0,2	2,5	0,0
Mg-Fe-chlorite	0,0	0,4	0,0
Molybdenite	0,0	0,0	0,0
Monazite_Ce	0,2	0,6	0,0
Monazite_Ce_La_Nd	0,0	0,0	0,0
Parisite_Ce	4,4	4,9	0,0
Parisite_Ce_La	3,2	3,8	0,0
Parisite_Ce_Nd	0,0	0,5	0,0
Pyrite	0,0	0,2	0,0
Quartz	14,2	22,3	0,0
REE-quartz mix	1,2	1,5	0,0
Si=O>Fe mix	0,0	0,5	0,0
Siderite	0,0	0,6	25,0
Synchysite_Ce	0,2	0,2	0,0
Synchysite_Ce-Nd	0,0	0,1	0,0
Synchysite_Nd	0,0	0,0	0,0
Talc	0,4	0,9	0,0
Thorite	0,0	4,7	0,0
Thorite_Ce_La_Mix	0,8	1,2	0,0
Thorite_Ce_Mix	3,2	4,0	0,0
Thorite2	46,8	0,0	50,0
Thorite2-Calcite mix	1,8	2,3	0,0
Thorite3	0,0	0,0	0,0
Thorite-Calcite mix	0,0	0,2	0,0
Uraninite	0,0	0,0	0,0
Background	1,2	3,9	0,0
Not Analysed	0,0	0,0	0,0
Not Classified	0,0	0,1	0,0
Unclassified	4,2	7,3	25,0

3-6_3	Thorite	Thorite2	Thorite3
Ankerite	4,0	12,8	25,0
Apatite	0,2	0,3	0,0
Barite	0,0	0,1	0,0
Bastnäsite_Ce_La	0,2	0,2	0,0
Burbankite_Y	0,2	0,2	0,0
Calcite	15,4	22,5	0,0
Calcite_w_Ce	0,0	0,3	0,0
Ce-quartz mix	0,0	0,1	0,0
Coffinite	0,0	0,1	0,0
Dolomite	0,5	1,2	0,0
Fe-Mg-chlorite	0,0	0,1	0,0
Galena	0,0	0,0	0,0
Gypsum	0,0	0,0	0,0
La-quartz mix	0,0	0,0	0,0
Magnetite	2,0	7,5	0,0
Mg-Fe-chlorite	0,0	0,0	0,0
Molybdenite	0,0	0,0	0,0
Monazite_Ce	0,7	0,9	0,0
Monazite_Ce_La_Nd	0,0	0,0	0,0
Parisite_Ce	4,2	3,5	0,0
Parisite_Ce_La	3,2	4,1	0,0
Parisite_Ce_Nd	0,0	0,0	0,0
Pyrite	0,0	0,4	0,0
Pyrrhotite	0,0	0,0	0,0
Quartz	16,2	21,2	0,0
REE-quartz mix	0,0	0,0	0,0
Si=O>Fe mix	1,2	1,1	0,0
Siderite	1,7	2,3	0,0
Synchysite_Ce	0,2	0,0	0,0
Talc	0,0	0,5	25,0
Thorite	0,0	3,9	0,0
Thorite_Ce_Mix	0,0	0,3	0,0
Thorite2	43,8	0,0	0,0
Thorite2-Calscte mix	2,7	6,6	0,0
Thorite-Calcite mix	0,0	0,2	0,0
Uraninite	0,0	0,0	0,0
Background	0,7	3,3	0,0
Not Classified	0,0	0,0	0,0
Unclassified	2,5	6,2	50,0

3-6_4	Thorite	Thorite2
Ankerite	0,0	5,8
Apatite	12,5	0,0
Barite	0,0	0,0
Bastnäsite_Ce_La	0,0	1,4
Burbankite_Y	0,0	0,0
Calcite	43,8	36,5
Coffinite	0,0	0,0
Dolomite	0,0	1,0
Fluorite	0,0	0,5
La-quartz mix	0,0	0,5
Magnetite	0,0	1,9
Mg-Fe-chlorite	0,0	0,0
Monazite_Ce	0,0	1,0
Nb_rutile	0,0	0,0
Parisite_Ce	0,0	5,3
Parisite_Ce_La	6,3	1,4
Pyrite	0,0	0,0
Quartz	6,3	30,3
Si=O>Fe mix	0,0	0,5
Siderite	0,0	1,0
Thorite	0,0	1,9
Thorite2	25,0	0,0
Thorite2-Calsite mix	6,3	7,2
Uraninite	0,0	0,0
Background	0,0	1,4
Unclassified	0,0	2,4

6_1	Thorite	Thorite2	Thorite3
Ankerite	3,0	7,3	0,0
Apatite	0,3	0,6	0,0
Barite	0,3	0,9	0,0
Bastnäsite_Ce	0,0	0,0	0,0
Bastnäsite_Ce_La	0,0	0,5	0,0
Bastnäsite_sulph	0,0	0,1	0,0
Burbankite_Y	0,3	0,9	0,0
Calcite	15,3	32,7	50,0
Calcite_w_Ce	0,2	0,2	0,0
Coffinite	0,0	0,0	50,0
Dolomite	0,2	0,4	0,0
Fe-Mg-chlorite	0,3	1,2	0,0
Gypsum	0,0	0,1	0,0
Magnetite	1,2	3,8	0,0
Mg-Fe-chlorite	0,7	1,2	0,0
Molybdenite	0,2	0,1	0,0
Monazite_Ce	2,3	5,9	0,0
Monazite_Ce_La_Nd	0,0	0,1	0,0
Monazite_La	0,0	0,1	0,0
Parisite_Ce	1,0	1,5	0,0
Parisite_Ce_La	0,3	1,4	0,0
Parisite_Ce_Nd	0,0	0,1	0,0
Pyrite	0,0	0,9	0,0
Pyrrhotite	0,0	0,2	0,0
Quartz	1,9	7,1	0,0
REE-quartz mix	0,0	0,1	0,0
Si=O>Fe mix	0,0	0,4	0,0
Siderite	0,7	1,5	0,0
Synchysite_Ce	0,0	0,0	0,0
Talc	0,2	0,1	0,0
Thorite	0,0	5,8	0,0
Thorite_Ce_La_Mix	0,0	0,0	0,0
Thorite_Ce_Mix	0,2	0,2	0,0
Thorite2	59,4	0,0	0,0
Thorite2-Calcite mix	6,4	13,6	0,0
Thorite3	0,0	0,0	0,0
Thorite-Calcite mix	0,2	0,3	0,0
Background	1,6	5,6	0,0
Not Classified	0,2	0,1	0,0
Unclassified	3,6	5,2	0,0

6_2

	Thorite	Thorite2	Thorite3
Ankerite	2,0	5,1	0,0
Apatite	0,1	0,3	0,0
Barite	0,0	0,1	0,0
Bastnäsite_Ce	0,0	0,0	0,0
Bastnäsite_Ce_La	1,6	3,3	0,0
Bastnäsite_La	0,0	0,0	0,0
Bastnäsite_sulph	0,1	0,1	0,0
Bastäsite_Ce_La_Nd	0,0	0,0	0,0
Burbankite_Y	0,1	0,3	0,0
Calcite	3,2	9,8	3,1
Calcite_w_Ce	0,1	0,1	0,0
Ce-quartz mix	0,0	0,0	0,0
Coffinite	0,0	0,0	0,0
Dolomite	0,0	0,1	0,0
Fe-Mg-chlorite	0,3	0,9	3,1
Gypsum	0,0	0,0	0,0
La-quartz mix	0,0	0,0	0,0
Magnetite	8,6	19,7	12,5
Mg-Fe-chlorite	4,5	9,1	15,6
Monazite_Ce	1,3	2,8	0,0
Monazite_Ce_La_Nd	0,0	0,0	0,0
Monazite_La	0,0	0,0	0,0
Nb_rutile	0,0	0,0	0,0
Parisite_Ce	3,0	6,1	3,1
Parisite_Ce_La	4,4	8,3	3,1
Parisite_Ce_Nd	0,1	0,2	0,0
Parisite_Nd_La	0,0	0,0	0,0
Pyrite	0,6	2,0	0,0
Pyrrhotite	0,1	0,2	0,0
Quartz	1,6	3,2	3,1
REE-quartz mix	0,0	0,0	0,0
Si=O>Fe mix	0,1	0,4	0,0
Siderite	2,2	5,2	3,1
Synchysite_Ce	0,1	0,1	0,0
Synchysite_Nd	0,0	0,0	0,0
Talc	0,0	0,1	0,0
Thorite	0,0	6,8	6,3
Thorite_Ce_La_Mix	0,0	0,2	0,0
Thorite_Ce_Mix	0,5	0,9	0,0
Thorite2	59,3	0,0	34,4
Thorite2-Calcite mix	1,2	2,5	0,0
Thorite3	0,0	0,0	0,0
Thorite-Calcite mix	0,0	0,1	0,0
Uraninite	0,0	0,0	0,0
Background	3,0	7,1	12,5
Not Classified	0,0	0,1	0,0
Unclassified	1,9	4,6	0,0

6_3

	Thorite	Thorite2	Thorite3
Actinolite	0,0	0,0	0,0
Ankerite	0,7	3,2	0,0
Apatite	5,9	16,4	0,0
Barite	0,0	0,3	0,0
Bastnäsite_Ce	0,1	0,1	0,0
Bastnäsite_Ce_La	0,5	1,5	5,0
Bastnäsite_sulph	0,0	0,0	0,0
Bastäsite_Ce_La_Nd	0,0	0,0	0,0
Biotite	0,0	0,0	0,0
Burbankite	0,0	0,0	0,0
Burbankite_Y	0,2	0,4	5,0
Calcite	2,7	10,3	0,0
Calcite_w_Ce	0,0	0,2	0,0
Ce-quartz mix	0,1	0,2	0,0
Coffinite	0,0	0,1	10,0
Dolomite	0,1	0,2	0,0
Fe-Mg-chlorite	0,1	0,6	0,0
Galena	0,0	0,0	0,0
Gypsum	0,0	0,0	0,0
Kaolinite	0,0	0,0	0,0
Magnetite	0,5	2,3	0,0
Mg-Fe-chlorite	4,3	12,4	35,0
Molybdenite	0,0	0,0	0,0
Monazite_Ce	1,2	4,6	0,0
Monazite_Ce_La_Nd	0,0	0,0	0,0
Monazite_La	0,0	0,1	0,0
Nb_rutile	0,0	0,0	0,0
Parisite_Ce	0,9	2,9	0,0
Parisite_Ce_La	1,1	3,2	0,0
Parisite_Ce_Nd	0,0	0,0	0,0
Pyrite	0,9	2,5	15,0
Pyrrhotite	0,1	0,2	0,0
Quartz	2,5	7,2	0,0
REE-quartz mix	0,0	0,0	0,0
Si=O>Fe mix	0,2	0,7	0,0
Siderite	0,4	1,1	0,0
Synchysite_Ce	0,0	0,0	0,0
Synchysite_Nd	0,0	0,0	0,0
Talc	0,0	0,1	0,0
Thorite	0,0	12,2	5,0
Thorite_Ce_La_Mix	0,1	0,2	0,0
Thorite_Ce_Mix	0,1	0,4	0,0
Thorite2	72,6	0,0	15,0
Thorite2-Calcite mix	1,2	3,7	0,0
Thorite3	0,0	0,0	0,0
Thorite-Calcite mix	0,0	0,2	0,0
Background	2,0	7,1	10,0
Not Analysed	0,0	0,0	0,0
Not Classified	0,0	0,2	0,0
Unclassified	1,7	4,9	0,0

6_4

	Thorite	Thorite2
Ankerite	3,0	5,6
Apatite	0,0	0,3
Barite	7,9	14,8
Bastnäsite_Ce	0,6	0,2
Bastnäsite_Ce_La	0,6	2,4
Bastnäsite_sulph	0,0	0,1
Bastäsite_Ce_La_Nd	0,0	0,1
Burbankite_Y	0,6	6,5
Calcite	3,7	8,2
Calcite_w_Ce	0,0	0,2
Ce-quartz mix	0,0	0,4
Dolomite	0,6	0,4
Fe-Mg-chlorite	0,6	0,2
Gypsum	0,0	0,1
La-quartz mix	0,0	0,0
Magnetite	0,6	0,8
Mg-Fe-chlorite	0,6	2,5
Molybdenite	0,0	0,2
Monazite_Ce	0,0	5,6
Monazite_La	0,0	0,1
Parisite_Ce	2,4	5,3
Parisite_Ce_La	0,0	3,2
Parisite_Ce_Nd	0,0	0,2
Pyrite	1,2	1,4
Quartz	4,9	13,3
REE-quartz mix	0,6	0,4
Si=O>Fe mix	1,8	0,6
Siderite	1,2	0,3
Synchysite_Ce	0,0	0,3
Synchysite_Ce-Nd	0,0	0,0
Synchysite_Nd	0,6	0,1
Talc	0,0	0,3
Thorite	0,0	4,7
Thorite_Ce_La_Mix	0,0	0,1
Thorite_Ce_Mix	0,0	2,0
Thorite2	61,0	0,0
Thorite2-Calcite mix	1,8	2,4
Background	3,0	11,7
Not Classified	0,0	0,3
Unclassified	2,4	4,4

Kjerne_V	Thorite	Thorite2
Ankerite	8,9	6,8
Apatite	1,0	0,0
Barite	6,5	0,0
Bastnäsite_Ce	0,4	0,0
Bastnäsite_Ce_La	1,0	0,0
Burbankite_Y	0,8	0,0
Calcite	17,7	10,2
Calcite_w_Ce	0,2	0,0
Ce-quartz mix	0,2	0,0
Dolomite	2,8	3,4
Fe-Mg-chlorite	0,2	0,0
Kaolinite	0,4	1,1
Magnetite	2,0	0,0
Mg-Fe-chlorite	0,2	0,0
Monazite_Ce	2,4	0,0
Parisite_Ce	3,6	3,4
Parisite_Ce_La	0,8	0,0
Plagioclase	0,2	1,1
Pyrite	1,0	1,1
Quartz	14,1	11,4
Si=O>Fe mix	0,2	0,0
Siderite	3,2	1,1
Synchysite_Ce	0,2	0,0
Talc	0,4	1,1
Thorite	0,0	50,0
Thorite2	8,9	0,0
Thorite2-Calcite mix	0,4	0,0
Thorite-Calcite mix	2,2	0,0
Background	9,1	5,7
Not Classified	3,2	0,0
Unclassified	7,7	3,4

Kjerne_H	Thorite	Thorite2
Ankerite	6,8	3,0
Barite	10,4	5,1
Bastnäsite_Ce	0,3	0,4
Bastnäsite_Ce_La	1,6	1,7
Bastnäsite_La	0,1	0,0
Biotite	0,1	0,0
Burbankite_Y	5,9	2,5
Calcite	7,5	5,5
Calcite_w_Ce	0,1	0,0
Ce-quartz mix	0,9	0,8
Dolomite	1,7	0,8
Fe-Mg-chlorite	0,3	0,0
Gypsum	0,1	0,0
Kaolinite	0,2	0,0
La-quartz mix	0,4	0,4
Magnetite	2,3	2,1
Mg-Fe-chlorite	0,4	0,0
Monazite_Ce	0,9	0,4
Monazite_Ce_La_Nd	0,1	0,0
Parisite_Ce	3,4	1,3
Parisite_Ce_La	2,6	3,0
Parisite_Ce_Nd	0,1	0,0
Pyrite	0,9	0,0
Quartz	23,6	16,5
REE-quartz mix	0,4	0,0
Si=O>Fe mix	0,4	0,0
Siderite	1,6	0,4
Synchysite_Ce	0,5	0,0
Synchysite_Ce-Nd	0,1	0,0
Synchysite_Nd	0,1	0,0
Talc	0,1	0,4
Thorite	0,0	44,1
Thorite_Ce_Mix	0,3	0,8
Thorite2	7,4	0,0
Thorite2-Calcite mix	0,4	0,4
Thorite-Calcite mix	1,0	0,0
Background	4,2	4,7
Not Classified	0,9	0,0
Unclassified	11,7	5,5

Shows full combined thorite associations

	3_1	3_2	3_3	3_4	3-6_1	3-6_2	3-6_3	3-6_4	6_1	6_2	6_3	6_4	Kjerne_V	Kjerne_H
Ankerite	16,2	5,0	11,0	1,6	4,5	5,5	12,3	5,5	7,1	5,0	3,0	5,5	8,7	6,5
Apatite	1,8	0,8	11,9	0,0	1,2	0,5	0,3	0,7	0,6	0,3	15,8	0,3	0,9	0,0
Barite	0,0	1,0	1,9	0,0	0,0	6,3	0,1	0,0	0,9	0,1	0,3	14,6	5,8	10,0
Bastnäsite_Ce	0,0	0,0	0,0	0,0	0,0	0,9	0,0	0,0	0,0	0,0	0,1	0,2	0,4	0,3
Bastnäsite_Ce_La	0,0	0,0	0,3	0,2	0,1	8,5	0,2	1,4	0,5	3,2	1,4	2,3	0,9	1,6
Bastnäsite_La	0,0	0,0	0,0	0,0	0,0	0,0	0,0	0,0	0,0	0,0	0,0	0,0	0,0	0,1
Bastnäsite_sulph	0,0	0,0	0,0	0,0	0,0	0,0	0,0	0,0	0,1	0,1	0,0	0,1	0,0	0,0
Bastäsite_Ce_La_Nd	0,0	0,0	0,0	0,0	0,0	0,1	0,0	0,0	0,0	0,0	0,0	0,1	0,0	0,0
Biotite	0,0	0,0	0,0	0,0	0,0	0,0	0,0	0,0	0,0	0,0	0,0	0,0	0,0	0,1
Burbankite	0,0	0,0	0,0	0,0	0,0	0,0	0,0	0,0	0,0	0,0	0,0	0,0	0,0	0,0
Burbankite_Y	0,1	0,5	0,0	0,6	0,0	2,7	0,2	0,0	0,9	0,2	0,4	6,3	0,7	5,6
Calcite	23,9	15,6	21,6	8,4	59,5	8,7	22,2	36,9	31,9	9,5	9,9	8,0	17,0	7,3
Calcite_w_Ce	0,2	0,2	0,0	0,0	0,8	0,5	0,3	0,0	0,2	0,1	0,2	0,2	0,2	0,1
Ce-quartz mix	0,0	0,2	0,0	0,1	0,0	1,2	0,1	0,0	0,0	0,0	0,1	0,4	0,2	0,9
Coffinite	0,0	0,0	0,0	0,0	0,0	0,0	0,1	0,0	0,0	0,0	0,1	0,0	0,0	0,0
Dolomite	3,8	1,8	3,2	0,4	0,9	0,6	1,1	0,9	0,4	0,1	0,2	0,4	2,9	1,6
Fe-Mg-chlorite	0,2	0,3	0,0	1,0	0,0	0,2	0,1	0,0	1,1	0,9	0,6	0,2	0,2	0,3
Galena	0,0	0,0	0,0	0,0	0,0	0,0	0,0	0,0	0,0	0,0	0,0	0,0	0,0	0,0
Fluorite	0,0	0,0	0,0	0,1	0,0	0,0	0,0	0,5	0,0	0,0	0,0	0,0	0,0	0,0
Gypsum	0,0	0,0	0,0	0,0	0,0	0,0	0,0	0,0	0,1	0,0	0,0	0,1	0,0	0,1
Kaolinite	0,0	0,0	0,0	0,0	0,0	0,0	0,0	0,0	0,0	0,0	0,0	0,0	0,5	0,2
La-quartz mix	0,0	0,0	0,0	0,1	0,0	0,2	0,0	0,5	0,0	0,0	0,0	0,0	0,0	0,4
Magnetite	6,7	6,9	0,6	6,6	0,8	2,4	7,2	1,8	3,7	19,1	2,2	0,8	1,8	2,3
Mg-Fe-chlorite	0,6	0,0	0,0	0,4	0,1	0,4	0,0	0,0	1,2	8,8	12,0	2,4	0,2	0,3
Molybdenite	0,0	0,5	0,3	0,0	0,0	0,0	0,0	0,9	0,1	0,0	0,0	0,2	0,0	0,0
Monazite_Ce	4,3	1,0	0,3	1,1	0,1	0,6	0,9	0,0	5,7	2,8	4,4	5,4	2,2	0,9
Monazite_Ce_La_Nd	0,2	0,0	0,0	0,0	0,0	0,0	0,0	0,0	0,1	0,0	0,0	0,0	0,0	0,1
Monazite_La	0,0	0,0	0,0	0,1	0,0	0,0	0,0	0,0	0,1	0,0	0,1	0,1	0,0	0,0
Nb_rutile	0,1	0,0	0,0	0,0	0,0	0,0	0,0	0,0	0,0	0,0	0,0	0,0	0,0	0,0
Parisite_Ce	1,2	5,0	0,6	1,6	0,2	4,8	3,5	5,0	1,5	5,9	2,8	5,2	3,6	3,2
Parisite_Ce_La	0,2	1,4	0,0	2,2	0,1	3,7	4,0	1,7	1,3	8,1	3,1	3,1	0,7	2,6
Parisite_Ce_Nd	0,0	0,2	0,0	0,0	0,0	0,4	0,0	0,0	0,0	0,2	0,0	0,2	0,0	0,1
Parisite_Nd_La	0,0	0,0	0,0	0,0	0,0	0,0	0,0	0,0	0,0	0,0	0,0	0,0	0,0	0,0
Plagioclase	0,0	0,0	0,0	0,0	0,0	0,0	0,0	0,0	0,0	0,0	0,0	0,0	0,3	0,0
Pyrite	6,6	0,8	0,3	0,2	0,3	0,2	0,4	0,0	0,9	2,0	2,4	1,4	1,0	0,9
Pyrrhotite	1,3	0,4	0,0	0,0	0,0	0,0	0,0	0,0	0,2	0,2	0,2	0,0	0,0	0,0
Quartz	5,0	38,0	28,0	59,5	2,5	21,8	20,9	29,0	6,8	3,1	7,0	13,0	13,8	23,0
REE-quartz mix	0,0	0,0	0,3	0,0	0,0	1,5	0,0	0,0	0,1	0,0	0,0	0,4	0,0	0,3
Si=O>Fe mix	0,1	1,2	0,3	1,9	0,0	0,5	1,1	0,5	0,4	0,4	0,7	0,7	0,2	0,4
Siderite	1,5	2,4	0,6	1,8	0,8	0,6	2,3	0,9	1,4	5,0	1,1	0,3	3,0	1,5
Synchysite_Ce	0,0	0,0	0,0	0,0	0,0	0,2	0,0	0,0	0,0	0,1	0,0	0,3	0,2	0,5
Synchysite_Ce-Nd	0,0	0,0	0,0	0,0	0,0	0,1	0,0	0,0	0,0	0,0	0,0	0,0	0,0	0,1
Synchysite_Nd	0,0	0,2	0,0	0,0	0,0	0,0	0,0	0,0	0,0	0,0	0,0	0,1	0,0	0,1
Talc	0,1	0,0	0,0	0,1	0,0	0,9	0,5	0,0	0,1	0,1	0,1	0,3	0,5	0,2
Thorite	2,6	2,6	2,7	1,8	3,5	4,4	3,7	1,8	5,5	6,5	11,5	4,5	4,9	3,7
Thorite2	4,4	3,9	3,8	2,5	6,8	2,8	2,2	1,3	2,8	3,0	4,1	2,6	8,0	6,8
Thorite3	0,0	0,0	0,0	0,0	0,0	0,0	0,0	0,0	0,0	0,0	0,0	0,0	0,0	0,0
Thorite_Ce_La_Mix	0,0	0,0	0,0	0,0	0,0	1,2	0,0	0,0	0,0	0,2	0,2	0,1	0,0	0,0
Thorite_Ce_Mix	0,0	0,0	0,0	0,0	0,0	3,9	0,2	0,0	0,2	0,9	0,4	1,9	0,0	0,3
Thorite2-Calcite mix	0,2	0,1	0,0	0,0	1,0	2,3	6,4	7,2	13,3	2,5	3,5	0,0	0,4	0,4
Thorite-Calcite mix	3,2	1,9	2,2	0,1	6,8	0,2	0,2	0,0	0,3	0,1	0,2	0,0	2,0	0,9
Background	6,1	1,6	1,3	2,1	1,1	3,8	3,1	1,4	5,4	6,9	6,8	11,3	8,7	4,2
Not Analysed	0,0	0,0	0,0	0,0	0,0	0,0	0,0	0,0	0,0	0,0	0,0	0,0	0,0	0,0
Not Classified	2,8	0,2	0,6	0,2	0,9	0,1	0,0	0,0	0,1	0,1	0,2	0,3	2,9	0,9
Unclassified	6,5	6,1	7,3	5,3	7,5	7,2	6,0	2,3	5,1	4,4	4,7	4,4	7,2	11,2

Element distribution

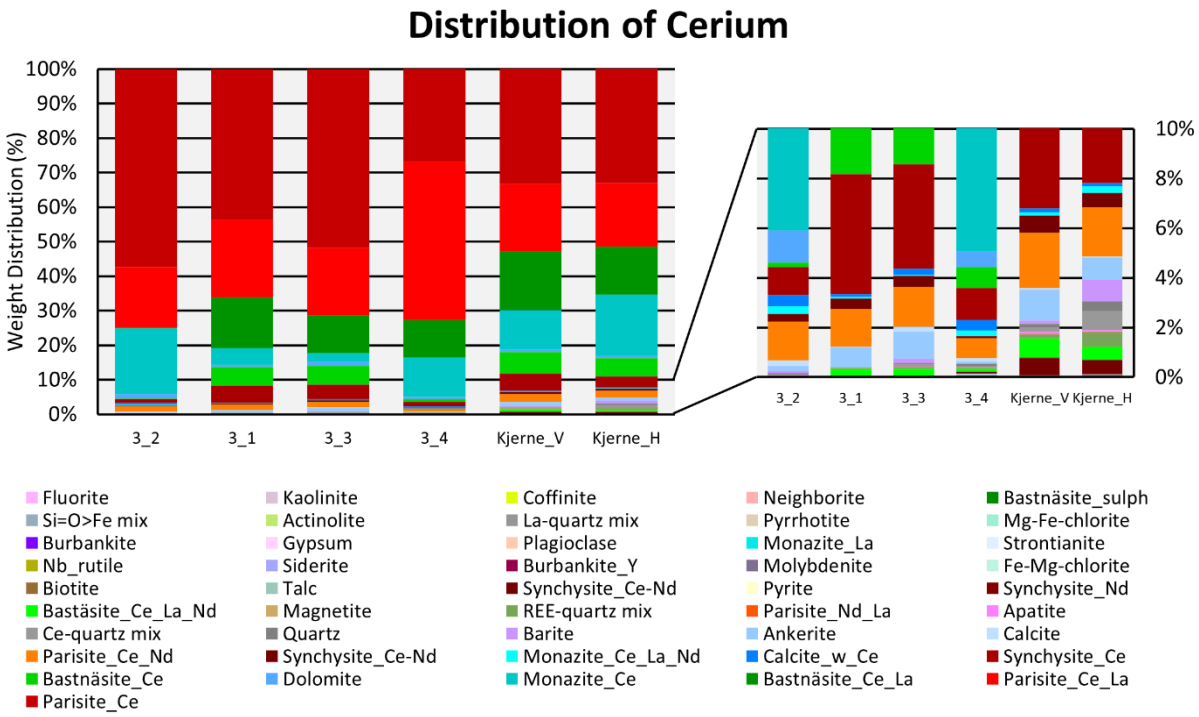

Shows distribution of cerium in the low radioactive and core specimen

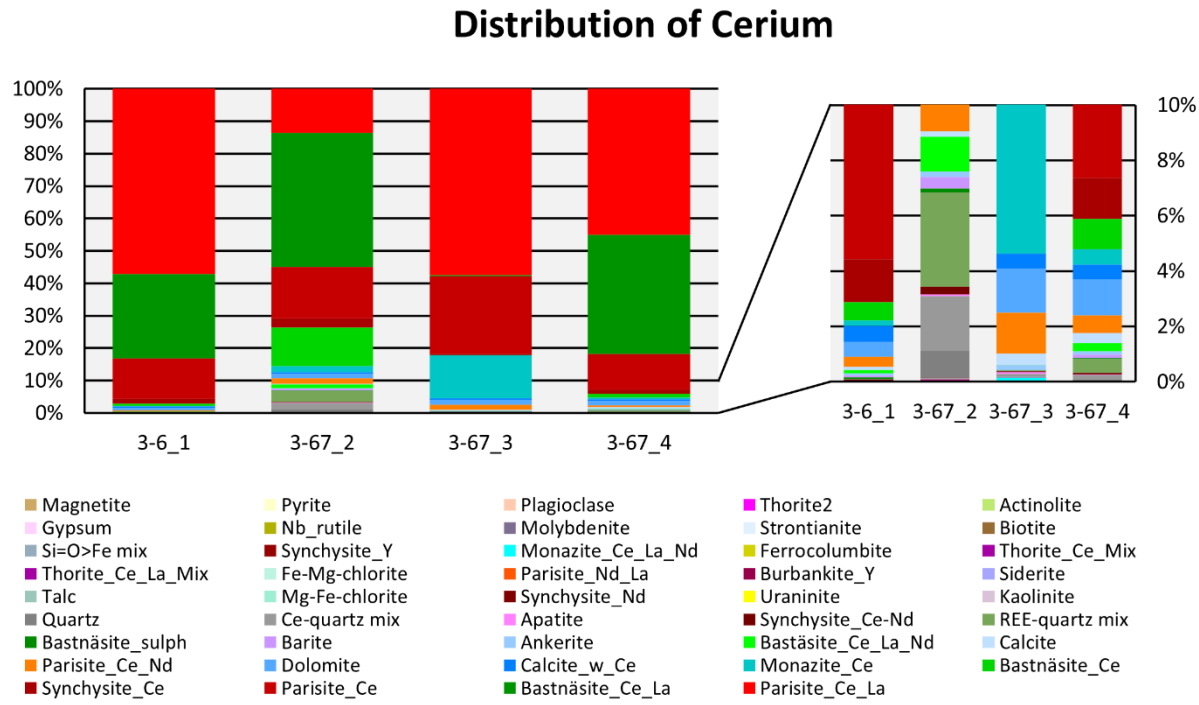

Shows distribution of cerium in the medium radioactive specimen

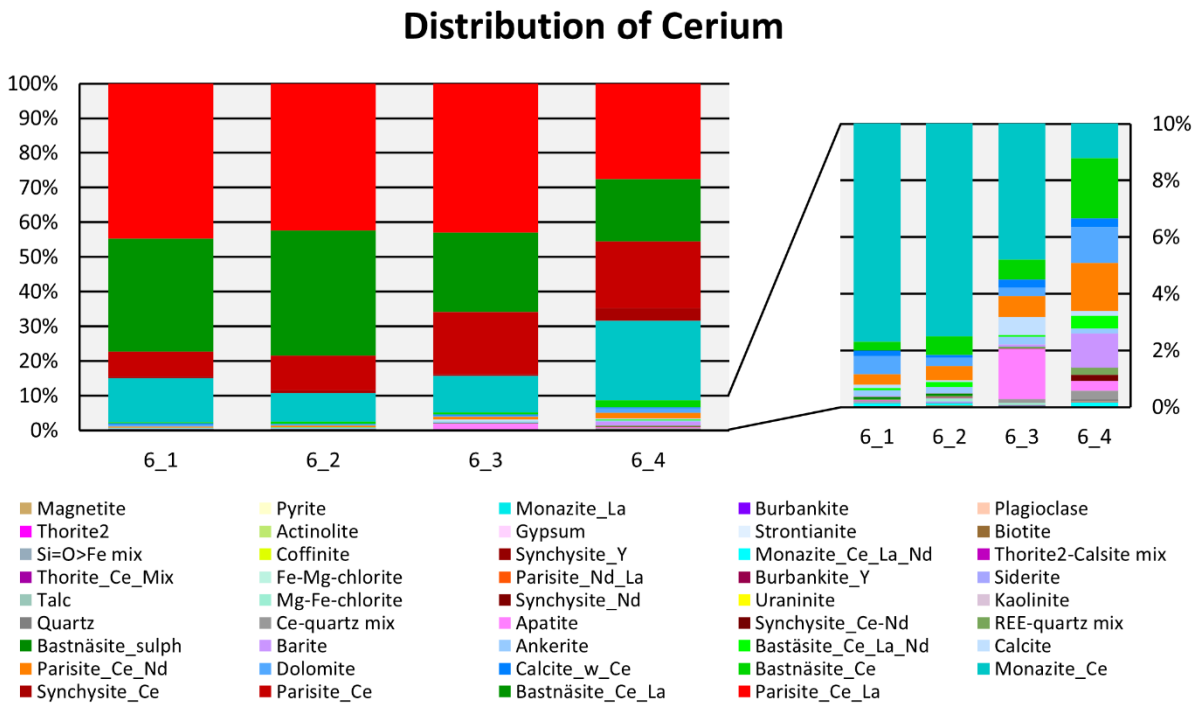

Shows cerium distribution in the high radioactive specimen

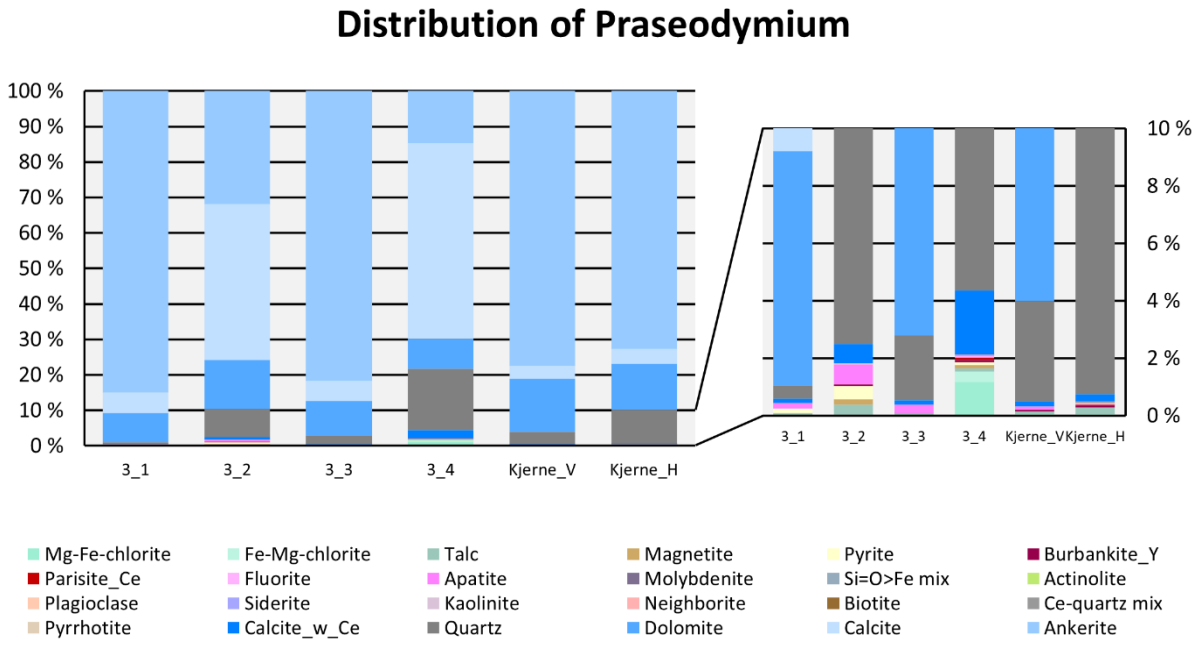

Shows praseodymium distribution in the low radioactive and core specimen

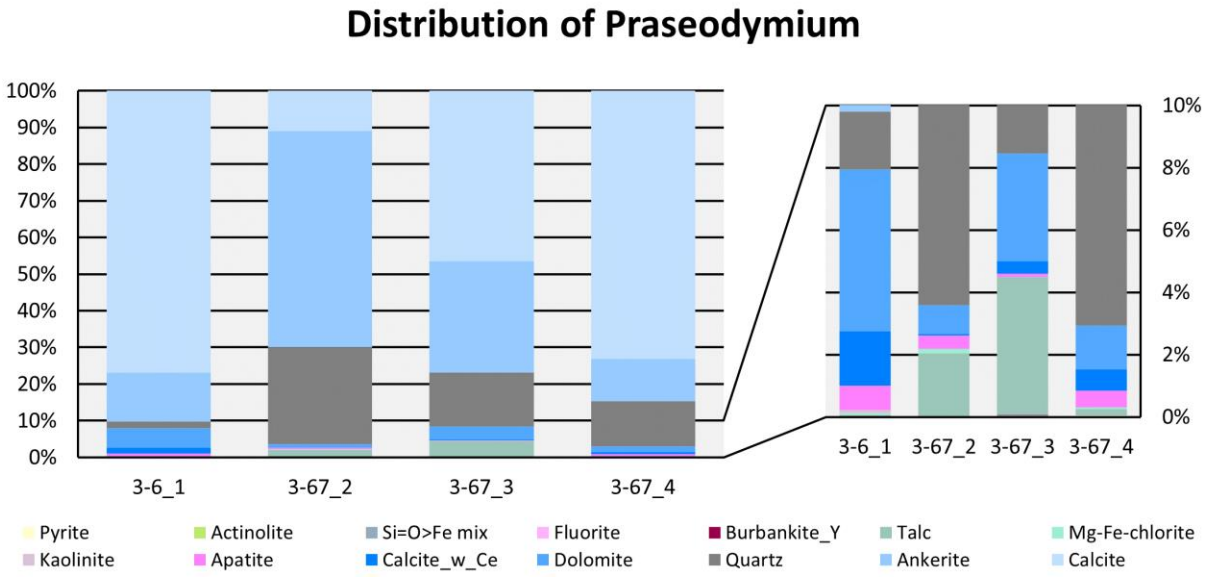

Shows praseodymium distribution in the medium radioactive specimen

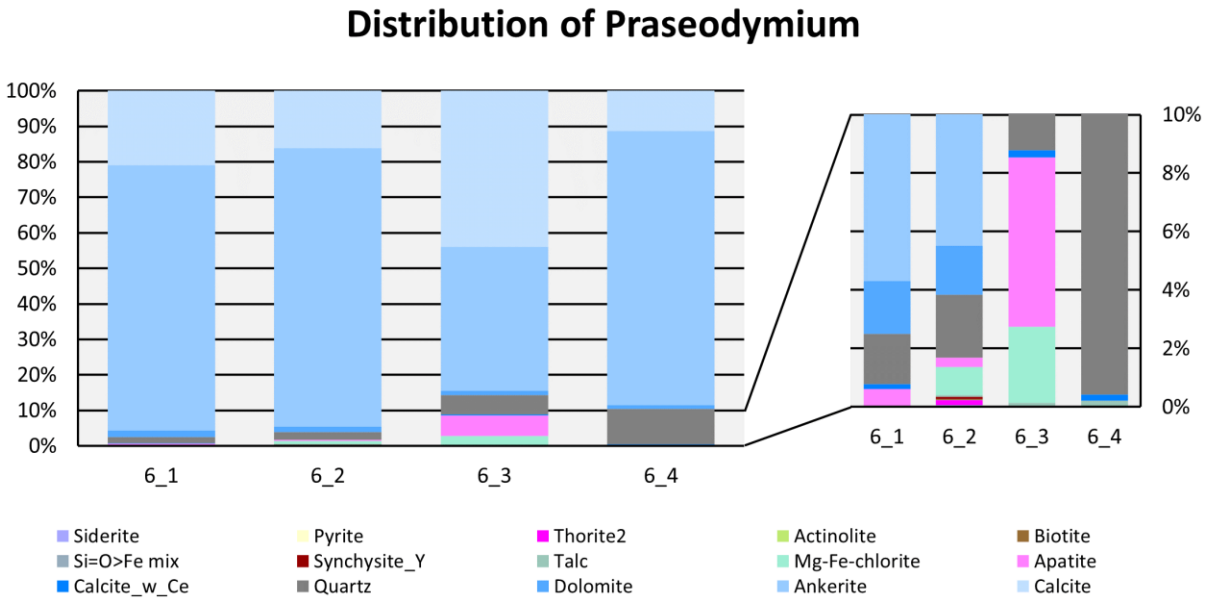

Shows praseodymium distribution in the high radioactive specimen

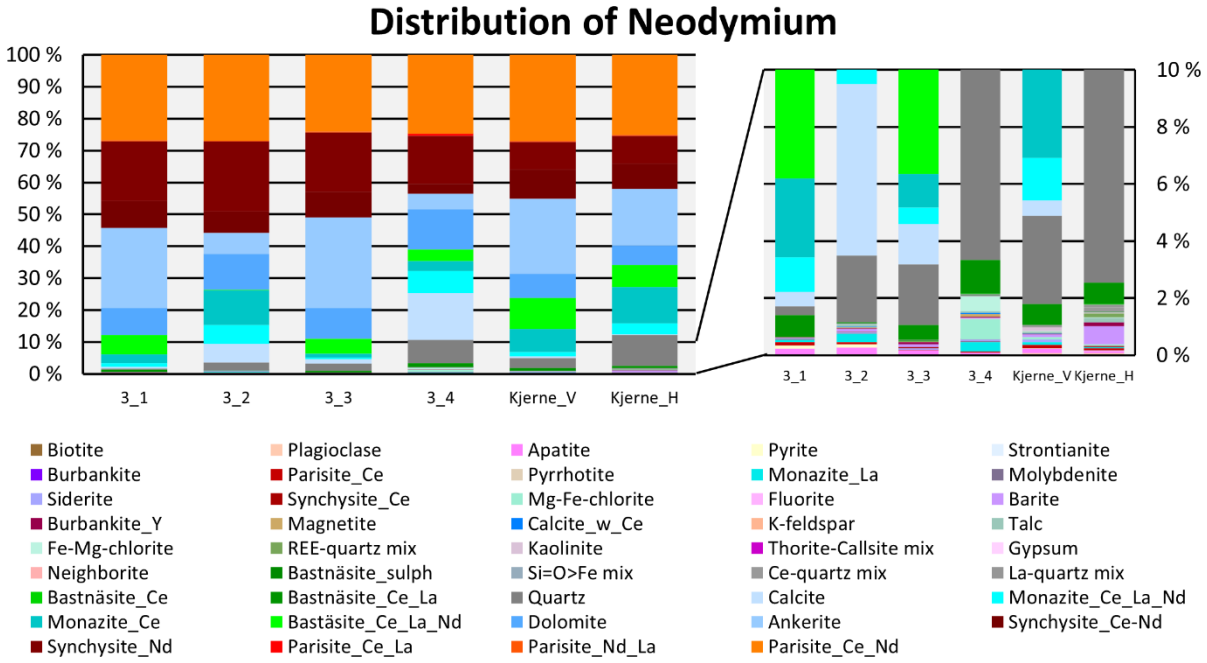

Shows the distribution of neodymium in the low radioactive and core sample specimen

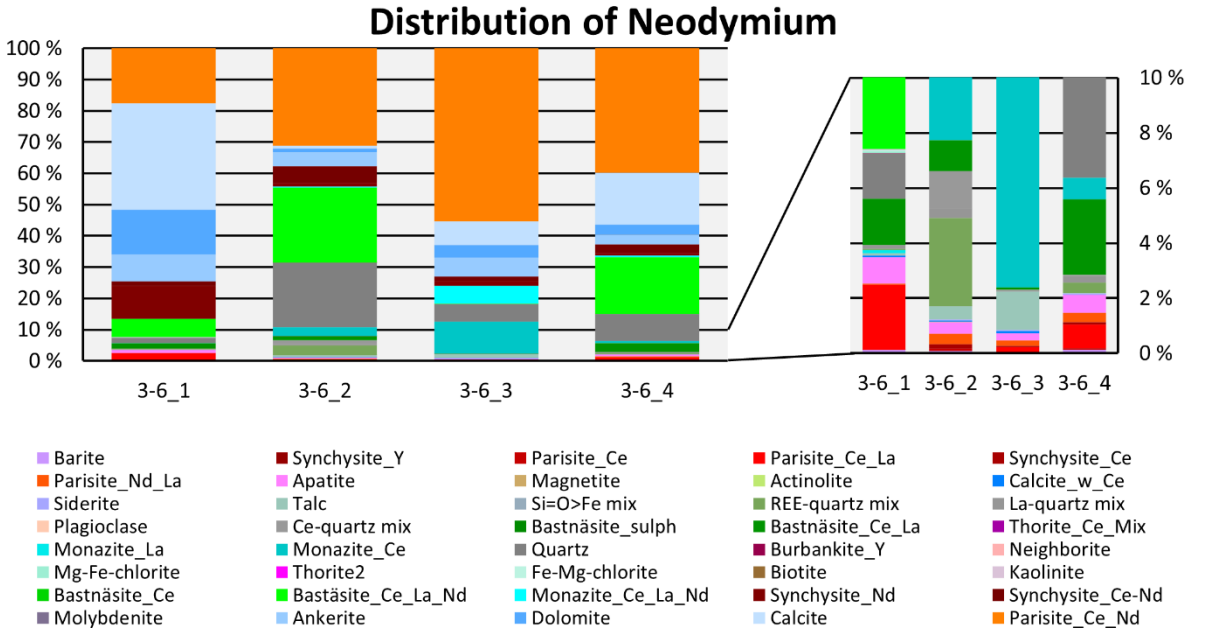

Shows distribution of neodymium in the medium radioactive specimen

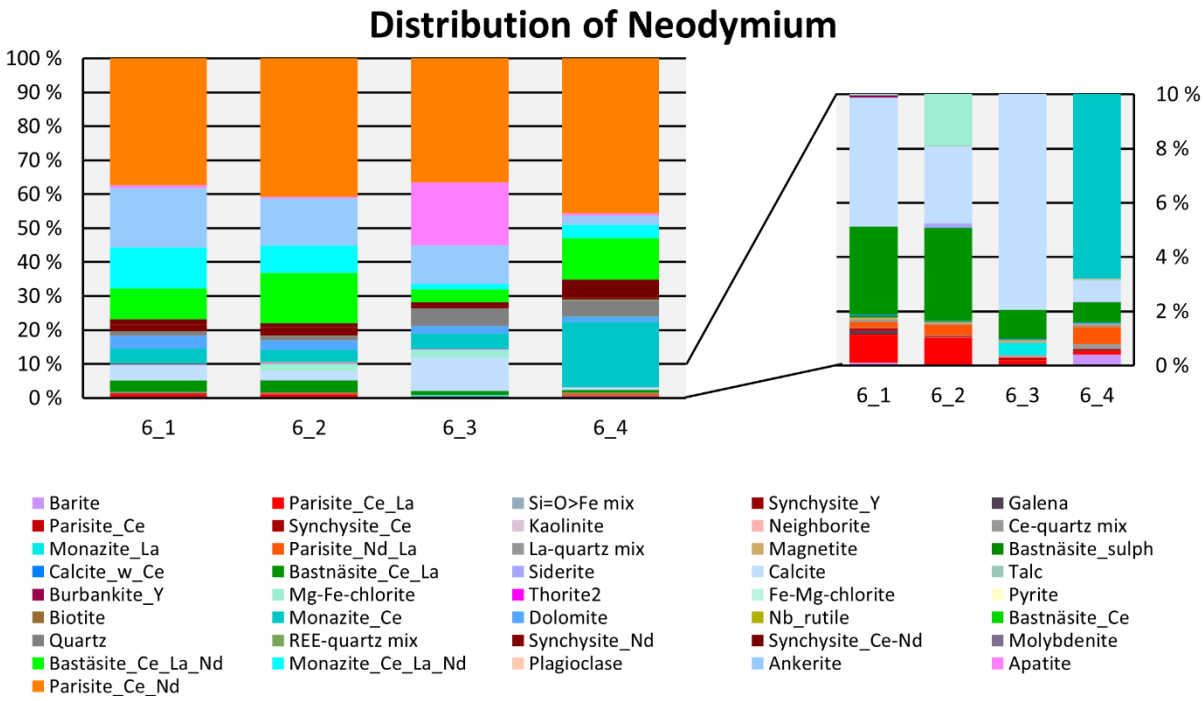

Shows distribution of neodymium in the high radioactive specimen

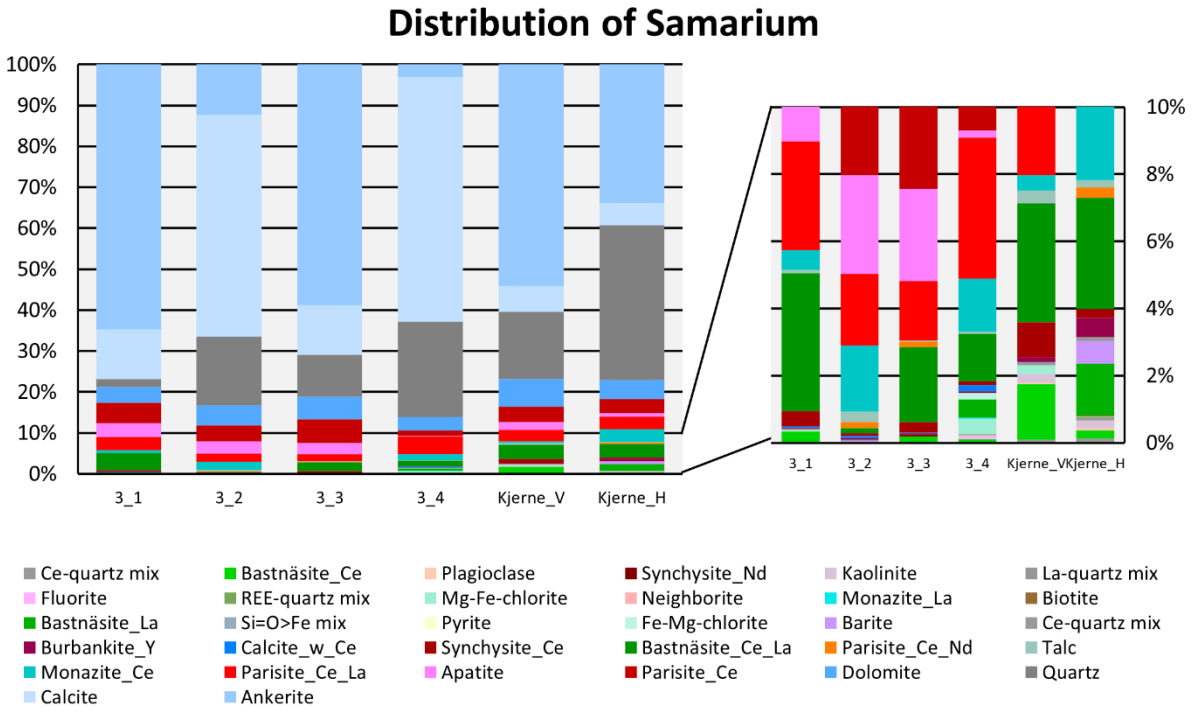

Shows distribution of samarium in the low radioactive and core specimens

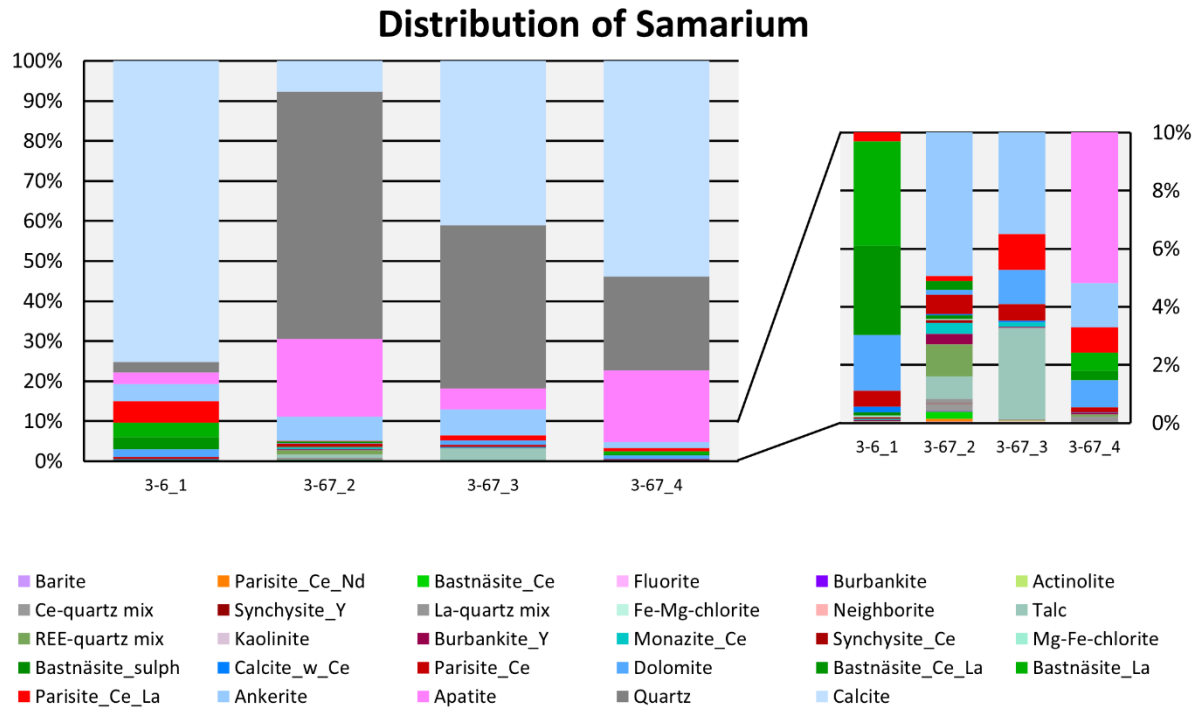

Shows distribution of samarium in the medium radioactive specimen

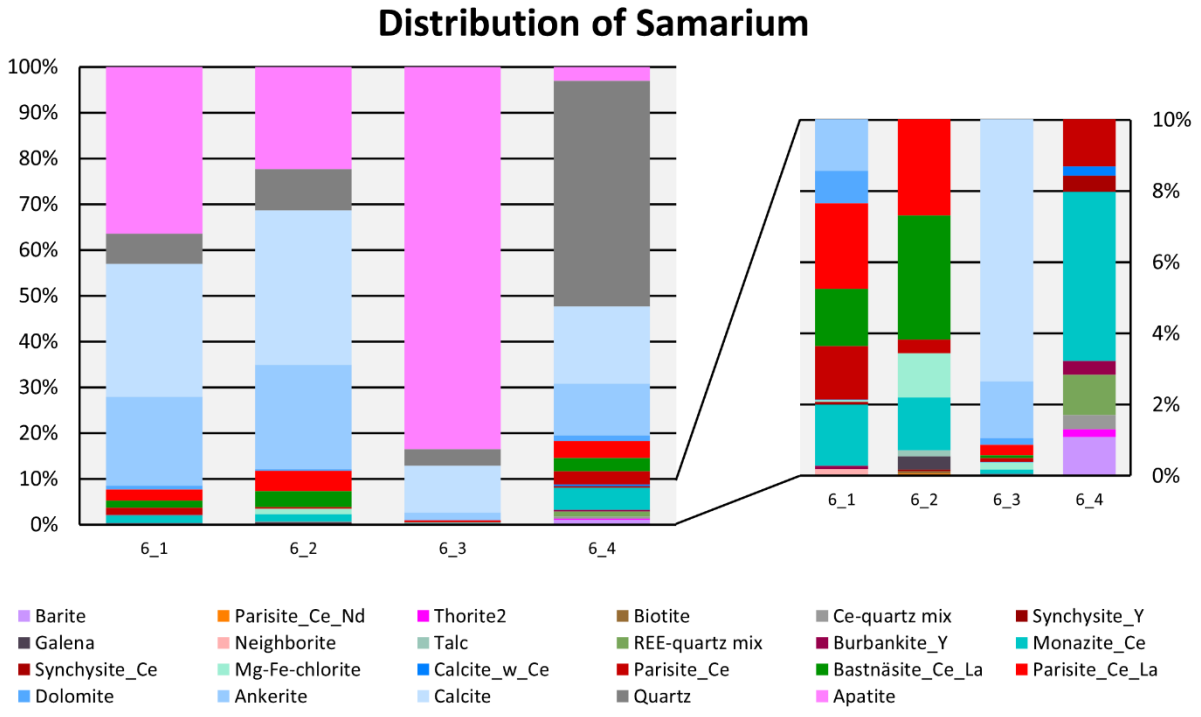

Shows distribution of samarium in the high radioactive specimen

Element size distribution

Size distribution cumulative percentage for thorite, uraninite, coffinite. including counts per specimen for all three minerals.

Size distribution Thorite grains

Size (um)	3_1	3_2	3_3	3_4	3-6_1	3-6_2	3-6_3	3-6_4	6_1	6_2	6_3	6_4	Kjerne_V	Kjerne_H
400	100	100	100	100	100	100	100	100	100	100	100	100	100	100
200	100	100	100	100	100	100	100	100	100	99,97527	100	100	100	100
100	100	100	100	100	100	100	100	100	100	99,92582	99,80411	100	100	100
50	99,72527	100	100	100	99,61832	99,73684	100	100	99,11504	98,83778	97,64936	100	100	100
25	96,7033	98,5782	100	98,90511	94,27481	97,36842	98,06763	100	93,51032	92,1365	89,71596	97,44526	96,25	97,5
15	89,56044	93,12796	96,36364	96,16788	88,54962	91,18421	90,49919	97,36842	85,25074	81,42928	78,51779	87,22628	88,75	88,5
10	75,54945	80,56872	89,09091	86,86131	74,80916	81,57895	67,47182	84,21053	71,38643	64,41642	64,7078	68,9781	80	70
3,5	56,04396	57,109	60	65,87591	53,05344	58,81579	37,03704	65,78947	51,62242	43,49654	46,52302	44,16058	62,5	49
Counts	364	422	55	548	262	760	621	38	678	4091	3063	274	80	200

Size distribution Uraninite grains

Size (um)	3_1	3_2	3_3	3_4	3-6_1	3-6_2	3-6_3	3-6_4	6_1	6_2	6_3	6_4	Kjerne_V	Kjerne_H
400	100	100	0	100	100	100	100	100	100	100	100	100	0	0
200	100	100	0	100	100	100	100	100	100	100	100	100	0	0
100	100	100	0	100	100	100	100	100	100	100	100	100	0	0
50	100	100	0	100	100	100	100	100	100	100	100	100	0	0
25	100	100	0	100	100	100	100	100	100	96	100	100	0	0
15	100	100	0	100	100	100	89,47368	100	100	84	77,77778	100	0	0
10	100	100	0	96,55172	88,88889	100	78,94737	100	100	64	77,77778	100	0	0
3,5	100	75	0	72,41379	66,66667	100	52,63158	75	100	44	66,66667	100	0	0
Counts	2	4	0	29	9	1	19	4	2	**25**	9	1	0	0

Size distribution Coffinite grains

Size (um)	3_1	3_2	3_3	3_4	3-6_1	3-6_2	3-6_3	3-6_4	6_1	6_2	6_3	6_4	Kjerne_V	Kjerne_H
400	0	100	100	100	100	100	100	100	100	100	100	100	0	0
200	0	100	100	100	100	100	100	100	100	100	100	100	0	0
100	0	100	100	100	100	100	100	100	100	100	100	100	0	0
50	0	100	100	98,3871	100	100	100	100	83,33333	100	100	100	0	0
25	0	100	100	98,3871	100	100	100	100	83,33333	100	100	100	0	0
15	0	96,66667	100	95,16129	100	100	93,10345	100	50	93,33333	85,71429	100	0	0
10	0	86,66667	100	82,25806	100	100	79,31034	100	33,33333	86,66667	66,66667	100	0	0
3,5	0	50	100	51,6129	100	100	58,62069	60	33,33333	60	33,33333	100	0	0
Counts	0	30	4	62	5	1	29	10	6	**15**	21	1	0	0

3_1

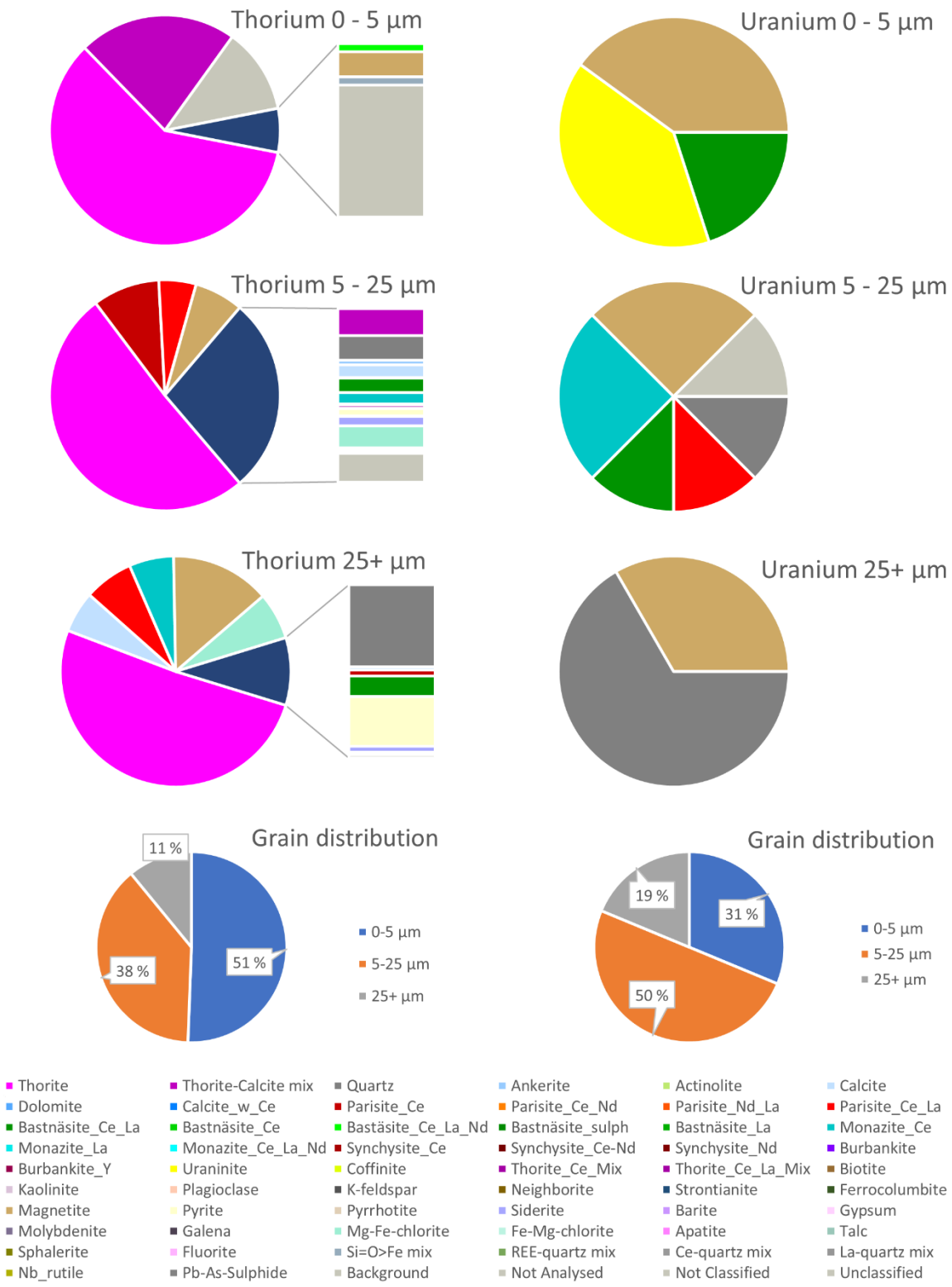

Shows distribution of thorium/ uranium in specimen 3_1 based on measured grain size. minerals under 5 % are placed in the column graph. Bottom graph shows the distribution between the three sizes.

3_2

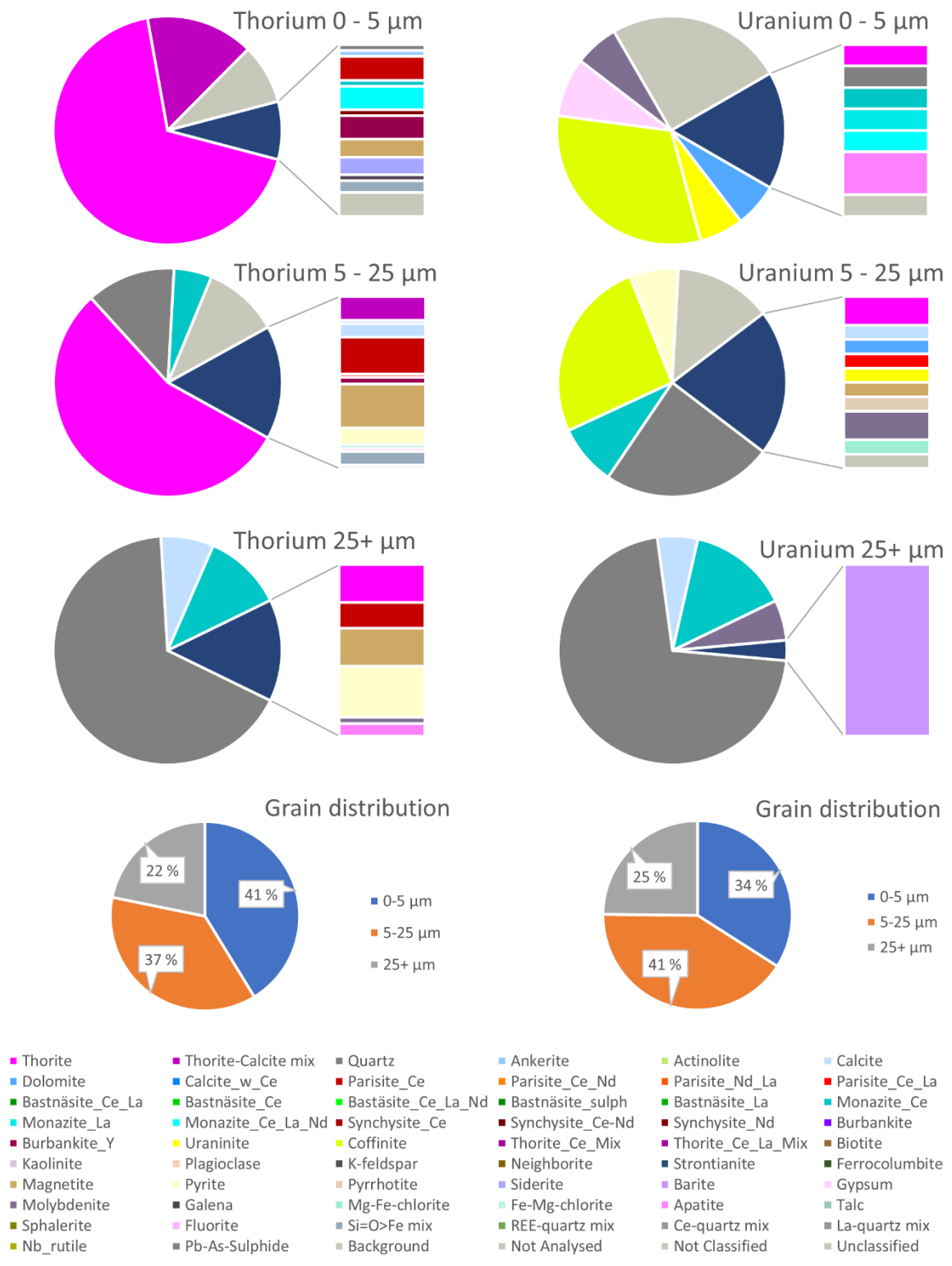

Shows distribution of thorium/ uranium in specimen 3_2 based on measured grain size. minerals under 5 % are placed in the column graph. Bottom graph shows the distribution between the three sizes.

3_3

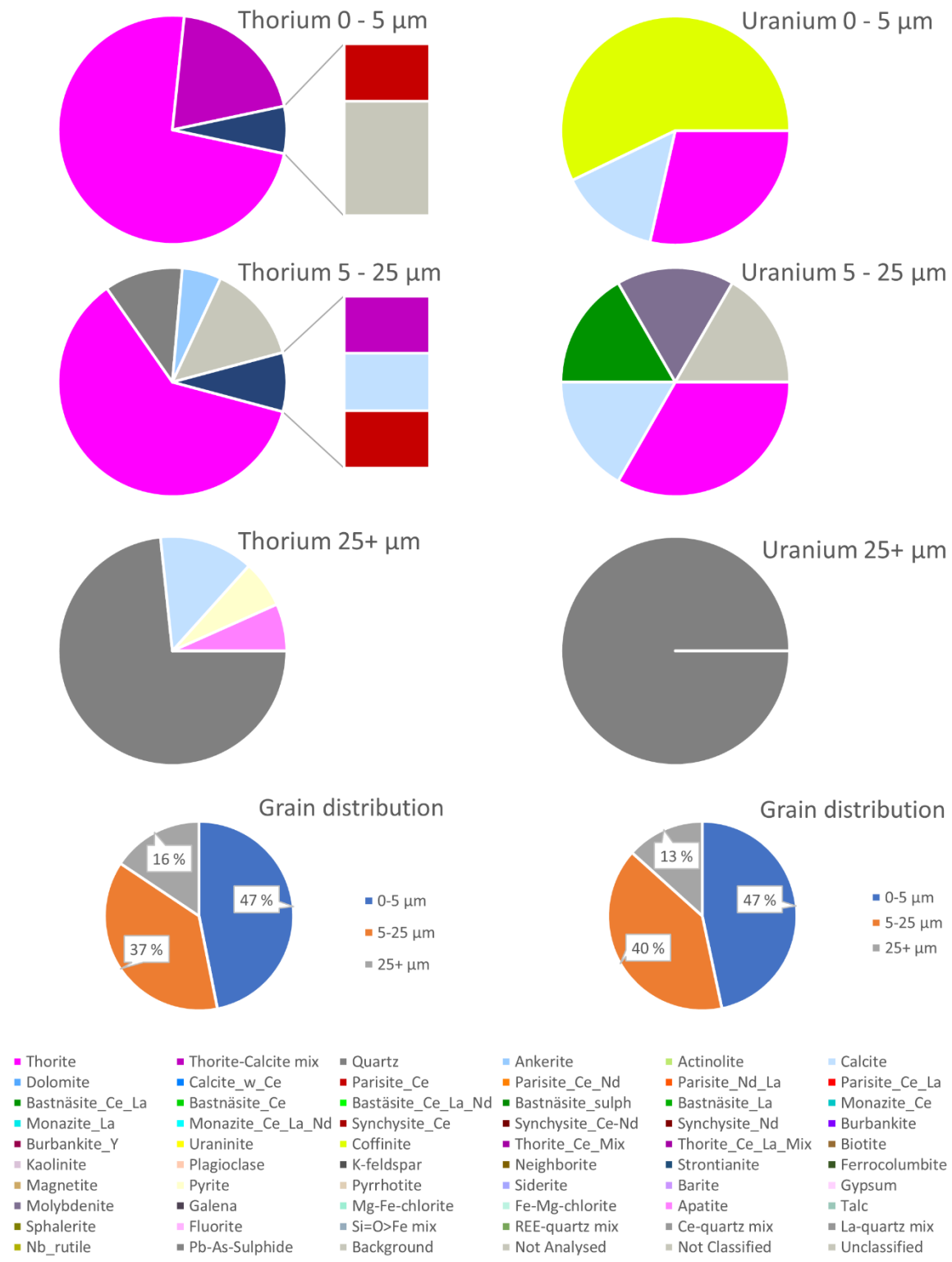

Shows distribution of thorium/ uranium in specimen 3_3 based on measured grain size. minerals under 5 % are placed in the column graph. Bottom graph shows the distribution between the three sizes.

3_4

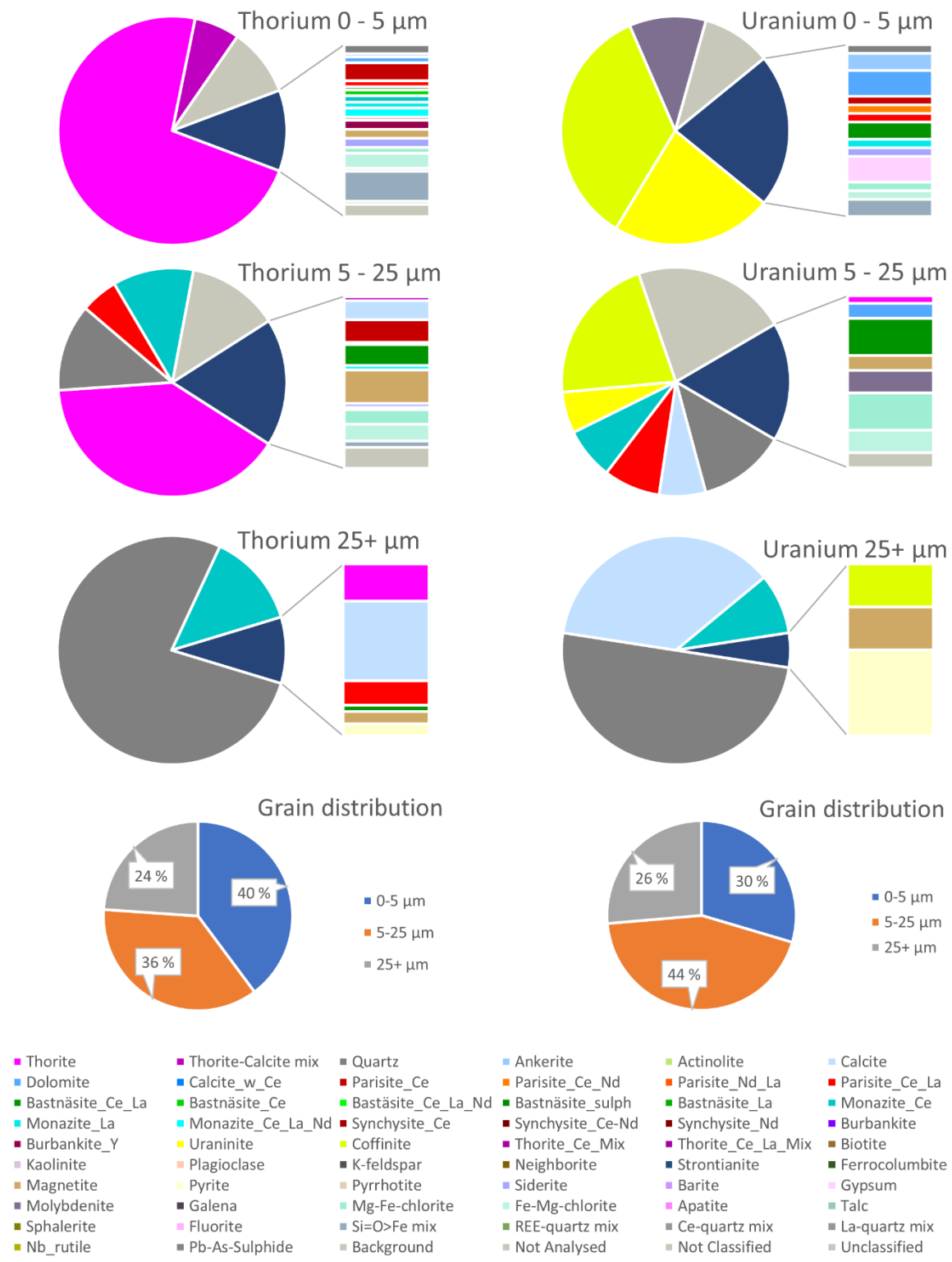

Shows distribution of thorium/ uranium in specimen 3_4 based on measured grain size. minerals under 5 % are placed in the column graph. Bottom graph shows the distribution between the three sizes.

3-6_1

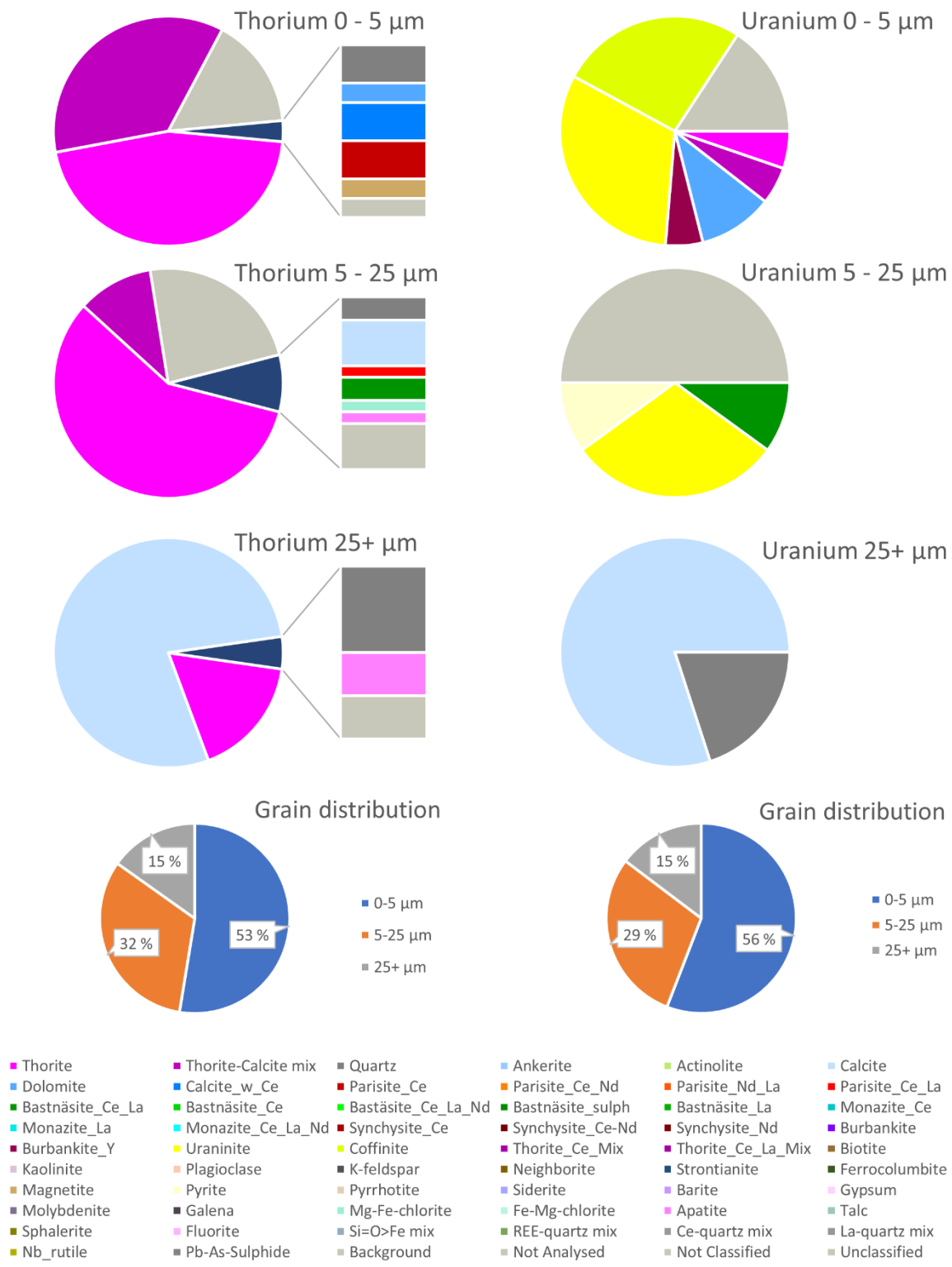

Shows distribution of thorium/ uranium in specimen 3-6_1 based on measured grain size. minerals under 5 % are placed in the column graph. Bottom graph shows the distribution between the three sizes.

3-6_2

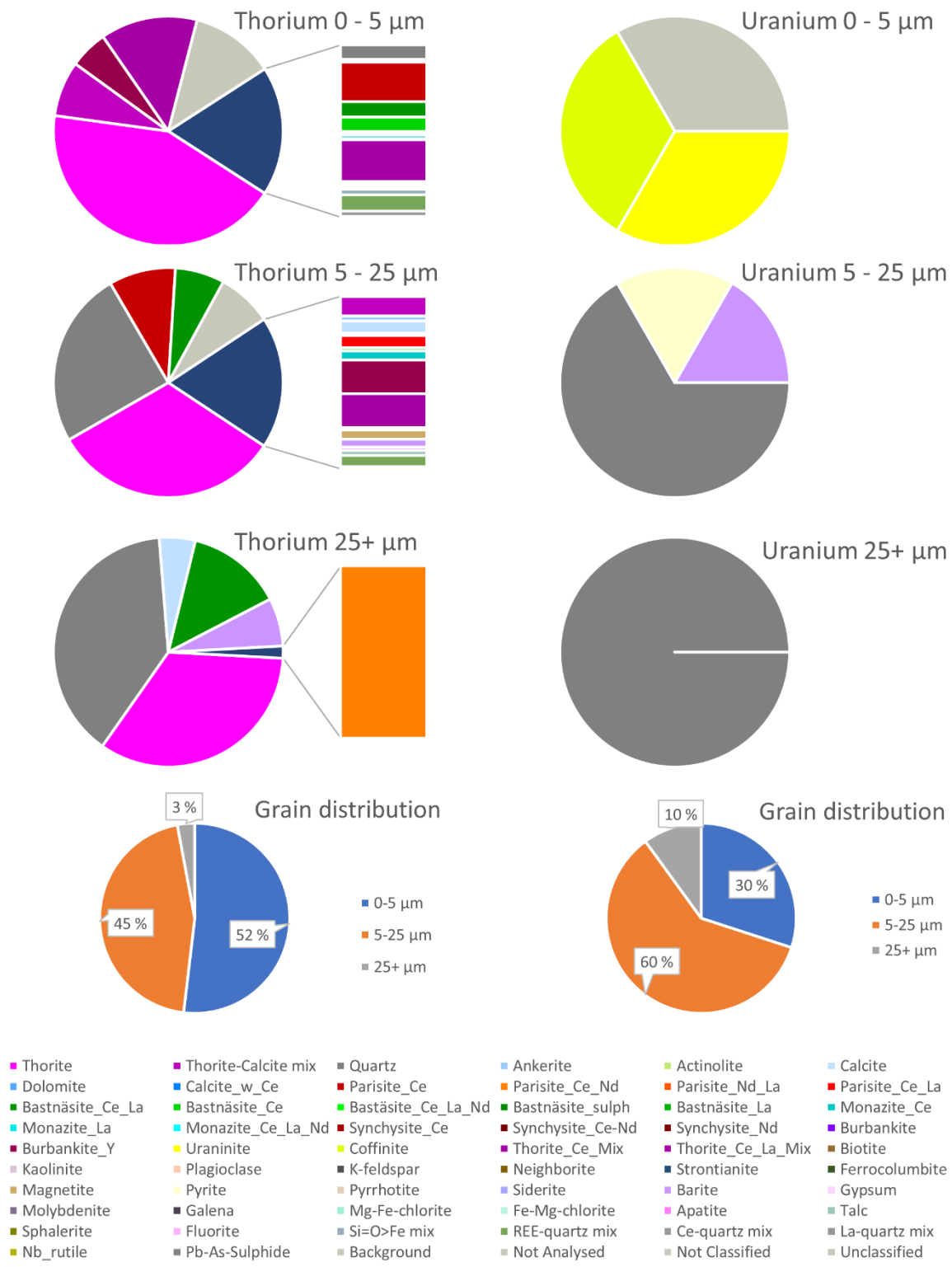

Shows distribution of thorium/ uranium in specimen 3-6_2 based on measured grain size. minerals under 5 % are placed in the column graph. Bottom graph shows the distribution between the three sizes.

3-6_3

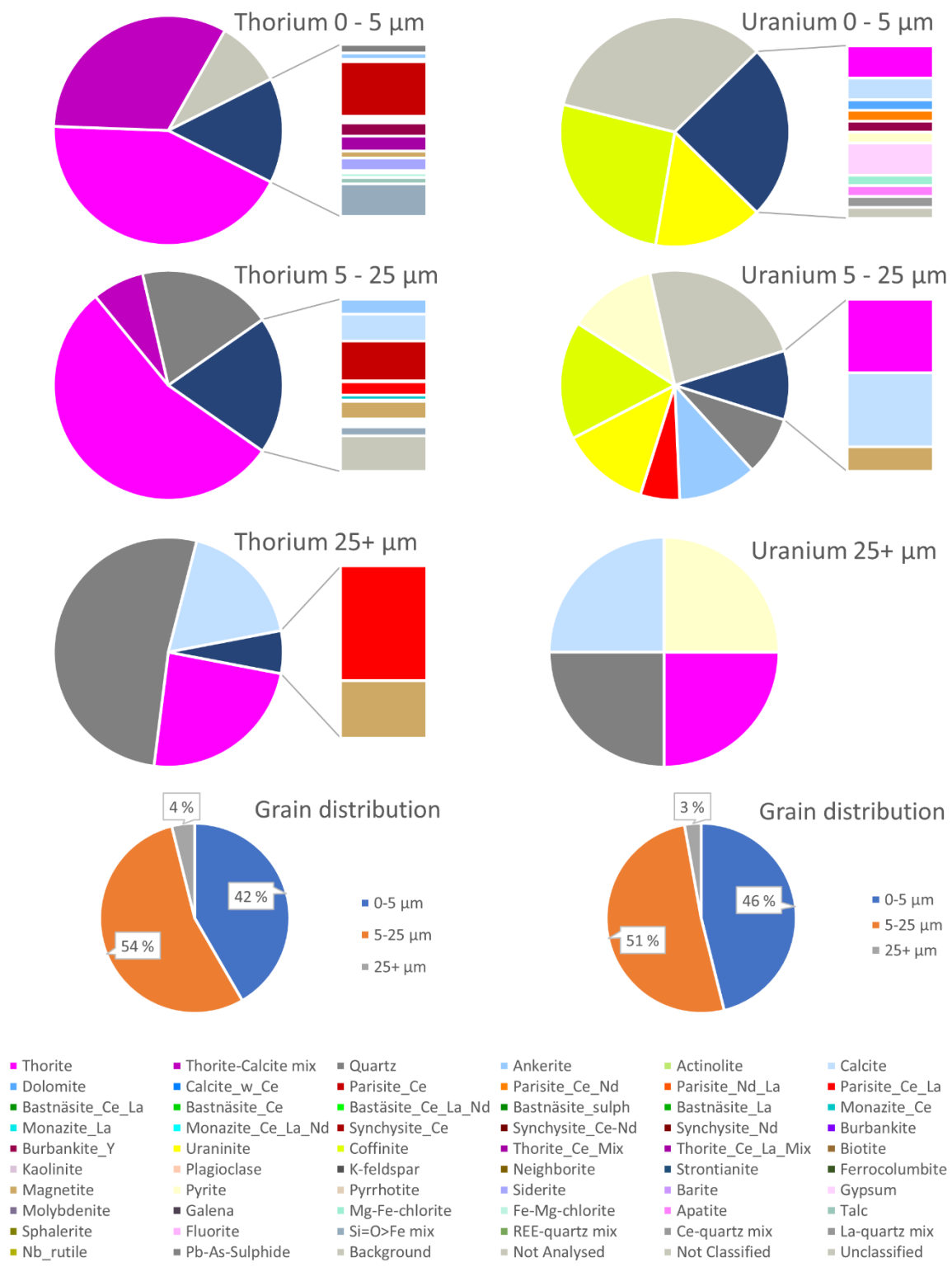

Shows distribution of thorium/ uranium in specimen 3-6_3 based on measured grain size. minerals under 5 % are placed in the column graph. Bottom graph shows the distribution between the three sizes.

3-6_4

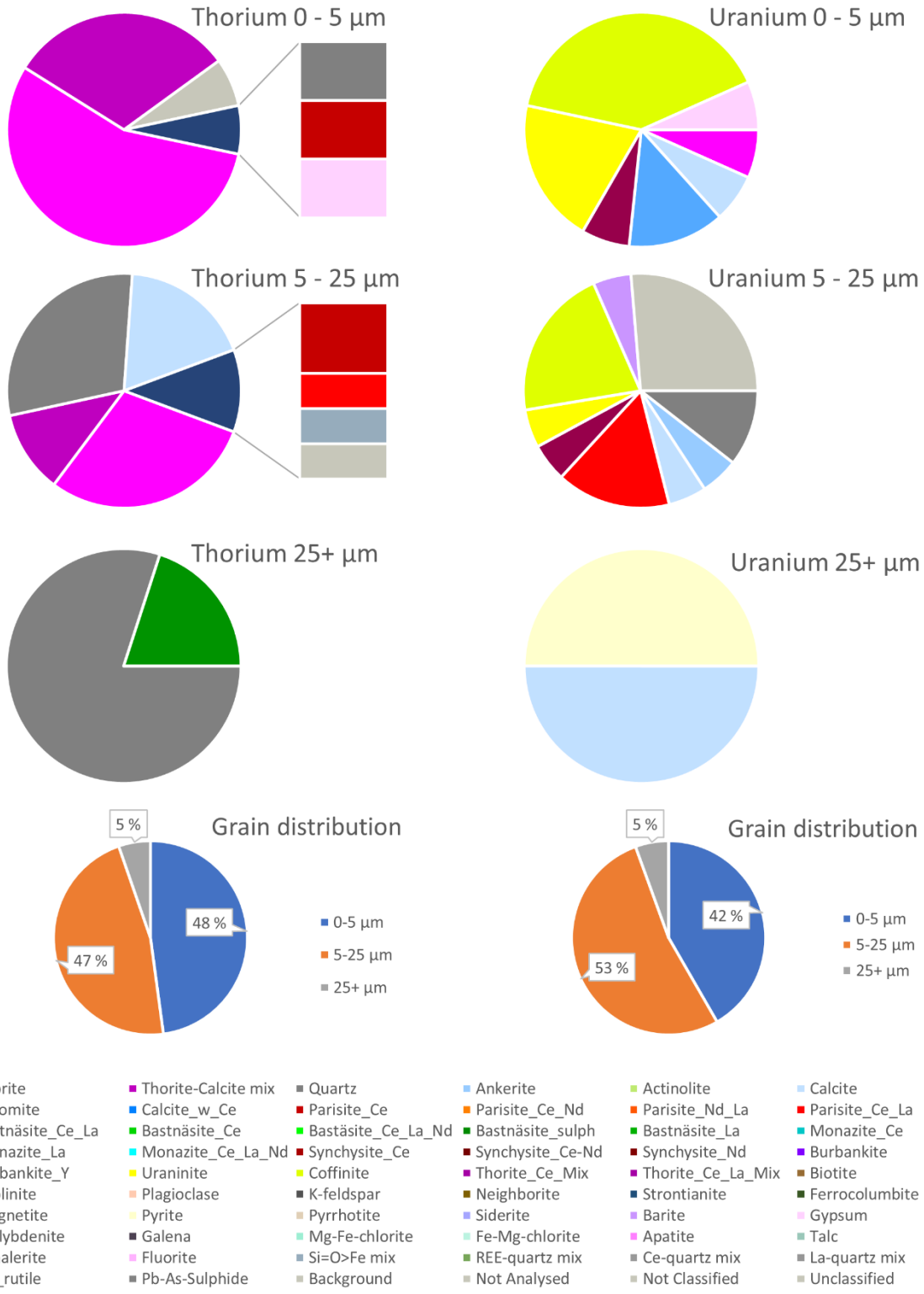

Shows distribution of thorium/ uranium in specimen 3-6_4 based on measured grain size. minerals under 5 % are placed in the column graph. Bottom graph shows the distribution between the three sizes.

6_1

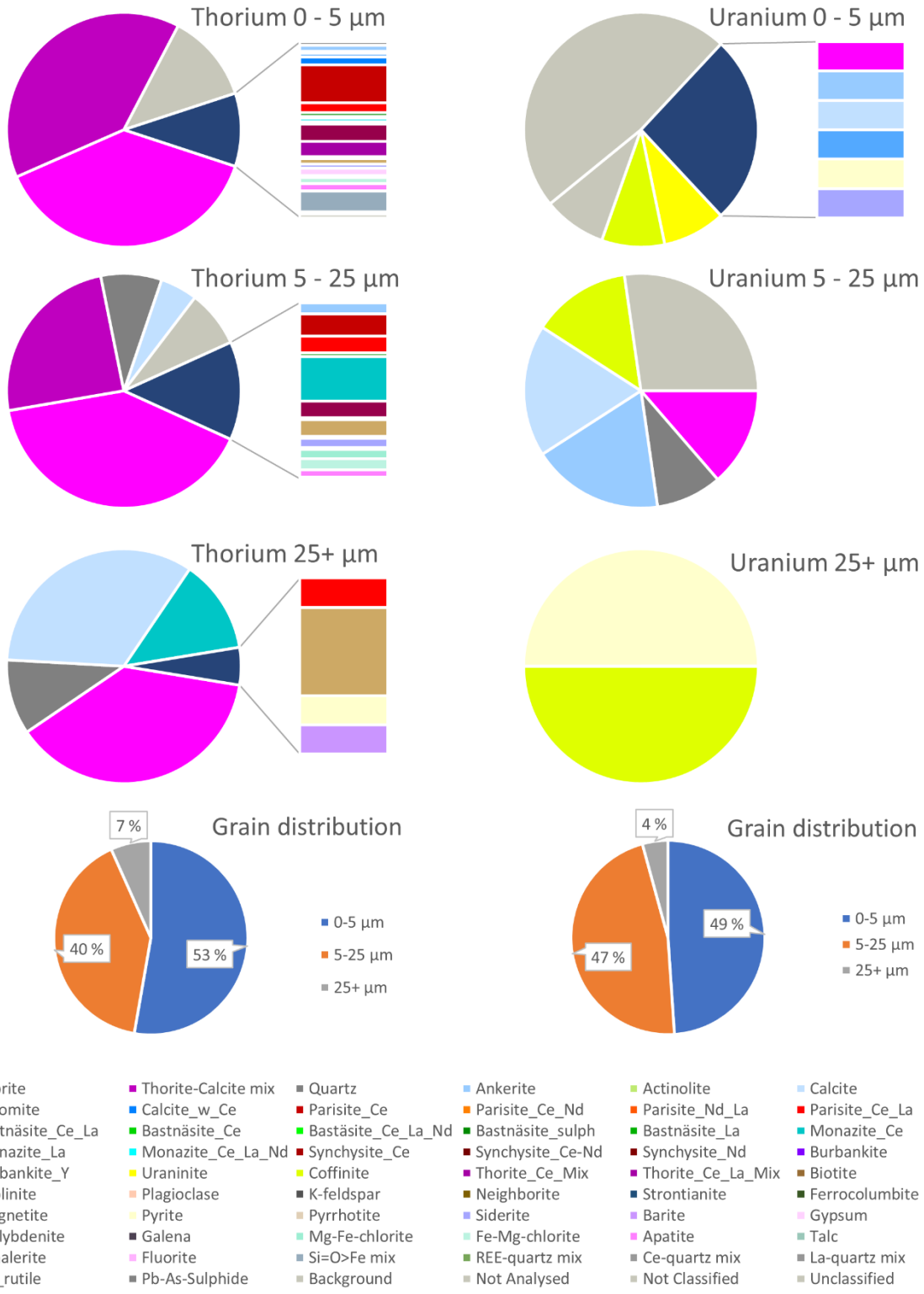

Shows distribution of thorium/ uranium in specimen 6_1 based on measured grain size. minerals under 5 % are placed in the column graph Bottom graph shows the distribution between the three sizes.

6_2

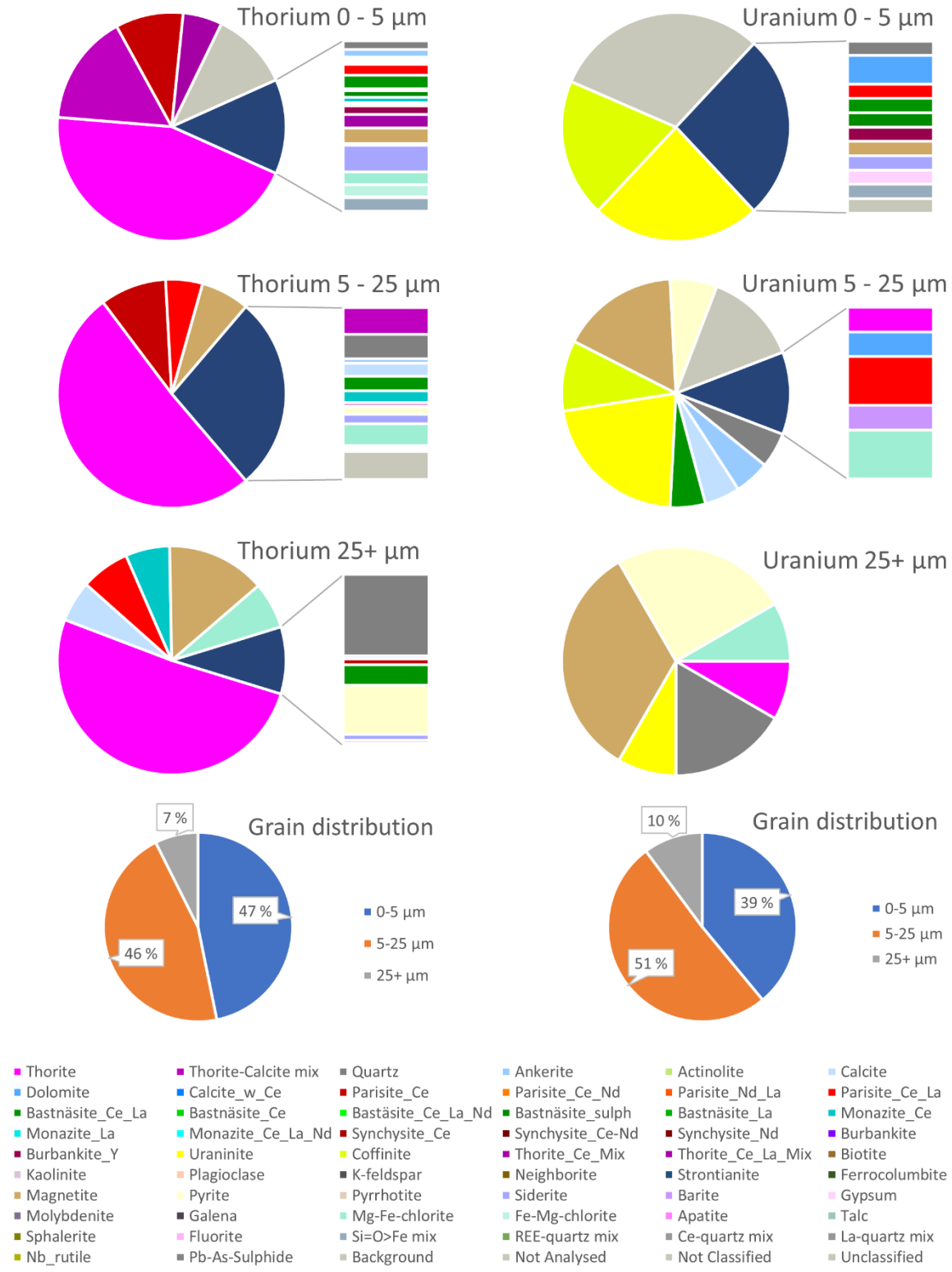

Shows distribution of thorium/ uranium in specimen 6_2 based on measured grain size. minerals under 5 % are placed in the column graph. Bottom graph shows the distribution between the three sizes.

6_3

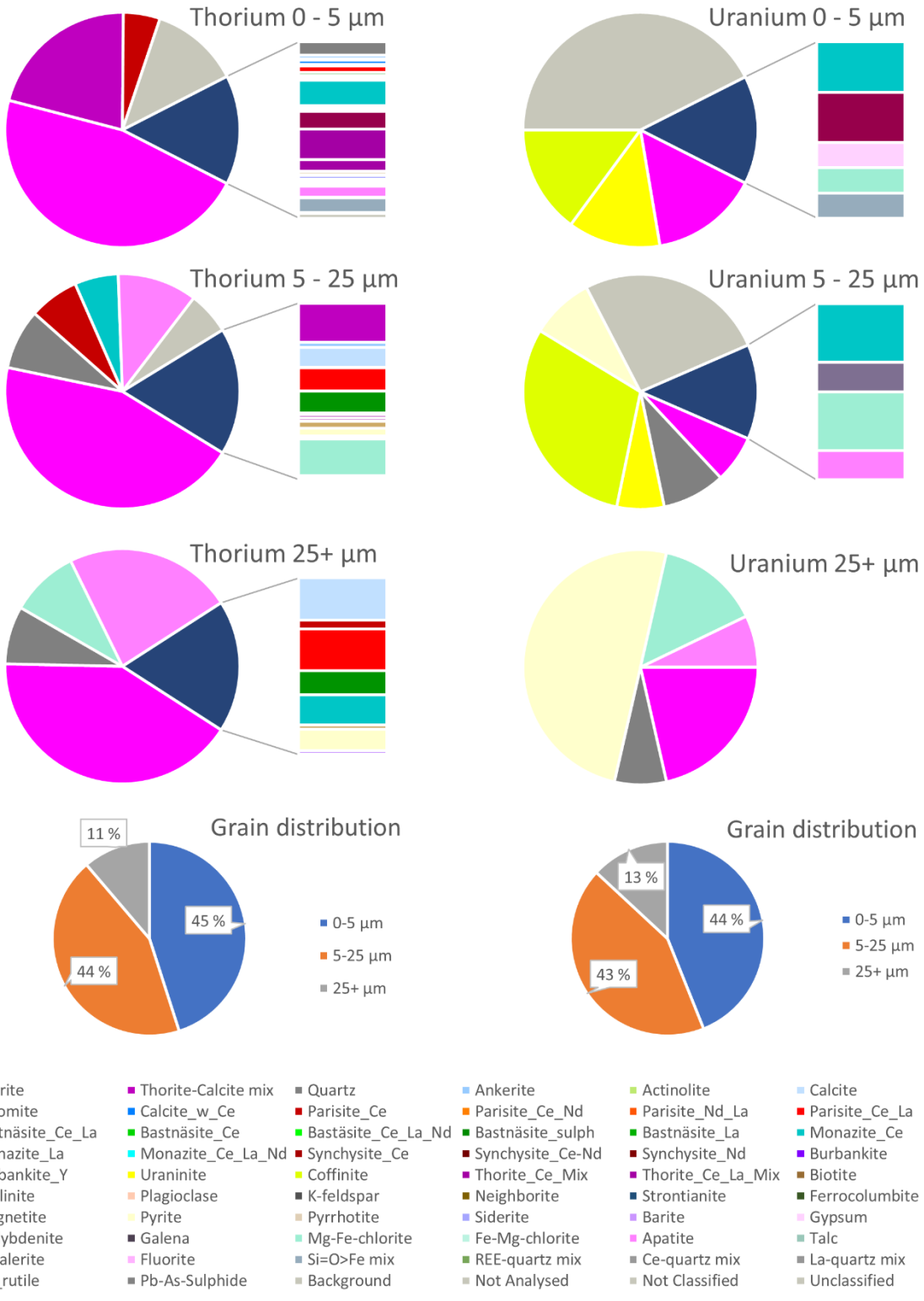

Shows distribution of thorium/ uranium in specimen 6_3 based on measured grain size. minerals under 5 % are placed in the column graph. Bottom graph shows the distribution between the three sizes.

6_4

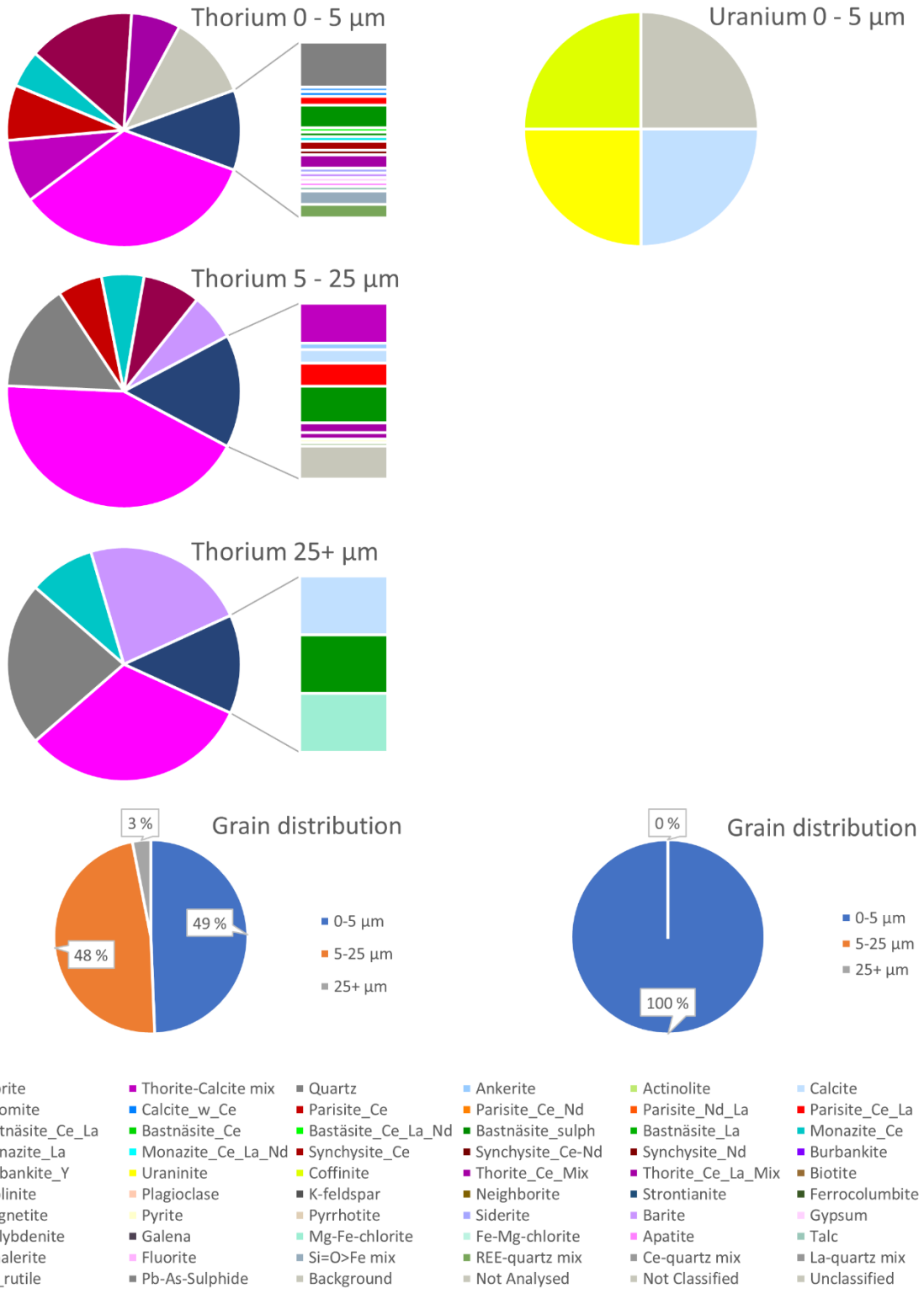

Shows distribution of thorium/ uranium in specimen 6_4 based on measured grain size. minerals under 5 % are placed in the column graph. Bottom graph shows the distribution between the three sizes.

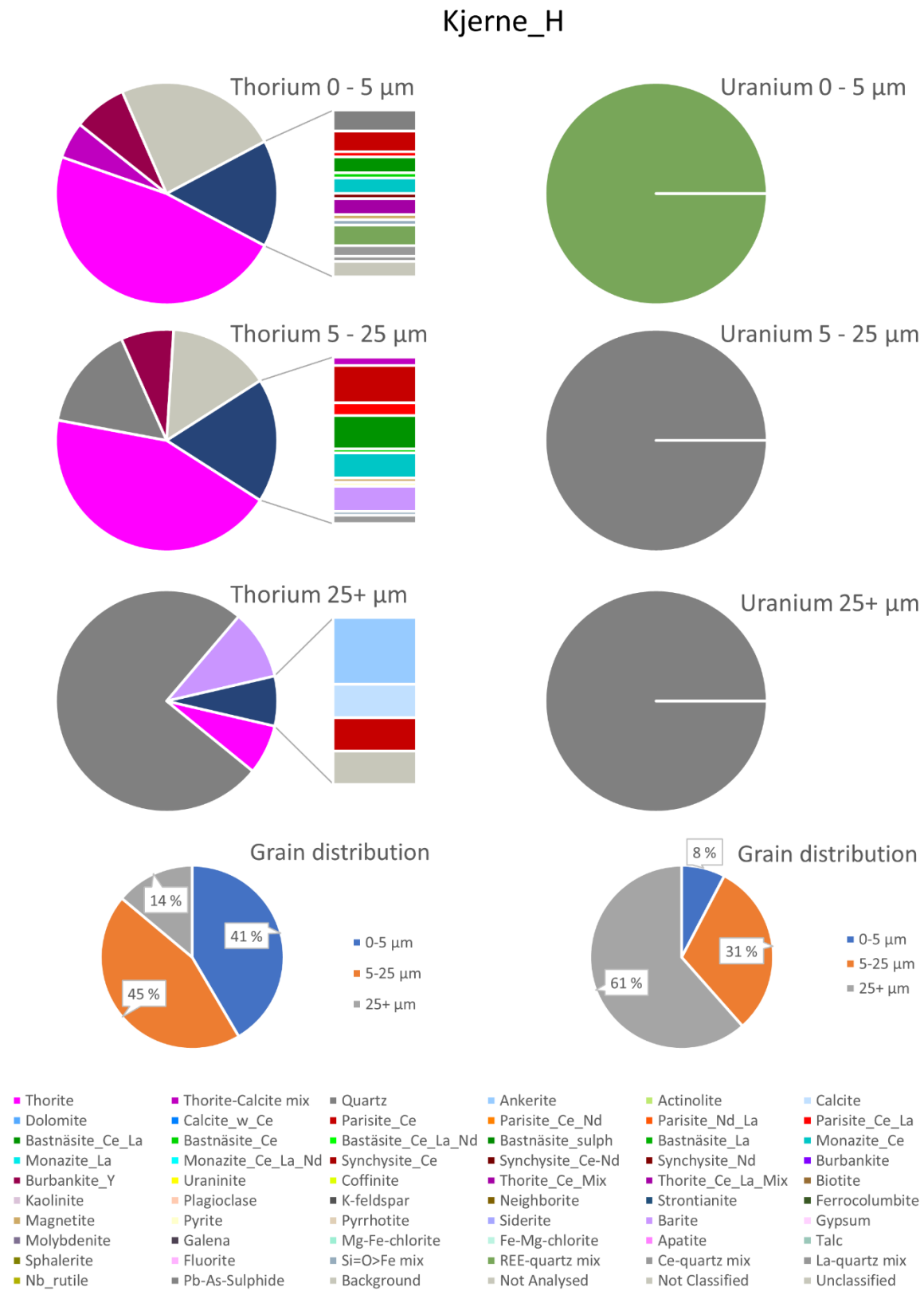

Shows distribution of thorium/ uranium in specimen Kjerne_H based on measured grain size. minerals under 5 % are placed in the column graph. Bottom graph shows the distribution between the three sizes.

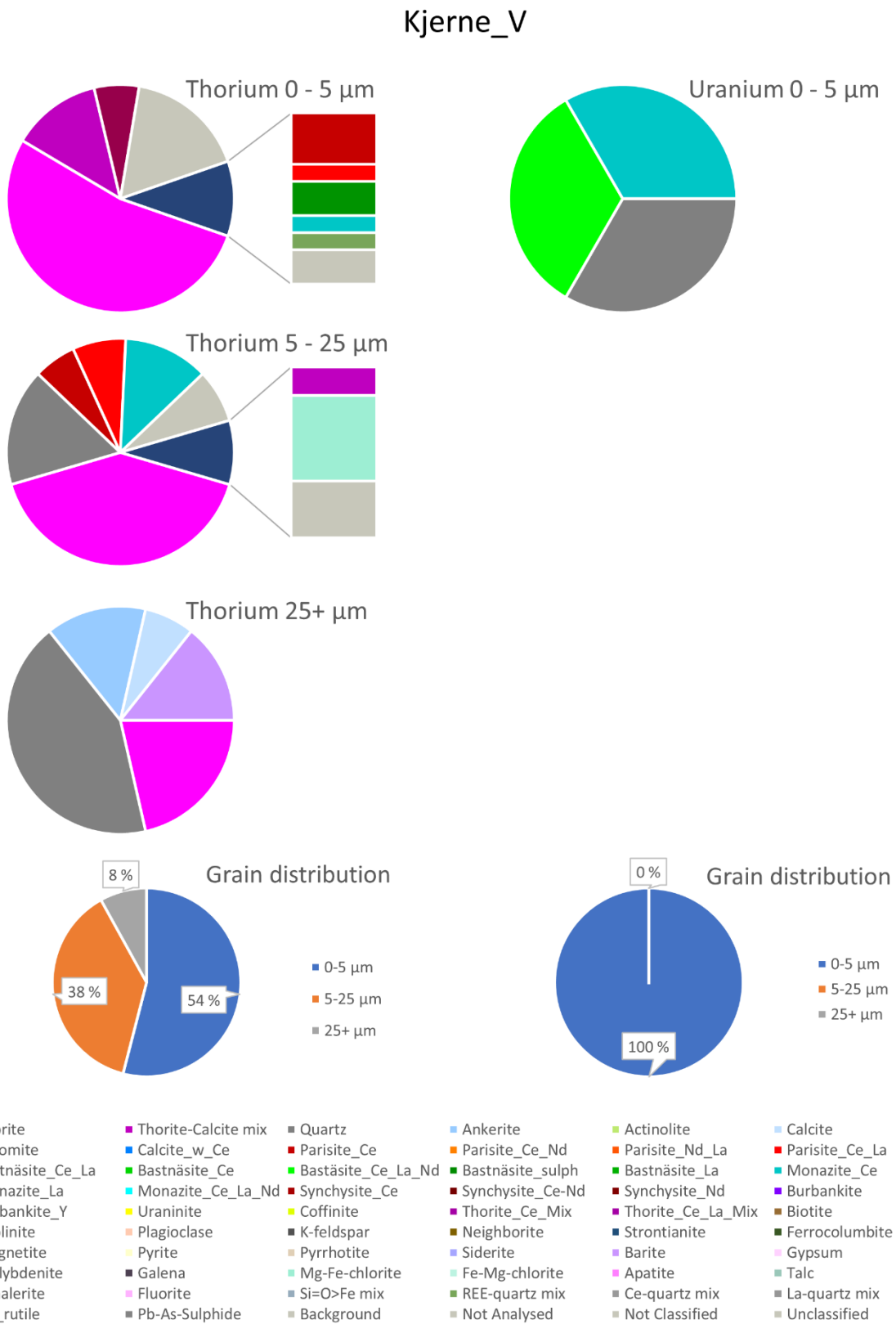

Shows distribution of thorium/ uranium in specimen Kjerne_V based on measured grain size. minerals under 5 % are placed in the column graph. Bottom graph shows the distribution between the three sizes.

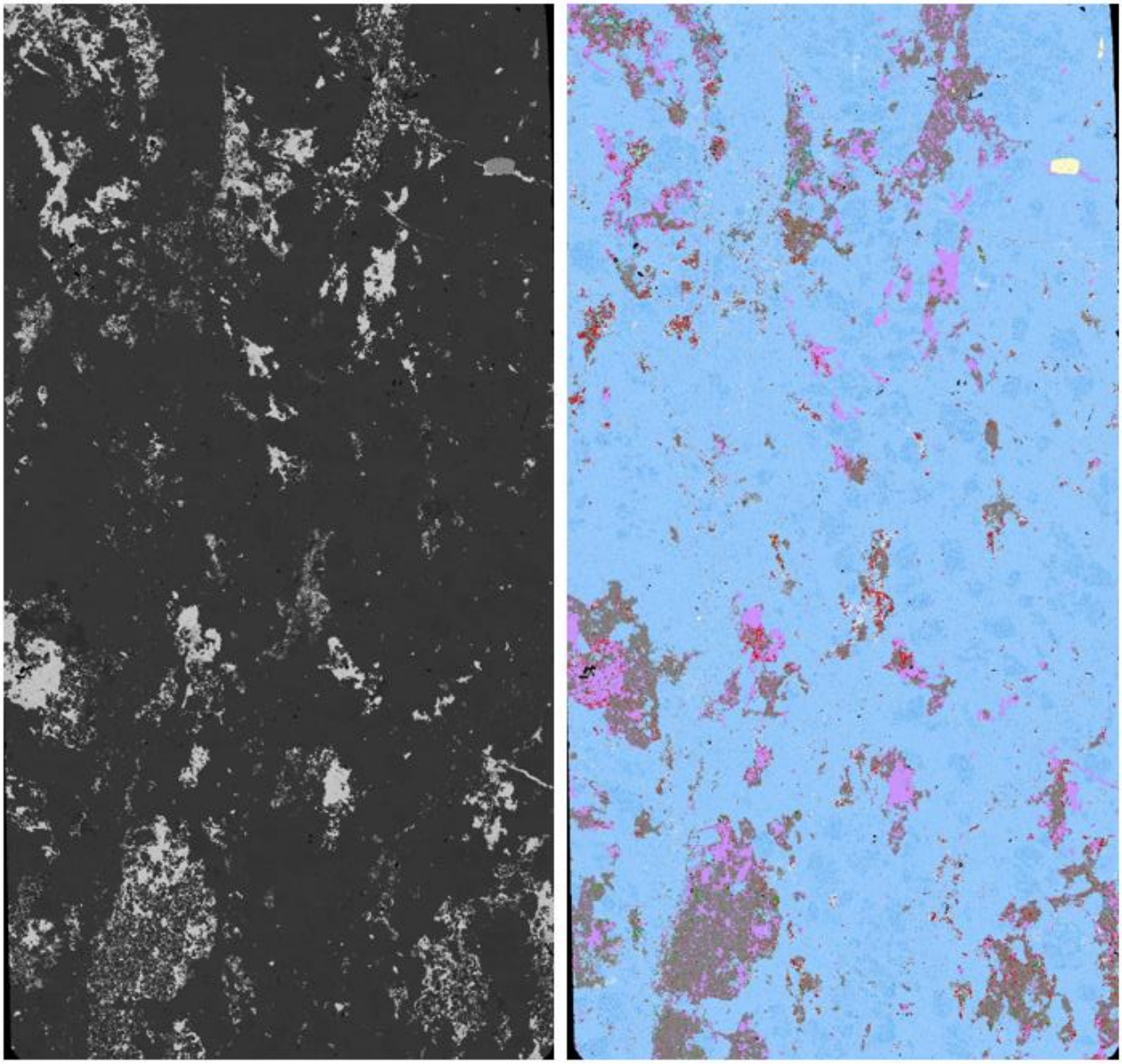

Shows BSE and AM OV of Kjerne_H

Gaute Magnushommen

Distribution of Th and U in the Fe-dolomite carbonatite from the Fen REE deposit

NTNU
Norwegian University of
Science and Technology